Doctoral Thesis

Inatel
Instituto Nacional de Telecomunicações

Machine Learning Applied to 5G and Towards 6G Fiber/Wireless Systems Linearization

Luiz Augusto Melo Pereira

July / 2023

MACHINE LEARNING APPLIED TO 5G AND TOWARDS 6G FIBER/WIRELESS SYSTEMS LINEARIZATION

LUIZ AUGUSTO MELO PEREIRA

Doctoral Thesis presented at National Institute of Telecommunications (Inatel), as part of the requirements for obtaining the Doctor Degree in Telecommunication Engineering.

ADVISOR: Prof. Dr. Arismar Cerqueira Sodré Junior.

CO-ADVISOR: Prof. Dr. Luciano Leonel Mendes.

Santa Rita do Sapucaí-MG
2023

Pereira, Luiz Augusto Melo
P436m
Machine Learning Applied to 5G and Towards 6G Fiber/Wireless Systems Linearization / Luiz Augusto Melo Pereira. – Santa Rita do Sapucaí, 2023.
148 p.

Orientador: Prof. Dr. Arismar Cerqueira Sodré Junior / Prof. Dr. Luciano Leonel Mendes.
Tese de Doutorado em Telecomunicações – Instituto Nacional de Telecomunicações – INATEL.
Inclui bibliografia.

1. 5G 2. 6G 3. linearization 4. machine learning 5. radio over fiber. 6. Doutorado em Telecomunicações. I. Sodré Junior, Arismar Cerqueira. II Mendes, Luciano Leonel. III. Instituto Nacional de Telecomunicações – INATEL. III. Título.

CDU 621.39

Ficha Catalográfica elaborada pelo Bibliotecário da Instituição
CRB6-2718 – Paulo Eduardo de Almeida

APPROVAL FORM

Thesis defended and approved in July 6th, 2023 by the judging committee:

Prof. Dr. Arismar Cerqueira Sodré Junior
Instituto Nacional de Telecomunicações (Inatel)

Prof. Dr. Marcelo Eduardo Vieira Segatto
Universidade Federal do Espírito Santo (UFES)

Prof. Dr. Felipe Augusto Pereira de Figueiredo
Instituto Nacional de Telecomunicações (Inatel)

Prof. Dr. José Antônio Justino Ribeiro

Profa. Dra. Antonella Bogoni
Scuola Superiore Sant'Anna

Graduate Course Coordinator
Prof. Dr. José Marcos Camara Brito

"Commit your works to the LORD,
and your plans will succeed."

Proverbs 16:3

To my friends and family,
for the patience, guidance and support.

Acknowledgments

I would like to express my deepest gratitude and appreciation to my doctoral advisor, Prof. Dr. Arismar Cerqueira Sodré Junior, for their guidance, unwavering support, and invaluable mentorship throughout my doctoral journey.

To my co-advisor Prof. Dr. Luciano Leonel Mendes, for the numerous contributions and immense attention dedicated to this work. His expertise and support were instrumental in the successful completion of my doctoral thesis. I am grateful for his insightful discussions, guidance, and contributions throughout the research process. His commitment to scientific excellence and dedication to the advancement of knowledge greatly enriched this study. It is an honor to have had the opportunity to work alongside him.

To the judging committee, for the guidelines to improve this work.

To my parents Altair and Gorete, for their unconditional love, support and for teaching me the most important lessons of life.

To my dear brothers Kalyne, Natalia, Pedro Henrique and Ana Júlia, for always being by my side, showing me the true meaning of patience and fraternity.

I also like to express my gratitude to my girlfriend Bruna for her unconditional love, patience, support and understanding. I am so fortunate to have you in my life.

To my friends and members of the Wireless and Optical Convergent Access (WOCA) laboratory, you have deeply contributed to my career development. Thank you for the partnership and shared laughs.

To Instituto Nacional de Telecomunicacões (Inatel), for providing the required infrastructure to develop this work.

I would like to express my sincere gratitude to Carmelo José Albanez Bastos Filho from Universidade de Pernambuco (UPE) for their valuable collaboration.

This work was partially supported by RNP, with resources from MCTIC, Grant No. 01245.020548/2021-07, under the Brazil 6G project of the Radiocommunication Reference Center (Centro de Referência em Radiocomunicações - CRR) of the National Institute of Telecommunications (Instituto Nacional de Telecomunicações - Inatel), Brazil, by Huawei, under the project Advanced Academic Education in Telecommunications Networks and Systems, contract No PPA6001BRA23032110257684, and by FAPESP, Grant No. 20/05127-2, under SAMURAI project. The authors also thank the financial support from CNPq, CAPES, FINEP, FAPEMIG and FAPESP (Contracts # 2021/06569-1 e # 2022/09319-9).

Luiz Augusto Melo Pereira

Index

List of Figures

List of Tables

List of Acronyms

3G	Third generation of mobile communication
3GPP	3rd Generation Partnership Project
4G	Fourth generation of mobile communication
5G	Fifth generation of mobile communication
5G NR	5G New Radio
5G-RANGE	Remote Area Access Network for the 5th Generation
6G	Sixth generation of mobile communication
A-RoF	Analog radio over fiber
ACLR	Adjacent channel leakage ratio
Adam	Adaptive momentum
ADC	Analog-to-digital converter
AM/AM	Amplitude-to-amplitude
AM/PM	Amplitude-to-phase
ANN	Artificial neural network
API	Application programming interface
ARIMA	Auto-regressive integrated moving average
ARMA	Auto-regressive moving average
ARVTDNN	Augmented real valued time delay neural network
AWG	Arbitrary waveform generator
AWGN	Additive white Gaussian noise
BBU	Base-band unit
BER	Bit error rate
BS	Base station
C-RAN	Centralized radio access network
CAPEX	Capital expenditure
CD	Chromatic dispersion
CO	Central Office
CP	Cyclic prefix
CPRI	Common Public Radio Interface
D-RAN	Distributed radio access network
D-RoF	Digital radio over fiber
DAC	Digital-to-analog converter
DC	Direct current
DCF	Dispersion compensation fiber
DD-MZM	Dual-drive Mach Zehnder modulator
DFB	Distributed feedback

DLA	Direct learning architecture
DPD	Digital pre-distortion
DSP	Digital signal processing
DTV	Digital television
DU	Distribution unit
E/O	Electrical-to-optical
EA	Electrical amplification
eCPRI	Enhanced Common Public Radio Interface
EDFA	Erbium doped fiber amplifier
Elu	Exponential linear unit
eMBB	Enhanced mobile broadband communication
eRAC	Enhanced remote areas communications
ESA	Electrical spectrum analyzer
EVM_{RMS}	Root mean square error vector magnitude
FIR	Finite impulse response
FiWi	Fiber/wireless
flop	Float-point operation
FR1	Frequency range 1
FR2	Frequency range 2
GPON	Gigabit passive optical network
GPU	Graphics processing unit
GRU	Gated recurrent unit
IB	In-band
IBI	Inter block interference
IIR	Infinite impulse response
ILA	Indirect learning architecture
IMD	Intermodulation distortion
IMD3	Third order intermodulation distortion
IMT	International Mobile Telecommunications-2020
IoT	Internet of things
ITU-R	International Telecommunication Union Radiocommunication Sector
LASSO	Least absolute shrinkage and selection operator
LD	Laser diode
Leaky ReLU	Leak rectified linear unit
LEO	Low Earth orbit
$LiNbO_3$	Lithium Niobate
LMS	Least Mean Square
LSTM	Long short-term memory
MAC	Medium access control
MATP	Maximum transmission point
MIMO	Multiple-input multiple-output
MITP	Minimum transmission point
ML	Machine learning
MLP	Multi-layer perceptron
mMTC	Massive machine type communication
MNO	Mobile network operator

MSE	Mean-squared error
MZM	Mach-Zehnder modulator
NMSE	Normalized mean squared error
O/E	Optical-to-electrical
OB	Out-band
OBSAI	Open Base Station Architecture Initiative
OFDM	Orthogonal frequency division multiplexing
OFDMA	Orthogonal frequency division multiple access
OOBE	Out-of-band emission
OPEX	Operational expenditure
OPM	Optical power monitor
ORI	Open Radio Equipment Interface
OSFL	Orthogonal scalar feedback linearization
PA	Power amplifier
PAPR	Peak to average power ratio
PC	Polarization controller
PD	Photodetector
PHY	Physical layer
PON	Passive optical network
PSD	Power spectrum density
QAM	Quadrature amplitude modulation
QoE	Quality of experience
QP	Quadrature point
RAN	Radio access network
RAU	Remote antenna unit
ReLU	Rectified linear unit
RF	Radiofrequency
RNN	Recurrent neural network
RRH	Remote radio head
RRU	Remote radio unit
SDN	Software defined network
SDR	Software defined radio
SELU	Scaled exponential linear unit
SER	Symbol error rate
SFDR	Spurious free dynamic range
SFL	Scalar feedback linearization
SMF	Single-mode fiber
SNR	Signal-to-noise ratio
SVM	Support Vector Machine
SVR	Support-vector regressor
tanh	Hyperbolic tangent
TDL	Time delay line
TV	Television
TVWS	TV white spaces
TX	Transmitter
UHF	Ultra-high frequency

URLLC	Ultra-reliable low latency communication
VHF	Very-high frequency
VOA	Variable optical attenuator
VSA	Vector signal analyzer

List of Symbols

α	Slope coefficient of Leaky ReLU activation function
$\mathbf{b}$	Bias vector
$\boldsymbol{\beta}$	Coefficients of the polynomial-based DPD
B_{I}	In-band frequency range
$\mathcal{O}$	Big O notation for complexity analysis
B_{O}	Out-of-band frequency range
c	Speed of light
$\mathbb{C}$	Set of complex numbers
$C(\zeta_j)$	Scalar cost function
c_n	Discrete OFDM signal linearized by the post-distortion scheme
$(.)*$	Convolution operation of (.)
D	Optical fiber dispersion parameter
Δ_{min}	Minimum loss function variation
d_m	Data symbol
$(.)_\ell$	ℓth layer from the ANN
e_n	Error signal
f	Frequency
G	Frequency response of single-model fiber
g_n	Impulse response of single-mode fiber
$\mathbf{h}$	Vector of coefficients of the memoryless polynomial model
$\mathbf{H}$	Frequency response of Rayleigh channel
$\odot$	Hadamard product
$(.)^{\text{H}}$	Hermitian operator
h_j	Coefficients of the memoryless polynomial model
$\in$	Belongs to
$(.)^{-1}$	Matrix inversion operation of $(.)$
J	Nonlinearity order of the memoryless polynomial model
K	Nonlinearity order of the memory polynomial model
L	Number of hidden layers of an artificial neural network
λ	Wavelength
$Loss$	Loss function
$\lfloor . \rfloor$	Largest integer smaller than the $(.)$
Lz	Optical fiber length
M	Number of subcarriers of the OFDM signal
m	mth subcarrier of the OFDM signal
$\mathcal{L}$	MSE loss function

N	Number of samples of the OFDM signal
n	nth time index of the OFDM signal
nf	Number of features
N_{t}	Number of taps of chromatic dispersion finite impulse response
N_{TR}	Number of training instances
O_ℓ	Number of neurons from the ℓth layer
$\mathbf{P}$	Frequency domain vectroed version of p_n
$\phi(.)$	Non-linear activation function
p_n	Discrete OFDM signal at power amplifier output
$\|(.)\|_p$	p-norm operator
$\mathbf{P}_{\text{R}}$	Regression matrix for closed-form solution coefficients estimation
$\mathbf{P}_{(t)}$	Input matrix of RNN for the current time-step
$P_z(f)$	Power Spectrum Density of z_n at frequency f
Q	Memory depth
$\mathbb{R}$	Set of real numbers
s_1	Switch 1
s_2	Switch 2
T	Sample period
$(.)^{\text{T}}$	Transposition operation of (.)
Ts	Time step
$\mathbf{V}$	Regression matrix for the pre-distorted signal
$\mathbf{v}$	Vectored version of v_n
V_{BIAS}	Polarization voltage
v_n	Discrete Pre-distorted signal
V_π	Half-wave voltage of MZM
$\hat{\mathbf{V}}_{(t-1)}$	Output matrix of RNN for the previous time-step
$\mathbf{w}$	Vectored version of w_n
$\mathbf{W}$	Matrix of weights of multi-layer perceptron artificial neural network
w_n	Discrete additive white Gaussian Noise
$\mathbf{W}_p$	Matrix of weights for the recurent neural network previou time-step
$\mathbf{W}_v$	Matrix of weights for the recurent neural network input vector
$\boldsymbol{\xi}$	Matrix of coefficients of memory polynomial model
$\xi_{q,k}$	Coefficients of the memory polynomial model
x_n	Discrete OFDM signal
$\mathbf{x}_{\text{R}}$	Vector of input samples for closed-form solution coefficients estimation
y_n	Discrete signal at MZM output
$\mathbf{Z}$	Matrix of delayed samples of z_n
ζ_j	Coefficients of the conventional OSFL DPD
ζ_{R_j}	Auxiliary coefficients generated by the orthogonalization process
z_n	Discrete signal at photodetector output

Summary of Original Works

This thesis is based on the following original publications:

(1) **L. A. M. Pereira**, L. L. Mendes, C. J. A. Bastos-Filho and Arismar Cerqueira S. Jr, "Linearization Schemes for Radio Over Fiber Systems Based on Machine Learning Algorithms," *IEEE Photonics Technology Letters*, vol. 34, no. 5, pp. 279-282, 1 March, 2022, DOI: 10.1109/LPT.2022.3151616.

(2) **L. A. M. Pereira**, L. L. Mendes, C. J. A. Bastos-Filho and Arismar Cerqueira S. Jr, "Machine Learning-based Linearization Schemes for Radio over Fiber Systems," *IEEE Photonics Journal*, vol. 14, no. 6, pp. 1-10, December, 2022, DOI: 10.1109/JPHOT.2022.3210454.

(3) **L. A. M. Pereira**, E. S. Lima, L. L. Mendes and Arismar Cerqueira S. Jr, "Machine Learning-based Digital Pre-Distortion Scheme for RoF Systems and Experimental 5G mm-waves Fiber-Wireless Implementation," *Journal of Microwaves, Optoelectronics and Electromagnetic Applications*, vol. 22, no. 1, pp. 172-183, March, 2023, DOI: 10.1590/2179-10742023v22i1270779.

(4) **L. A. M. Pereira**, L. L. Mendes, C. J. A. Bastos-Filho and Arismar Cerqueira S. Jr, "Amplified Radio-over-Fiber System Linearization Using Recurrent Neural Networks," *IEEE/Optica Journal of Optical Communications and Networking*, vol. 15, no. 3, pp. 144-154, 15 February, 2023, DOI: 10.1364/JOCN.474290.

(5) **L. A. M. Pereira**, L. L. Mendes, C. J. A. Bastos-Filho and Arismar Cerqueira S. Jr, "Machine Learning Applied to 6G Radio over Fiber Systems Linearization," in *2nd International Conference on Electrical, Computer, Communications and Mechatronics Engineering (ICECCME)*, Maldives, 2022, pp. 1-6, DOI: 10.1109/ICECCME55909.2022.9988151.

(6) **L. A. M. Pereira**, L. L. Mendes, C. J. A. Bastos-Filho and Arismar Cerqueira S. Jr, "Novel Machine Learning Linearization Scheme for 6G A-RoF Systems," in *IEEE/Optica Journal of Lightwave Technology*, (accepted for publication in August 8, 2023), DOI: 10.1109/JLT.2023.3304281.

(7) **L. A. M. Pereira**, L. L. Mendes and Arismar Cerqueira S. Jr, "Proposal of a Fiber/Wireless System Assisted by Machine Learning Towards 6G Communications," in *20th SBMO/IEEE MTT-S International Microwave and Optoelectronics Conference*, (accepted for publication in July 30, 2023).

Other associated scientific reports:

(8) **L. A. M. Pereira**, P. H. F. Santos, R. M. Borges, L. L. Mendes, C. J. A. Bastos-Filho and Arismar Cerqueira S. Jr. "Sistema Rádio sobre Fibra assistido por Inteligência Artificial para aplicações 5G/6G", *Brazilian Journal of Development*, vol. 7, pp. 48948-48958, May, 2021.

(9) **L. A. M. Pereira**, C. H. S. Lopes, R. M. Borges, E. S. Lima, A. C. Ferreira, M. Abreu, L. L. Mendes and Arismar Cerqueira S. Jr., "Implementation of a Multiband 5G NR Fiber-Wireless System using Analog Radio over Fiber Technology," *Optics communications*. vol. 474, pp. 126112, May, 2020.

(10) **L. A. M. Pereira**, E. S. Lima, Arismar Cerqueira S. Jr., "A Multi-band 5G-NR Fiber-wireless System for Next-generation Networks," In *2021 SBMO/IEEE International Microwave and Optoelectronics Conference (IMOC)*, Fortaleza-CE, October, 2021.

(11) **L. A. M. Pereira**, L. L. Mendes, Arismar Cerqueira S. Jr., "Machine Learning-based Fiber-Wireless Channel Estimation," In "Frontiers in Optics Laser Science Conference and Exhibition", Washington, D.C, November, 2021.

(12) R. M. Borges, C. H. de Souza Lopes, E. S. Lima, M. A. de Oliveira, M. S. B. Cunha, L. C. Alexandre, L. G. da Silva, **L. A. M. Pereira**, D. H. Spadoti, M. A. Romero and Arismar Cerqueira S. Jr. "Integrating Optical and Wireless Techniques Towards Novel Fronthaul and Access Architectures in a 5G NR Framework," *Applied Sciences*, vol. 11, no. 11, pp. 5048, May, 2021.

(13) E. S. Lima, R. M. Borges, **L. A. M. Pereira**, H. R. D. Filgueiras, A. M. Alberti, Arismar Cerqueira S. Jr ., "Multiband and Photonically Amplified Fiber-Wireless Xhaul," *IEEE Access*. vol. 8, pp. 44381-44390, March, 2020.

(14) E. S. Lima, **L. A. M. Pereira**, R. M. Borges and Arismar Cerqueira S. Jr., "Brillouin Effect Impact in RoF Systems with Photonic-Assisted RF amplification," *Journal of Communication and Information Systems*. vol. 35, pp. 162-170, June, 2020.

(15) R. M. Borges, **L. A. M. Pereira**, A. C. Ferreira, L. L. Mendes, D.H. Spadoti, Arismar Cerqueira S. Jr., "Fifth-generation New Radio Fiber-wireless System for Long-reach and Enhanced Mobile Broadband Scenarios," *Microwave and Optical Technology Letters* , vol. 1, pp. 1-8, August, 2020.

(16) E. S. Lima, **L. A. M. Pereira**, R. M. Borges, Arismar Cerqueira S. Jr., "5G New Radio Photonically-amplified Xhaul," *Optical Fiber Technology* , vol. 60, pp. 102358, December 2020.

(17) H. R. D. Filgueiras, T. H. Brandão, **L. A. M. Pereira** and Arismar Cerqueira S. Jr. "Antenna Array Diversity Evaluation Under Multipath Environments with Digital Beamforming," *IEEE Open Journal of Antennas and Propagation*, (accepted for publication).

(18) L. F. F. De Almeida, j. R. D. Santos, **L. A. M. Pereira**, Arismar Cerqueira S. Jr., L. L. Mendes, J. J. P. C. Rodrigues, R. A. L. Rabelo, and A. M. Alberti, "Control Networks and Smart Grid Teleprotection: Key Aspects, Technologies, Protocols, and Case-Studies," *IEEE Access*, vol. 8, pp. 174 049–174 079,

September, 2020.

(19) C. H. S. Lopes, E. S. Lima, **L. A. M. Pereira**, R. M. Borges, A. C. Ferreira, M. Abreu, W. D. Dias, D. H. Spadoti, L. L. Mendes, and Arismar Cerqueira S. Jr., "Non- Standalone 5G NR Fiber-Wireless System Using FSO and Fiber-Optics Fronthauls," *Journal of Lightwave Technology*, vol. 39, no. 2, pp. 406–417, October, 2021.

(20) C. H. S. Lopes, E. S. Lima, **L. A. M. Pereira**, Arismar Cerqueira S. Jr., "Peaceful Coexistence Between 5G NR and LTE-A Over a RoF-Based Fronthaul," In *2021 SBFoton International Optics and Photonics Conference (SBFoton IOPC)*, São Carlos, May, 2021.

(21) C. H. S. Lopes, **L. A. M. Pereira**, Arismar Cerqueira S. Jr., "Coexistência entre 5G NR e LTE-A em Sistemas Fiber/Wireless,". *XXXVIII Simpósio Brasileiro de Telecomunicações e Processamento de Sinais (SBrT)*, Florianópolis-SC, September, 2020.

(22) P. H. Santos, **L. A. M. Pereira**, R. M. Borges, L. L. Mendes, C. J. A. B. Filho and Arismar Cerqueira S. Jr., "Inteligência Artificial Aplicada a Sistemas 5G com Tecnologia Rádio sobre Fibra," In *X Conferência Nacional em Comunicações, Redes e Segurança da Informação (ENCOM)*, Natal-RN, December, 2020.

(23) C. H. S. Lopes, **L. A. M. Pereira**, Arismar Cerqueira S. Jr., "Coexistência entre LTE-A e 5G NR em Fronthaul Móvel," In *19º SBMO- Simpósio Brasileiro de Micro-ondas e Optoeletrônica (MOMAG)*, Niterói- RJ, November, 2020.

(24) H. R. D. Filgueiras, E. S. Lima, M. S. B. Cunha, C. H. S. Lopes, L. C. de Souza, R. M. Borges, **L. A. M. Pereira**, T. H. Brandão, T. P. V. Andrade, L. C. Alexandre, G. Neto, A. Linhares, L. L. Mendes, M. A. Romero and Arismar Cerqueira S. Jr., "Wireless and Optical Convergent Access Technologies Toward 6G," *IEEE Access*, vol. 11, pp. 9232-9259, 2023, DOI: 10.1109/ACCESS.2023.3239807.

Resumo

O objetivo deste trabalho é propor e avaliar o desempenho de esquemas de linearização baseados em aprendizado de máquina (ML - *machine learning*), aplicados a sistemas analógicos rádio sobre fibra (A-RoF - *analog radio over fiber*) para o transporte de sinais da quinta geração de comunicações móveis (5G - *fifth generation of mobile communications*) e das futuras redes de comunicações móveis de sexta geração (6G - *sixth generation of mobile communications*). As análises de desempenho das técnicas de linearização baseiam-se na utilização de modelos polinomiais para modelar as não-linearidades do sistema A-RoF e utilizar redes neurais para realizar a pre-e/ou pós-distorção do sinal transmitido.

Considerou-se os principais componentes do sistemas A-RoF que apresentam comportamento não-linear. Inicialmente, propõe-se um esquema de linearização para o modulador eletro-óptico de Mach-Zehnder (MZM - Mach-Zehnder *modulator*). Nesta abordagem, emprega-se uma rede neural perceptron com múltiplas camadas (MLP - *multi-layer perceptron*) para realizar a pré- e/ou pós-distorção do sinal transmitido. Avalia-se também os efeitos não-lineares do amplificador de potência elétrico (PA - *power amplifier*), comumente utilizado em sistemas A-RoF para amplificar o sinal de radio-frequência (RF - *radio frequency*) antes da radiação. Neste caso, utiliza-se a rede neural recorrente (RNN - *recurrent neural network*), que é capaz de lidar com o efeito memória do amplificador. A RNN possui uma estrutura de memória interna, que pode ser devidamente dimensionada para compensar as degradações não-lineares sem memória do MZM e com memória do PA. Finalmente, a dispersão cromática da fibra óptica também foi considerada, uma vez que o enlace óptico de transporte precisa ser estendido visando fornecer cobertura em áreas remotas. Para tal, utiliza-se a rede neural de atraso de tempo real aumentada (ARVTDNN - *augmented real-valued time delay neural network*), pois esta arquitetura permite compensar os efeitos acima mencionados. Todos os resultados destas análises foram obtidos usando simulações em Python.

Este trabalho também apresenta a aplicação da técnica ARVTDNN em um sistema fibra/rádio (FiWi - *fiber/wireless*). Em linhas gerais, os resultados obtidos nessa tese demonstram que o uso de esquemas de linearização baseados em ML são potenciais para maximizar o desempenho de sistemas A-RoF em redes de transporte 5G e 6G.

***Palavras-Chave*:** 5G, 6G, aprendizado de máquina, pós-distorção, pré-distorção, redes neurais artificiais e rádio sobre fibra analógico.

Abstract

The thesis main goals are proposing and evaluating machine learning (ML)-based linearization schemes for analog radio over fiber (A-RoF) systems from the fifth and sixth generations of mobile communications (5G and 6G). The performance analyses of the linearization techniques were based on the use of polynomial models to represent the non-linearities of the A-RoF system and artificial neural networks (ANNs) to perform pre-and/or post-distortion of the transmitted signal.

The main A-RoF system non-linear components were taken into account. First, a linearization scheme was developed for the Mach-Zehnder modulator (MZM). It employs a multi-layer perceptron (MLP) ANN to perform the pre-and/or post-distortion of the transmitted signal. The electrical power amplifier (PA) non-linear effects were also evaluated. PA is commonly used in A-RoF systems to amplify the radio frequency (RF) signal before being radiated. In this case, it is required a recurrent neural network (RNN), which is able to deal with the power amplifier memory effect. RNN has an internal memory structure that can be properly designed to compensate for the non-linear degradation, considering the memoryless non-linear distortions introduced by the MZM and the memory non-linear distortion introduced by the PA. Finally, the chromatic dispersion (CD) introduced by the optical fiber was also taken into account, since the transport optical link needs to be extended to provide coverage in remote areas. The augmented real-valued time delay neural network (ARVTDNN) was used, since it allows simultaneously compensating all the aforementioned effects. All results were obtained by using Python simulations.

This work also presents the application of ARVTDNN linearization scheme into a fiber/wireless (FiWi) system. Basically, the obtained results from this thesis demonstrate that ML-based linearization schemes represent potential solutions to maximize the performance of A-RoF systems from the 5G and 6G transport networks.

***Keywords*:** 5G, 6G, analog radio over fiber, ANN, machine learning, post-distortion and pre-distortion.

Chapter 1

Introduction

DURING the concept and standardization of the fifth generation of mobile communication (5G), which has led to the 5G New Radio (5G NR) definition, new audacious and futuristic use case scenarios were defined for encompassing a plurality of new applications [1]. The 5G NR is a standardized technology for 5G communications. It encompasses a set of specifications and recommendations defined by the 3rd Generation Partnership Project (3GPP) [2]. The 5G NR aims to provide enhanced capabilities, including higher data rates, lower latency, improved energy efficiency, and increased scalability compared to previous generations of mobile networks. The standardization process of 5G NR started in 2017, at the end of Release 14 [3]. This marked the initial phase of defining the specifications and requirements for 5G NR. One of the main concerns of 5G NR standardization was to ensure compatibility and coexistence with the legacy technologies while enabling seamless integration with future advancements.

The International Telecommunication Union Radiocommunication Sector (ITU-R) has highlighted the following three main 5G scenarios accordingly with the International Mobile Telecommunications-2020 (IMT) vision [4]: The enhanced mobile broadband communication (eMBB) scenario, focuses on significantly increasing data rates for end users, supporting peak data rates of up to 20 Gbit/s and 100 Mbit/s in a high mobility condition [5]; massive machine type communication (mMTC) scenario, in which is expected a high density of connections from power-limited devices, with estimates reaching up to 1 million connections per square kilometer [6]; ultra-reliable low latency communication (URLLC), aiming to reduce the network time response to values below 1ms with reliability of 99.9999% [7]. Figure 1.1 demonstrates the mains use cases of 5G networks. The foreseen 5G applications impose strict, contrasting and very challenging requirements on the physical layer (PHY), which must be flexible for

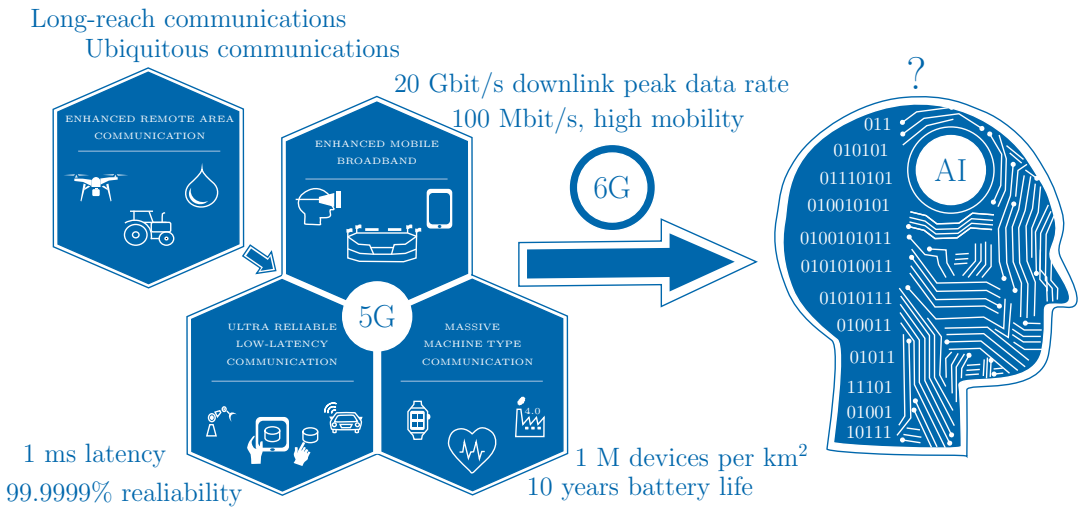

Figure 1.1: *Use Cases for 5G Networks and the Intriguing Prospect of AI Integration.*

covering the three defined use case scenarios [8].

The 5G ecosystem encompasses a broad range of new applications, which are related to the most diverse sectors of the economy and market verticals [9]. Such verticals are composed of many applications and services, such as collaborative robots, remote surgeries, autonomous vehicles, real-time immersive games, augmented reality and tactile Internet [10]. Many enabling technologies are used to support the services and applications expected in each scenario, including the integration of optical and wireless techniques in the fronthaul architecture [11]. Most of the applied technologies are prone to reduce cell coverage. Moreover, coverage is also limited in the URLLC and the mMTC scenarios since the power limitation in the device and restriction on the symbol duration will limit the link budget and robustness against long channel delay profile, respectively [12, 13]. Although 5G networks are currently being globally deployed, academia, operators and industry are already defining the sixth generation of mobile communication (6G) networks. One of the main 6G visions is to overcome the already known limitations of the 5G NR and also to introduce new services and use cases based on the integration of new features besides communication, such as localization, positioning, imaging, mapping and sensing [1, 14, 15].

Although the three main 5G scenarios were already defined by 3GPP, one important use case scenario is not being properly addressed. The enhanced remote areas communications (eRAC) scenario focus on providing broadband communications in remote and rural areas [16]. Continental-sized countries are likely to be the main beneficiaries of this scenario since large territorial extensions are prone to have many remote inhabited areas. As a consequence, the low population density, infrastructure scarcity and high deployment and maintenance costs are the main challenges for mo-

bile network operators (MNOs) to provide digital services in these areas. This means that the network operating model is usually economically unattractive in these locations. Therefore, cost-effective solutions and new business models are crucial for reducing the capital expenditure (CAPEX) and operational expenditure (OPEX) for the MNOs [17]. Moreover, frequency licenses have also hindered the remote area network deployment [16]. These restrictions must be overcome to finally offer connectivity to a large parcel of the unconnected population in remote areas. Some initiatives have been proposed to address this problem. The Remote Area Access Network for the 5th Generation (5G-RANGE) project aimed for exploiting television (TV) white spaces (TVWS) for 5G communications in remote areas [18], as demonstrated in Figure 1.2. The TVWS PHY must have low out-of-band emission (OOBE) waveform, which means the adjacent channel leakage ratio (ACLR) must be kept as low as possible for avoiding interference in the adjacent digital television (DTV) channels. Since spectral mobility is essential for TVWS exploitation, the low OOBE must be achieved without the use of radiofrequency (RF) filters. Another example is the One5G project [19], which proposed a flexible architecture to provide Internet of things (IoT) and Big Data in underserved areas. In parallel, the 5G rural first project aims to allow local communities to exploit idle 3GPP bands in remote areas [20].

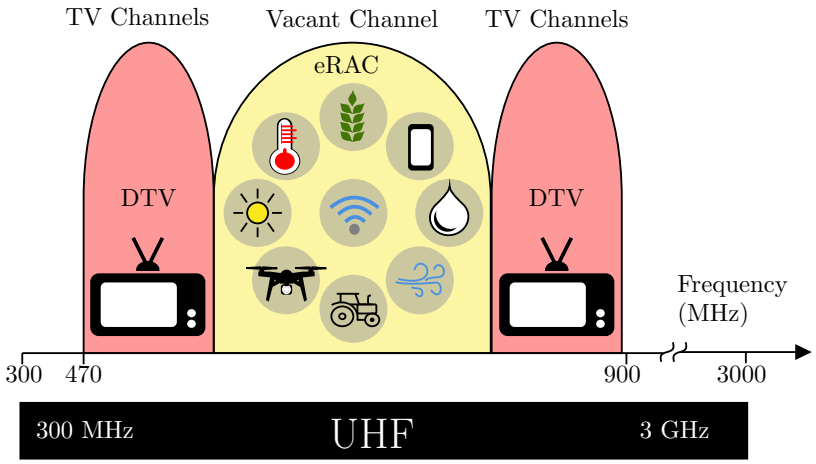

Figure 1.2: *TV white spaces for mobile communications that allow the exploitation of unused spectrum to improve connectivity in remote areas.*

Considering the aforementioned limitations for providing connectivity in remote areas, it becomes clear that future mobile networks must benefit from solutions that offer cost advantages, where centralized radio access network (C-RAN), multiple-input multiple-output (MIMO), satellites network, TVWS and analog radio over fiber (A-RoF) deserve special attention [17]. The C-RAN architecture simplifies the network maintenance by sharing processing resources among distinct services, which

enables for reducing the radio access network (RAN) implementation and operation costs [21, 22]. On the other hand, MIMO systems increase communication robustness by exploiting diversity. The stand-alone satellite networks aim to provide ubiquitous connectivity by using air/spaceborne platforms, such as low Earth orbit (LEO), and can also be jointly used with terrestrial networks to complement coverage. TVWS can also be employed to reduce OPEX, since no license is required to exploit ultra-high frequency (UHF) DTV vacant channels to provide connectivity services.

In particular, A-RoF offers an interesting solution to transport and distribute analog RF signals to a simplified remote radio head (RRH), which can be tens of kilometers distant from central office (CO). In this case, the fronthaul link needs to be extended, which endorses the use of microwave and optical technologies [23]. However, A-RoF systems present non-linear distortions as RF and optical power increases. The A-RoF system non-linear distortion can be neglected if the entire signal excursion is restricted to the A-RoF linear region. For instance, authors have shown that an A-RoF system can be used to provide multiple services to a simple RRH without introducing performance loss among these services since a controlled low RF power was employed [24]. However, a dynamic RF power allocation is required to simultaneously take advantage of TVWS, C-RAN and A-RoF in remote areas without producing prohibitive adjacent channel interference. Therefore, a linearization technique can be applied to reduce the non-linear distortions of the signal, which enables operating with high-power RF signals to cover distinct remote regions.

The Mach-Zehnder modulator (MZM) is typically employed in A-RoF systems to modulate the optical carrier with the RF signal. One challenge in this approach is to deal with the non-linearities introduced by the MZM as the input level of the RF signal increases. The MZM non-linear response leads to a spectral regrowth, which is produced by the intermodulation products of the RF signal and it is of major concern in TVWS application. Once the dynamic allocation of RF power is desirable in eRAC applications for serving different regions, a linearization technique must be employed to minimize the signal distortion [25]. The specialized literature presents many solutions for the linearization of A-RoF systems, which might be applied either in the optical or electrical domains [26, 27]. Moreover, recent advances in computational capacity and the increase in the available data sets have enabled new machine learning (ML) approaches, which might be applied in distinct network layers, aiming to deal with the unprecedented growth in the complexity of the communication systems [28, 29].

ML-based solutions can be considered a powerful tool for linearizing complex systems. This methodology enables precise modeling of complex systems and potentially provides multiple benefits when compared to conventional polynomial models, which

frequently rely on simplified approximations of real-world systems. This means that ML-based solutions can capture the non-linear dynamics and complex relations between variables that are often neglected in conventional models. Moreover, the ML-based linearization schemes are more flexible, since they can be adapted for distinct operating scenarios and conditions. Despite its manifold advantages, ML-based solutions also exhibit several limitations and challenges, including the requirement for large amounts of training data, the inherent difficulty in interpreting the models generated by ML algorithms, the definition of the hyperparameters and the performance estimation.

1.1 Aim of the Research

Figure 1.3 depicts the centralized radio access network architecture, assisted by analog radio-over-fiber transport network aiming to cover eRAC applications. The approach used in this thesis relies on integrating the machine learning-based linearization schemes in a conventional analog radio-over-fiber system, illustrated in Figure 1.3 (a). In a C-RAN architecture, the base-band unit (BBU) plays an important role in handling digital signal processing and base-band functions for multiple RRHs, optimizing resource allocation and network performance. The A-RoF link connects the BBU to

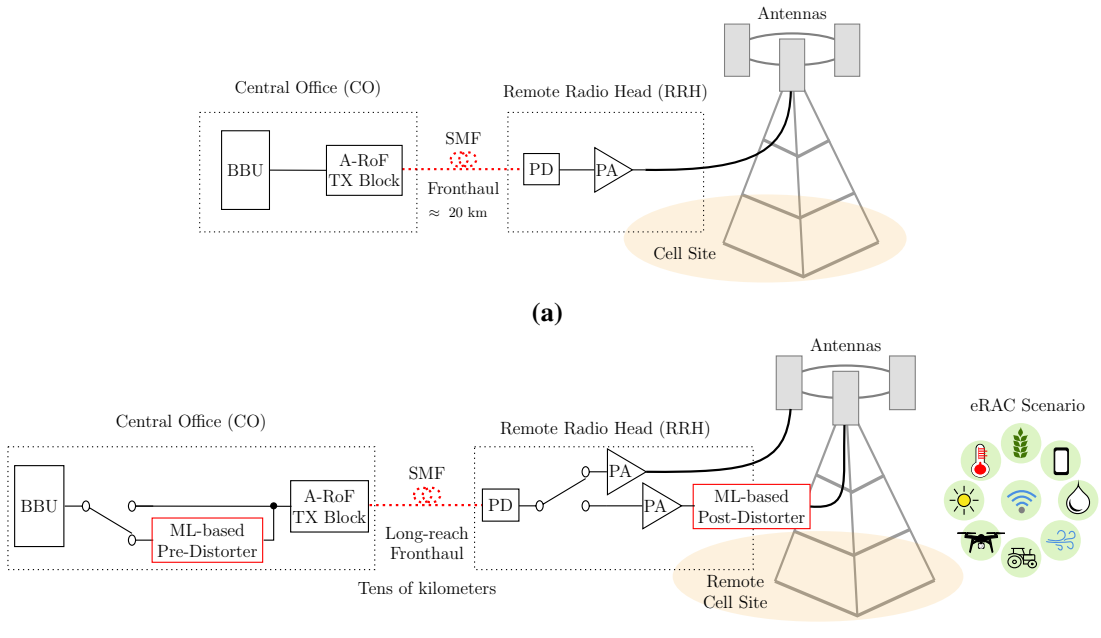

Figure 1.3: *C-RAN architecture using A-RoF system in the transport network (a) Conventional A-RoF system (b) A-RoF system assisted by machine learning for supporting eRAC applications.*

RRHs via optical fiber, enabling the transmission of analog radio signals. At the remote cell site side, the photodetector (PD) converts optical signals back into electrical signals at the RRHs. The power amplifier (PA) amplifies the radio signals for transmission to user devices. By centralizing base-band processing and using optical fiber links, C-RAN enhances connectivity in remote areas while providing more efficient resource management. In Figure 1.3 (b), one can see the integration of ML-based pre- and post-distorter blocks, which enable extending the fronthaul link to support eRAC applications. We have considered that the core network is connected to the CO using an optical-fiber backhaul link. The PHY and medium access control (MAC) functions of the base station (BS) are performed at CO, by taking advantage of software defined radio (SDR) implementation. It was assumed that TVWS was employed to provide eRAC services [16]. We have also assumed that the RRH will be located in the region where the services will be provided and the optical link can be several miles long. The base-band signal generated by the SDR is upconverted to a RF channel, which modulates an optical carrier using an MZM, resulting in an A-RoF system. The RF signal is linearized by a linearization scheme, aiming to reduce the non-linear distortions caused either by the MZM and/or PA components [30]. At the RRH, the signals are converted to the electrical domain, amplified and radiated by the remote antenna unit (RAU) to cover remote areas. In the uplink transmission, the RAU is also responsible for receiving the signals from the users, which will be converted to the optical domain to be transmitted to the BS.

The aim of this research is to conceive, design, implement and evaluate ML-based linearization schemes for amplified-A-RoF systems. All the linearization algorithms developed in this thesis were designed upon the application programming interface (API) Keras from Tensorflow. Equivalent base-band models for A-RoF were employed, which enables modeling the distortions introduced by the system. The linearization schemes are based on pre- and post-distortion concepts. The pre-distortion applies an intentional distortion to the input signal. On the other hand, the post-distortion scheme act as an equalizer at the RRH. We have assumed that the non-linear response of the system comes only from the MZM and PA components. The PD might also introduce non-linear distortions. However, for the investigated scenario, the PD will be located at several miles from CO, in the RRH. In this case, the non-linear distortions of the PD might be neglected due to the low optical power of the incident signal [31]. The PA presents memory effect, which means that its output at a specific time instant depends not only on the current input but also on previous inputs [32]. The memory polynomial model has been widely used for modeling devices with memory effects, which is the case of PA [33]. Many approaches based on computational in-

telligence are commonly employed to deal with memory-temporal signals, including recurrent neural networks (RNNs) and augmented real valued time delay neural networks (ARVTDNNs), which are capable of compensating memory non-linear distortions [34–36].

One of the main goals of this thesis is to propose ML-based linearization techniques for A-RoF with lower complexity, yet more robust and adaptable solution than those found in existing specialized literature. Although, when considering an optimal scenario where traditional models accurately describe the non-linear system response, ML algorithms does not outperform conventional linearization schemes, they achieve similar linearization performance with much lower complexity. When there is a mismatch between the real system response and the mathematical model, ML-based solutions become even more appealing. In such cases, ML-based solutions can outperform classic models, since it presents a remarkable non-linear representation and generalization capacity. Furthermore, when there is a variation in the non-linear system response, classic models require an expensive re-calibration process to estimate a new set of coefficients. In contrast, ML-based solutions can be designed to generalize possible variations in the non-linear system response, which means that ML-based linearization systems does not require re-calibrations.

1.2 Literature Review

Linearization techniques for A-RoF systems have been discussed since the late of the 20th century. Many approaches were studied and demonstrated, including dual parallel linearization, optical feedforward, analog pre-distortion and digital pre-distortion (DPD) [26, 37–40]. Many optical linearization techniques have been presented [26, 41–43].

An optical feed-forward linearization scheme was presented in [26]. Authors aim for linearizing the laser diode (LD) non-linear response, which produces intermodulation distortion (IMD) products. The concept of this linearization scheme is based on creating a counter-phase version of the IMD products at the LD output to be combined with the original distorted signal, resulting in the desired linearization [26]. Figure 1.4 presents the block diagram of the feed-forward linearization scheme. The input RF signal is split by the splitter, with upper path modulating the LD_1, and the other serving as an error-free reference. Nevertheless, the inherent nonlinearity of LD_1 from the upper path leads to the presence of IMD products in the modulated optical output. Subsequently, the split output traverses through a 50:50 optical coupler, is detected by PD_1 and enters a variable gain amplifier. The variable amplifier generates a com-

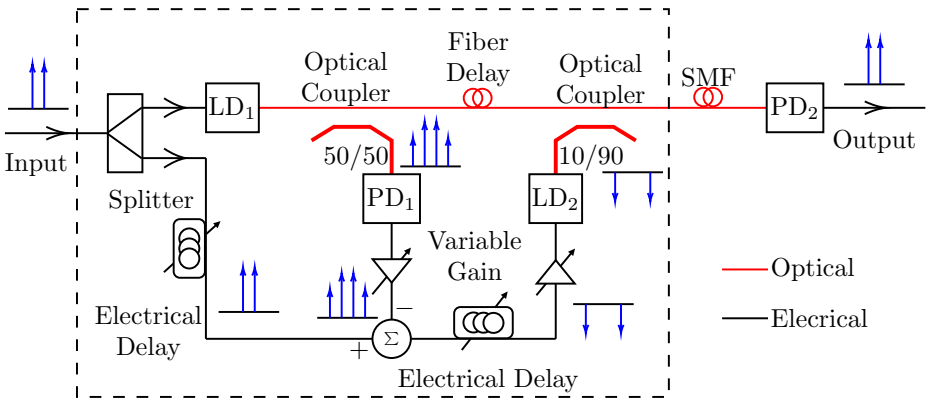

Figure 1.4: *Diagram of the optical feed-forward linearization scheme: LD- laser diode; PD-photodetector [adapted from [26]].*

posite signal, encompassing distortion products and intensity noise originating from laser LD_1. These composite components are then combined with the electrical reference signal phase-shifted by 180° through an electrical delay. In an ideal scenario, the resulting output should solely comprise the error signal, encompassing non-linear distortion products and detected noise from LD_1. The error signal undergoes a 180° phase shift through an electrical delay, gets amplified, and then modulates the LD_2. The modulated optical output signal from laser LD_2 represents distortion products from LD_1. Since laser LD_2 is directly modulated with low-level distortion products, it operates linearly without significant distortion generation. By combining the output of laser LD_2 with the optical signal from laser LD_1 in the 90:10 optical coupler, an efficient transportation over fiber is achieved, which facilitate the mitigation of distortion and laser intensity noise at the receiver. Finally, PD_2 coherently adds the detected RF signals, resulting in the suppression of unwanted distortion products through counter-phase addition. In summary, several additional components are employed in this scheme when compared with conventional A-RoF systems, including an electrical splitter, LD, PD, two variable electrical amplifiers, two electrical delays, two optical couplers and a hybrid electrical coupler. The main drawback of this scheme is the high complexity, cost and the need for precise adjustments to properly reduce the IMD products at the system output.

In [43], authors presented the dual-parallel linearization technique, in which the polarization voltage of the MZMs are independently controlled to mitigate the IMD products. This scheme is illustrated by Figure 1.5. The linearization is achieved by using the distortions produced by the MZM_1 to interact with the distortions from MZM_2 [43]. In this diagram, MZM_1 is biased at V_π with a π phase difference between the electrical signals modulated on its electrodes, while MZM_2 is biased at $V_{\pi/2}$, assuming equal half-wave voltages ($V_{\pi/2}$) for both MZMs. This configuration results in carrier suppres-

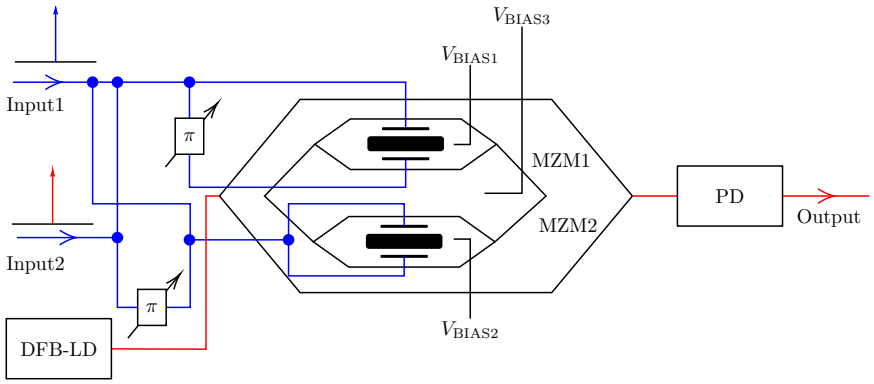

Figure 1.5: *Diagram of the dual-parallel linearization scheme: [adapted from [41]].*

sion in MZM_1, ensuring efficient information transmission, while MZM_2 operates at quadrature point. This innovative scheme holds promise for improving high-linearity performance in optical communication systems. Recent studies have demonstrated that this technique can effectively mitigate non-linear distortions [41, 44, 45]. However, its implementation can be very challenging. Factors such as cost, complexity of the required components and the need for accurate adjustments for properly compensating the distortions should be taken into consideration.

In summary, a large portion of optical-domain linearization approaches requires additional components, precise, adaptive, and fast response control at different operating points. In parallel, electrical-domain linearization techniques have been proposed for simplifying the linearization process [27, 46–50].

The analog pre-distortion technique is one approach for linearizing A-RoF systems [38, 51, 52]. Figure 1.6 depicts the simplified block diagram of the analog-predistortion, which splits the RF signal into two branches. One parcel of the RF signal is applied to an electrical delay, whereas the second part is applied to a non-linear path. The non-linear device component is designed to create IMD products, which have its magnitude and phase controlled by an amplifier and phase shifter, respectively. To

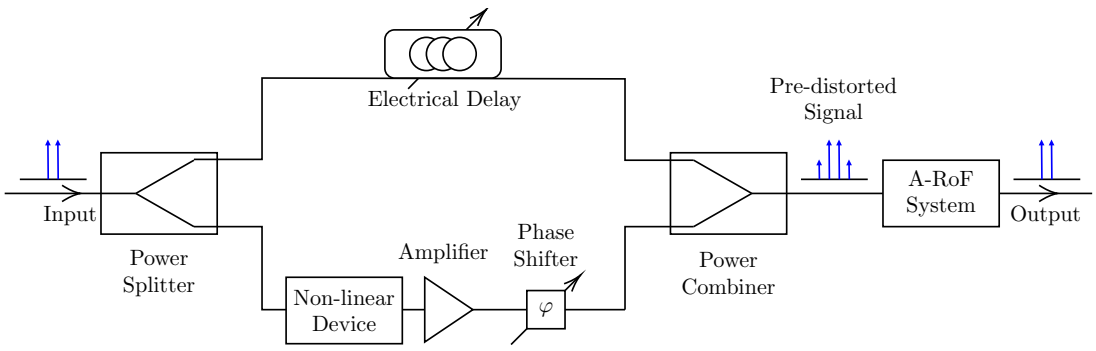

Figure 1.6: *Diagram of the analog pre-distortion [adapted from [38]].*

linearize the A-RoF system, the generated IMD produced by the analog pre-distortion circuit must be precisely adjusted to cancel with the IMD generated by the A-RoF system. The major analog pre-distortion drawback is related to limitations on linearization bandwidth. Additionally, the linearization performance also can be affected by the non-linearities produced by the amplifier and phase shifter. Besides the electrical delay, the phase shifter and amplifier must be precisely controlled, increasing the operation complexity.

The DPD has been considered the most prominent solution for linearization in the electrical domain [27,53–55]. The DPD concept lies in compensating for nonlinearities within systems through pre-distorting the input signal, leading to a notable enhancement in the output signal, increasing the overall signal quality. Moreover, DPD plays a important role in optimizing efficiency by mitigating power losses arising from unwanted harmonics and intermodulation products. The cost-effectiveness and standardized nature of DPD have significantly contributed to its widespread adoption across various applications. Nevertheless, to keep pace with the dynamic technological landscape, continuous monitoring of the latest advancements in distortion reduction techniques remains essential. In the context of A-RoF systems, the DPD operating principle consists of pre-distorting the input signal by a function that is complementary to the non-linear A-RoF system. Therefore, the distortions introduced by A-RoF system will reduce the distortions introduced by the DPD, linearizing the system response. The DPD distortions are ruled by a set of coefficients calculated according to a linearization algorithm. One of the most popular approaches to extract the DPD coefficients is the Least Mean Square (LMS) algorithm. Figure 1.7 illustrates the block diagram of a conventional DPD system, in which G is the linear gain of the system. To control the power input into the acquisition unit, it is customary to employ an attenuator within the feedback loop. During the training, the input and output signals fed the linearization algorithm, which calculates the coefficients that produce an output signal as similar as possible to the input signal by reducing a cost function training error.

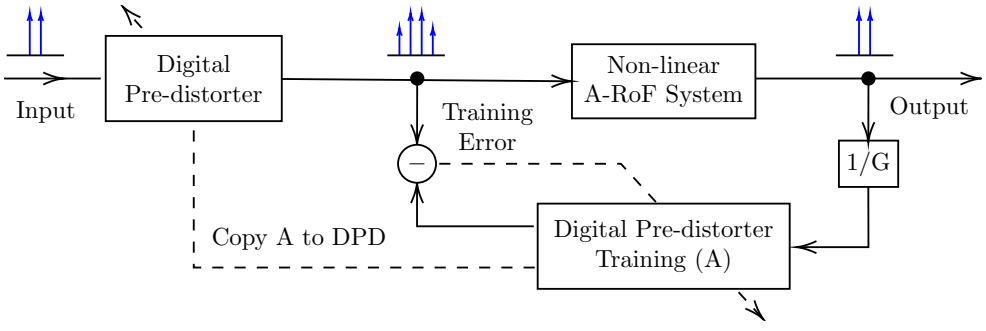

Figure 1.7: *Diagram of the digital pre-distortion scheme [adapted from [27]].*

Table 1.1 summarizes the main optical and electrical linearization techniques applied to A-RoF systems. Distinct performance metrics are usually evaluated when analyzing linearization schemes, including: spurious free dynamic range (SFDR), which measures the range between the maximum desired signal level and the highest unwanted spurious signals in the system output, this means that a higher SFDR value indicates better performance with less unwanted interference and improved signal accuracy; third order intermodulation distortion (IMD3), which stands for unwanted frequencies at the third harmonic or third-order intermodulation product of the original input signals; ACLR, which is a metric used to measure the interference caused by a transmitted signal in adjacent channels in communication systems, such as wireless transmission in mobile networks and radio communications; root mean square error vector magnitude (EVM_{RMS}), which quantifies the difference between the actual received signal and the ideal signal and is often used to assess the performance of communication systems; normalized mean square error (NMSE), which is a metric used to evaluate the accuracy of an estimation or prediction model by measuring the average squared difference between the predicted values and the true values normalized by the variance of the true values.

Table 1.1: *Comparison of A-RoF linearization techniques.*

Reference-Year	Authors	Linearization Type	Evaluated Metrics	Memory Effect	Modulation Method
[26]-(2007)	T. Ismail *et al.*	Optical Feed-forward	SFDR and IMD3 Suppression	No	Direct
[27]-(2018)	M. Noweir *et al.*	DPD	EVM and NMSE	Yes	External
[38]-(2010)	Y. Shen *et al.*	analog pre-distortion	SFDR and IMD3 Suppression	No	External
[41]-(2015)	W. Jiang *et al.*	Dual-Parallel	SFDR and IMD3 Suppression	No	External
[51]-(2016)	R. Zhu *et al.*	analog pre-distortion	SFDR, EVM and IMD3 Suppression	No	External
[54]-(2018)	X. Xie *et al.*	Hybrid analog pre-distortion and DPD	EVM and ACLR	Yes	Direct
[56]-(2006)	S-H. Lee *et al.*	Cross-gain Modulation	SFDR and IMD3 Suppression	No	Direct
[57]-(2021)	M. Noweir *et al.*	DPD	EVM, ACLR and NMSE	Yes	External
[58]-(2010)	B. Hraimel *et al.*	Mixed-Polarization	SFDR and IMD3 Suppression	No	External
[59]-(2014)	Y. Cui *et al.*	Digital Post-processing	IMD3 Suppression	No	External

These metrics enable to evaluate the RF signal in-band (IB) and out-band (OB) distortions. The linearization techniques were applied in directly and externally modulated A-RoF systems, since both schemes present non-linear behavior. In directly modulated systems, non-linearities are specially produced by the LD. On the other hand, in

externally modulated systems, non-linearities come specially from the MZM. In summary, A-RoF linearization techniques improves the performance of MZM in optical communication systems. Nonetheless, all techniques have limitations and trade-offs, and the most suitable approach will depend on the specific requirements of the system. Further researches regarding ML-based approaches have been conducted aiming developing more robust and efficient methods for linearizing A-RoF systems.

Recent advances in computational capacity and the increase in the available data sets have enabled new ML approaches, which might be applied in distinct network layers, aiming to deal with the unprecedented growth in the complexity of the communication systems [28, 29]. For instance, in the 6G conception, ML-based solutions are considered an enabling technology for increasing the efficiency of distinct levels of the mobile networks [60].

In this context, Najarro *et al.* have described a model based on an artificial neural network (ANN) for distortion compensation by estimating the inverse response of a A-RoF system [61]. The received EVM_{RMS} was the metric evaluated. They have varied the number of hidden layers and neurons per hidden layer to properly estimate the A-RoF system inverse response. The estimate inverse response was used for compensating the non-linear distortions at the A-RoF output. In other words, they have proposed an ANN equalizer for A-RoF system, which has improved the received EVM_{RMS} from 4.027% to 2.605%.

A DPD approach based on ANNs was investigated by Hadi *et al.* to overcome the A-RoF system impairments caused by non-linearities [62]. They have compared the ANN-based DPD solution with the conventional Volterra-based DPD scheme, which is commonly implemented using indirect learning architecture (ILA) or direct learning architecture (DLA). Authors showed a reduction in EVM_{RMS} and ACLR, when compared to the Volterra approach. Moreover, they demonstrated that the ANN DPD solution enhances the trade-off between linearization performance and complexity.

A deep ANN for decoding RF signals was reported in [63]. Their goal was to provide a low-cost decoder and equalizer for mobile fronthaul links. Authors have taken advantage of the powerful fitting capability of ANN to decode the received signals and simultaneously mitigate the signal impairments due to the A-RoF system non-linearities. Their ANN solution has outperformed the conventional Volterra equalization followed by a hard decision detection.

In [30], authors have demonstrated an A-RoF system equalization using an ANN equalizer for compensating the non-linear signal compression due to the in-band distortions. They have introduced the concept of multi-level activation function, which

enhances the ANN non-linearity representation capability for properly compensating the A-RoF non-linear response. The goal was to mitigate the cross-modulation effect, which is the non-linear interaction between the signal in-phase and quadrature components, caused by in-band distortions. This effect results in compression in the signal and it is more severe when high-peak to average power ratio (PAPR) waveforms are employed. Authors have investigated signal compression by analyzing the constellation of the received signal. Later, authors also proposed an ANN equalizer to mitigate the interference between multiple users in uplink transmissions [64].

In summary, ANNs have been applied to A-RoF system for overcoming the non-linear degradation that reduces the overall performance of the system. It has been demonstrated that ANN solutions are a powerful tool to learn complex behavior, which is the case of the non-linear effects of the A-RoF systems. Additionally, the ANN solutions simplify or even outperform the conventional linearization solutions.

1.3 Research Contribution

The main contribution of this thesis is the proposal and implementation of novel ML-based schemes for linearizing A-RoF systems. Firstly a ML-based linearization was designed for compensating memoryless non-linear distortions introduced by the MZM. The ML-based linearization can be used as a pre- or post- distortion scheme, with similar linearization performance. The pre-distortion scheme compensates the MZM non-linearities before the signal transmission, avoiding the spectrum regrowth that could add interference to the adjacent channels. Moreover, the effect of the non-linearities on the noise is also significant. While the pre-distortion schemes operate at high signal-to-noise ratio (SNR), the post-distortion scheme operates on the received signal, in which the noise is more prominent, degrading the SNR. The post-distortion operation affects the noise statistics, meaning that the detector designed to deal with additive white Gaussian noise (AWGN) can underperform under this situation. A study regarding the generalization capabilities of these approaches was also performed. The goal was to propose a robust linearization scheme against time-variations of the MZM behavior, such occurrences may arise due to aging or variations in the MZM feed structure, for example. The linearization schemes proposed in this thesis does not require complex and laborious re-calibration procedures over time. Typically, the variation due to the component aging and/or fluctuations in the MZM polarization voltage is expected to fall within a range of 10% over a period of five years. The novel linearization approach does not require new training campaigns when the MZM parameters change over time promoting robustness against time variations in the non-linear A-RoF system

response. Hence, this approach reduces the network CAPEX and OPEX

In A-RoF systems, a PA is employed for amplifying the RF signal before radiation over the covered area. It is well known that PA introduces memory non-linear distortions to the signal, which also must be take in consideration during the design of the linearization algorithm. Therefore, a second ML-based linearization scheme was proposed for linearizing an amplified-A-RoF system. This approach is based on RNN since this ANN has an internal memory structure that can be used for compensating the memory effect. In this case, the goal was to reduce the CAPEX of the mobile network infrastructure and to increase the flexibility of the mobile network operators for allocating RF power to serve different remote regions.

The proposed ML-based linearization schemes were envisioned for eRAC applications. In this scenario, it is interesting to extend the optical fronthaul link aiming to cover remote regions. When the optical fronthaul link is extended, linear distortion may arise due to especially chromatic dispersion (CD). In addition to mitigating memoryless and memory non-linear distortions, the linearization algorithm must address CD linear distortion as well. Hence, a yet another scheme was proposed to compensate the aforementioned distortions. Finally, Table 1.2 summarizes the main contributions and aspects of the ML-based linearization schemes proposed and evaluated in this thesis.

Table 1.2: *Summary of the proposed ML-based linearization schemes.*

Paper Number	Journal or Conference	Linearization Technique	Linearization Scheme	Non-linear Distortion Type	Non-Linear Device	Main Contribution
PAPER 1	IEEE PTL	Pre- and Post Distortion	MLP	Memoryless	MZM	Proposal of MLP-based linearization schemes
PAPER 2	IEEE Phot. Journal	Pre-Distortion	MLP OSFL	Memoryless	MZM	Proposal of a MLP-based linearization scheme for time-varying A-RoF systems
PAPER 3	JMOe	Pre-Distortion	MLP	Memoryles	MZM	Further discussion on the proposed MLP-based linearization schemes
PAPER 4	IEEE/Optica JOCN	Pre- and Post Distortion	RNN MLP	Memoryles and Memory	MZM + PA	Proposal of RNN-based schemes for amplified A-RoF systems
PAPER 5	IEEE ICECCME	Pre-Distortion	RNN	Memoryless and Memory	MZM + PA	Evaluation of activation functions of RNN for amplified A-RoF systems
PAPER 6	IEEE/Optica JLT	Pre-Distortion	ARVTDNN	Memoryless, Memory and linear CD	MZM + PA	Proposal of an ARVTDNN-based scheme for linearizing amplified A-RoF systems considering chromatic dispersion
PAPER 7	IEEE IMOC	Pre-Distortion	ARVTDNN Polynomial Regression	Memoryless and Memory	MZM + PA	Integration of the ARVTDNN-based linearization scheme in a FiWi system

1.4 Thesis Outline

This thesis is structured in four chapters. Chapter 2 presents the technical background of C-RAN, A-RoF systems, non-linear devices, ANNs and linearization schemes for A-RoF systems, which are the main technologies and techniques studied in this thesis. Chapter 3 brings the main results obtained during this work, which are presented in form of original scientific papers. It is important to mentioned that the version of the papers included in this thesis underwent modifications in comparison to the original published papers. The intent behind these modifications was to achieve uniformity in variables across the text while also integrating supplementary results. Finally, the conclusions and future works are drawn in Chapter 4.

Chapter 2

Technical Background

THIS chapter describes the main techniques, technologies, components, architectures and theoretical foundations encompassing C-RAN, A-RoF, non-linear devices, ANNs and linearization schemes for A-RoF systems.

2.1 Centralized Radio Access Network (C-RAN)

The demands of 5G necessitate a scalable and efficient RAN solution. In distributed radio access network (D-RAN) architectures, the BBU and RRH are located at the cell sites of mobile networks. Typically, the base-band processing functions are integrated within the BS, with the RRH placed close to the antennas and connected with BBU. Although is widely employed, D-RAN suffers from scalability issues and efficiency, which might hinder its use for attaining the high bandwidth and low latency demanded for 5G. Moreover, the OPEX and CAPEX of D-RAN significantly increases as the number of BS is expanded, since each new site will require a complete energy and cooling infrastructure, along with a considerable physical area. The CAPEX encompasses the costs associated with network construction, including site acquisition, RF and base-band hardware, software licenses, and installation. On the other hand, OPEX refers to the costs incurred for network operation, such as electricity, site rental, maintenance, and upgrades. These expenditures pose a significant challenge for future wireless generations due to the anticipated increase in the number of cell sites. Consequently, D-RAN is not considered a competitive RAN solution for 5G and beyond [21, 65, 66]. As a result, the industry has shifted towards newer architectural approaches like C-RAN, which offers enhanced flexibility and centralized base-band processing, making it better suited to meet the requirements of 5G and future networks.

Figure 2.1 shows the C-RAN architecture, which has been considered the most

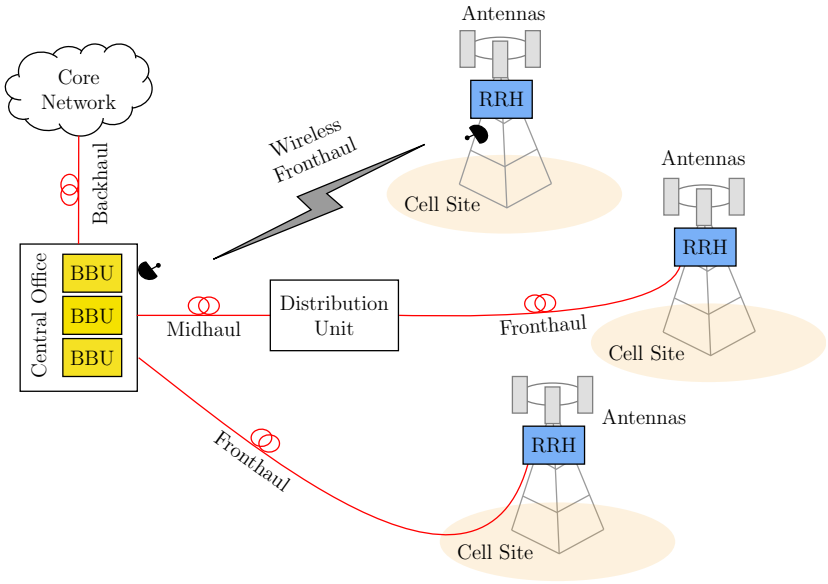

Figure 2.1: *Centralized radio access network: BBU- baseband unit; RRH- remote radio head.*

prominent RAN architecture for 5G networks. This fact can be attributed to its centralized base-band processing, scalability, cost efficiency, and dynamic resource allocation capabilities. Through centralization, C-RAN efficiently manages network resources, reducing redundancy and operational expenses for operators. Its scalability facilitates seamless expansion to address the increased capacity demands of 5G, with easy integration of RRHs into the centralized BBU pool. The low latency and high capacity of C-RAN are pivotal for real-time applications and MIMO technology. Furthermore, virtualization fosters energy efficiency, streamlined software upgrades, and simplified maintenance procedures, making it a promising solution to cater to the diverse requirements of 5G networks. While C-RAN stands out, selecting the optimal architecture hinges on deployment scenarios and specific use cases, with alternatives like D-RAN or hybrid approaches [21]. In C-RAN architectures, the core network is connected to the CO using a backhaul link. A functional split can be applied by placing a distribution unit (DU) between the CO and RRH. This approach enables for minimizing latency and increasing the system flexibility. In this case, an optical midhaul link is employed to connect the CO and DU. Otherwise, the remote radio unit (RRU) is directly connected to the CO by a fronthaul link. Microwave and optical technologies might be applied in these links.

In recent years, the use of digital radio over fiber (D-RoF) techniques for data transmission over fronthaul links has intensified. Commonly used digital transmission standards are: Common Public Radio Interface (CPRI); enhanced Common Public Radio Interface (eCPRI); Open Base Station Architecture Initiative (OBSAI); Open Radio Equipment Interface (ORI). Although D-RoF is widely employed, increas-

ing data throughput and implementing MIMO transmissions in 5G networks require extremely high transmission rates, which hardly can be accomplished using D-RoF. This fact is related to the low bit transmission efficiency of the CPRI standard used in D-RoF [67,68]. This becomes even more critical as the operating frequency increases, due to the need for increasing the sampling frequency. In summary, the CPRI standard has low spectral efficiency since the available bandwidth resources are quickly depleted as the transmission rate increases. Therefore, methods to improve transmission efficiency in D-RoF systems, applying data compression, have been proposed [69,70]. At the same time, the interest in the A-RoF solution in the fronthaul has intensified.

2.2 Radio over Fiber (RoF) Systems

In millimeter wave transmissions employing D-RoF, the signal sampling becomes even more critical factor since high sampling frequency bandwidth analog-to-digital converters (ADCs) and digital-to-analog converters (DACs) are required. Although modern fronthaul links widely employ D-RoF, it presents scalability issues, high-power consumption and costly operation considering the millimeter-wave operating scenario [71,72]. The focus of this thesis relies on A-RoF that employs external modulation. Figure 2.2 illustrates the A-RoF solution, in which the simplified RRH is composed by only electrical-to-optical (E/O) or optical-to-electrical (O/E) conversions and PAs. Simplification is achieved by moving the RF front-end to the CO, as well as eliminating the ADC and DAC from the RRH [73]. Therefore, the RF might be transported in the fronthaul link at the wireless channel radio frequency of the access network. However, this approach presents higher susceptibility to chromatic dispersion and non-linear distortions, compared to the D-RoF solution [74]. The RF signal also can be transported in the fronthaul link in intermediate frequency or in its base-band form. In this case, the RF front-end must to placed in the RRH to up-convert the RF

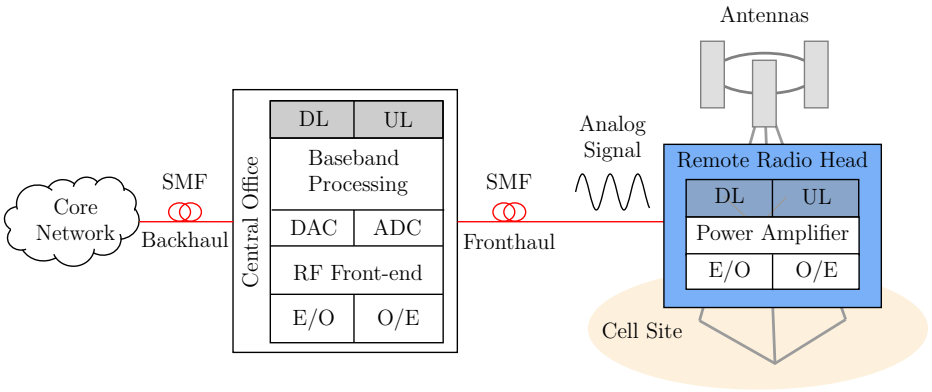

Figure 2.2: *Centralized radio access network assisted by the analog radio over fiber system.*

signal to channel central frequency.

A-RoF systems perform the E/O conversion through direct or external modulation techniques, in contrast to D-RoF systems that rarely employ external modulation [75]. The primary reasons are complexity and bandwidth constraints. Furthermore, employing external modulators can lead to increased costs, larger system size, and signal degradation compared to direct modulation, which offers a simpler and more cost-effective solution. Figure 2.3 shows the block diagram of the direct modulation A-RoF system. In direct modulation, the RF signal is applied directly to the laser driven current. The RF signal modulates the optical signal by modifying the light intensity, producing an intensity modulation in the optical carrier. It is important to notice that a bias tee component is used for combining the analog signal with a direct current (DC) source for modulating the optical carrier. Therefore, the envelope of the optical signal at the laser output follows the RF signal. The direct modulation technique has lower costs compared to external modulation, which makes it attractive especially for applications with data rates of up to 10 Gbit/s. The data rate limitation is imposed by the laser time response and the chirp, caused by optical carrier phase variations over time. In parallel, external modulation is employed to overcome these issues.

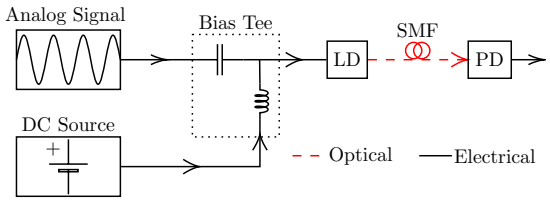

Figure 2.3: *Simplified block diagram of the directly modulated A-RoF system.*

Figure 2.4 illustrates the external modulation scheme, in which an MZM Lithium Niobate ($LiNbO_3$)-optical modulator is typically employed. The modulated signal at the MZM output is launched into a single-mode fiber (SMF) and photodetected by PD. As demonstrated in Figure 2.5, the optical signal is split into two branches. In the superior branch, the RF signal is applied to the MZM electrodes and the effective modal index of the waveguide is modified by a polarization voltage (V_{BIAS}), resulting in

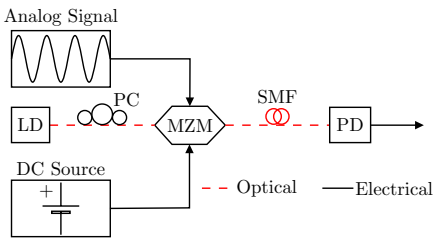

Figure 2.4: *Simplified block diagram of the externally modulated A-RoF system.*

a phase variation. Sequentially, the two branches of the MZM are combined to create an intensity modulation in the optical signal.

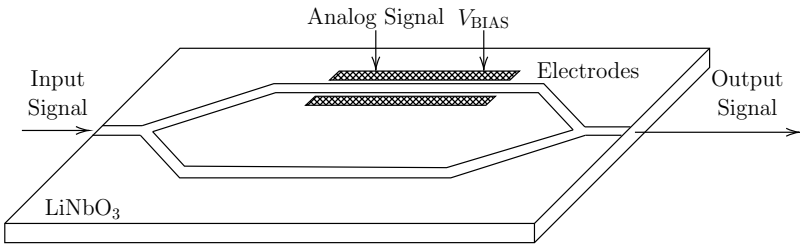

Figure 2.5: *Single-drive Mach-Zehnder modulator schematic.*

The MZM transfer function is commonly approximated by a cosine shape function [76]. The optical carrier modulation process creates spaced optical carrier sidebands according to the frequency of the RF signal (f). The main operating points of the optical modulator are demonstrated in Figure 2.6. These operating points are set by varying V_{BIAS} in relation to the half-wave voltage of MZM (V_π), which is the voltage necessary to introduce phase of π radians between the branches. In the absence of polarization voltage, the electric fields of the optical carrier in the two branches have equal phases and, therefore, are constructively combined at the output of the device, which is known as maximum transmission point (MATP). The minimum transmission point (MITP) is achieved when V_{BIAS}=V_π, which means that a phase shift of 180° is produced between the modulator branches. In this case, the RF signal at the frequency of interest is attenuated since the signal at the optical carrier frequency are destructively combined. Finally, the quadrature point (QP) occurs when V_{BIAS} = V_π/2, which is typically employed in A-RoF to reduce the non-linear distortions. It can be observed

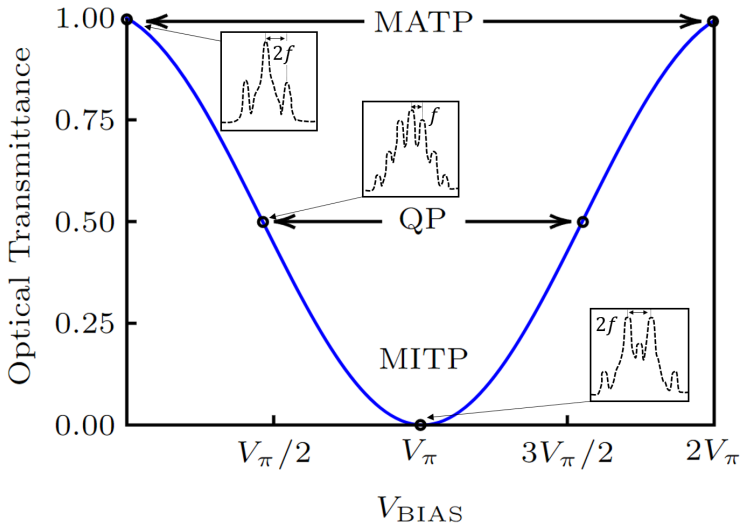

Figure 2.6: *Transfer function and main operating points of the Mach-Zehnder modulator.*

infinity operating points and phase combinations between the modulator branches, depending on the chosen operating point on the optical transmittance curve.

The optical spectrum for each operating point can be observed from the insets of Figure 2.6. At the MATP point, the detected RF carrier frequency is twice that of the RF-driven signal, resulting from the suppression of the first sidebands, spaced at the RF frequency from the optical carrier. Conversely, the QP point maintains the detected signal frequency identical to the RF-driven signal, facilitating signal recovery at the PD output. Lastly, in the MITP point, the direct detection process generates an RF carrier with a frequency again twice that of the RF-driven signal, as the optical carrier is considered suppressed.

2.3 Non-linear Devices

Many devices have non-linear behavior, for instance, PA, LD, transistors and diodes. This work focuses only on the MZM and PA non-linearities, which are commonly employed for implementing the transport link of C-RAN networks. Non-linearities appear when a signal with a variable envelope is applied to the non-linear device input, generating intermodulation products. This unwanted effect appears at frequencies outside the signal band, interfering with adjacent channels, as well as within the signal band, interfering with the signal to be transmitted.

Let x_n represent the input, and y_n represent the output of a device, representing the discrete samples of complex input and output signals. Here, n denotes the index of each sample in time. Depending on the signal power, distortions in the signal might be observed at the device output, which can be noticed in time and frequency domains. In the time domain, the distortions will affect the signal magnitude and phase, as illustrated in Figure 2.7 (a) and (b). In this figure, the signal magnitude has been normalized to ensure that the maximum value of the signal is unity, and the minimum value corresponds to zero. This normalization was solely performed to enhance visualization. It can be noticed that both magnitude and phase of the signal at the device output are changed as a function of the input signal magnitude, decreasing the overall system performance. As RF signal power increases, the distortions will become more severe, which will demand a linearization scheme to keep the system performance. It is important to emphasize that even in linear systems, distortions may be present. In this way, the observed distortion may not necessarily be attributed to a non-linear behavior. Therefore, a practical investigation was conducted to assess the non-linear distortion in external modulation and direct detection, which is more discernible in the frequency domain.

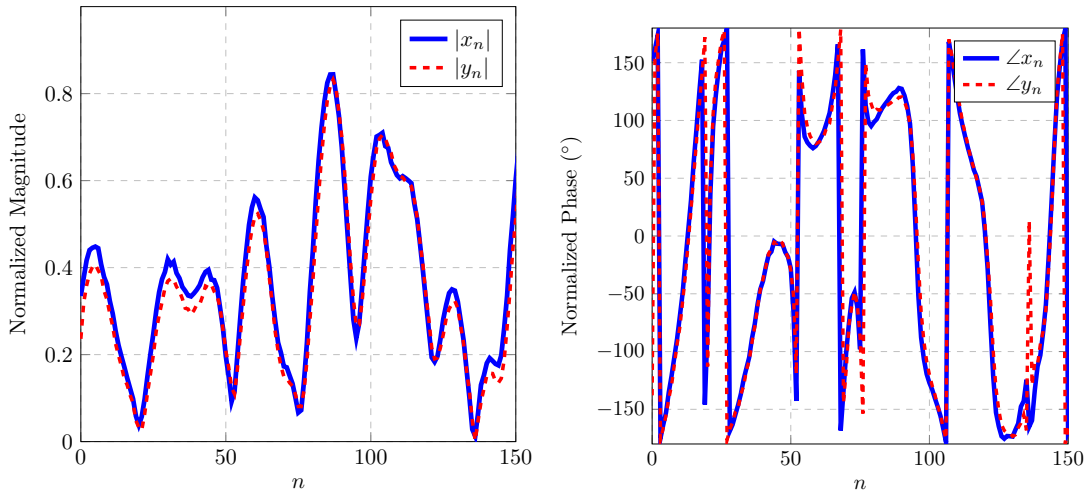

(a) *Distortion on the signal magnitude.* **(b)** *Distortion on the signal phase.*

Figure 2.7: *Distortions in time-domain, where x_n and y_n are the samples of the input and output signals, respectively, where $|\cdot|$ stands for the module of a complex signal and $\angle\cdot$ denotes the phase of a complex symbol.*

An investigation of harmonic distortions for an external modulation and direct detection was performed, which means that a MZM modulator and a PD was used. In this investigation, the RF signal was generated by an analog signal generator (PSG-E8267D) operating at 500 MHz. This RF signal was then applied to a Fujitsu FTM7939 EK MZM, capable of supporting up to 23.5 dBm RF power. The optical carrier, generated at 1550 nm with an optical power of 12 dBm, was produced using a tunable Golight laser source. This optical carrier was also directed to the MZM, where it underwent modulation with the RF signal. The maximum optical input power allowed for the FTM7939 EK is 17 dBm. A EoT ET-5000F PD was employed for direct signal detection, followed by analysis using a Keysight DSAV084A oscilloscope. Figure 2.8 presents a photography of the harmonic distortion experiment.

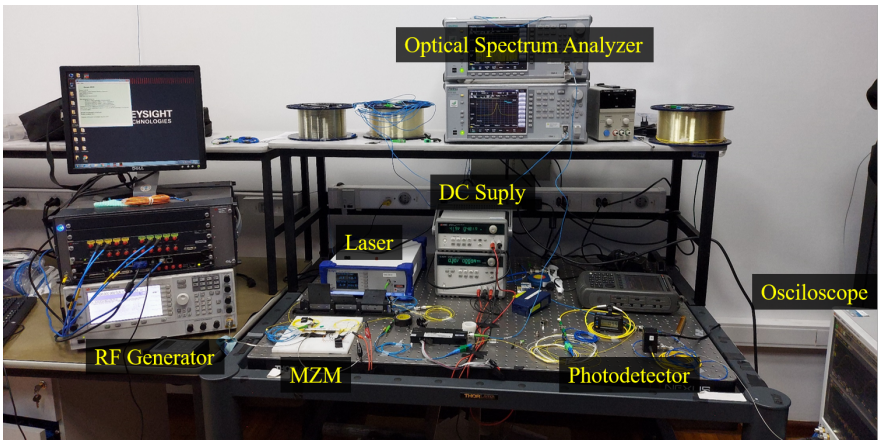

Figure 2.8: *Photography of the harmonic distortion experiment.*

In this analysis, only harmonic distortions will be observed as we are applying a one-tone signal solely to the electro-optic modulator input. The input RF signal power was varied from 1 to 20 dBm and the output RF power was measured at PD. Figure 2.9 illustrates the harmonic generation due to MZM non-linear response. The 2nd harmonic corresponds to $2f$, the 3rd harmonic corresponds to $3f$, and so on. Moreover, we have applied approximately 3 V DC voltage to the MZM, which results in operation at the quadrature point. It can be observed that the RF power of harmonics rapidly increases as RF power at MZM input increases, becoming even higher than the fundamental component. Although there is a considerable difference between the fundamental signal and spurious harmonics ($\geq$ 40 dB), non-linear distortions can significantly impact signal quality, especially for high-level RF input and when broadband modulated signals is transmitted.

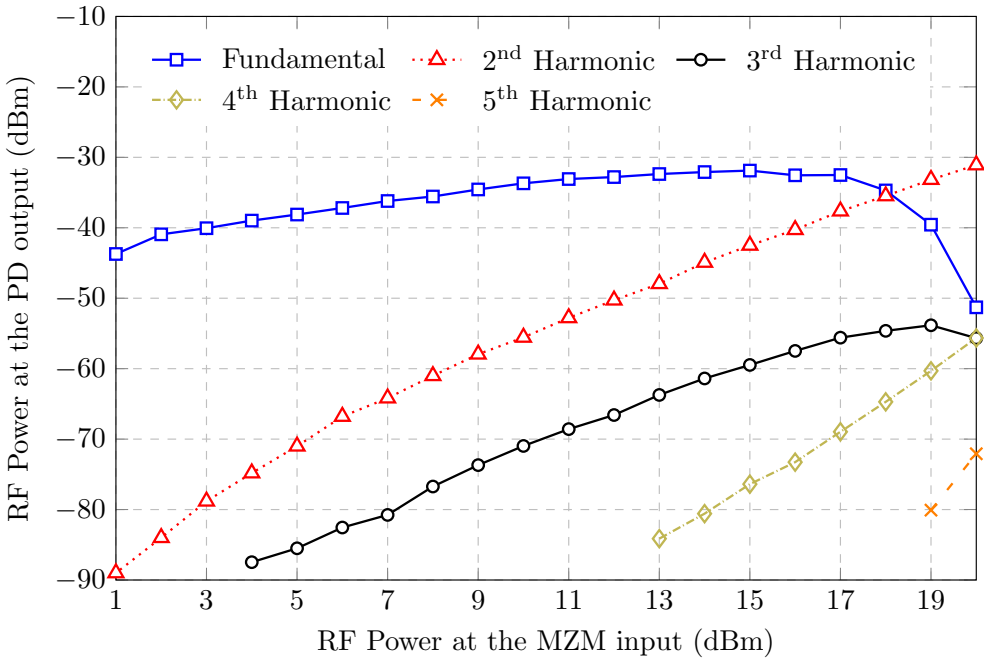

Figure 2.9: *MZM harmonic generation.*

Figure 2.10 illustrates optical power spectrum at MZM input for a double-sideband modulation, considering a two-tone signal, with same RF power as input. This result was obtained by using the Optisystem software, which is designed for simulating optical communications systems. It can be observed that harmonics, sum and subtraction intermodulation products are generated and upconverted by the optical carrier at 1,552.525 nm or $\approx$ 193.1 THz. We can notice that the MZM non-linear IMD and harmonics generation it is similar to the well known PA. Considering that a memory polynomial model is widely adopted for modeling PA non-linearities, this result suggests that a polynomial model can also be used for representing the MZM non-linear

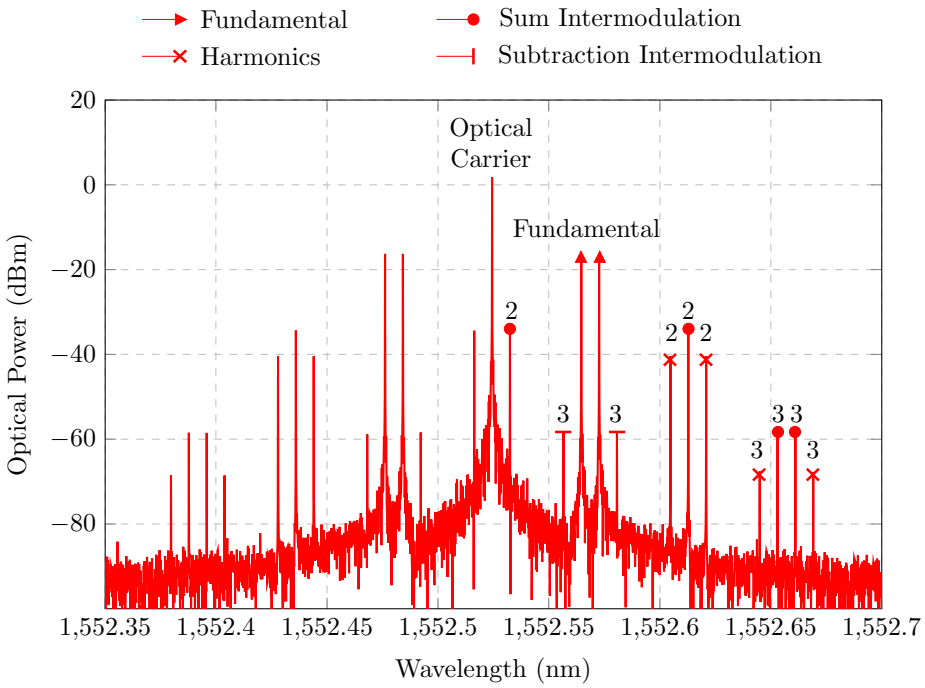

Figure 2.10: *Spectrum of the optical signal at the MZM output.*

power response.

Considering the mentioned non-linearities, a signal processing tool will be required to remove the distortions imposed by the MZM and PA. Pre-distortion and equalization techniques are commonly employed to perform this task, which often requires a mathematical model to represent the non-linear behavior. This model has a set a coefficients that are evaluated during the training process. In this model, the output samples are defined by the input samples taken to different powers and weighted by the coefficients of the model. A non-linear system model enables to properly represent a non-linear device output as close as possible to the real measured output for the same input signal. The memoryless and memory system models are often employed for representing non-linear devices, which is the case of the MZM and PA, considered in this work.

2.4 Artificial Neural Networks (ANNs)

The ANN is a subclass of the ML algorithms that has been widely employed to solve complex computational tasks [77]. An ANN used for analog radio over fiber linearization can be compared with conventional linearization schemes in terms of their effectiveness, complexity, and adaptability.

The ANN-based A-RoF linearization employs a machine learning approach that

can efficiently learn the non-linear characteristics of the A-RoF system. The ANN is trained with input-output data pairs to create a model that maps the non-linear input-output relation, enabling it to compensate for distortions effectively. The advantage of this approach lies in its ability to adapt and handle complex non-linearities without the need for detailed mathematical models.

On the other hand, conventional linearization schemes are based on established signal processing techniques or pre-determined mathematical models. While these techniques can provide good performance under certain conditions, they may struggle to address more complex non-linearities effectively.

The key differences between ANN-based RoF linearization and conventional schemes are as follows:

- Adaptability: ANN-based approaches can adapt to changing A-RoF system characteristics and can account for non-linearities beyond the scope of conventional techniques.
- Complexity: ANN-based linearization can handle complex A-RoF non-linearities without the need for a detailed mathematical model, whereas conventional schemes may require precise system modeling and calibration.
- Learning from Data: The ANN learns from input-output data pairs, enabling it to capture complex effects in the A-RoF system. Conventional techniques rely on predetermined algorithms, which might not be as flexible in adapting to different scenarios.
- Performance: ANN-based linearization has the potential to achieve higher performance in mitigating non-linear distortions compared to conventional methods, especially in scenarios where conventional techniques may become less effective.

The ANNs was inspired by the biological brain and was first proposed by Warren McCulloch and Walter Pitts in 1943 [78]. In 1980, more sophisticated training methods and architectures were proposed, which has increased the interest in ANNs by the scientific community. However, at that time, the computational capacity has limited the ANNs employment. Moreover, other ML-based techniques, such as Support Vector Machine (SVM) have been proposed and offer more interesting results and theoretical foundations when compared with ANNs [79]. Therefore, the study of ANNs was put aside.

Advances in computing power and the increase in available data sets have contributed to the recent interest in ML [28, 29]. Many ML techniques have been studied over the years. Supervised, unsupervised and reinforcement learning are some exam-

ples of ML techniques. In supervised learning, the model learns from a desired labeled data set. In contrast, unsupervised learning does not require the labeled data set and the model is trained without any guidance. Finally, reinforcement learning is when the model interacts with the environment to learn using the trial-and-error approach based on rewards [79, 80]. In this thesis, only supervised learning is considered.

A supervised ANN learns the relation among the input samples and the target labeled samples by using a set of training instances N_{TR}, with the purpose of creating an approximated function to map the input and target data samples. An ANN has been considered an interesting tool to deal with non-linear systems since it is capable of learning complex non-linear behaviors.

In this thesis, the ANN is employed as a linearization scheme for A-RoF systems. For instance, an ANN can be used for implementing pre- and post-distortion linearization techniques based on a linear regression operation. In this case, a supervised ANN can learn a behavioral model given its input and output samples.

2.5 Linearization Schemes for A-RoF Systems

The DPD has been considered the most prominent solution for linearization of digital communication systems, once it can be designed using conventional methods, based on LMS, or innovative ML-based solutions [81]. Considering non-linear A-RoF systems, the DPD operating principle consists of pre-distorting the input signal by a function that is complementary to the non-linear A-RoF system. By leveraging ML-based solutions, the response of the A-RoF system can be obtained by training neural networks with samples of the signal at the system input and output. This requires creating a data set, enabling the use of a supervised learning approach. Once the A-RoF system response is effectively modeled by the neural network, it can be employed to construct either a pre-distortion or post-distortion scheme. Therefore, the distortions introduced by the A-RoF system will considerably mitigate the distortions introduced by the DPD, linearizing the system response. Figure 2.11 presents the magnitude of the RF signal in the discrete-time domain, which allows us to verify the influence of the DPD scheme in the waveform. The DPD block applies the A-RoF post-inversion response for pre-distorting the orthogonal frequency division multiplexing (OFDM) signal. As a result, the cascade response of the DPD block and the A-RoF system produces a linear response. Figures 2.11 (a) and (b) demonstrate that in the regions in which the non-linear A-RoF response compress the signal, the DPD expands and vice versa. In other words, in the time domain, the cascade response of the DPD block and the A-RoF TX block produces a signal close to the non-distorted original signal. The

next sub-chapters present some linearization schemes for A-RoF systems.

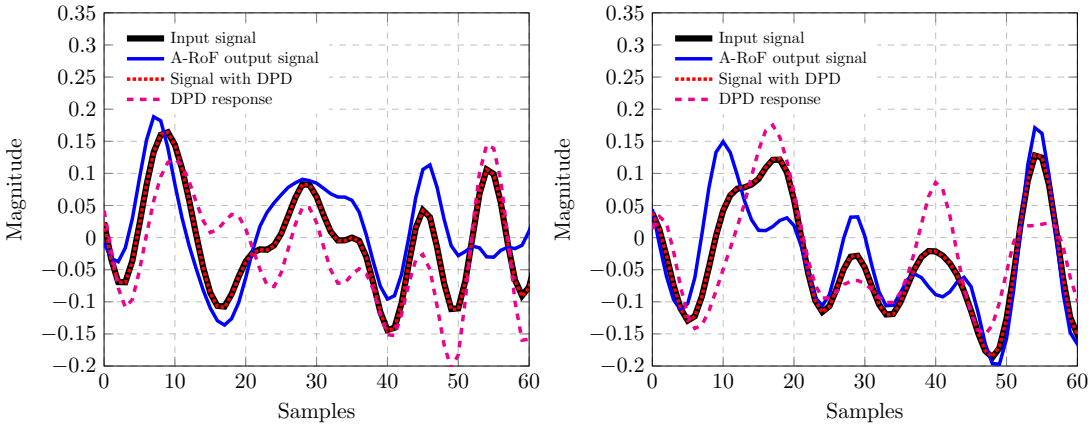

(a) *Real part* **(b)** *Imaginary part*

Figure 2.11: *OFDM signal magnitude as a function of time samples.*

2.5.1 Orthogonal Scalar Feedback Linearization

The waveform employed in the mobile communication network is assumed to be OFDM, which is given by

$$x_n = \sum_{m=0}^{M-1} d_m e^{-j2\pi \frac{m}{M}(n+1)}, \tag{2.1}$$

where d_m is quadrature amplitude modulation (QAM) symbol carried by the mth sub-carrier, $m \in \{0,\ 1,\ 2,\ \ldots,\ M-1\}$ and $n \in \{0, 1, \ldots, N-1\}$ is the time index. In this case, the orthogonal scalar feedback linearization (OSFL) DPD, proposed in [49], was employed. Digital samples of the pre-distorted signal are applied to the MZM. The MZM modulates the optical carrier from LD and the power of the LD beam affects the non-linear behavior of the optical modulator, as well as the DC voltage coming from the V_{BIAS} component. The effects of LD and V_{BIAS} might be inherently considered in the polynomial model coefficients. The MZM, polarized by a DC voltage provided by the V_{BIAS} block, presents a memoryless non-linear behavior. This implies that instantaneous samples at the device output depend solely on the input samples at the same moment and are not influenced by past samples. This memoryless behavior can be modeled by a transfer function given by [27]

$$y_n = \sum_{j=0}^{J-1} h_j |v_n|^j v_n, \tag{2.2}$$

where J stands for the non-linear order of the memoryless polynomial model, v_n are

the samples input signal, y_n the samples of output signal and h_j are the polynomial model coefficients. In this work, the coefficients are given by

$$h_j = \begin{bmatrix} 1.1 + j0.4 \\ 0.2 + j0.6 \\ 0.7 + j0.2 \\ 0.5 + j0.7 \\ 0.3 + j0.5 \end{bmatrix}. \tag{2.3}$$

It is worth to mention that the coefficients were randomly generated since will change for distinct MZMs components. It is important to emphasize that the coefficients of the MZM component were generated with the specific goal of achieving convergence between the models described in the literature and the benchtop components in our laboratory. Consequently, the coefficients may exhibit variation for distinct MZM models. The employed non-linearity order was $J = 5$, aligning with prior research that has already conducted practical investigations into the polynomial model for A-RoF links [53, 82].

The OSFL DPD is a pruned version of scalar feedback linearization (SFL) [83]. The basic idea of SFL is to optimize a scalar cost function ($C(\zeta_j)$) for obtaining the DPD coefficients. The scalar feedback does not require time synchronization and magnitude normalization, as the linear regression-based approaches [49]. Distinct cost functions can be selected aiming for reducing the out-band or in-band distortions, or even both interference. The main metrics used by the SFL DPD are the ACLR, EVM_{RMS}, and mean-squared error (MSE). While the ACLR is used to minimize the out-band distortions, the EVM_{RMS} is used to minimize the in-band interference. The MSE is employed to reduce both interference. It is important to notice that by improving one metric, the other one will be also improved. For instance, a DPD optimized for the ACLR will also improve the EVM_{RMS} and vice-versa [49]. Since $C(\zeta_j)$ changes at each iteration, any generic mathematical linearization algorithm might be employed to optimize the cost function. The main drawback of the SFL is the inter-dependency among the coefficients. In other words, the evaluation of the jth coefficient of ζ_j leads to the reevaluation of all previous coefficients $\zeta_1, \zeta_2, \ldots, \zeta_{J-1}$, which must be re-defined. This procedure significantly increases the overall convergence time.

On the other hand, the OSFL performs an orthogonalization process of the coefficients ζ_j, followed by numerical optimization of the scalar cost function aiming to reduce the algorithm convergence time. The main goal of the OSFL is to remove the inter-dependency among the coefficients, which means that the evaluation of one co-

efficient does not affect the previous ones. The orthogonalization process is based on minimizing the difference (residual vector) when a new coefficient order is being adjusted. In other words, the orthogonalization produces a new set of coefficients (ζ_{R_j}) that is incorporated in the DPD coefficients for promoting orthogonality. The coefficients ζ_{R_j} are obtained using a least squares estimation algorithm. It is important to highlight that this process might be repeated for enhancing the pre-distortion accuracy. The OSFL approach provides faster convergence when compared with the SFL technique since the orthogonalization of the coefficients simplifies the optimization process. More details and mathematical description of OSFL DPD can be found in [49]. In this thesis, the OSFL scheme was used as a benchmark for our proposed ANN-based DPD linearization method. This analysis is presented in **PAPER 2**.

2.5.2 MLP-Based Linearization for Memoryless Non-linear Distortions

The multi-layer perceptron (MLP)-based linearization scheme presented in this thesis is designed to compensate for the non-linear distortions produced by the MZM. Let us consider the block diagram of the equivalent base-band system model of A-RoF system depicted in Figure 2.12. The data symbols (d_m) are applied to the base-band OFDM modulator, which applies (2.1) to generate x_n. The first step for linearizing an A-RoF system employing an ANN consists of training the ANN. Supervised learning might be used during the training process. This means that a data set containing the training instances and their desired labels is required. Considering the block diagram presented in Figure 2.12, the data set can be generated when none of the linearization schemes are employed, i.e., s_1 and s_2 are in position 0. After generating the data set, the ANN might be trained. Details of the MLP-based linearization scheme training process are presented in **PAPERS 1, 2** and **3**.

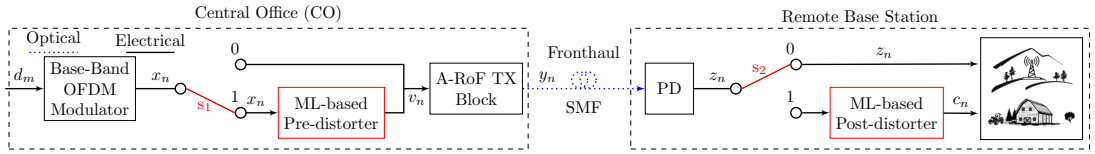

Figure 2.12: *Block diagram of the equivalent base-band system model of analog radio-over-fiber system.*

Creating a comprehensive and a representative data set is of utmost importance for training neural networks effectively. Such data sets play an important role in enhancing the overall performance of ML models. By providing a diverse and representative set of examples, the neural network can learn robust features and patterns, enabling it to

make accurate predictions on new, unseen data. A high-quality data set ensures that the neural network can generalize well beyond the training samples, which is crucial to avoid overfitting and achieve reliable performance on real-world data. Therefore, the initial step in designing an ML-based linearization scheme involves creating the data set for the A-RoF system. The process of creating the data set is outlined in Algorithm 1.

Algorithm 1 Generating the training data set for A-RoF Systems

Switch the switches s_1 and s_2 from Figure 2.12 to the 0 position
for $i = 1$ **to** Number of OFDM blocks **do**
Generate the ith training OFDM block by applying (2.1), with $M = 2048$
Generate the signal at the MZM output by applying (2.2), using $J = 5$ and the coefficients presented by (2.3)
Storage the samples of the OFDM symbols at MZM input and output to be used as training labels and to feed the ANN, respectively
end for

Now, considering that the ANN is already trained, the MLP-based linearization schemes can be used. Two possibilities for introducing the linearization schemes were considered. The switches from Figure 2.12 define which scheme is employed. For s_1 in position 1 and s_2 in position 0, the pre-distortion scheme is employed, whereas post-distortion is employed when s_1 is in position 0 and s_2 is in position 1. It is important to highlight that the same training process is used for both approaches.

Given the utilization of the pre-distortion scheme, the pre-distorted signal can be generated through the application of the ANN prediction method, a process accomplished by employing [79]

$$\mathbf{v} = \sum_{\ell=0}^{L+1} \phi(\mathbf{W}_\ell \times \mathbf{x}_\ell + \mathbf{b}_\ell), \tag{2.4}$$

where $\mathbf{v}$ is the vectored version of v_n, $(.)_\ell$ is the ℓth layer from the ANN, $\mathbf{W}$ is the matrix of weights, $\mathbf{b}$ is the biases vector and $\phi(.)$ is the non-linear activation function.

Regarding the MLP neural network architecture, Figure 2.13 presents the block diagram of the MLP ANN. It is important to note that for the input layer ($\ell = 0$), $\mathbf{x}_0$ is given by (2.1), with $\mathbf{x} = [x_0, x_1, ..., x_{N-1}]^T, \mathbf{x} \in \mathbb{C}^{N\times 1}$. For the next layers ($\ell = 1, ..., L+1$), $\mathbf{x}$ is given by the preceding layer output, since the ℓth layer is fully connected with the $(\ell - 1)$th layer.

The pre-distorted signal is applied to the MZM, which can be represented by (2.2). At the MZM output, the signal is launched in an SMF that can have tens of kilometer

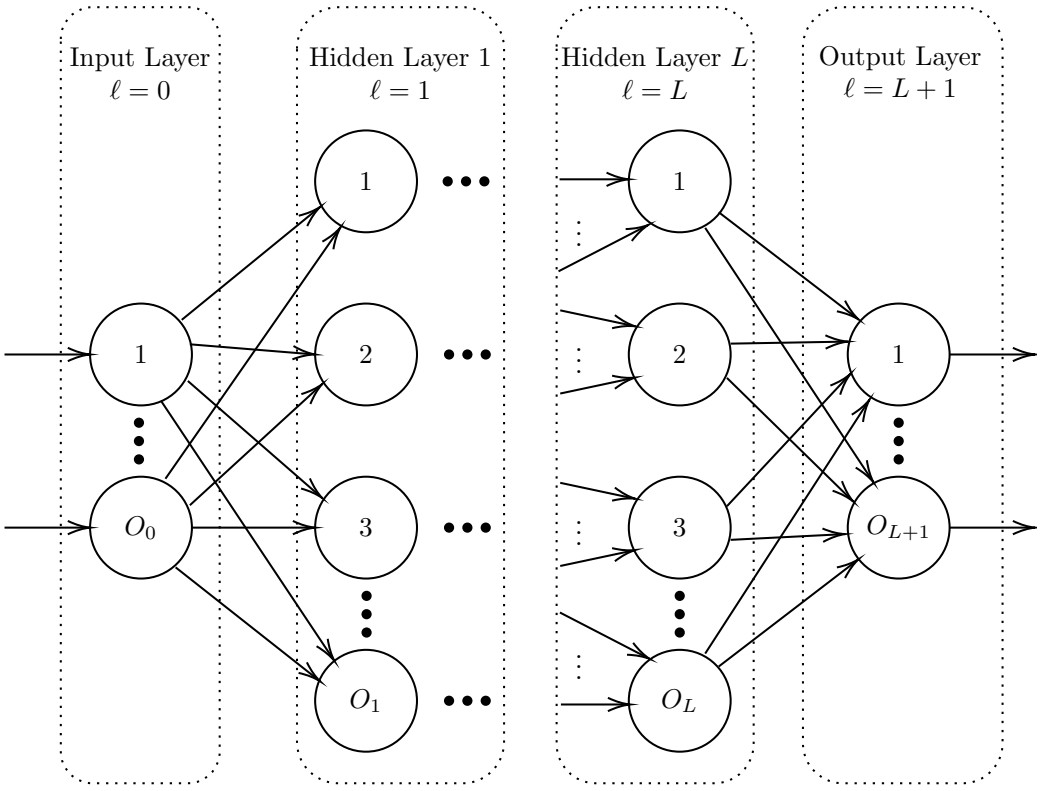

Figure 2.13: *Multi-layer perceptron ANN architecture composed of the following layers: input layer ($\ell = 0$); hidden layers ($\ell = 1, ..., L$); output layer ($\ell = L + 1$). Each layer has O_ℓ neurons.*

to deliver the signal at the RRH. In this first analysis, it was assumed that the SMF and PD responses are impulsive denoted by $g_n = \delta_n$. In other words, we have not considered the linear and non-linear effects of fiber-optics transmissions and also the noises produced in the photodetection process. Thereby, the proposed ML-based schemes focus on reducing the MZM non-linearities. Considering the above assumptions, the linearized signal is given by

$$z_n = y_n * g_n + w_n, \tag{2.5}$$

where g_n is the nth sample of the impulse response and w_n is the AWGN. Algorithm 2 summarizes the pre-distortion scheme process.

The post-distortion scheme might also be employed. This means that s_1 is in position 0 and s_2 is in position 1 ($x_n = v_n$). In this case, samples of the non-distorted discrete OFDM signal are directly applied to the MZM. Again, the discrete signal at PD output is given by (2.5) and is applied to the ML-based post-distorter, which applies (2.4), with z_n as input, to obtain the linearized signal (c_n). Algorithm 3 summarizes the post-distortion scheme, considering a data set that is unknown to theANN.

Algorithm 2 Proposed MLP-based pre-distortion scheme

Select the number of OFDM blocks considered for the performance evaluation of the linearization scheme
Position switch s_1 to position 1 and s_2 to position 0
for $i = 0$ **to** number of OFDM blocks **do**
Generate the ith test OFDM block by applying (2.1), with $M = 2048$
Apply the generated OFDM block to the MLP-based pre-distorter, and get the output applying the ANN predict method
Generate the signal at the MZM output by applying the non-linear model (2.2) using samples of the signal at the MLP-based pre-distorter output as input. Use $J = 5$ and the coefficients provided by (2.3)
Obtain the signal at the PD output by utilizing (2.5)
Conduct the OFDM symbol demodulation
Utilize the EVM, NMSE, and ACLR metrics for evaluating the linearization performance of the pre-distortion scheme
end for

The performance evaluation of this ML-based approach is demonstrated in **PAPERS 1** and **3**. We have also applied the aforementioned approach to design a novel linearization scheme capable of generalizing possible variations of MZM parameter, leading to a non-recalibrated linearization scheme. This scheme introduces robustness to the system against time variations dispensing new costly training campaigns. Moreover, the linearization performance of the proposed scheme was also compared with a conventional state-of-the art solution, aiming evaluating the linearization performance and algorithm complexity. This analysis can be found in **PAPER 2**.

Algorithm 3 Proposed MLP-based post-distortion scheme

Select the number of OFDM blocks considered for the performance evaluation of the linearization scheme.
Position switch s_1 to position 0 and s_2 to position 1.
for $i = 0$ **to** number of OFDM blocks **do**
Generate the ith test OFDM block by applying (2.1), with $M = 2048$
Generate the signal at the MZM output by applying the non-linear model (2.2) with samples of OFDM symbol as input. Use $J = 5$ and the coefficients provided by (2.3).
Obtain the signal at the PD output by utilizing (2.5).
Apply the samples of the signal at PD output to the MLP-based post-distorter, and get the output applying the ANN predict method
Conduct the OFDM symbol demodulation
Utilize the EVM, NMSE, and ACLR metrics for evaluating the linearization performance of the pre-distortion scheme.
end for

2.5.3 RNN-Based Linearization for Memory Non-linear Distortions

In C-RAN architectures based on A-RoF transport network, the photodetected signal at the RRH must to be amplified before being radiated to the covered area. An electrical PA is used to perform this task. Similar to the MZM, the PA also has a non-linear behavior, which means that the linearization scheme must also deal with the PA non-linearity, which has a dynamic behavior that can not be represented by a memoryless polynomial model, since a memory effect at the PA output is observed. The memory effect is a variation of the amplitude-to-amplitude (AM/AM) and amplitude-to-phase (AM/PM) functions due to the past input levels, which means that the instantaneous PA output does not depends only on the corresponding instantaneous input. The memory depth (Q) parameter defines how many previous samples have an influence on the instantaneous signal at the PA output. In this case, the memory polynomial model, is widely adopted for modeling the PA behavior. Since the PA non-linearities has memory, an ANN capable of dealing with a system with memory effect is necessary. For this reason, we have employed a RNN, since it has an internal memory structure. Additionally, memoryless devices, such as MZM, can be considered a special case of memory system and, therefore, also can be modeled using this ANN architecture. This implies that even a memoryless system can be represented by a memory model by setting the memory depth parameter to zero [84].

Figure 2.14 depicts the block diagram of the equivalent base-band system model of an amplified A-RoF. Firstly, it is necessary to create the training data set. This data set must contain the desired labels, which are the original OFDM signal (x_n) and the distorted signal at the PA output p_n, as describe by Algorithm 4. Details of RNN training process, as well as its hyperparameters, can be found in **PAPERS 4** and **5**.

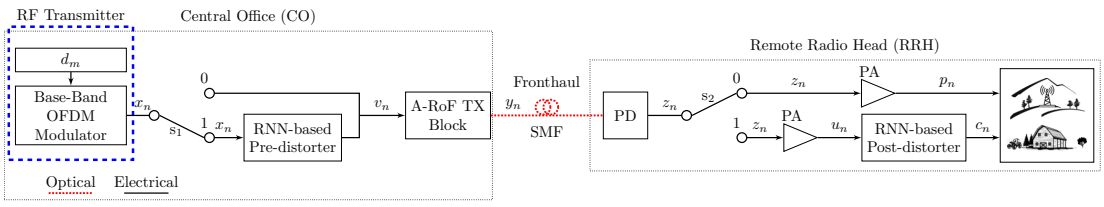

Figure 2.14: *Block diagram of the equivalent base-band model of amplified A-RoF system.*

Once trained, the RNN might be used as a pre- or post-distortion scheme aiming to achieve the desired linearization. Considering that the pre-distortion scheme was employed, the output of each hidden layer at time step t with $t \in \{1, \cdots, Ts\}$, is given by [79]

$$\hat{\mathbf{V}}_{(t)} = \phi\left(\mathbf{P}_{(t)}\mathbf{W}_p + \hat{\mathbf{V}}_{(t-1)}\mathbf{W}_v + \mathbf{b}\right), \tag{2.6}$$

where Ts is the RNN internal memory depth. Let $\mathbf{P}_{(t)} \in \mathbb{R}^{N\times nf}$ denote the input matrix at $Ts{=}\ t$, where nf corresponds to the input training number of features instances. Furthermore, we define $\hat{\mathbf{V}}_{(t-1)} \in \mathbb{R}^{N\times O_\ell}$ as the output matrix from the previous Ts. It is important to highlight that the output of the ℓth layer will be the input of the $(\ell+1)$th layer. Additionally, as illustrated in Figure 2.15, the input ($\ell = 0$) and output layer ($\ell = L+1$) are composed of non-recurrent neurons, meaning that $\hat{\mathbf{V}}_{(t-1)}$ and $\mathbf{W}_v$ are zeroed in these layers. The ℓth hidden layer, $\ell \in \{1, \cdots, L\}$, has two sets of weights matrices $\mathbf{W}_p \in \mathbb{R}^{O_{\ell-1}\times O_\ell}$ and $\mathbf{W}_v \in \mathbb{R}^{O_\ell\times O_\ell}$, in which are stored the input vector weights of the current Ts and for the output of the previous Ts, respectively.

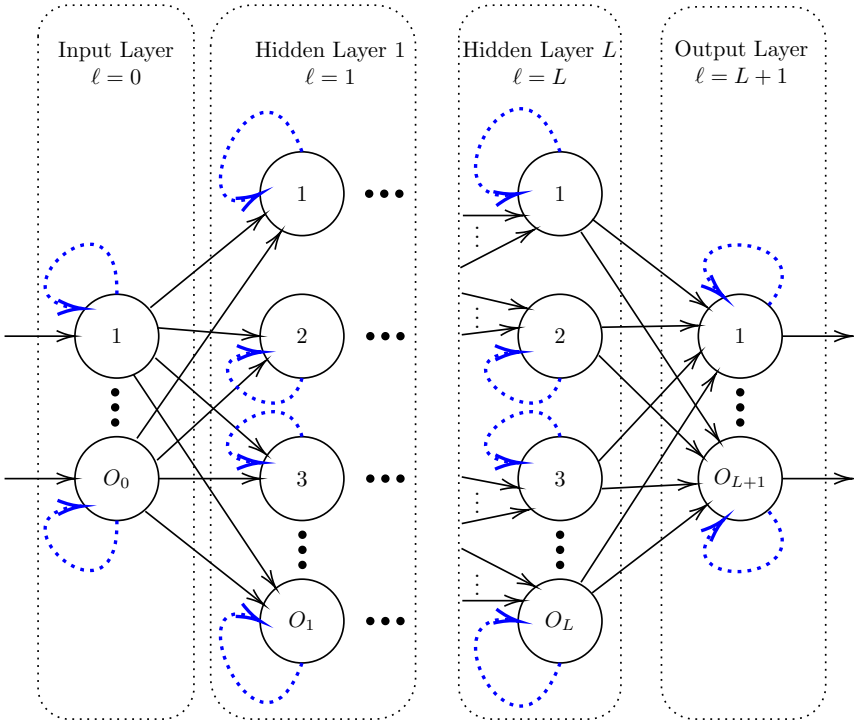

Figure 2.15: *RNN architecture composed of the following layers: input layer ($\ell = 0$); hidden layers ($\ell = 1, ..., L$); output layer ($\ell = L+1$). Each layer has O_ℓ neurons.*

The pre-distorted signal (v_n) is applied to the A-RoF TX block, which is described by (2.2). At the MZM output, the signal is launched in an SMF to be delivered at the RRH. Again, g_n stands for the combined impulse response of SMF and PD, which means that z_n is obtained by applying (2.5). The signal at PD output is amplified before being radiated. Typically, the PA is modeled using a memory polynomial model.

The PA usually operates close to its 1-dB saturation point, introducing memory

non-linear distortions that can be modeled as [85, 86]

$$p_n = \sum_{q=0}^{Q-1} \sum_{k=0}^{K-1} \xi_{q,k} \left| z_{n-q} \right|^k z_{n-q}, \tag{2.7}$$

where $\xi_{q,k}$ are coefficients of the PA model, with $q \in \{0, 1, \cdots, Q-1\}$ and $k \in \{0, 1, \cdots, K-1\}$, in which Q is the memory depth and K the non-linear order of the model. It is important to highlight that K and Q depend on the specific components and architecture used to build the PA [85].

For the sake of simplicity, (2.7) can be written in matrix form. Firstly, let us define $\boldsymbol{\xi}$ as the matrix of coefficient of the memory polynomial model, $\boldsymbol{\xi} \in \mathbb{C}^{Q \times K}$, which was randomly generated. The chosen values of K and Q align with commonly employed parameters for modeling amplifiers in mobile communication systems [53, 82, 85]. Through extensive preliminary testing and studies, we have observed that our proposed linearization scheme effectively operates across a wide range of coefficient combinations One example of this matrix is given by

$$\boldsymbol{\xi} = \begin{bmatrix} 1.077 + j0.06 & 0.04 + j0.09 & 0.08 + j0.08 & 0.07 + j0.02 & 0.01 + j0.03 \\ 0.097 + j0.09 & 0.07 + j0.01 & 0.08 + j0.08 & 0.01 + j0.08 & 0.04 + j0.04 \\ 0.03 + j0.03 & 0.09 + j0.03 & 0.06 + j0.02 & 0.08 + j0.04 & 0.04 + j0.05 \end{bmatrix}. \tag{2.8}$$

For the sake of simplicity, consider $\mathbf{Z} \in \mathbb{C}^{Q \times K}$, as a matrix containing samples of the input signal, which are organized as follows

$$\mathbf{Z} = \begin{bmatrix} z_n & z_n|z_n| & \cdots & z_n|z_n|^{K-1} \\ z_{n-1} & z_{n-1}|z_{n-1}| & \cdots & z_{n-1}|z_{n-1}|^{K-1} \\ \vdots & \vdots & \ddots & \vdots \\ z_{n-Q+1} & z_{n-Q+1}|z_{n-Q+1}| & \cdots & z_{n-Q+1}|z_{n-Q+1}|^{K-1} \end{bmatrix}, \tag{2.9}$$

where the nth output sample of the memory polynomial model is obtained by performing the sum of all elements of the matrix resulted from the Hadamard product between $\boldsymbol{\xi}$ and $\mathbf{Z}$ as follows

$$p_n = \sum_{q,k} \left[\boldsymbol{\xi} \odot \mathbf{Z} \right]_{q,k}, \tag{2.10}$$

where $\odot$ is the Hadamard product, $q \in \{0, 1, \cdots, Q-1\}$ and $k \in \{0, 1, \cdots, K-1\}$. Finally, we can rewrite (2.7) as a column vector given by $\mathbf{p} = [p_0, p_1, \cdots, p_{N-1}]^{\mathrm{T}}$, $\mathbf{p} \in$

$\mathbb{C}^{N\times 1}$. Due to the causal response of the PA, the samples with negative indexes in (2.10) are considered to be zeroed. This representation considerably simplifies the implementation of the model in a numerical simulator, for instance, using Python. This is achieved since only matrix operations is required, while still yielding the exact same result as expected when applying (2.7).

The training process is similar to the one presented for the MLP-based linearization scheme. However, now we need to account for the PA both in data set creation and performance evaluation. Algorithm 4 outlines the data set generation process for amplified A-RoF systems with memory effect.

Algorithm 4 Generating the training data set for amplified A-RoF Systems with memory effect

Switch the switches s_1 and s_2 from Figure 2.14 to the 0 position..
for $i = 1$ **to** Number of OFDM blocks **do**
Generate the ith training OFDM block by applying (2.1), with $M = 2048$
Generate the signal at the MZM output by applying (2.2), using $J = 5$ and the coefficients presented by (2.3)
Generate the signal at the PA output by applying (2.10), using $K = 5$, $Q = 3$ and the coefficients presented by (2.8)
Storage the samples of the OFDM symbols at MZM input and PA output to be used as training labels and to feed the ANN, respectively
end for

Algorithm 5 encompasses all processes related to the pre-distortion approach. It is important to note PA was considered during the RNN training process and is also considered for the performance evaluation.

Alternatively, the OFDM signal could also be linearized using the post-distortion scheme showed in Figure 2.14, considering that s_1 is in position 0 and s_2 is in position 1. Algorithm 6 summarizes all the process involved with the RNN-based post distortion approach. In this case, $x_n = v_n$ is directly applied to the MZM. Similarly to the pre-distortion approach, the signal at the PD output is given by (2.5). This discrete signal is applied to the RNN-based post-distorter, which applies (2.6) for obtaining the linearized signal (c_n).

The performance evaluation of this ML-based approach is demonstrated in **PAPER 4**. We also investigated the impact of Ts and compared it with a memoryless ANN (MLP). Moreover, **PAPER 5** reports the investigation of activation function influence on the algorithm linearization performance.

Algorithm 5 Proposed RNN-based pre-distortion scheme

Select the number of OFDM blocks considered for the performance evaluation of the linearization scheme.
Position switch s_1 to position 1 and s_2 to position 0.
for $i = 0$ **to** number of OFDM blocks **do**
Generate the ith test OFDM block by applying (2.1), with $M = 2048$
Apply the generated OFDM block to the RNN-based pre-distorter, and get the output applying the ANN predict method
Generate the signal at the MZM output by applying the non-linear model (2.2) using samples of the signal at the RNN-based output as input. Use $J = 5$ and the coefficients provided by (2.3)
Obtain the signal at the PD output by utilizing (2.5).
Generate the signal at the PA output by applying the non-linear model (2.10) using samples of the signal at the PD output as input. Use $K = 5$, $Q = 3$ and the coefficients provided by (2.8)
Conduct the OFDM symbol demodulation
Utilize the EVM, NMSE, and ACLR metrics for evaluating the linearization performance of the pre-distortion scheme.
end for

Algorithm 6 Proposed RNN-based post-distortion scheme

Select the number of OFDM blocks considered for the performance evaluation of the linearization scheme.
Position switch s_1 to position 0 and s_2 to position 1.
for $i = 0$ **to** number of OFDM blocks **do**
Generate the ith test OFDM block by applying (2.1), with $M = 2048$
Generate the MZM output signal by applying the non-linear model (2.2), with OFDM symbol samples as input. Use $J = 5$ and the coefficients provided by (2.3)
Obtain the signal at the PD output by utilizing (2.5).
Generate the signal at the PA output by applying the non-linear model (2.10) with samples of the signal at PD output as input. Use $K = 5$, $Q = 3$ and the coefficients provided by (2.8).
Apply the samples of the signal at PA output to the RNN-based post-distorter, and get the output applying the ANN predict method
Conduct the OFDM symbol demodulation
Utilize the EVM, NMSE, and ACLR metrics for evaluating the linearization performance of the pre-distortion scheme.
end for

2.5.4 Polynomial-Based Linearization for Memory Non-linear Distortions

Considering that the relation between an input and output signal of an A-RoF system might be modeled by a polynomial expression, a polynomial-based linearization might also be employed. The goal here is to fit a polynomial regression to the data from a data set containing the training instances (p_n) and desired labels (x_n). In this case, the normal equation can be employed to obtain the model coefficients. The normal equation requires that the number of rows be much greater than the number of columns. In this case, this condition is satisfied with $(N - Q + 1) \gg (QK)$. In this way, the normal equation is given by [87]

$$\boldsymbol{\beta} = \left[\mathbf{P}_{\mathrm{R}}^{\mathrm{H}}\mathbf{P}_{\mathrm{R}}\right]^{-1}\mathbf{P}_{\mathrm{R}}^{\mathrm{H}}\mathbf{x}_{\mathrm{R}}, \tag{2.11}$$

where $(.)^{-1}$ is the matrix inversion operation, $(.)^{\mathrm{H}}$ is the Hermitian operator, $\boldsymbol{\beta} \in \mathbb{C}^{(QK)\times 1}$ and $\mathbf{P}_{\mathrm{R}}$ is given by

$$\mathbf{P}_{\mathrm{R}} = \begin{bmatrix} p_{Q-1}\left|p_{Q-1}\right|^{0} & \cdots & p_{0}\left|p_{0}\right|^{0} & \cdots & p_{Q-1}\left|p_{Q-1}\right|^{K-1} & \cdots & p_{0}\left|p_{0}\right|^{K-1} \\ p_{Q}\left|p_{Q}\right|^{0} & \cdots & p_{1}\left|p_{1}\right|^{0} & \cdots & p_{Q}\left|p_{Q}\right|^{K-1} & \cdots & p_{1}\left|p_{1}\right|^{K-1} \\ \vdots & \ddots & \vdots & \ddots & \vdots & \ddots & \vdots \\ p_{N-1}\left|p_{N-1}\right|^{0} & \cdots & p_{N-Q}\left|p_{N-Q}\right|^{0} & \cdots & p_{N-1}\left|p_{N-1}\right|^{K-1} & \cdots & p_{N-Q}\left|p_{N-Q}\right|^{K-1} \end{bmatrix}, \tag{2.12}$$

where $\mathbf{P}_{\mathrm{R}} \in \mathbb{C}^{(N-Q+1)\times(QK)}$ and

$$\mathbf{x}_{\mathrm{R}} = \begin{bmatrix} x_{Q-1} \\ x_{Q} \\ \vdots \\ x_{N-1} \end{bmatrix}, \tag{2.13}$$

is a vector containing $(N - Q + 1)$ samples of x_n.

Figure 2.16 depicts the block diagram of the scheme used for estimating the coefficients of the polynomial-based DPD. In this diagram, x_n is the original discrete OFDM signal and p_n is the discrete signal at the PA output. The coefficients of the polynomial-based linearization ($\boldsymbol{\beta}$) are obtained by employing (2.11). The first step for training a polynomial-based linearization scheme relies on choosing the degree of the polynomial. This enables properly fitting the model to the data.

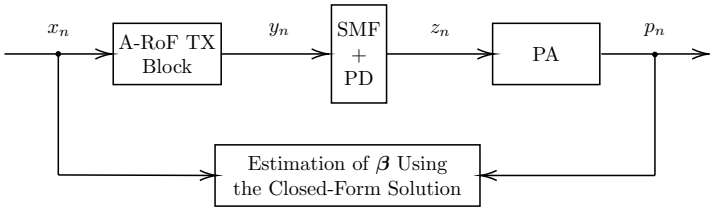

Figure 2.16: *Block diagram of the scheme used to train the polynomial-based DPD.*

Once trained, the coefficients of the model ($\boldsymbol{\beta}$) are copied to the linearization block, which can be a pre- or post-distortion schemes. Now, let us consider that the RNN pre- and post- distorter blocks from Figure 2.14 are exchanged by processing blocks based on polynomial linearization. When pre-distortion is employed, the pre-distorted signal (v_n) is given by (2.10) with $\boldsymbol{\beta}$ and $\mathbf{X}$ and as inputs. It is important to notice that $\mathbf{X}$ is obtained using (2.9) and $\boldsymbol{\beta}$ needs to be re-arranged to a $(Q \times K)$ matrix. Similarly to the pre-distortion scheme, the post-distortion can be accomplished by using (2.10) with p_n as input and the calculated coefficients $\boldsymbol{\beta}$.

The normal equation for polynomial regression has several advantages. It provides a solution to the problem of finding the coefficients of the polynomial that best fits the data. Moreover, it can be easily implemented. On the other hand, this solution has some important disadvantages. For instance, the degree of the polynomial must be chosen carefully to avoid overfitting, otherwise it can hinder the algorithm generalization capability. This solution is also high-sensitive to outliers in the data, which can become a problem, since OFDM has high PAPR. In addition, the normal equation might also not be suitable for high-correlated signals. This is known as multicollinearity and can hinder the accurate estimation of the coefficients of the regression model. In this case, the coefficients become very sensitive to small changes in the data, which can lead to unstable and unreliable results. Finally, this model also may not work well for data sets with a large number of variables. Although its disadvantages, the polynomial model was used as a benchmark for our proposed ML-based linearization techniques and the results are discussed in **PAPER 7**.

2.5.5 Compensating Chromatic Dispersion, Memoryless- and Memory Distortions using ARVTDNN

Now, let us consider that the optical fronthaul link needs to be extended to cover remote areas. For this long-reach optical fronthaul, chromatic dispersion kicks in and introduces linear distortions as well. This means that besides memoryless and memory non-linear distortions, the system will also be affected by a linear distortion. All these interference must be compensated in a A-RoF. Otherwise, in-band distortions will

deteriorate quality of service to the end user, whereas out-band distortions may cause interference in services operating adjacent channels.

Figure 2.17 shows the block diagram of the equivalent base-band model for the scenario considered in the analysis. For this case, an ARVTDNN was employed, since an ANN capable of dealing with linear and non-linear distortions is required. Although RNN can deal with memory effect by employing an internal memory structure, it was observed that recurrent neurons are not the best option when a linear effect is also observed. An ARVTDNN might be used to overcome this issue since it receives the base-band samples of the transmit waveform and stores them in a time delay line (TDL). This means that all the information necessary to compensate time correlated effects is available for the ML algorithm.

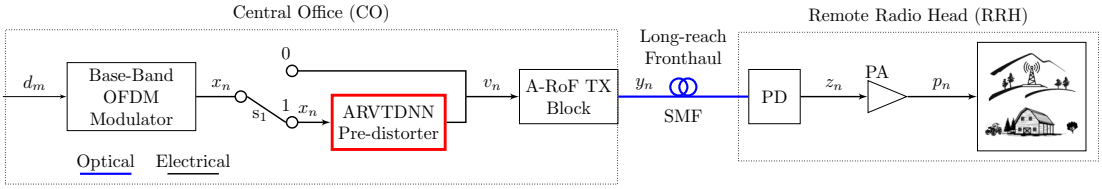

Figure 2.17: *Block diagram of the equivalent base-band system model considering CD.*

Consider now that the ARVTDNN was trained, according with the details presented in **PAPER 6**. The ARVTDNN is trained using a data set containing the original input signal (v_n) and the distorted signal at PA output (p_n).

From the system model point-of-view, the base-band equivalent representation can be used considering the new ANN and the linear CD effect. Figure 2.18 depicts the block diagram of the ARVTDNN, which is composed of $L+1$ layers. The ℓth layer has O_ℓ neurons, with $\ell \in \{0, ..., L+1\}$. In this diagram, the first 2 blocks receive the real and imaginary values of the waveform. The remaining $K-1$ blocks receive the absolute value of the Q samples raised to the k power. Therefore, the input layer has $Q(K+1)$ neurons, meaning that the ANN has all the necessary information to compensate for the memory effect. Therefore, the input layer depends on the PA memory depth Q and non-linear order K, since the ANN is fed with $K+1$ blocks of Q samples to compensate for the memory effect. This approach enables capturing time-varying patterns and dependencies in the data, which is the case of the memory effect of PAs.

Like the MLP-based linearization scheme presented in Sub-chapter 2.5.2, the pre-distorted signal (v_n) will be given by (2.4). It is important to notice that, for this case, the ANN input will be composed of $Q(K+1)$ neurons. It is assumed that the impulse response of SMF can no longer be considered impulsive. The SMF introduces CD that leads to a variation in the fiber frequency response, which is given by [88, 89]

$$G\left(e^{j\omega T}\right) = e^{-jA(\omega T)^2}, \quad A = \frac{D\lambda^2 Lz}{4\pi cT^2}, \tag{2.14}$$

where D is the SMF dispersion parameter, λ is the optical carrier wavelength, Lz is the SMF length and c is the speed of light. The digital frequency is represented by $\omega T = 2\pi fT$, in which T stands for the sampling period. The CD impulse response is given by the inverse Fourier transform of (2.14), which leads to non-causal and infinite impulse response (IIR). The authors in [88] have shown that the CD can be properly represented using a finite impulse response (FIR) filter by truncating the IIR with an odd number of taps N_t, leading to

$$g_n = \sqrt{\frac{1}{j4A\pi}} e^{j\frac{n^2}{4A}}, -\left\lfloor \frac{N_\mathrm{t}}{2} \right\rfloor \leq n \leq \left\lfloor \frac{N_\mathrm{t}}{2} \right\rfloor, N_\mathrm{t} = 2\left\lfloor 2A\pi \right\rfloor + 1, \tag{2.15}$$

in which $\lfloor . \rfloor$ returns the largest integer smaller than the argument. It is important to mention that the optical fiber exhibits an impulse response at the sample signaling rate of the OFDM symbol. However, the system response is obtained through the

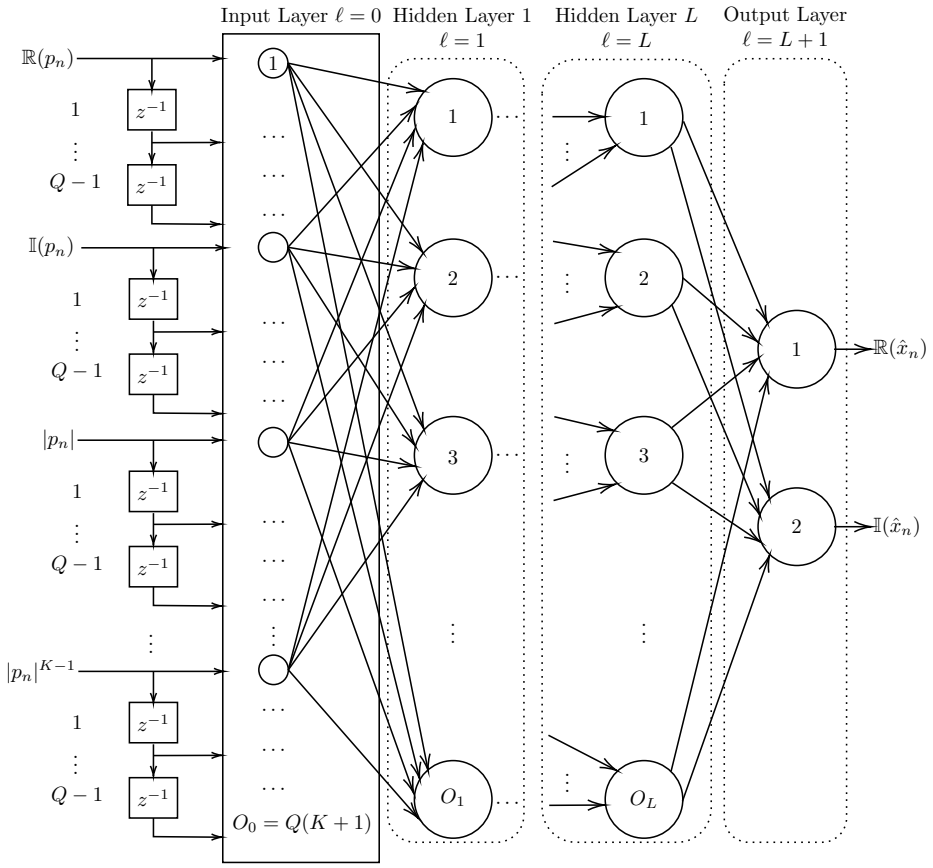

Figure 2.18: *ARVTDNN architecture composed of the following layers: input layer ($\ell = 0$); hidden layers ($\ell = 1, ..., L$); output layer ($\ell = L + 1$). Each layer has O_ℓ neurons*

convolution between the fiber response and the wireless channel response. This leads to spreading in the resultant impulse response. Consequently, the cyclic prefix (CP) needs to be sized to cover the wireless channel convolved with the response of the fiber. Hence, the analysis should be performed at the sample signaling rate, considering the system as a whole.

The training process is similar for the previous proposed schemes. However, now we need to account for the power amplifier and chromatic dispersion both in data set creation and performance evaluation. Algorithm 7 outlines the data set generation process for this case.

Algorithm 7 Generating the training data set for amplified A-RoF Systems with memory effect and chromatic dispersion

Position switch s_1 to position 0
for $i = 1$ **to** Number of OFDM blocks **do**
Generate the ith training OFDM block by applying (2.1), with $M = 2048$
Add the cyclic prefix to protect the OFDM block from inter-block interference
Generate the signal at the MZM output by applying (2.2), using $J = 5$ and the coefficients presented by (2.3)
Generate the signal at the PD output by applying (2.5), incorporating g_n described by (2.15)
Generate the signal at the PA output by applying (2.10), using $K = 5$, $Q = 3$ and the coefficients presented by (2.8)
Storage the samples of the OFDM symbols at MZM input and PA output to be used as training labels and to feed the ANN, respectively
end for

Using this model and assuming that the PD does not introduce distortions, the signal at the PA input and output are given by (2.5) and (2.7), respectively. Algorithm 8 describes all process related to the ARVTDNN-based pre-distortion process, considering the chromatic dispersion. During the training phase, the target labels will be $\mathbb{R}(\mathbf{v})$ and $\mathbb{I}(\mathbf{v})$, where $\mathbf{v}$ is the vectored version of v_n with Q samples. During the ARVTDNN training, a loss function is minimized, in other words, the ANN is trained to compensate the A-RoF by learning the inverse response of the A-RoF system. This estimated response is afterward used in the pre-distortion block, producing the desired linearization.

The performance evaluation of the proposed ARVTDNN-based linearization scheme is reported in **PAPER 6**. In addition, the proposed scheme was also evaluated for a fiber/wireless (FiWi) system. The goal was to demonstrate that the linearization scheme enables a seamless integration of the A-RoF system to a wireless link.

Algorithm 8 Proposed ARVTDNN-based pre-distortion scheme

Select the number of OFDM blocks for the performance evaluation
Position switch s_1 to position 1
for $i = 0$ **to** number of OFDM blocks **do**
Generate the ith test OFDM block by applying (2.1), with $M = 2048$
Add the cyclic prefix to protect the OFDM block from inter-block interference
Apply the generated OFDM block to the RNN-based pre-distorter, and get the output applying the ANN predict method
Generate the signal at the MZM output by applying the non-linear model (2.2) using samples of the signal at the RNN-based output as input. Use $J = 5$ and the coefficients provided by (2.3)
Obtain the PD output by utilizing (2.5), incorporating g_n described by (2.15).
Generate the signal at the PA output by applying the non-linear model (2.10) using samples of the signal at the PD output as input. Use $K = 5$, $Q = 3$ and the coefficients provided by (2.8)
At the receiver side, remove the cyclic prefix
Conduct the OFDM symbol demodulation
Utilize the EVM, NMSE, and ACLR metrics for evaluating the linearization performance of the pre-distortion scheme.
end for

2.6 Conclusions

In this chapter, the necessary foundation for designing linearization schemes for A-RoF systems was discussed, including concepts of C-RAN, A-RoF, non-linear devices, ANNs and linearization schemes. The C-RAN and A-RoF are key cost-effective solutions for providing connectivity in remote and rural areas, since reduce the maintenance and implementation costs. It was also discussed the concepts of non-linear devices. Understanding the non-linear device response allows for the identification and mitigation of undesirable effects on the system. By comprehending non-linear system behavior, it is possible accurately modeling and characterize the non-linearities present in the system. This knowledge serves as the foundation for developing effective linearization techniques that counteract the non-linear effects and restore linearity within the system. Moreover, the knowledge of the system non-linear behavior is also required to select the most appropriated approach to effectively mitigate the non-linear effects.

This chapter also presented a discussion about ANNs which is crucial for designing ML-based linearization schemes. ML-based solutions enable accurate modeling of complex non-linear systems. Understanding ML allows for choosing the most appropriated ANN architecture, and optimization techniques for improving the system linearity, reducing distortions, and enhancing the overall system performance.

Chapter 3

Summary of Original Work

This thesis is based on a set of papers published or submitted for publication in peer-reviewed journals, conference proceedings. These papers present the main results on the use of ML-based algorithms for linearization of A-RoF systems. The set of papers bringing the main contributions of this work are presented below.

Paper 1: Linearization Schemes for Radio Over Fiber Systems Based on Machine Learning Algorithms

Luiz Augusto Melo Pereira, Luciano Leonel Mendes, Carmelo José Albanez Bastos-Filho and Arismar Cerqueira Sodré Junior. " Linearization Schemes for Radio Over Fiber Systems Based on Machine Learning Algorithms", *IEEE Photonics Technology Letters*, vol. 34, no. 5, pp. 279-282, March, 2022.3

Publisher: IEEE Photonics Society

Linearization Schemes for Radio over Fiber Systems Based on Machine Learning Algorithms

Luiz A. M. Pereira, Luciano L. Mendes, Carmelo J. A. Bastos-Filho and Arismar Cerqueira S. Jr

***Abstract*—This work is regarding the concept and implementation of pre- and post-distortion schemes idealized for analog radio-over-fiber (A-RoF) systems. A-RoF systems have been considered potential to increase the capillarity of future mobile networks. However, the integration of the radiofrequency (RF) and optical systems might introduce nonlinearities that increase the in-band and out-band interferences. The proposed schemes employ a multi-layer perceptron (MLP) artificial neural network (ANN) linearization for reducing the signal distortions. We have applied our linearization schemes to orthogonal frequency division multiplexing (OFDM) signals for investigating its performance, in terms of root mean square error vector magnitude (EVM_{RMS}), normalized mean square error (NMSE) and adjacent channel leakage ratio (ACLR). Numerical results demonstrate promising linearization performance, since the EVM_{RMS} has been kept as low as 3%, attaining NMSE and ACLR lower than below -30 dB and -35 dB, for input RF power up to 23 dBm.**

***Index Terms*—Artificial neural network, machine learning, pre-distortion, post-distortion and radio-over-fiber.**

I. Introduction

OPTICAL communication systems have been integrated with wireless access networks for combining fiber optics high capacity and wireless transmission flexibility. Analog RoF (A-RoF) systems constitute a key solution for fifth generation of mobile communications (5G) that exploit centralized radio access networks (C-RANs) [1]. A-RoF favors the network function centralization, which brings important benefits, such as sharing the network's resources, reduction of deployment costs and the system maintenance/operation simplification [2].

One of the 5G premises is to provide ubiquitous connectivity, which includes covering the enhanced remote area communications (eRAC) scenario [3]. However, in this operating scenario, the few potential subscribers discourage infrastructure investment. In this context, some cost-effective solutions are being conducted, including the Remote Area Access Network for the 5th Generation (5G-RANGE) project [4], which aims for exploiting TV white space (TVWS) opportunities for providing 5G communications in eRAC scenario. In this way, reducing the signal's out-of-band emissions (OOBEs) is of major concern to avoid co-channel interference.

In A-RoF systems, a Mach-Zehnder modulator (MZM) is employed for modulating the optical carrier with the radiofrequency (RF) signal. The MZM response might be modeled as a linear function for small signals. However, in this work we are especially interested in a flexible RF power allocation to maximize the electrical-to-optical conversion efficiency, enabling to cover different remote regions [5]. Therefore, a linearization scheme might be applied to reduce the signal OOBE due to a nonlinear RF-photonics response. Table I presents a comparison among our proposals and others form the state-of-art linearization schemes. One can note our approach provides lower complexity when compared to other solutions. The main reason for this outcome is the fact that memory effect can be neglected to properly tackle the non-linearities introduced by the MZM [6]. As a result, a simple artificial neural network (ANN) structure is recommended and employed, allowing the use of a multi-layer perceptron (MLP) ANN.

TABLE I
State-of-the-art on A-RoF Linearization Schemes

Reference	Type	Memory	Complexity
[7]	Volterra-based	Yes	High
[8]	ANN-based	Yes	High
[9]	ANN-based	No	Medium
[This work]	ANN-based	No	Low

This letter reports the proposal and implementation of two machine learning (ML)-based linearization schemes especially designed to reduce the RF-photonics distortions. Typically, pre-distortion schemes are preferable over post-distortion ones, since they are able to mitigate the spectral regrowth produced by the MZM non-linearities, preventing the occupation of a wider channel bandwidth. Moreover, the pre-distortion schemes operate at high signal-to-noise ratio (SNR), which means that the noise statistics on the receiver side are unchanged. On the other hand, the main advantage of the post-distortion scheme is that it can be employed to also compensate the linear distortions introduced by the channel, acting as an equalizer, although it would not prevent the channel spectrum regrowth and the noise at its output will be colored. Therefore, it is expected that the pre-distortion schemes outperform the post-distortion ones.

The paper main goal is to expand the dynamic range of the A-RoF system, which enables to extend the mobile communication coverage. Our proposal also benefits a flexible

This work was supported by RNP-MCTIC Grant No. 01245.020548/2021-07, under the 6G project, CNPq, CAPES, FINEP and FAPEMIG.

L. A. M. Pereira, L. L. Mendes and Arismar Cerqueira S. Jr are with the Inatel, Santa Rita do Sapucaí, MG 37540-000 Brazil (e-mails: luiz.augusto@dtel.inatel.br, {luciano,arismar}@inatel.br).

C. J. A. Bastos-Filho is with the University of Pernambuco, Recife, PE 50100-010 Brazil (e-mails: carmelo.filho@upe.br).

Digital Objective Identifier 10.1109/LPT.2022.3151616

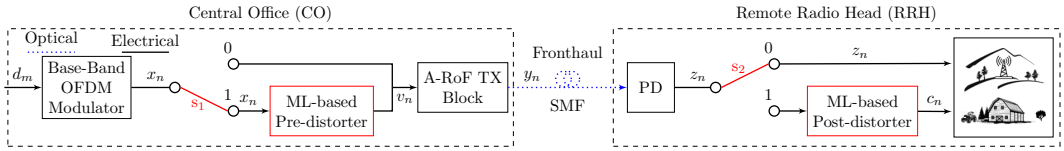

Fig. 1. Analog Radio over fiber block diagram assisted by the proposed machine learning-based linearization schemes.

and dynamic RF power allocation to serve distinct unserved or underserved remote regions. Moreover, the proposed linearization schemes also allow the transmitted RF power increment without producing significant distortions, favoring the peaceful coexistence with legacy systems in TVWS applications.

II. ML-based Pre- and Post-Distortion Schemes

A flexible RF power allocation is a key feature to cover distinct remote regions. However, as RF power increases, the RF signal distortions become more severe, decreasing the overall system performance. In this case, a linearization scheme must be employed for reducing the signal distortions. In this paper we will consider two possibilities for introducing the linearization scheme, as presented in Fig. 1. In this diagram, the switches s_1 and s_2 define which scheme is employed. For s_1 in position 1 and s_2 in position 0, pre-distortion scheme is selected. For s_1 in position 0 and s_2 in position 1, the post-distortion scheme is used. It will be assumed that the central office (CO) is connected with the core network by an optical backhaul link. The CO is composed of an orthogonal frequency division multiplexing (OFDM) baseband modulator, a pre-distorter block (when applicable), and a A-RoF TX block, which is composed of a laser diode (LD) and a MZM, located at remote radio head (RRH). The generated OFDM signal is given by

$$x_n = \sum_{m=0}^{M-1} d_m e^{-j2\pi \frac{m}{M}(n+1)}, \tag{1}$$

where n represents the nth sample from the total N samples, d_m is the quadrature amplitude modulation (QAM) data symbols, which are split in M orthogonal subcarriers. The complete linearization process was divided into two major distinct steps as shown in Sections II-A, and II-B.

A. Post-inversion Model Estimation

In this first step, we have used an ANN for estimating the system post-inversion model. We fed the ANN with a data set containing samples from an OFDM signal distorted by the MZM nonlinearities. The aforementioned data set was generated by considering s_1 and s_2 in position 0, leading to $v_n = x_n$. In this case, y_n is given by

$$y_n = \sum_{j=0}^{J-1} h_j |v_n|^j v_n, \tag{2}$$

where h_j is the model coefficients, with $j = 0, 1, ..., J-1$, J stands for the nonlinearity model order, v_n is the nth sample of the OFDM signal described by (1) and y_n is the nth sample at the A-RoF TX block output. The nonlinear model represented by (2) refers to a memoryless polynomial model [6]. Similarly to [6], we have used $J = 5$ for modeling the MZM nonlinearities.

We have employed a MLP ANN for obtaining the A-RoF post-inversion model. As illustrated in Fig. 2, the ANN is composed of $L+1$ layers, each one of them containing O_ℓ neurons with $\ell \in \{0, ..., L+1\}$. The input and output layers have two neurons ($O_0 = O_{L+1} = 2$), since we have fed the ANN with the real $\mathbb{R}(z_n)$ and imaginary $\mathbb{I}(z_n)$ parts of z_n. The ANN is trained using the backpropagation algorithm for calculating the gradient descent. In this algorithm, the error between an estimated output ($\hat{x}_n$) and the desired labeled samples (x_n) are backpropagated for optimizing the weights and, consequently, minimizing the cost function.

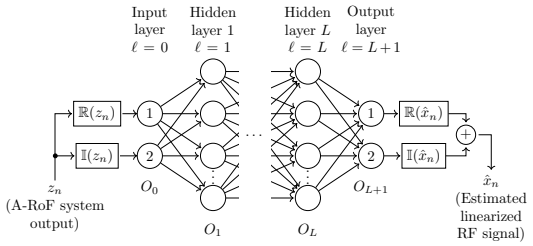

Fig. 2. Diagram of MLP artificial neural network architecture

Fig. 3 illustrates the ANN training process for obtaining the post-inversion estimation, which is based on a linear regression technique. A matrix of weights ($\mathbf{W}$) is calculated for producing the MZM component nonlinear inverse response. The $Loss$ function represents the training error or loss given by

$$Loss(\mathbf{W}, \mathbf{b}) = \frac{1}{N_{\text{TR}}} \sum_{n=1}^{N_{\text{TR}}} \mathcal{L}(x_n, \hat{x}_n(\mathbf{W}, \mathbf{b})), \tag{3}$$

for which N_{TR} is the number of training instances and $\mathcal{L}$ represents the loss function. During the ANN training process, the loss function is minimized to reduce the discrepancy

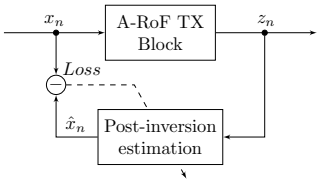

Fig. 3. Block diagram of the ML-based post-inversion estimation.

between the estimated ANN output ($\hat{x}_n$) and the labeled training signal (x_n).

B. Pre- and Post-distortions Schemes

Fig. 4 presents the pre-distortion block diagram, which was selected by setting s_1 and s_2 switches to positions 1 and 0, respectively. The pre-distorter block applies the previously trained ANN for producing a pre-distorted signal given by

$$\mathbf{v} = \sum_{\ell=0}^{L+1} \phi(\mathbf{W}_\ell \times \mathbf{x}_\ell + \mathbf{b}_\ell), \tag{4}$$

where $\mathbf{v}$ is the vectored version of v_n, $(.)_\ell$ denotes the ℓth layer from the ANN, $\mathbf{W}$ is the matrix of trained weights, $\mathbf{b}$ is the biases vector and $\phi(.)$ is the nonlinear activation function. It is important to note that for the input layer ($\ell = 0$), $\mathbf{x}_0$ is given by (1), with $\mathbf{x} = [x_0, x_1, ..., x_{N-1}]^T, \mathbf{x} \in \mathbb{C}^{N\times 1}$. For the next layers ($\ell = 1, ..., L+1$), $\mathbf{x}$ is given by the preceding layer output, since the ℓth layer is fully connected with the $(\ell-1)$th layer.

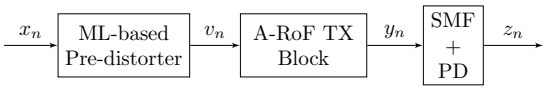

Fig. 4. Block diagram of the pre-distortion scheme

After the pre-distortion, v_n is applied to the A-RoF TX block, which is modeled by (2). The signal at A-RoF TX block output (y_n) is launched into a single-mode fiber (SMF) up to a photodetector (PD). In this paper, we generically assume that the SMF and PD responses are given by an unit impulse response g_n. In other words, we have not considered the linear and nonlinear effects of fiber-optics transmissions and also the noises produces in the photodetection process. Thereby, the proposed ML-based schemes focus on reducing the MZM nonlinearities. Considering the above assumptions, the linearized signal is given by

$$z_n = y_n * g_n + w_n, \tag{5}$$

where $(.)*$ represents the convolution operation, g_n is the nth sample of the impulse response and w_n is the nth sample of the uncorrelated Gaussian noise.

Alternatively, the RF signal could also be linearized using the post-distortion scheme depicted in Fig. 5, considering that s_1 is in position 0 i.e. $x_n = v_n$ and s_2 is in position 1. Considering the same assumptions made in the pre-distortion case, the signal at PD output is obtained by applying (5). Similarly to the pre-distorter block, the post-distorter block applies the trained ANN for obtaining a linearized version of the OFDM signal (c_n) by applying (4), with z_n as input.

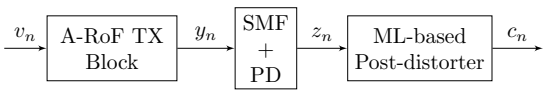

Fig. 5. Block diagram of the post-distortion scheme

III. Results

This Section reports the proposed linearization schemes results, aiming to cover eRAC applications by exploiting TVWS opportunities. We also report the procedure for training the ANN, including its hyperparameters. The MLP architecture used in this work presents a trade-off between simplicity and capacity for operating with nonlinear continuous variables.

In our proposed MLP ANN input layer, two neurons were employed with no activation function. Such network configuration was also applied to the output layer since the ANN output must be the linearized version of the OFDM signal. In summary, two hidden layers are capable of performing a regression task if the used activation function are nonlinear. Considering the aforementioned proposed operating scenario, two hidden layers were the smallest tested dimension that produced a trade-off between complexity and performance. In the first and second hidden layers, 32 and 16 neurons were employed, respectively. Such neuron numbers were obtained by accomplishing preliminary tests. Regarding the activation function, we have tested rectified linear unit (ReLU), scaled exponential linear unit (SELU) and tanh, which have produced similar results, so we have opted for ReLU for performance evaluation. Furthermore, we have noted that increasing the neuron numbers in the hidden layers will only generate unnecessary complexity since no performance increase was noted. We have used $N_{\text{TR}} = 71680$ and 30720 samples for training and validating the ANN, respectively. The training was done using the Adaptive Momentum (Adam) solver [10], considering batch sizes with 1024 samples throughout 5000 epochs. We have monitoring the mean-squared error (MSE) as a stop criterion ($\Delta_{min} = 10^{-15}$), with patience hyperparameter set to 250, which has lead to 2252-epochs training. The ANN was trained using the MSE loss function, defined as

$$\mathcal{L} = (a_n - b_n)^2, \tag{6}$$

We have trained the ANN considering 20-dBm OFDM signals at 45 dB SNR, resulting in an initial 0.5% root mean square error vector magnitude (EVM_{RMS}).

The performance of the linearization schemes was evaluated in terms of EVM_{RMS}, which is given by

$$\text{EVM}_{\text{RMS}}(\%) = 100\sqrt{\frac{\sum_{m=0}^{M-1} \left|d_m - \hat{d}_m\right|_2^2}{\sum_{m=0}^{M-1} |d_m|_2^2}}, \tag{7}$$

where $|(.)|_p$ is the p-norm operator and $\hat{d}_m$ is the mth complex data received on the mth subcarrier of the OFDM signal. The normalized mean squared error (NMSE) is another important metric. It enables to evaluate the discrepancy between two signals and is defined as

$$\text{NMSE (dB)} = 10\log\left(\frac{\sum_{n=0}^{N-1} |x_n - z_n|_2^2}{\sum_{n=0}^{N-1} |x_n|_2^2}\right). \tag{8}$$

The adjacent channel leakage ratio (ACLR) metric is used for evaluating the signal OOBE and is defined as

$$\text{ACLR (dB)} = 10\log\left(\frac{\int_{f\in B_O} P_y(f)df}{\int_{f\in B_I} P_y(f)df}\right), \quad (9)$$

where $P_y(f)$ denotes the power spectrum density (PSD) of y_n at frequency f, B_O defines the out-band and B_I defines the in-band-frequencies range.

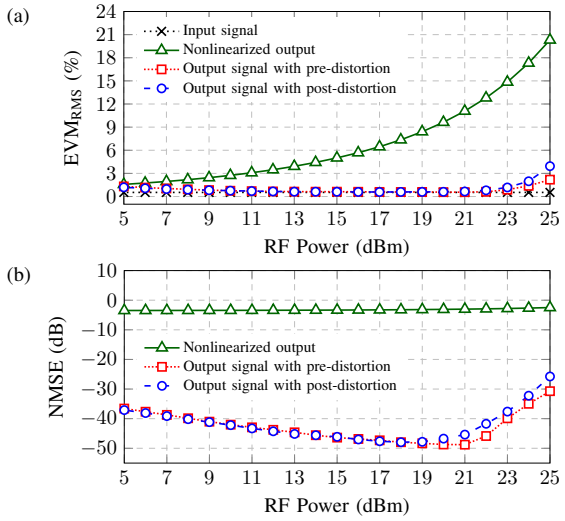

Fig. 6. Proposed linearization schemes performance as a function of RF Power at MZM input: (a) EVM$_{RMS}$; (b) NMSE.

Fig. 6 (a) presents the EVM$_{RMS}$ as a function of RF power at the MZM input for pre- and post-distortion schemes. The performance evaluation was carried out considering RF powers from 5 to 25 dBm. The pre-distortion slightly outperforms the post-distortion, however, both schemes present a remarkable improvement of the EVM$_{RMS}$ when compared with the nonlinearized signal, resulting in EVM$_{RMS}$ as low as 3% for almost the entire analyzed RF power range. Fig. 6 (b) presents the NMSE results. We can note that the NMSE is minimum at 19 dBm, which is close to the RF power used for training the ANN. Furthermore, for almost the entire analyzed RF power range, the NMSE was kept below than -30 dB, which can be considered an excellent ANN generalization capability.

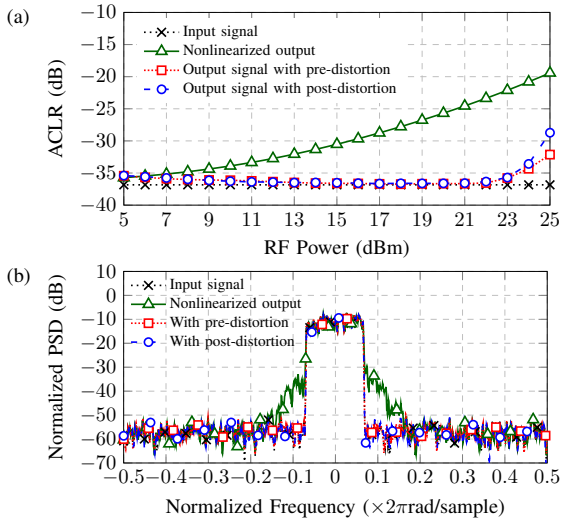

Fig. 7. Proposed linearization schemes performance in terms of OOBE: (a) ACLR; (b) normalized PSD.

We have also investigated the linearization schemes performance in terms of OOBE. Fig. 7 (a) reports the ACLR results. We can note that both linearization schemes have produced a significant ACLR reduction when compared to the nonlinearized output. When applying one of the proposed schemes, the ACLR was kept below -35 dB for the input RF power below 23 dBm. The ACLR reduction can also been seen in Fig. 7 (b) for input RF power of 20 dBm. We can observe that without a linearization technique, the A-RoF nonlinearities results in high OOBE, which might become prohibitive in TVWS applications. As demonstrated in Fig. 7 (b), the pre- and post-distortion schemes are able to drastically reduce the OOBE. Hence, the linearization schemes allows the coexistence of A-RoF signals with legacy technologies.

IV. Conclusions

This paper presented novel pre- and post-distortion schemes based on ML for A-RoF systems. Our proposed schemes employ a MLP artificial neural network for linearizing an OFDM signal at A-RoF system output. It was numerically demonstrated both schemes provide high performance in terms of EVM$_{RMS}$, NMSE and ACLR. Moreover, it allows increasing of the transmitted RF power without producing significant signal distortions, favoring the peaceful coexistence with other systems, including Digital Television in TVWS applications. Finally, the proposed ML-based schemes might increase mobile telecommunication operators flexibility to dynamically allocate RF power in distinct remote regions. As future works, we envisage to validate and evaluate both pre- and post-distortion techniques in a real 5G fiber-wireless system.

References

[1] Y. Li, K. Satyanarayana, M. El-Hajjar, and L. Hanzo, "Analogue Radio Over Fiber Aided MIMO Design for the Learning Assisted Adaptive C-RAN Downlink," *IEEE Access*, vol. 7, pp. 21 359–21 371, 2019.

[2] M. A. Habibi *et al.*, "A Comprehensive Survey of RAN Architectures Toward 5G Mobile Communication System," *IEEE Access*, vol. 7, pp. 70 371–70 421, 2019.

[3] L. L. Mendes *et al.*, "Enhanced Remote Areas Communications: The Missing Scenario for 5G and Beyond 5G Networks," *IEEE Access*, vol. 8, pp. 219 859–219 880, 2020.

[4] W. Dias *et al.*, "Performance Analysis of a 5G Transceiver Implementation for Remote Areas Scenarios," in *2018 European Conference on Networks and Communications (EuCNC)*, 2018, pp. 363–367.

[5] X. Fan, X. Zhang, and Y. Liu, "Investigation on Nonlinear Characteristics of the Mach-Zehnder Intensity Modulator based on Bessel Series Expansion," in *Photonics and Optoelectronics Meetings (POEM) 2011: Optoelectronic Devices and Integration*, vol. 8333. International Society for Optics and Photonics, 2012, p. 833310.

[6] H. Chen *et al.*, "Experimental Investigation on Multi-Dimensional Digital Predistortion for Multi-Band Radio-over-Fiber Systems," *Optics express*, vol. 22, no. 4, pp. 4649–4661, 2014.

[7] M. Noweir *et al.*, "Digitally Linearized Radio-over Fiber Transmitter Architecture for Cloud Radio Access Network's Downlink," *IEEE Transactions on Microwave Theory and Techniques*, vol. 66, no. 7, pp. 3564–3574, 2018.

[8] G. Paryanti *et al.*, "A Direct Learning Approach for Neural Network based Pre-distortion for Coherent Nonlinear Optical Transmitter," *Journal of Lightwave Technology*, vol. 38, no. 15, pp. 3883–3896, 2020.
[9] H.-M. Nguyen *et al.*, "> 55-Gbps and 30-dB Loss Budget LR-OFDM PON Downstream Enabled by ANN-based Predistortion," in *Optical Fiber Communication Conference*, 2021, pp. M3G–4.
[10] D. Kingma and J. Ba, "Adam: A Method for Stochastic Optimization," *International Conference on Learning Representations*, 12 2014.

Paper 2: Machine Learning-based Linearization Schemes for Radio over Fiber Systems

Luiz Augusto Melo Pereira, Luciano Leonel Mendes, Carmelo José Albanez Bastos-Filho and Arismar Cerqueira Sodré Junior. " Machine Learning-based Linearization Schemes for Radio over Fiber Systems", *IEEE Photonics Journal*, vol. 14, no. 6, pp. 1-10, September, 2022.

Publisher: IEEE Photonics Society

Machine Learning-based Linearization Schemes for Radio over Fiber Systems

Luiz A. M. Pereira, Luciano L. Mendes, Carmelo J. A. Bastos-Filho and Arismar Cerqueira S. Jr

***Abstract*—This manuscript proposes a novel machine learning (ML)-based linearization scheme for analog radio-over-fiber (A-RoF) systems with external modulation. The proposed approach has the advantage of not requiring new training campaigns in case the Mach-Zehnder modulator (MZM) parameters are changed over time. Our innovative digital pre-distortion (DPD) was designed to favor enhanced remote areas (eRAC) scenarios, in which the non-linearities introduced by the MZM become more severe. It employs a multi-layer perceptron (MLP) artificial neural network (ANN) to model the A-RoF system and estimate its post-inverse response, which is then applied to the DPD block. We investigate the ML-based DPD performance in terms of adjacent channel leakage ratio (ACLR), normalized mean square error (NMSE), resultant signal root mean square error vector magnitude error (EVM_{RMS}), and complexity. Numerical results demonstrate that the intended DPD method is less complex and outperforms the orthogonal scalar feedback linearization (OSFL) scheme, which has been considered a state-of-the-art DPD technique. The proposal has the potential to effectively and efficiently compensate for the A-RoF nonlinear distortions, especially in a time-variant system, without needing new training campaigns.**

***Index Terms*—Artificial intelligence, digital pre-distortion, machine learning, neural network and radio-over-fiber.**

I. Introduction

OVER the past few years, new services and applications for mobile communication networks have emerged, resulting in an exponential growth in data traffic at the radio access network (RAN) and backhaul network [1]. The fifth-generation of mobile network (5G) ecosystem encompasses a broad range of new applications, which are related to the most diverse sectors of the economy and market verticals [2].

To deal with the plethora of services, the 5G network was divided into three scenarios [3]: enhanced mobile broadband (eMBB), for providing higher data rates for the end-user; massive machine type communication (mMTC), for supporting a large number of power-limited devices connected to the network; ultra-reliable low-latency communication (URLLC), for reducing the network time response. Many enabling technologies are used to support the services expected in each scenario, including optical/wireless techniques employed in the fronthaul architecture [4]. Most of the applied technologies are prone to reduce cell coverage. Moreover, coverage is also limited in the URLLC and the mMTC scenarios, since the power limitation in the device and restriction on the symbol duration will limit the link budget and robustness against the long channel delay profile, respectively [5,6].

One scenario that has been attracting attention, especially in continental-sized countries, is known as enhanced remote area communications (eRAC) [7]. In this scenario, new business models and cost-effective solutions are required to offer connectivity for subscribers in remote and rural areas [8]. However, this network operating model is usually economically unattractive, since there are a few potential subscribers at these locations. Moreover, the capital expenditures (CAPEX) and frequency licenses have hindered the remote network deployment [7]. These restrictions must be overcome to finally offer connectivity in remote areas. Some initiatives have been proposed to address this problem. The Remote Area Access Network for the 5th Generation (5G-RANGE) project aims to exploit TV white space (TVWS) for 5G communications in remote areas [9]. The TVWS usage demands a low out-of-band emission (OOBE) waveform, which means the adjacent channel leakage ratio (ACLR) must be kept as low as possible for avoiding co-channel interference. The 5G Rural First project aims to allow local communities to exploit idle 3rd Generation Partnership Project (3GPP) bands in remote areas [10].

All the initiatives mentioned above show that reducing the cost of deploying the telecommunication infrastructure is key for successfully covering remote areas. In this case, analog RoF (A-RoF) technology [11] can play an important role in bringing connectivity to unserved or underserved regions since it might be efficiently used in the transport centralized radio access network (C-RAN) [12]. The centralization of the RAN functions allows sharing the processing resources among different services and applications, favoring the dynamic allocation and simplifying the network operation and maintenance. This approach reduces the CAPEX [1] and brings more flexibility for the Telecom operators since the radiofrequency (RF) power for one base station (BS) can be dynamically allocated according to the demand in each region. In C-RAN architectures, the core network is connected to the central office (CO) using a backhaul link. In contrast, the remote radio unit (RRU) is connected to the CO using a fronthaul link. Microwave and optical technologies might be applied in these links. A-RoF is particularly interesting since

This work was supported by RNP-MCTIC Grant No. 01245.020548/2021-07, under the 6G project, FAPESP Grant No. 20/05127-2, under SAMURAI project, CNPq, CAPES, FINEP and FAPEMIG.

L. A. M. Pereira, L. L. Mendes and Arismar Cerqueira S. Jr are with the Inatel, Santa Rita do Sapucaí, MG 37400-000 Brazil (e-mails: luiz.augusto@dtel.inatel.br, lucianol@inatel.br, arismar@inatel.br).

C. J. A. Bastos-Filho is with the University of Pernambuco, Recife, PE 50100-010 Brazil (e-mails: carmelo.filho@upe.br).

Manuscript received 4 August 2022; revised 15 September 2022, accepted 22 September 2022.

Digital Objective Identifier 10.1109/JPHOT.2022.3210454

it reduces the RRU complexity and occupied bandwidth in the optical link when compared to the digital RoF (D-RoF) [13].

Recent advances on 5G fronthaul solutions indicate to the replacement of D-RoF by A-RoF technology. Although D-RoF is currently widely employed, it presents scalability issues, high-power consumption and costly operation in the millimeter-wave frequency range. In [14], authors present a dual-band A-RoF system using a polarization control to switch the RF operating frequency and single-sideband modulation for reducing distortions caused by intermodulation products. A digital signal processing (DSP)-assisted A-RoF was proposed in [15], focused on reducing the sampling rate for a high-speed analog-to-digital converter (ADC) and digital-to-analog converter (DAC) in fronthaul links. Regarding fronthaul flexibility and latency demands, Datsika *et al.* demonstrate an A-RoF fronthaul assisted by a software-defined network (SDN), which enables dynamically performing network functional splits for minimizing the system latency.

In order to achieve high-speed modulation, the Mach-Zehnder modulator (MZM) is typically used to externally modulate the optical carrier with the RF signal. One challenge in this approach is to deal with the non-linearities introduced by the MZM as the input level of the RF signal increases. The MZM nonlinear response leads to a spectral regrowth, which is produced by the intermodulation products of the RF signal and is of major concern in TVWS application. Therefore, a limited input power must be applied to the MZM input or a linearization technique must be employed in order to minimize the signal distortion [16].

The digital pre-distortion (DPD) has been considered the most prominent solution for the linearization of nonlinear devices [17–20]. Recent advances in computational capacity and the increase in the available data sets have enabled new machine learning (ML) approaches, which might be applied in distinct network layers, aiming to deal with the unprecedented growth in the complexity of the communication systems [21,22]. For instance, in the sixth-generation of mobile network (6G) conception, ML-based solutions are considered an enabling technology for increasing the efficiency of distinct levels of the mobile networks [23]. Najarro *et al.* have described a model based on an artificial neural network (ANN) for distortion compensation by estimating the inverse response of a A-RoF system [24] . The received root mean square error vector magnitude (EVM_{RMS}) was the metric evaluated. Additionally, a DPD approach based on ANNs has been proposed by Hadi *et al.* [25]. Authors have shown a substantial reduction in EVM_{RMS} when compared to a Volterra-based approach. An ANN for simultaneously equalizing and decoding RF signals was reported in [26]. The ANN solution has outperformed the conventional Volterra equalization followed by a hard decision detection. In [27], authors have demonstrated an A-RoF system equalization using a multi-level ANN equalizer for compensating the nonlinear signal compression due to the in-band distortions. Liu *et al.* have proposed an ANN equalizer to mitigate the interference between multiple users in uplink transmissions [28].

Although the above works have considerably reduced the A-RoF distortions, a natural component response variation with time, due to aging and temperature drift, will require new training campaigns to maintain the system high-performance level. Moreover, the replacement of silicon components and/or fluctuations in the MZM polarization voltage might also demand for a new training campaign, since these variations would imply in a different nonlinear function [29].

This work main contribution is the proposal and implementation of a novel ML-based scheme for linearizing A-RoF systems, which is able to generalize possible variations of the MZM parameters for enabling a non-recalibrated DPD. The proposed linearization scheme does not demand new training campaigns when the MZM parameters change over time, promoting robustness against time variations in the nonlinear A-RoF system response in eRAC applications. The manuscript is structured in six sections. Section II describes the nonlinear model used for modeling the A-RoF system. Section III presents the theoretical background on DPD techniques. Section IV introduces the proposed ML-based DPD concepts, whereas the Section V reports its results. Finally, the conclusions and future works are drawn in Section VI.

II. Base-Band Equivalent Radio-over-Fiber Model

The scenario considered in this paper is depicted in Fig. 1. The Software-defined radio (SDR) approach is used to implement all the physical layer (PHY) and medium access control (MAC) functions of the base stations, which run at the CO server. It will be assumed that BSs will be used to provide connectivity to remote areas using eRAC, which means that low out-of-band emission is necessary [7]. The signal from remote radio head (RRH) is linearized by the proposed ML-based DPD approach and then applied to MZM. The fronthaul link is implemented using A-RoF due to its lower operational expenditure (OPEX), compared to the D-RoF solution. In case D-RoF is employed, OPEX is significantly increased for each additional kilometer between CO and RRH, which might hinder its use in the eRAC scenario [30]. A single CO might serve multiple eRAC sites. A single-mode fiber (SMF) is used to distribute the signal to all eRAC sites, where a photodetector (PD) converts the signal from the optical to electrical domain and a RRU radiate it over the covered area, giving rise to a fiber/wireless (FiWi) system. The RRU also receives the signals from the mobile users and converting them to the optical domain to be transmitted to the respective BS.

Typically, the MZM transfer function has a nonlinear periodical behavior, more specifically a cosine-shape function [31]. Although the MZM transfer function might be considered approximately linear for small signals [32], in this work we are interested in maximizing the electrical-to-optical (E/O) conversion efficiency by operating with flexible RF power for covering distinct remote regions. The E/O conversion efficiency is directly proportional to the RF input power, which will produce high levels of signal distortion, which consists of intermodulation products and harmonics of the carrier frequency. This distortion increases the OOBE parameter and reduces the EVM_{RMS}, affecting the overall performance of the system. Depending on the levels of the OOBE, it can even hinder the exploitation of TVWS [7].

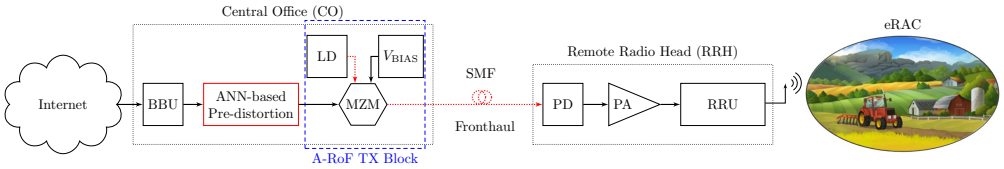

Fig. 1. Machine learning-assisted eRAC scenario; BBU-baseband unit; MZM-Mach-Zehnder modulator; SMF-single-mode fiber; PD-photodetector; PA-power amplifier; RRU-remote radio unit; eRAC-enhanced remote area communications.

The aforementioned operating scenario claims for a linearization technique to make possible increasing the RF input power and simultaneously reduce the signal distortion. One of the main approaches to achieve linearization consists of using a DPD technique before transmitting the RF signal to RRU. The DPD power response is the reciprocal of the MZM power response. Therefore, the combined power response of DPD and MZM is linear. The behavior of the classic DPD is defined by a model based on a set of coefficients, which are defined by a linearization algorithm.

A simplified version of the polynomial model from [17,33] has been applied to digitally linearize a A-RoF system. In our investigation, we have not considered the laser diode (LD) non-linearities, which might introduce a memory effect. However, as demonstrated in [33], the memory effect can be neglected in A-RoF systems, since it will not produce significant performance degradation. We have assumed a memoryless polynomial model with five coefficients, i.e. $J = 5$, which represents a trade-off between performance and complexity [33]. This non-linearity order was assumed in all evaluated scenarios. The memoryless polynomial model is given by

$$y_n = \sum_{j=0}^{J-1} h_j |v_n|^j v_n, \tag{1}$$

where J is the polynomial order, h_j are the model coefficients, with $j = 0, 1, ..., J-1$, v_n is the orthogonal frequency division multiplexing (OFDM) signal given by

$$x_n = \sum_{m=0}^{M-1} d_m e^{-j2\pi \frac{m}{M}(n+1)}, \tag{2}$$

with n representing the nth sample with $n = 0, 1, ..., N-1$ from the total N samples, d_m is the quadrature amplitude modulation (QAM) data symbols, which are split in M orthogonal subcarriers. y_n is the output discrete signal.

III. Digital Predistortion

The DPD has been widely used for mitigating signal distortions caused by nonlinear devices. The main DPD application is the linearization of high-power amplifier (PA), which typically presents a nonlinear system response. Similarly, the A-RoF systems also present a nonlinear response, imposed mainly by the MZM modulator. The DPD operating principle consists of pre-distorting the input signal by a function that is complementary to the nonlinear system. Therefore, the distortions introduced by the nonlinear device will cancel those added by DPD, linearizing the system response. The DPD distortions are ruled by a set of coefficients obtained according to a linearization algorithm. One of the most popular approach to extract the DPD coefficients is the Least Mean Square (LMS) algorithm. Fig. 2 illustrates the block diagram of a conventional DPD system. In this diagram, x_n is the discrete input signal, v_n is the pre-distorted signal with shape ruled by the coefficients ζ_j, and e_n is the error signal used to estimate the system response. The input signal x_n and output signal y_n feed the linearization algorithm, which calculates the coefficient ζ_j that produces an output signal y_n as similar to x_n as possible.

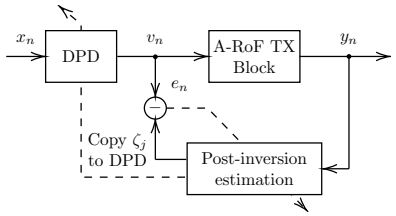

Fig. 2. Conventional DPD block diagram.

The scalar feedback linearization (SFL) is an alternative solution to linear-regression DPDs [34]. The basic idea of SFL is to optimize a scalar cost function ($C(\zeta_j)$) for obtaining the DPD coefficients. The scalar feedback does not require time synchronization and magnitude normalization, as the linear regression-based approaches. Distinct cost functions can be selected for reducing the OOBE, in-band distortions, or even both interferences. The main metrics used by the SFL DPD are the ACLR, EVM_{RMS}, and mean-squared error (MSE). While the ACLR is used to minimize the OOBE, the EVM_{RMS} is used to minimize the in-band interference. The MSE is employed to reduce both interferences. It is important to notice that by improving one metric, the other one will be also improved. For instance, a DPD optimized for the ACLR will also improve the EVM_{RMS} (and vice-versa). Since $C(\zeta_j)$ changes at each iteration, any generic mathematical linearization algorithm might be employed to optimize the cost function. The main drawback of the SFL is the inter-dependency among the coefficients. In other words, the evaluation of the jth coefficient ζ_j leads to the reevaluation of all previous coefficients $\zeta_1, \zeta_2, \ldots, \zeta_{J-1}$, which must be readjusted. This procedure increases significantly the overall convergence time.

In this paper we have compared our ML-based DPD solution with a state-of-the-art DPD technique known as orthogonal scalar feedback linearization (OSFL) [35], which represents a

pruned version of the SFL. Basically, the OSFL principle consists of the orthogonalization of the coefficients ζ_j, followed by numerical optimization of the scalar cost function. The main goal of the OSFL is to remove the inter-dependency among the coefficients, which means that the evaluation of one coefficient does not affect the previous one. The orthogonalization process is based on minimizing the difference (residual vector) when a new coefficient order are being adjusted. In other words, the orthogonalization produces a new coefficient set (ζ_{R_j}) that is incorporated in the DPD coefficients for promoting orthogonality. The coefficients ζ_{R_j} are obtained using a least squares estimation algorithm. It is important to highlight this process might be repeated for enhancing the predistortion accuracy. The OSFL approach provides faster convergence when compared with the SFL technique, since the orthogonalization of the coefficients simplifies the optimization phase.

The DPD algorithm complexity is an important parameter to be taken into account. The complexity analysis was carried out using the float-point operations (flops) counter method, where one flop is defined as one multiplication followed by and addition of two float-point numbers [36]. The orthogonalization algorithm applied to the SFL DPD reduces the complexity, since only J matrix inversion operation are required (once for each order) regardless the iterations of the optimization algorithm [35]. The complexity of an $n \times n$ matrix inversion is $\mathcal{O}(n^3)$. Since this process is going to be repeated J times, we can infer a computation cost of OSFL will be

$$\mathcal{O}\left(J\left((J-1)^3 + 2(J-1)^2(N+1) + 2(J-1)N\right)\right), \quad (3)$$

which has its complexity mainly governed by the least square estimation of ζ_{R_j}. Considering the dominant term of $\mathcal{O}$, we can infer that the OSFL DPD computation complexity will cubically increase with the polynomial model non-linearity order.

IV. ML-BASED DPD FOR A-ROF SYSTEMS

The ANN is a subclass of the ML algorithms that has been widely employed to solve complex computational tasks. A supervised ANN learns the relation among the input samples and the target labeled samples by using a set of training instances (N_{TR}), with the purpose of creating an approximated function to map the input and target data samples. An ANN has been considered an interesting tool to deal with nonlinear systems since it is capable of learning complex nonlinear behaviors.

This section presents two distinct A-RoF system DPD schemes based on machine learning. The first one was designed to linearize time-invariant systems, while the second one is used for time-variant systems. The second approach is interesting for optical/electronic components since their nonlinear responses can change over time due to aging and temperature drift. In a conventional DPD, the previously calculated coefficients must be recalculated to avoid signal distortion, while the solution for time-variant system proposed in this paper will accommodate these changes, adding robustness to the pre-distortion process and minimizing the need for periodical maintenance for the coefficients recalculation.

A. MLP ANN-based DPD for Time-Invariant Systems

Many nonlinear regression techniques have been widely adopted in recent works, such as Least Absolute Shrinkage and Selection Operator (LASSO), Random Forest, Support-vector Regressor (SVR) and multi-layer perceptron (MLP) [37–39]. The MZM non-linearities can be entirely modeled by a memoryless polynomial model. This statement is supported by [33], in which authors have proved that modeling the A-RoF system nonlinearities considering the memory effect will only unnecessarily increase the overall system complexity. For this reason, ANNs-based pre-distortion schemes that consider the memory effect were classified as high complexity solutions in our analysis. On the other hand, our proposed schemes employ a memoryless polynomial model, which is more appropriate to tackle the non-linearities introduced by the MZM. Once the memory effect might be neglected, a simpler ANN structure could be employed. Therefore, we have chosen the MLP for developing the ANN-based DPD, since it can be successfully deployed to represent continuous variables with nonlinear behavior. Although its simplicity, the MLP can be efficiently used for solving complex tasks.

The MLP is composed of several units or neurons densely connected in sequential layers. At least three layers are required for designing a MLP network, namely input layer, hidden layer and output layer. It has already been demonstrated in the specialized literature that a single-layer network can approximate any continuous function if there is enough data to train the neural network [40]. This means that a very simple neural network can already present high non-linear representation capacity, as long as we employ non-linear activation functions, have enough examples and computational resources to train the neural network. In this work, two hidden layers are enough to represent the nonlinearities imposed by MZM. Each connection between neurons is represented by a weights matrix $\mathbf{W}$ and a bias vector $\mathbf{b}$, which are calculated accordingly to the backpropagation algorithm to minimize a cost function. In summary, the backpropagation algorithm jointly with the solver compute the gradient of the loss function for the ANN current weights. Sequentially, the algorithm backpropagates the error for identifying its parcel related to each connection. Finally, the weights are updated aiming for minimizing the cost function.

Fig. 3 illustrates the proposed ML-based DPD for time-invariant systems. It is based on the indirect learning architecture, in which a post-inversion system response is obtained and the matrix of weights $\mathbf{W}$ is copied to the DPD block. In our approach, x_n is the original OFDM signal, whereas v_n is the pre-distorted signal at MZM input and y_n is the signal at MZM output, which is obtained by applying (1). In our work, an ideal feedback loop was considered for training the DPD coefficients. However, in real A-RoF systems, the required output feedback signal is typically a few kilometers far from CO. Our goal is to perform the training in an offline fashion rather than on-the-fly. This strategy implies in transmitting the labeled data from CO to the RRH, where signals are collected for the ANN training; once trained, ANN is not updated anymore. As a consequence, although costly, the training phase

only takes place once, since our solution is able to generalize variations in the A-RoF system time-response.

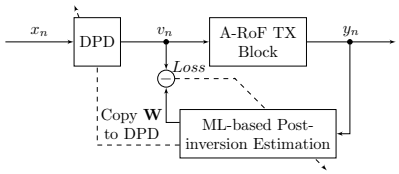

Fig. 3. Block diagram of the MLP ANN DPD designed for time-invariant systems

.

The MLP ANN is composed of $L+1$ layers, where each one of them contains O_ℓ neurons per layer with $\ell \in \{0, ..., L+1\}$. The post-inversion estimation is obtained by the ANN, as described in Fig.4. The ANN is fed by a data set containing two features, which represent the real $\mathbb{R}(\mathbf{y})$ and imaginary $\mathbb{I}(\mathbf{y})$ parts of an OFDM signal at the A-RoF system output. The target labels are composed of the real $\mathbb{R}(\mathbf{x})$ and the imaginary $\mathbb{I}(\mathbf{x})$ parts of a non-distorted OFDM signal at the MZM input.

Once trained, an MLP layer performs the following operation for a given input vector $\mathbf{x}$

$$\mathbf{v} = \phi(\mathbf{W} \times \mathbf{x} + \mathbf{b}), \tag{4}$$

where $\mathbf{W}$ is a matrix containing the MLP weights, $\mathbf{x}$ is the input vector, $\mathbf{b}$ is the biases vector, and $\phi(.)$ is the nonlinear activation function. Several activation functions, including sigmoid, rectified linear unit (ReLU), hyperbolic tangent function (tanh), scaled exponential linear unit (SELU) might be used [41]. Finally, the loss function to be minimized, which depends on the estimated instance $\hat{x}_n$ and desired instance x_n, is described as follows

$$Loss(\mathbf{W}, \mathbf{b}) = \frac{1}{N_{\text{TR}}} \sum_{n=0}^{N_{\text{TR}}-1} \mathcal{L}(x_n, \hat{x}_n(\mathbf{W},\mathbf{b})), \tag{5}$$

where N_{TR} is the size of the training set and $\mathcal{L}(.)$ is the loss function to be minimized by tuning $\mathbf{W}$ and $\mathbf{b}$.

The neural network performs nonlinear transformations in the input signal to compensate the A-RoF system distortions. It means that both input and output layers of the neural network must contain two features i.e., $O_0 = O_{L+1} = 2$, which represent the real and imaginary part of the OFDM symbol.

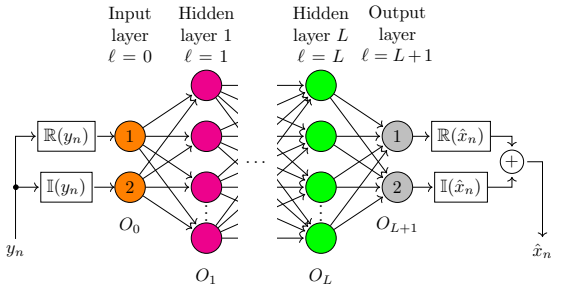

Fig. 4. Multi-layer perceptron artificial neural network architecture composed of the following layers: input layer ($\ell = 0$); hidden layers ($\ell = 1, ..., L$); output layer ($\ell = L + 1$). Each layer has O_ℓ neurons.

TABLE I
MULTI-LAYER PERCEPTRON ARTIFICIAL NETWORK HYPERPARAMETERS

	Input Layer	Hidden Layer 1	Hidden Layer 2	Output Layer
Number of Neurons	2	32	16	2
Activation Function	None	ReLU	ReLU	None
Learning Rate	10^{-3}			
Solver	Adam			

The training data set relied on a hundred OFDM symbols; each of them with a signal-to-noise ratio (SNR) equal to 45 dB and 1024 samples, resulting in 102400 instances. The other system hyperparameters are summarized in Table I. The hyperparameters were configured using a heuristic methodology, which means without a sophisticated random or grid search. Initially, we started with a few neurons per hidden layer. Sequentially, these hyperparameters were gradually increased accordingly with the DPD performance. According to our observations, 32 neurons in the first hidden layer and 16 neurons in the second one are the smallest dimensions for the hidden layers that outperform the conventional DPD. Additionally, we have noted that incrementing the number of neurons of each layer will only unnecessarily increase the algorithm complexity, with no additional performance gain. Regarding the activation function, we have tested the ReLU, SELU and tanh. However, the activation function has not considerably impacted on the results. Therefore, we have chosen the ReLU for performance evaluation. The number of hidden layers depends on the application however, typically one to five hidden layers are employed in regression problems [42]. We have chosen two hidden layers in our ML-based DPD, which have enabled a remarkable performance and employing more hidden layers will only unnecessarily increase the computational complexity.

We have also estimated the complexity of the ML-based DPD using the flops counting method. Since each layer output is obtained by (4), we can express the MLP complexity by

$$\mathcal{O}\left(\dim(\mathbf{y})O_0 + \sum_{\ell=1}^{L} O_{\ell-1}O_\ell + O_L O_{L+1}\right), \tag{6}$$

where $\dim(\cdot)$ returns the size of the input vector. Considering an ANN-based DPD, in which $O_{\ell-1} = 2O_\ell$ for $\ell \in \{2, \ldots, L\}$, wherein O_1 is the number of neurons from the first hidden layer and $O_0 = O_{L+1}$, the total cost is simplified to

$$\mathcal{O}\left(O_0(\dim(\mathbf{y}) + O_L) + 2LO_\ell^2\right). \tag{7}$$

Assuming now that $\dim(\mathbf{y}) \gg O_L$, then

$$\mathcal{O}\left(\dim(\mathbf{y})O_0 + 2LO_\ell^2\right), \tag{8}$$

which shows that the complexity of the proposed DPD grows linearly with the dimension of the input vector, the number of neurons of the input layer O_0 and the number of hidden layers L. Additionally, the complexity grows quadratically with the number of neurons from the hidden layers O_ℓ.

B. MLP Dual-ANN-based DPD for Time-Variant Systems

Two MLP ANNs were employed for dealing with the variability of the nonlinear system over time, since the nonlinear behavior of the MZM is not constant over time. Aging, temperature variation and fluctuations of the MZM polarization voltage can cause the nonlinear behavior of the system to vary over time. In order to analyze the proposed scheme capacity of accommodating these variations, a Gaussian distributed random variation of approximately 10% of the coefficient value has been added to each coefficient of the memoryless polynomial model, with the purpose of representing the time-variable non-linear behavior of the MZM. Our strategy for this case was to apply the ANN for modeling the A-RoF system and obtaining the post-inversion system estimation using another independent MLP ANN, as illustrated in Fig. 5. We have named this scheme as dual-ANN-based DPD. This enhanced approach brings robustness against time-variations of the A-RoF system nonlinear response.

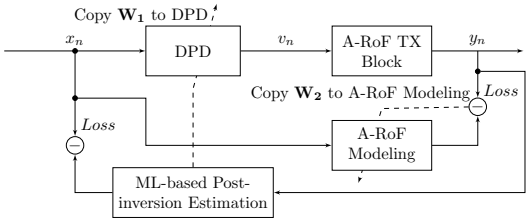

Fig. 5. Block diagram of MLP dual-DPD for time-variant systems

.

The post-inversion estimation from the time-variant system was obtained by applying the same approach from the time-invariant systems, generating the weights matrix $\mathbf{W_1}$, which is copied to DPD. To model the A-RoF system, the ANN must be fed with the non-distorted samples and the label samples are the distorted signal at the A-RoF output. The A-RoF ML-based modeling produces the second matrix of weights $\mathbf{W_2}$, which might be used for emulating the A-RoF system. Modeling the A-RoF system with an ANN has an important advantage that comes from the high capacity of ANN to mimic nonlinear systems. That means, the ANN is able to capture nonlinear behaviors that a polynomial model can not represent. Additionally, such modeling might contribute to simultaneously compensate other distortions beyond those from MZM.

Table I summarizes the main hyperparameters employed by the dual-ANN DPD for time-variant systems. Assuming that both ANNs were trained offline, the DPD process applied to the A-RoF system will have the same complexity derived in Section IV-A. Hence, considering the two ANN will run independently, the dual-ANN DPD scheme will present twice complexity when compared with the MLP ANN-based DPD presented in Section IV-A.

V. Performance Evaluation

This Section presents the proposed ML-based DPD results applied to the eRAC scenarios, aiming the exploitation of TVWS opportunities. All simulations presented in this work were performed for base-band discrete-time signals, since the pre-distortion processing is accomplished in the digital domain. In this case, we consider the OFDM signal at the reception side is in its base-band format and has already been converted from analog to digital. One important motivation for applying a DPD technique in this scenario is the possibility of dynamically allocate RF power to cover distinct regions, without producing prohibitive adjacent channels interference.

The novel ML-based DPD was implemented in Python using the high-level Tensorflow application programming interface (API) Keras. Its performance was investigated using three figures of merit, namely: EVM_{RMS}, ACLR and normalized mean square error (NMSE). The NMSE was used for estimating the time-domain error between the MZM input signal and linearized signal at the photodetector output. Moreover, we have compared our ML-based DPD with the OSFL scheme for two distinct cases, i.e. time-invariant and time-variant systems, which were described in Sections IV-A and IV-B, respectively. The same data set have been used for both cases, which was generated for a OFDM signals at 20-dBm electrical power, which produces considerable distortion in the A-RoF system output, in case no linearization technique is applied. The performance evaluation of the proposed DPD scheme for both scenarios, i.e. time-invariant and time-variant systems, was carried out using 16-QAM. The data set was partitioned into 70% of training instances, leading to N_{TR} = 71680 and 30% for validating the ANN. The MSE loss function, which is one of the metrics for evaluating regressors [43], was used for training the ANNs and is defined as

$$\mathcal{L} = (a_n - b_n)^2 \tag{9}$$

Fig. 6(a) depicts the MSE between the predicted and real target labels, as a function of the training epoch for the time-invariant system. This result might be extended for the time-variant system post-inverse estimation, once the same hyperparameters and data set were used. Once no overfitting or underfitting behaviors were observed, we can infer that all configured hyperparameters have produced an appropriate generalization capability. Such conclusion is ratified by Fig. 6(b), which is regarding the ML-based A-RoF modeling.

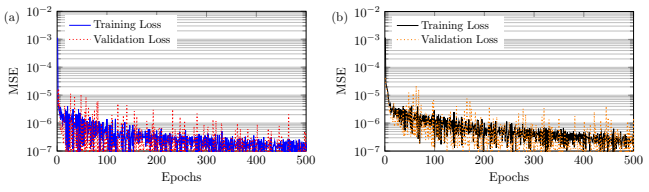

Fig. 6. Training and validation errors as a function of training epochs: (a) ML-based post-inversion esimation; (b) A-RoF modeling.

A. Performance of the MLP ANN DPD for time-invariant systems

Fig. 7 reports the EVM_{RMS} as a function of the electrical power at the MZM input for the time-invariant system. We have considered electrical power levels from 15 to 28 dBm

and an OFDM signal composed of 1024 samples for demonstrating the ML-based linearization performance compared to the OSFL and long short-term memory (LSTM) schemes. It is important to highlight the ANN DPD training was realized only for a specific power for the entire tested RF power range. Additionally, we have performed new training campaigns to investigate the best training RF power in terms of performance. As show in Fig. 7, using OFDM training symbols at 20 dBm leads to the best linearization result, for almost the entire analyzed RF power range, in comparison with the cases when the 15 and 28 dBm RF power levels are employed. The LSTM has only increased the complexity without improving the system performance, when compared with MLP and OSFL, since it was designed to process temporal data, which does not necessarily help to model the A-RoF system non-linearities. We are currently using ReLU activation function. Nonetheless, preliminary studies have demonstrated SELU can result in faster convergence time, without degrading the linearization performance. For the time-invariant system, we can note both DPD scheme has considerably reduced the EVM_{RMS} in comparison to the results without DPD. Furthermore, it is possible to observe that our proposed scheme has performed slightly better than the OSFL method for almost the entire analyzed power range. In addition, our approach is less complex, as already discussed in the previous Sections, making it promising for PHY layer optimization using machine learning.

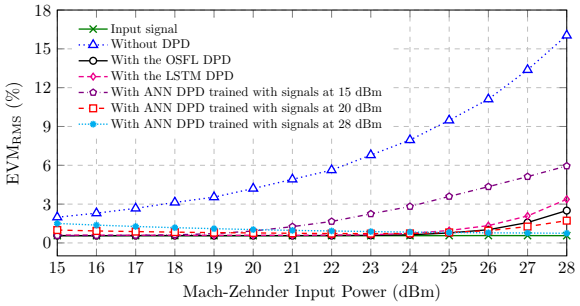

Fig. 7. EVM_{RMS} as a function of electrical power at the MZM input considering the time-invariant systems.

The second investigation was conducted by analyzing the frequency domain intermodulation using ACLR and the time-domain metric NMSE for calculating the error between the linearized and A-RoF output signals. Fig. 8 shows a normalized power spectrum density (PSD) for a 25-dBm OFDM signal. The ACLR metric defines the ratio between the undesired OOBE mean power and assigned channel frequency mean power. When DPD is not applied, the OOBE might become prohibitive, hindering the exploitation of TVWS. As can be seen, both DPD techniques have substantially reduced OOBE. Table II compiles the DPD techniques results. Our ML-based DPD solution provided ACLR = -36.2 dB and NMSE = -40.9 dB for an EVM_{RMS} of 0.91%. These results is close to the OSFL benchmarking, which achieved -36.6 and -43.44 dB for the ACLR and NMSE parameters, respectively, with EVM_{RMS} equal to 0.84%. It is important to note that for the analyzed polynomial model and ANN parameters, the computational complexity of the OSFL and ANN DPDs was 205.280k and 3.072k flops, respectively.

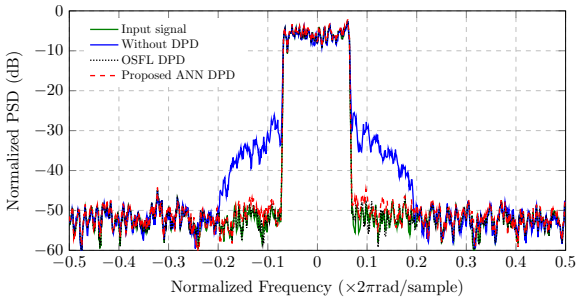

Fig. 8. Frequency spectrum for an OFDM signal without and with DPD for the time-invariant system at 25 dBm.

TABLE II
DPD PERFORMANCE FOR THE TIME-INVARIANT SYSTEM AT 25 DBM.

	Without DPD	OSFL DPD	LSTM DPD	ANN DPD
EVM_{RMS}(%)	9.62	0.84	0.96	0.91
ACLR (dB)	-23.1	-36.6	-36.0	-36.2
NMSE (dB)	-2.44	-43.44	-40.3	-40.9

We have also investigated the impact of variations in the A-RoF system nonlinear model, as a result of fluctuations in the MZM polarization voltage, in the ML-based DPD results. We refer to this case as a time-variant system. Table III shows a comparison of the DPD performance between the OSFL scheme and the proposed ML-based ANN DPD approach. The variation in the A-RoF system model coefficients has degraded the signal quality, which can be noted by comparing each column from Table II with the correspondent from Table III. As a conclusion, a new training campaign must be conducted in both cases for enhancing the DPD distortion reduction. In the next section, we present a second approach (dual-ANN DPD) to deal with this challenge feature in a dynamic scenario.

TABLE III
DPD PERFORMANCE FOR THE TIME-VARIANT SYSTEMS AT 25 DBM.

	Without DPD	OSFL DPD	LSTM DPD	ANN DPD
EVM_{RMS}(%)	9.85	5.05	5.11	4.60
ACLR (dB)	-23.02	-34.79	-35.80	-36.20
NMSE (dB)	-2.47	-27.45	-28.10	-28.99

B. Performance of the MLP dual-ANN DPD for time-variant systems

The dual-ANN DPD has been idealized to operate in cases that the nonlinear system response changes over time. In any case, it might also be applied to the static operating condition, in spite of presenting higher complexity, when compared to our first ML-based DPD approach. We have assumed that a time-variant nonlinear response has short and long terms components. The temperature drift over time results in a short-term instability to the system response. For instance, the environment temperature variation along the day might produce

fluctuations in the MZM polarization voltage, which could imply in the MZM operating point variation and, consequently, performance fluctuation. The long-term instabilities will be observed as the components ages. In this case, a new training session needs to be performed. Alternatively, we can employ the MLP dual-ANN DPD for time variant-systems, that is able to generalize the variations of the polynomial model coefficients, outperforming the OSFL scheme.

Any required change in the system will generate considerable expenses, since the skilled team would be necessarily sent to field, implying in travel and accommodation costs. This scenario could be even worse if the remote site is placed at hard-to-reach areas. In addition, the communication system must be periodically turned off for re-training the DPD algorithm whenever necessary, leaving customers without coverage. Therefore, although the time-variant response of the A-RoF components is typically slow, implementing a system that does not require changes will significantly reduce network operational expenditure.

Fig. 9 presents the EVM_{RMS} performance as a function of the electrical power at the MZM input. We have used a set of 100 OFDM symbols at 20 dBm for training the OSFL, LSTM and dual-ANN DPDs schemes. Our goal was to evaluate the generalization capacity of the DPD schemes when distinct RF powers are applied to the MZM input. Considering the time-variant system, the OSFL and LSTM scheme have not been shown efficient in terms of performance, since both will require a new training campaign because its polynomial model does not consider any changes in the coefficients model. Additionally, for low RF input power, using a DPD trained at 20 dBm might produce an overestimated pre-distortion that is not correspondent to the real observed distortion. In this case, the DPD block might produce a signal distortion that is even higher than not applying any DPD scheme. Therefore, the coefficients of the DPD must be re-estimated for low RF powers or DPD could even be turned off if the distortion level is acceptable. On the other hand, the dual-ANN DPD approach provided a remarkable distortion reduction, as a result of applying a second ANN for modeling the A-RoF system, which allowed to take advantage of the high-capacity of ANN to generalize and represent a nonlinear system. Therefore, in contrast to the OSFL and LSTM models, we can infer that our dual-ANN DPD scheme is capable to absorb variations in the model that represents the nonlinear system.

Similarly to the time-invariant system, we have also investigated the ACLR and NMSE metrics for the time-variant systems considering a 25-dBm OFDM signal. Fig. 10 reports the normalized PSD for the time-variant system. As expected, the OSFL scheme has presented higher intermodulation levels than the dual-ANN DPD approach, since it had not been designed for this operating condition. This result endorses the importance of a dynamic approach for linearizing signals in TVWS, by reason of high levels of spectral regrowth might severely interfere with adjacent channels. Table IV summarizes the statistics of the performance results for the time-variant system based on 10,000 runs. Our dual-ANN DPD solution enabled significantly reduce the mean EVM_{RMS} from 9.52 to 0.92%. The obtained mean ACLR=-36.54 dB and NMSE=-41.31 dB have also demonstrated its potential for distortion compensation. Furthermore, the dual-ANN DPD also has less computational complexity (6.144k flops) when compared with OSFL (205.280k flops).

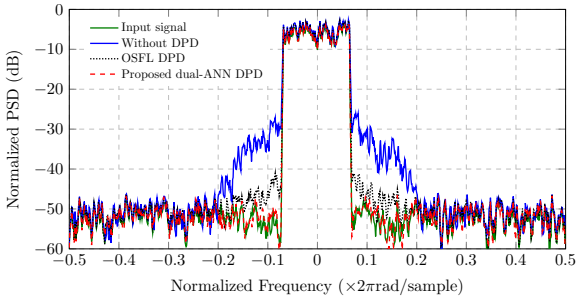

Fig. 10. Frequency spectrum for an OFDM signal without and with DPD for the time-variant system at 25 dBm.

TABLE IV
DPD PERFORMANCE FOR THE TIME-VARIANT SYSTEM AT 25 DBM.

	Without DPD		OSFL DPD		LSTM DPD		Dual-ANN DPD	
	μ	σ^2	μ	σ^2	μ	σ^2	μ	σ^2
EVM (%)	9.52	3.6	4.92	10.2	4.85	11.3	0.92	0.014
ACLR (dB)	-23.14	1.4	-35.61	1.2	-35.81	0.63	-36.54	0.10
NMSE (dB)	-2.48	0.3	-27.87	34.9	-28.3	39.5	-41.31	2.3

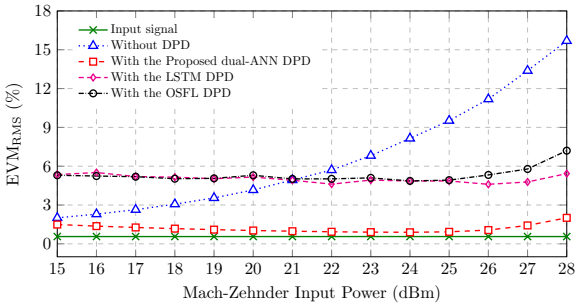

Fig. 9. EVM_{RMS} as a function of electrical power at the MZM input considering the time-variant systems.

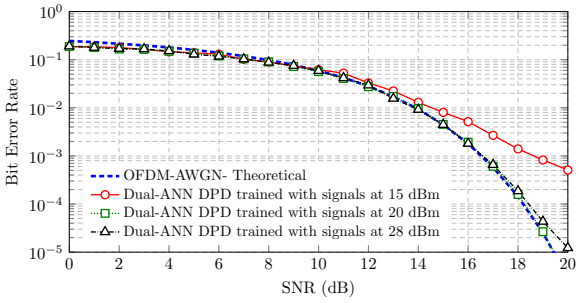

Fig. 11. Dual-ANN DPD performance as a function of SNR.

Finally, we have evaluated our proposed dual-ANN DPD performance in terms of bit error rate (BER). Fig. 11 presents the results of our proposed scheme compared with the theoretical OFDM-additive white Gaussian noise (AWGN) system, as a function of SNR. In this analysis, we have considered 15, 20 and 28 dBm of RF power at MZM input. It can be observed that for 20 dBm, our proposed dual-ANN DPD has produced a BER performance similar to the theoretical OFDM-AWGN. This achievement proves the excellent linearization performance of our DPD scheme, in case nonlinear distortions are introduced by the MZM. Additionally, we believe that the dual-ANN can play a distinguish role on the future mobile communication system, since ANN can learn complex nonlinear behaviors, such as the interactions between the linear and nonlinear effects of A-RoF systems.

VI. Conclusions

This paper presented, for the first time in literature, a digital pre-distortion scheme based on machine learning for radio over fiber systems considering a time-variant response. It employs an MLP artificial neural network to model the A-RoF system and estimate its post-inverse response, which is then applied to the DPD block. The main advantage of our dual-ANN DPD approach relies on not requiring new training campaigns when the A-RoF system parameters change over time, due to temperature variations, aging or fluctuation on the electro-optic modulator polarization voltage. Its performance has been compared to that of the OSFL scheme, considered a state-of-the-art solution, as a function of the three following figures of merit: ACLR, NMSE and EVM_{RMS}. It outperformed and has been shown simpler than OSFL. Particularly, the proposed ML-based linearizer allowed to significantly reduce mean EVM_{RMS} from 9.52 to 0.92% with mean ACLR=-36.54 dB and NMSE=-41.31 dB.

Moreover, our DPD solution is potential for reducing CAPEX and increase flexibility to the mobile network operators for dynamically allocating RF power for serving different regions. Furthermore, it can be efficiently applied to the future 5G networks in the eRAC scenario, exploiting TV white space. As future works, we envisage utilizing an even more realistic nonlinear model and testing other artificial neural network architectures. Additionally, we aim to experimentally validate our approach in a real 5G network.

References

[1] M. A. Habibi, M. Nasimi, B. Han, and H. D. Schotten, "A Comprehensive Survey of RAN Architectures Toward 5G Mobile Communication System," *IEEE Access*, vol. 7, pp. 70 371–70 421, 2019.

[2] H. Tullberg *et al.*, "The METIS 5G System Concept: Meeting the 5G Requirements," *IEEE Communications Magazine*, vol. 54, no. 12, pp. 132–139, 2016.

[3] A. Osseiran *et al.*, "Scenarios for 5G Mobile and Wireless Communications: The Vision of the METIS Project," *IEEE Communications Magazine*, vol. 52, no. 5, pp. 26–35, 2014.

[4] G. Kalfas *et al.*, "Next Generation Fiber-Wireless Fronthaul for 5G mmWave Networks," *IEEE Communications Magazine*, vol. 57, no. 3, pp. 138–144, 2019.

[5] M. Kamel, W. Hamouda, and A. Youssef, "Uplink Coverage and Capacity Analysis of mMTC in Ultra-Dense Networks," *IEEE Transactions on Vehicular Technology*, vol. 69, no. 1, pp. 746–759, 2020.

[6] C. Bockelmann *et al.*, "Massive Machine-Type Communications in 5G: Physical and MAC-layer Solutions," *IEEE Communications Magazine*, vol. 54, no. 9, pp. 59–65, 2016.

[7] L. L. Mendes *et al.*, "Enhanced Remote Areas Communications: The Missing Scenario for 5G and Beyond 5G Networks," *IEEE Access*, vol. 8, pp. 219 859–219 880, 2020.

[8] A. M. Cavalcante, M. V. Marquezini, L. Mendes, and C. S. Moreno, "5G for Remote Areas: Challenges, Opportunities and Business Modeling for Brazil," *IEEE Access*, vol. 9, pp. 10 829–10 843, 2021.

[9] W. Dias *et al.*, "Performance Analysis of a 5G Transceiver Implementation for Remote Areas Scenarios," in *2018 European Conference on Networks and Communications (EuCNC)*, 2018, pp. 363–367.

[10] 5G RuralFirst consortium, "5G RuralFirst: New Thinking Applied to Rural Connectivity," Departure for Digital, Culture, Media and Sports, Technical Report, October 2019, available at: https://www.5gruralfirst.org/wp-content/uploads/2019/10/5G-RuralFirst-New-Thinking-Applied-to-Rural-Connectivity-1.pdf.

[11] R. M. Borges *et al.*, "DSP-Based Flexible-Waveform and Multi-Application 5G Fiber-Wireless System," *Journal of Lightwave Technology*, vol. 38, no. 3, pp. 642–653, 2019.

[12] J. Capmany and D. Novak, "Microwave Photonics Combines Two Worlds," *Nature photonics*, vol. 1, no. 6, p. 319, 2007.

[13] I. Chih-Lin, H. Li, J. Korhonen, J. Huang, and L. Han, "RAN Revolution With NGFI (xHaul) for 5G," *Journal of Lightwave Technology*, vol. 36, no. 2, pp. 541–550, 2017.

[14] F. Shi, Y. Fan, X. Wang, W. Zhang, and Y. Gao, "High-Performance Dual-Band Radio-over-Fiber Link for Future 5G Radio Access Applications," *Journal of Optical Communications and Networking*, vol. 14, no. 4, pp. 267–277, 2022.

[15] P.-H. Ting, S.-H. Yu, Z.-W. Huang, C.-C. Wei, S. Chi, and C.-T. Lin, "Fronthaul Optical Links Using Sub-Nyquist Sampling Rate ADC for B5G/6G Sub-THz Ma-MIMO Beamforming," *IEEE Access*, vol. 10, pp. 236–243, 2021.

[16] J. Wang, C. Liu, M. Zhu, A. Yi, L. Cheng, and G.-K. Chang, "Investigation of Data-Dependent Channel Cross-Modulation in Multiband Radio-Over-Fiber Systems," *Journal of Lightwave Technology*, vol. 32, no. 10, pp. 1861–1871, 2014.

[17] M. Noweir *et al.*, "Digitally Linearized Radio-over Fiber Transmitter Architecture for Cloud Radio Access Network's Downlink," *IEEE Transactions on Microwave Theory and Techniques*, vol. 66, no. 7, pp. 3564–3574, 2018.

[18] A. Hekkala *et al.*, "Predistortion of Radio Over Fiber Links: Algorithms, Implementation, and Measurements," *IEEE Transactions on Circuits and Systems I: Regular Papers*, vol. 59, no. 3, pp. 664–672, 2012.

[19] X. Xie, M. Hui, T. Liu, and X. Zhang, "Hybrid Linearization of Broadband Radio-over-Fiber Transmission," *IEEE Photonics Technology Letters*, vol. 30, no. 8, pp. 692–695, 2018.

[20] L. A. M. Pereira, L. L. Mendes, C. J. A. Bastos-Filho, and S. Arismar Cerqueira, "Linearization Schemes for Radio Over Fiber Systems Based on Machine Learning Algorithms," *IEEE Photonics Technology Letters*, vol. 34, no. 5, pp. 279–282, 2022.

[21] J. He, J. Lee, S. Kandeepan, and K. Wang, "Machine Learning Techniques in Radio-over-Fiber Systems and Networks," in *Photonics*, vol. 7, no. 4. Multidisciplinary Digital Publishing Institute, 2020, p. 105.

[22] F. N. Khan, Q. Fan, C. Lu, and A. P. T. Lau, "An Optical Communication's Perspective on Machine Learning and Its Applications," *Journal of Lightwave Technology*, vol. 37, no. 2, pp. 493–516, 2019.

[23] K. B. Letaief, W. Chen, Y. Shi, J. Zhang, and Y.-J. A. Zhang, "The Roadmap to 6G: AI Empowered Wireless Networks," *IEEE communications magazine*, vol. 57, no. 8, pp. 84–90, 2019.

[24] A. C. Najarro and S.-M. Kim, "Nonlinear Compensation Using Artificial Neural Network in Radio-over-Fiber System," *Journal of information and communication convergence engineering*, vol. 16, pp. 1–5, 2018.

[25] M. U. Hadi, M. Awais, M. Raza, K. Khurshid, and H. Jung, "Neural Network DPD for Aggrandizing SM-VCSEL-SSMF-Based Radio over Fiber Link Performance," in *Photonics*, vol. 8, no. 1. Multidisciplinary Digital Publishing Institute, 2021, p. 19.

[26] Q. Zhou *et al.*, "Enhanced Multi-Level Signal Recovery in Mobile Fronthaul Network Using DNN Decoder," *IEEE Photonics Technology Letters*, vol. 30, no. 17, pp. 1511–1514, 2018.

[27] S. Liu *et al.*, "A Multilevel Artificial Neural Network Nonlinear Equalizer for Millimeter-Wave Mobile Fronthaul Systems," *Journal of Lightwave Technology*, vol. 35, no. 20, pp. 4406–4417, 2017.

[28] S. Liu, Y. M. Alfadhli, S. Shen, M. Xu, H. Tian, and G.-K. Chang, "A Novel ANN Equalizer to Mitigate Nonlinear Interference in Analog-RoF Mobile Fronthaul," *IEEE Photonics Technology Letters*, vol. 30, no. 19, pp. 1675–1678, 2018.

[29] D. Idris, Y. Le Moullec, and P. Eggers, "Design and Implementation of Self-Calibration for Digital Predistortion of Power Amplifiers," *WSEAS Transactions on Circuits and Systems*, vol. 7, p. 75, 02 2008.
[30] A. Udalcovs *et al.*, "Total Cost of Ownership of Digital vs. Analog Radio-over-Fiber Architectures for 5G Fronthauling," *IEEE Access*, vol. 8, pp. 223 562–223 573, 2020.
[31] V. J. Urick, J. F. Diehl, J. D. McKinney, J. M. Singley, and C. E. Sunderman, "Nonlinear Optical Angle Modulation for Suppression of RF Interference," *IEEE Transactions on Microwave Theory and Techniques*, vol. 64, no. 7, pp. 2198–2204, 2016.
[32] X. Fan, X. Zhang, and Y. Liu, "Investigation on Nonlinear Characteristics of the Mach-Zehnder Intensity Modulator Based on Bessel Series Expansion," in *Photonics and Optoelectronics Meetings (POEM) 2011: Optoelectronic Devices and Integration*, vol. 8333. International Society for Optics and Photonics, 2012, p. 833310.
[33] H. Chen *et al.*, "Experimental Investigation on Multi-Dimensional Digital Predistortion for Multi-Band Radio-over-Fiber Systems," *Optics express*, vol. 22, no. 4, pp. 4649–4661, 2014.
[34] B. D. Laki and C. J. Kikkert, "Adaptive Digital Predistortion for Wideband High Crest Factor Applications Based on the WACP Optimization Objective: A Conceptual Overview," *IEEE Transactions on Broadcasting*, vol. 58, no. 4, pp. 609–618, 2012.
[35] H. D. e. a. Rodrigues, "Orthogonal Scalar Feedback Digital Pre-Distortion Linearization," *IEEE Transactions on Broadcasting*, vol. 64, no. 2, pp. 319–330, 2018.
[36] S. Boyd, S. P. Boyd, and L. Vandenberghe, *Convex optimization*. Cambridge university press, 2004.
[37] K. et al, "A Least Absolute Shrinkage and Selection Operator (LASSO) for Nonlinear System Identification," *IFAC proceedings volumes*, vol. 39, no. 1, pp. 814–819, 2006.
[38] M. A. H. Shaikh and K. Barbé, "Study of Random Forest to Identify Wiener–Hammerstein System," *IEEE Transactions on Instrumentation and Measurement*, vol. 70, pp. 1–12, 2021.
[39] J. Xu, W. Jiang, L. Ma, M. Li, Z. Yu, and Z. Geng, "Augmented Time-Delay Twin Support Vector Regression-Based Behavioral Modeling for Digital Predistortion of RF Power Amplifier," *IEEE Access*, vol. 7, pp. 59 832–59 843, 2019.
[40] M. Sahay, "Neural Networks and the Universal Approximation Theorem," 2020. [Online]. Available: https://towardsdatascience.com/neural-networks-and-the-universal-approximation-theorem-8a389a33d30a
[41] C. Zhang, P. Patras, and H. Haddadi, "Deep learning in Mobile and Wireless Networking: A survey," *IEEE Communications surveys & tutorials*, vol. 21, no. 3, pp. 2224–2287, 2019.
[42] A. Géron, *Hands-on Machine Learning With Scikit-Learn, Keras, and TensorFlow: Concepts, Tools, and Techniques to Build Intelligent Systems*. O'Reilly Media, 2019.
[43] S. Singh and P. Dayan, "Analytical Mean Squared Error Curves for Temporal Difference Learning," *Machine Learning*, vol. 32, no. 1, pp. 5–40, 1998.

Luiz Augusto Melo Pereira received the B.Sc. and the M.Sc. degree in telecommunications engineering from the National Institute of Telecommunications (Inatel), Brazil, in 2017 and 2020, respectively and is a PhD student in telecommunications in the same institution.

Luciano Leonel Mendes received the B.Sc. and M.Sc. degrees from Inatel, Brazil, in 2001 and 2003, respectively, and the Doctor degree from Unicamp, Brazil, in 2007, all in electrical engineering. From 2013 to 2015, he was a Visiting Researcher with the Technical University of Dresden in the Vodafone Chair Mobile Communications Systems, where he has developed his postdoctoral. Since 2001 he is a professor at Inatel, where currently he acts as the Research Coordinator of the Brasil 6G project.

Carmelo José Albanez Bastos Filho (Senior Member, IEEE) was born in Recife, Brazil, in 1978. He received the B.Sc. degree in electronics engineering and the M.Sc. and Ph.D. degrees in electrical engineering from the Federal University of Pernambuco (UFPE) in 2000, 2003, and 2005, respectively. He is currently an Associate Professor with the Polytechnic School, University of Pernambuco. He authored or coauthored roughly 300 full papers in journals and conferences and advised more than 50 Ph.D. and M.Sc. candidates.

Arismar Cerqueira Sodré Junior received his Ph.D. degree from Scuola Superiore Sant'Anna-Italy in 2006. He was Invited Researcher and Professor from many world-recognized universities, such as Scuola Superiore Sant'Anna-Italy, University of Oulu, Danish Technical University-Denmark, Max-Planck Institute-Germany and University of Bath-UK. He is a holder of 12 patents, has transferred 25 products to the industry and has published over 300 scientific papers.

Paper 3: Machine Learning-based Digital Pre-Distortion Scheme for A-RoF Systems and Experimental 5G mm-waves Fiber-Wireless Implementation

Luiz Augusto Melo Pereira, Eduardo Saia Lima, Luciano Leonel Mendes and Arismar Cerqueira Sodré Junior. " Machine Learning-based Digital Pre-Distortion Scheme for A-RoF Systems and Experimental 5G mm-waves Fiber-Wireless Implementation", *Journal of Microwaves, Optoelectronics and Electromagnetic Applications*, vol. 22, no. 1, pp. 172-183, March, 2023.

Publisher: SciELO

Journal of Microwaves, Optoelectronics and Electromagnetic Applications, Vol. 22, No. 1, March 2023
DOI: https://doi.org/10.1590/2179-10742023v22i1270779

Machine Learning-based Digital Pre-Distortion Scheme for A-RoF Systems and Experimental 5G mm-waves Fiber-Wireless Implementation

Luiz A. M. Pereira, Eduardo S. Lima, Luciano L. Mendes, Arismar Cerqueira S. Jr.
National Institute of Telecommunications (Inatel)
510 João de Camargo Av., Santa Rita do Sapucaí-MG, Brazil, 37540-000.
luiz.melo@inatel.br, elima@get.inatel.br, lucianol@inatel.br, arismar@inatel.br

***Abstract*— The advent of the 5th generation of mobile networks brought a large number of new use case and applications to be supported by the physical layer (PHY), which must be more flexible than all previous radio access networks (RAN). The concept of the centralized RAN (C-RAN) allows all the baseband processing to be performed in the central office, simplifying the network deployment and also allowing the operators to dynamically control the PHY according with the applications requirements. The radio-frequency (RF) signal generated by the C-RAN can be transported to the remote radio unit (RRU) by using an analog radio over fiber (A-RoF) system. In this paper, we propose two A-RoF approaches for composing the transport and access networks of the next-generation systems. The first investigation relies on the implementation of a machine learning-based digital pre-distortion (DPD), designed for A-RoF systems. In the second approach, we implement an A-RoF system and characterize the optical and electrical power levels aiming to reduce the A-RoF non-linear distortions. The overall link performance is evaluated by measuring the error vector magnitude (EVM_{RMS}) and 590 Mbit/s is achieved with EVM_{RMS} as low as 4.4% in a 10 m reach cell.**

***Index Terms*—** 5G NR, digital pre-distortion, fiber-wireless system, machine learning, radio over fiber.

I. Introduction

Mobile communication systems have been continuously evolving to support new communications features and enhance user experience. The introduction of the fifth-generation of mobile network (5G) has been remodeling the way that society uses telecommunication systems. The previous mobile networks, especially the third and fourth generations (3G and 4G) were mainly focused on redesigning the radio access network (RAN) in order to increase the system throughput. On the other hand, the 5G networks aim to bring innovative services and applications, favoring new vertical services, such as security improvement, agribusiness, vehicular communications, logistics, education, and health. These new applications and services impose contrasting and conflicting requirements to the physical layer (PHY), which must be flexible to be dynamically adapted for each scenario [1]–[4].

The optical/wireless convergence brings remarkable advantages, in particular, analog RoF (A-RoF) technology is a key solution for transporting high-speed communications signals. The aforementioned technology favors the centralized radio access network (C-RAN) design [5]. In such a system, the

Brazilian Microwave and Optoelectronics Society-SBMO *received 0 Month 2020; for review 0 Month 2020; accepted 0 Month 2020*
Brazilian Society of Electromagnetism-SBMag *ISSN 2179-1074*

baseband processing is moved to a central office (CO), which allows sharing equipment and dynamic resource allocation leading to an expressive reduction in deployment costs [6]. The fronthaul link, which connects the CO and remote radio units (RRUs), might be implemented using wireless or optical technology. Typically, the optical link employs digital RoF (D-RoF) or A-RoF [7]. In addition, signal transmission using A-RoF allows combining optical and wireless advantages, giving rise to the fiber-wireless (FiWi) system.

In an A-RoF implementation, the RF signal is applied to a Mach-Zehnder modulator (MZM) in order to modulate the optical carrier. This solution increases the transmission data rate compared to direct modulation. However, the MZM presents a non-linear behavior, which means that the ratio between the MZM output and input signals is a function of the radiofrequency (RF) input power. Typically, the non-linearities become more severe as the RF input power increases, producing in-band and out-of-band distortions. As a consequence, a limited RF power must be applied to the MZM input for minimizing the non-linearities in the MZM output. On the other hand, for specific applications, such as enhanced remote area communications (eRAC), high RF power is desirable to overcome the long optical link distance. In this case, a digital pre-distortion (DPD) technique must be employed to reduce the impacts of the non-linearities in the A-RoF signal [8].

The A-RoF system linearization might be performed either in the electrical or optical domain [9]–[13]. The DPD is the most prominent electrical-domain linearization technique. In A-RoF systems, DPD is commonly based on the non-linear Volterra model and Volterra derived models, such as memory and memoryless polynomial models [14]–[16]. Recently, machine learning (ML) solutions have attracted considerable attention in the context of signal processing techniques, since it is capable of performing complex computational tasks while requiring small computational power, making it an interesting tool for DPD implementation [17]–[19]. Therefore, ML algorithms can have a distinguish role in A-RoF systems employed in future FiWi communication.

The state-of-the-art on FiWi-based 5G architectures includes the coexistence investigation of 4G and 5G services [20], digital signal processing (DSP) for mitigating A-RoF degradation [21] and 5G signals distribution over passive optical networks (PON) [22]. Specifically, our research group has recently reported a non-standalone FiWi system for simultaneously transmitting 4G and 5G signals [23]. In the context of DSP-assisted 5G systems, we have used DSP for generating and pre-distort 5G signals, in the frequency range 1 (FR1) and frequency range 2 (FR2), in a multi-band FiWi system [24]. Moreover, we have presented a 5G multi-band system, which takes advantage of an active gigabit passive optical network (GPON) capillarity to distribute 5G signals.

The current paper is an extended version of our previous work [25]. It reports a validation of a ML-based technique for linearizing a A-RoF system. Additionally, we have implemented a multi-band FiWi system focused on the enhanced mobile broadband (eMBB) scenario for next-generation networks [26]. Our demonstration reports the following 5G applications: a 3.5-GHz 5G new radio (5G-NR) signal transport and transmission to cover outdoor eMBB scenario; a 26-GHz 5G-NR signal transport and transmission for covering indoor eMBB applications. The manuscript is structured in five sections. Section II introduces the ML-based DPD scheme proposed to mitigate the non-linearities introduced by the MZM and evaluates its performance. Section III describes the multi-band FiWi system, whereas Sections IV and V present the experimental results and conclusions, respectively.

Brazilian Microwave and Optoelectronics Society-SBMO *received 0 Month 2020; for review 0 Month 2020; accepted 0 Month 2020*
Brazilian Society of Electromagnetism-SBMag *ISSN 2179-1074*

II. A Digital Pre-Distortion Scheme Based on a Machine Learning Technique

A. Methodology

A-RoF system can reduce the deployment and operational costs of mobile networks in remote areas. However, it is necessary to assure that the signals' characteristics at the A-RoF output, such as root mean square error vector magnitude (EVM_{RMS}) and out-of-band emission (OOBE), must be preserved. This means that the non-linearities introduced by the MZM must be compensated and the DPD is an efficient approach to achieve this goal. Conventional DPD schemes are very complex [15] and might require re-calibration over time. Therefore, we are proposing an ML linearization solution that is based on a linear regression technique. The employed artificial neural network (ANN) is composed of at least one input layer, one hidden layer, and one output layer, with non-linear activation functions.

The first architecture investigated in this paper is a multi-layer perceptron (MLP) ANN, which is the simplest ANN presented in the literature. In the MLP architecture, the neurons are densely connected. Each connection has its adjustable weights and bias. During the ANN training, the weights and bias parameters are adjusted accordingly to the backpropagation algorithm. In summary, the backpropagation training method uses a loss function to estimate the discrepancy between the ANN desirable training label and the ANN estimated output. During the training, the goal is to reduce the aforementioned discrepancy by updating the weights and bias set of parameters. The details of the architecture used to build the ML-based linearization scheme are presented below.

B. Artificial Neural Network Training

Fig. 1 illustrates the ANN training process. The desirable training labels consist of samples from a baseband orthogonal frequency division multiplexing (OFDM) signal (x_n), which are given by

$$x_n = \sum_{m=0}^{M-1} d_m e^{-j2\pi \frac{m}{M}(n+1)}, \tag{1}$$

where d_m represents the quadrature amplitude modulation (QAM) symbols that are mapped into M orthogonal subcarriers and $n \in \{0, 1, \ldots, N-1\}$ is the time index. Next, the OFDM signal is applied to the A-RoF TX block, which is composed by a laser diode (LD) and an MZM. The MZM has a non-linear power response, which can be represented by the base-band memoryless polynomial model, defined as [17]

$$y_n = \sum_{j=0}^{J-1} h_j |v_n|^j v_n, \tag{2}$$

where h_j is the jth model coefficient, with $j = 0, 1, \ldots, J-1$, in which J is the model non-linearity order. In this paper, we have used $J = 5$ to represent the MZM non-linearities. Since we are only interested in the MZM non-linearities, we have assumed that the single-mode fiber (SMF) and photodetector (PD) combined impulse response is $g_n = \delta_n$, leading to

$$z_n = y_n * g_n = y_n. \tag{3}$$

Brazilian Microwave and Optoelectronics Society-SBMO *received 0 Month 2020; for review 0 Month 2020; accepted 0 Month 2020*
Brazilian Society of Electromagnetism-SBMag *ISSN 2179-1074*

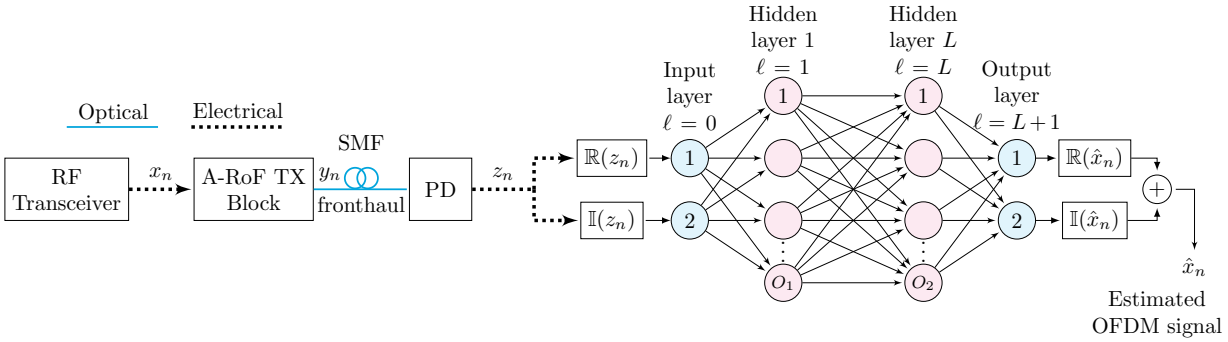

Fig. 1. MLP artificial neural network training process.

The PD output, z_n, is applied to train the ANN, whereas the training labels are the non-distorted OFDM signal, x_n. During the training, the ANN learns a function that approximates the A-RoF TX block post-inversion response, that will be used to pre-distort the OFDM signal.

The proposed ANN is composed of one input layer, two hidden layers, and one output layer. The number of neurons used in the ℓth hidden layer, with $\ell \in \{1, 2, \ldots, L\}$, is denoted by O_ℓ, with $O_1 = 64$ and $O_2 = 32$. The input and output layers have two neurons, i.e. $O_0 = O_{L+1} = 2$, being one for the real part and the other for the imaginary part of the OFDM signal. Table I summarizes the ANN hyperparameters that were tuned for optimizing the training process. The adaptive momentum (Adam) optimization algorithm was employed for training the ANN. It is well known that an ANN with a single hidden layer is capable of approximating any continuous function if enough data to train the ANN is provided. Considering the non-linear behavior of MZM, an elementary ANN employing non-linear activation functions can represent its non-linearities. Nevertheless, increasing the number of hidden layers also increases the non-linearities representation capability. Therefore, according to our empirical investigation and observations, a MLP ANN with two hidden layers and rectified linear unit (ReLU) activation function were enough to represent the non-linearities imposed by MZM. Furthermore, we have used a data set containing 20480 samples, which was split into a $N_{\text{TR}} = 14336$ training samples and $N_{\text{VAL}} = 6144$ validating samples. An early stop technique was employed to prevent overfitting in the ANN. We have set the patience hyperparameter to 100 and the training is concluded when the a mean-squared error (MSE) variation higher than 10^{-9} ($\Delta_{\text{min}} = 10^{-9}$) is not observed during 100 epochs.

TABLE I. MULTI-LAYER PERCEPTRON ANN HYPERPARAMETERS.

	Input Layer	**Hidden Layer 1**	**Hidden Layer 2**	**Output Layer**
Number of Neurons	2	64	32	2
Activation Function	-	ReLU	ReLU	Identity
Learning Rate		10^{-3}		
Solver		Adam		
Loss Function		Mean-squared error		

C. Performance Analysis

After training the ANN, the obtained A-RoF TX block post-inversion estimation response are used to pre-distort the OFDM signal. Fig.2 depicts the block diagram of the A-RoF system, in which the

ML-based DPD block are placed between the RF transceiver and the A-RoF TX block. In this diagram, x_n, generated by (1), are applied to the ML-based DPD block, which has its output given by

$$\mathbf{v} = \sum_{\ell=0}^{L+1} \phi(\mathbf{W}_\ell \times \mathbf{x}_\ell + \mathbf{b}_\ell), \tag{4}$$

where $\mathbf{W}$ is a matrix of weights, $\mathbf{v}$ is the vectored version of v_n, $\mathbf{x}$ is the input vector, $\mathbf{b}$ is the biases vector and $\phi(.)$ is the nonlinear activation function. It is important to highlight that in the first layer, $\mathbf{x}$ is a vector produced by (1) containing all N samples and, in the sequential layers, $\mathbf{x}$ is the output of the previous layer, since the layers are fully connected in the MLP architecture. The pre-distorted signal, v_n, is applied to the A-RoF TX block, which outputs y_n by applying (2) with v_n as input. Finally, the linearized version of the OFDM signal is given by (3). At the RRU the linearized signal must be upconverted and amplified for the wireless transmission.

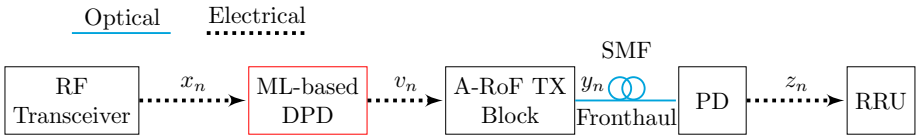

Fig. 2. Block diagram of the A-RoF system linearized using a ML DPD technique.

Fig. 3 presents the magnitude of the RF signal in the discrete time domain, which allows us verify the influence of the DPD scheme in the waveform. The DPD block applies the A-RoF TX block post-inversion response for pre-distorting the OFDM signal. As a result, the cascade response of the DPD block and the A-RoF TX block produces a linear response. Figs 3 (a) and (b) demonstrate that in the regions in which the non-linear A-RoF TX block response compress the signal, the DPD expands and vice versa. In other words, in the time-domain, the cascade response of the DPD block and the A-RoF TX block produces a signal as close as possible to x_n. It is well known that OFDM waveform presents a high peak-to-average power ratio (PAPR), which further aggravates the non-linear signal degradation. Once the linearization process produces a signal as close as possible to the original OFDM signal, the The PAPR of the linearized signal will similar to the original signal's PAPR.

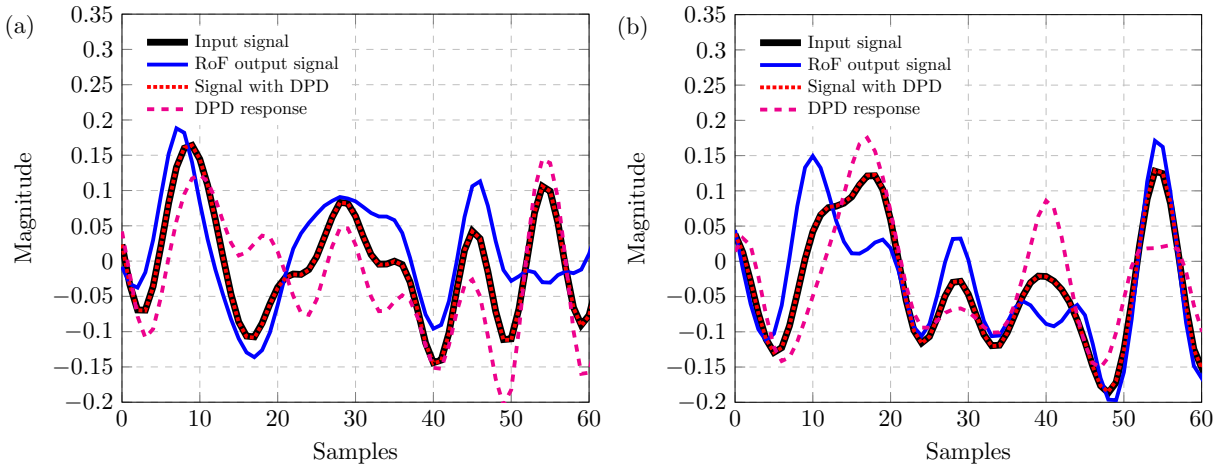

Fig. 3. OFDM Signal magnitude as a function of samples: (a) Real part; (b) Imaginary part.

ISSN 2179-1074

We have also investigated the DPD effect on the OFDM signal in the frequency domain. Fig 4 (a) illustrates the normalized power spectrum density of the OFDM signal. We can note that our proposed ML-based DPD technique considerably reduces the OOBE, resulting in an adjacent channel leakage ratio (ACLR) 10.5 dB bellow than the non-linearized signal. It is important to highlight that the DPD also reduces the in-band distortions resulting in the desired linear response. The DPD effect can also be seen in the signal constellation. Fig 4 (b) illustrates the constellation of the A-RoF output signal (blue circles) and the signal with DPD (red circles). The proposed technique has considerably reduced the symbols dispersion, leading to a EVM_{RMS} reduction from 6.35 to 0.92%.

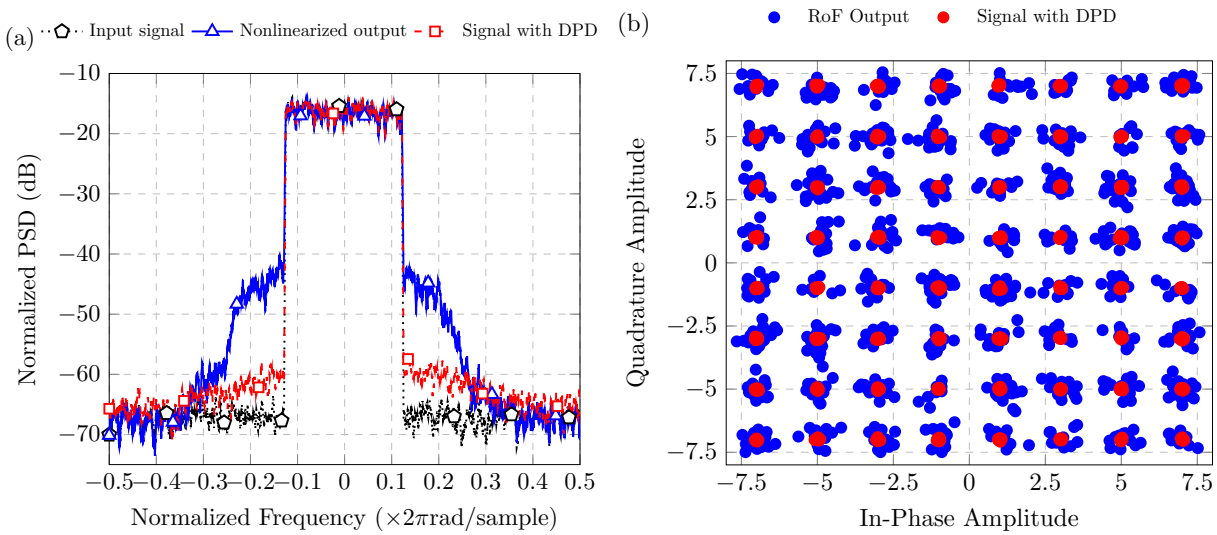

Fig. 4. Proposed DPD applied to an OFDM-16-QAM signal: (a) Normalized Power Spectrum Density; (b) Constellation.

III. 5G NR Fiber-wireless System

Fig. 5 describes the block diagram of our multi-band 5G-NR fiber-wireless system implementation. A LD from Golight generated a 10-dBm optical carrier at 1555 nm. Subsequently, a polarization controller (PC) has been employed to properly adjust and control the state of light polarization. A dual-drive Mach-Zehnder modulator (DD-MZM) has been used for simultaneously transmitting two distinct RF signals, namely: a 50-MHz bandwidth *M*-QAM 5G-NR signal at 3.5 GHz and a 100-MHz bandwidth *M*-QAM 5G-NR signal at 26 GHz, both in accordance to the 3rd Generation Partnership Project (3GPP) Release 15 [26]. The 5G signals were generated by Keysight arbitrary waveform generator (AWG) M8190A, using the Signal Studio software. Afterwards, the modulated optical carrier inset (i) propagated throughout a 12.5-km SMF fronthaul.

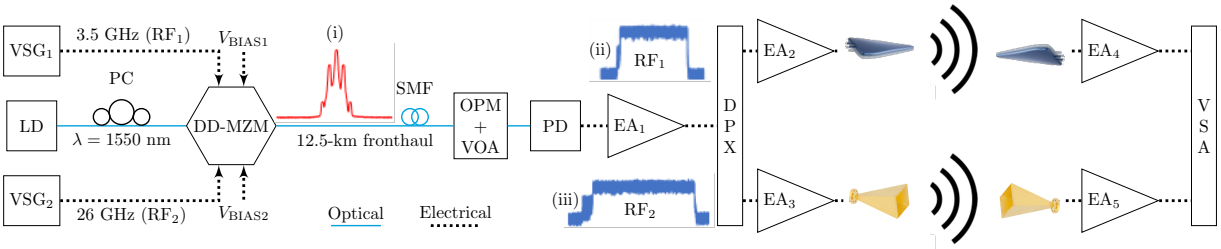

Fig. 5. FiWi system for the next-generation networks.

ISSN 2179-1074

At the optical receiver, a variable optical attenuator (VOA) and an optical power monitor (OPM) ensured 2-dBm optical power at the PD input. The photodetector performed the optical-to-electrical conversion and launched the RF signals to a 24-dB gain broadband electrical amplification stage (EA_1). An electrical spectrum analyzer (ESA) has been used to measure the resultant electrical spectrum for both signals, which are presented in the insets (ii) and (iii). Afterward, a diplexer has separated the 5G-NR signals, which were individually transmitted employing proper antennas based on the frequency range.

The signal at 26 GHz has been amplified using (E_3) with 35-dB gain before feeding a 25-dBi gain horn antenna. On the other hand, a 20-dB gain amplifier (EA_2) has amplified the 3.5 GHz signal, which is subsequently transmitted by a 5-dBi gain log-periodic antenna, giving rise to 10-m wireless access implemented as a proof-of-concept. At the reception side, identical antennas have been used for receiving the 5G-NR signals. Sequentially, the received signals at 3.5 and 26 GHz have been individually amplified by (EA_4) and (EA_5) with 20-dB gain and 35-dB gain, respectively. Finally, a vector signal analyzer (VSA) has been used for evaluating the FiWi system performance based on EVM_{RMS}. Fig. 6 shows experimental setup photographs, including the transmitter and receiver sides.

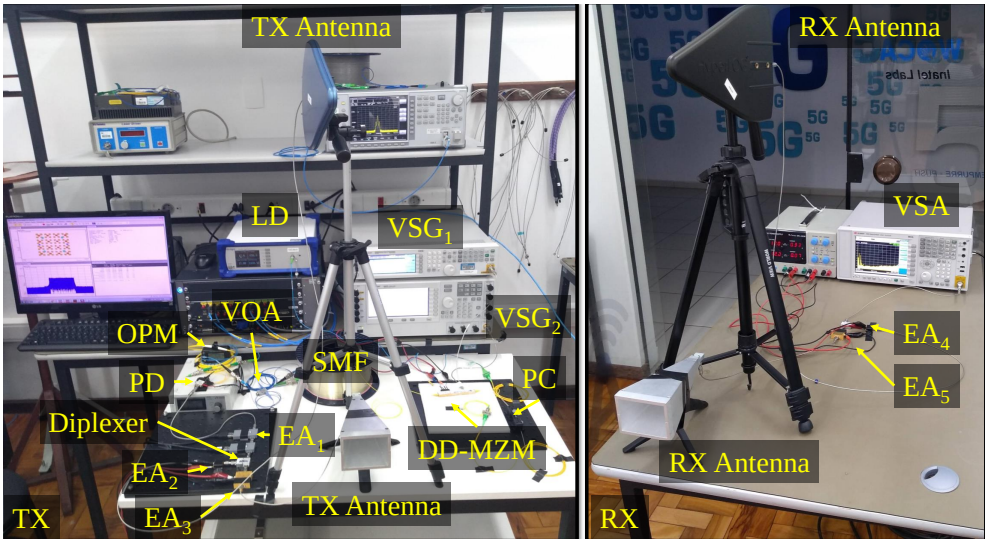

Fig. 6. Photography of the experimental setup.

IV. Experimental Results

This section presents an experimental investigation regarding the 5G-NR signals transport and transmission using our proposed FiWi System. Firstly, we have evaluated the transport A-RoF system performance, in terms of EVM_{RMS}, at two distinct setup stages, the photodetector input and the EA_1 output. Sequentially, we have investigated the wireless transmission system by transmitting the 3.5 and 26-GHz signals over a 10-m cell reach as a proof of concept.

Fig. 7 shows the EVM_{RMS} measurements as a function of the optical power at the photodetector input for the 3.5 and 26 GHz frequencies. In this analysis, we have used two modulation orders to investigate two distinct standardized 5G-NR bandwidths. Fig. 7 (a) shows the EVM_{RMS} performance for the 3.5-GHz 5G-NR signal modulated using 64/256-QAM and operating with 20 and 50-MHz bandwidths. One can note the EVM_{RMS} has kept below the 3GPP requirements from -16 to 2 dBm optical power

ISSN 2179-1074

for the 64-QAM, whereas for the 256-QAM, the feasible EVM_{RMS} has varied from -12 to 2 dBm. It is worth mentioning the photodetector maximum optical input power has established the superior limiting power (2 dBm). Fig 7 (b) shows the EVM_{RMS} performance for the 26-GHz 5G-NR signal modulated with 16 and 64-QAM and operating with 50 and 100-MHz bandwidths. One can observe the higher operating frequency and bandwidths, in comparison to the 3.5GHz analysis, have required more optical power for achieving the 3GPP requirements, as expected. Finally, we can conclude the best A-RoF received optical power was about 0 dBm, considering both operating frequencies analyses.

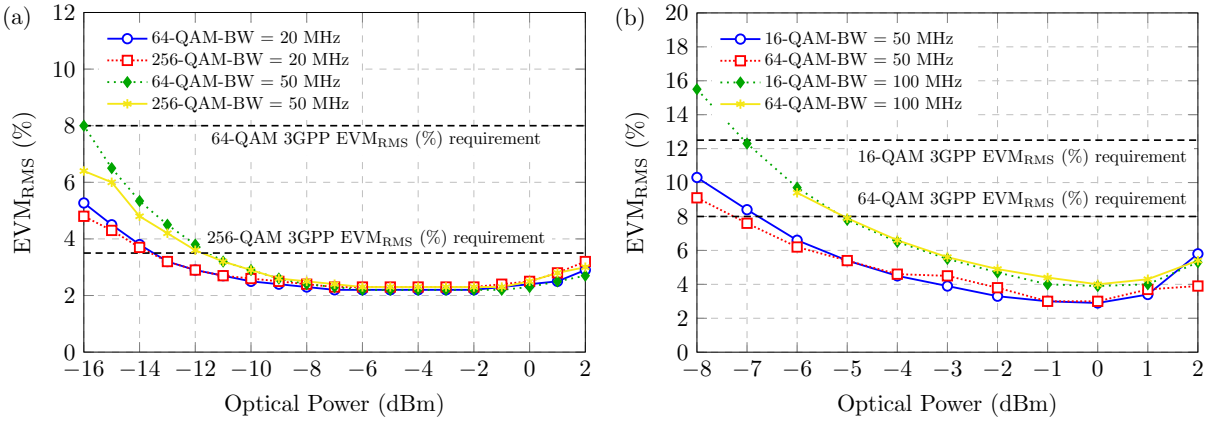

Fig. 7. EVM_{RMS} measurements as a function of the optical power at the photodetector input: (a) 3.5 GHz; (b) 26 GHz.

Our later analysis has consisted of varying the RF Mach-Zehnder modulator input power and measure the EVM_{RMS} at the EA_1 output, in order to obtain the best RF transmission power. Similarly to the optical power analysis, we have used the same modulation orders and bandwidths for this evaluation. Fig. 8 (a) and (b) report the EVM_{RMS} measure as a function of DD-MZM RF input power for the 3.5 and 26-GHz signals, respectively. The RF input power was varied from -26 to 6 dBm for the 3.5 GHz, whereas for the 26 GHz, the signal input powers varied from -8 to 6 dBm. One can note the EVM_{RMS} has increased for RF power above 1 dBm, decreasing the signal quality for both operating frequencies. This signal degradation occurs due to the DD-MZM non-linear response, which generates significant harmonics and inter-modulation products for powers higher than 1 dBm.

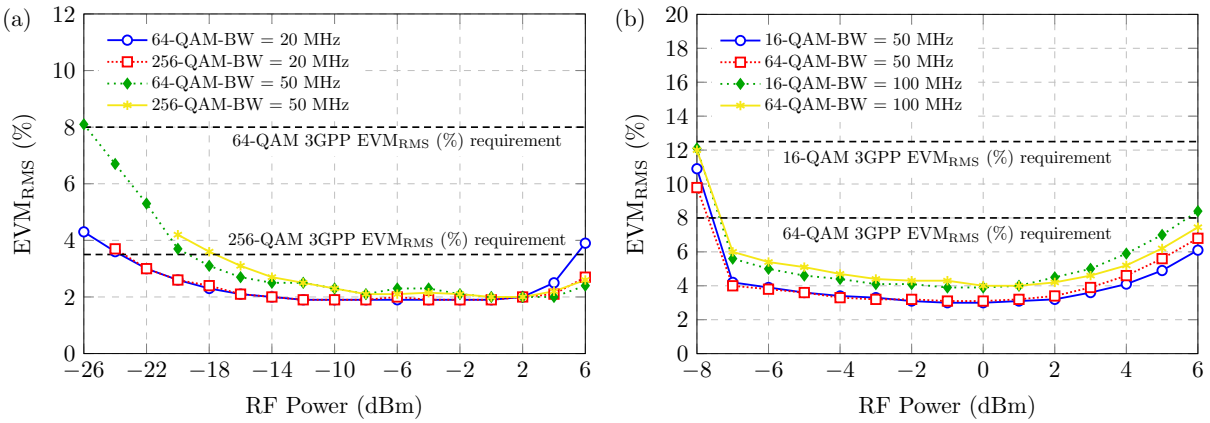

Fig. 8. EVM_{RMS} measurements as a function of RF power at EA_1 output: (a) 3.5 GHz; (b) 26 GHz.

One more time, the analyzed signals presented the same modulation orders and bandwidths from the previous results. We have implemented a 10-m reach FiWi system with 0 dBm received optical power at PD input and 0 dBm input RF power, which were the best configuration from our previous A-RoF performance evaluation. Fig. 9 shows the EVM_{RMS} measurements at the RX side for the 3.5 GHz and 26 GHz. The results show the received signals EVM_{RMS} measurements in the FR1 and FR2 bands, which has achieved EVM_{RMS} as low as 2.2 and 2.7% and 4.2 and 4.4%, respectively. For both operating frequencies, the FiWi system has been capable of recovering the signals with margins. These margins might be used to extend the link reach or to transmit signals with higher bandwidths. The joint transmission of signal with 50 MHz and 100 MHz bandwidths, has enabled attaining 590 Mbit/s throughput. Finally, our setup might be efficiently applied for composing the fronthaul and access networks for future communication systems.

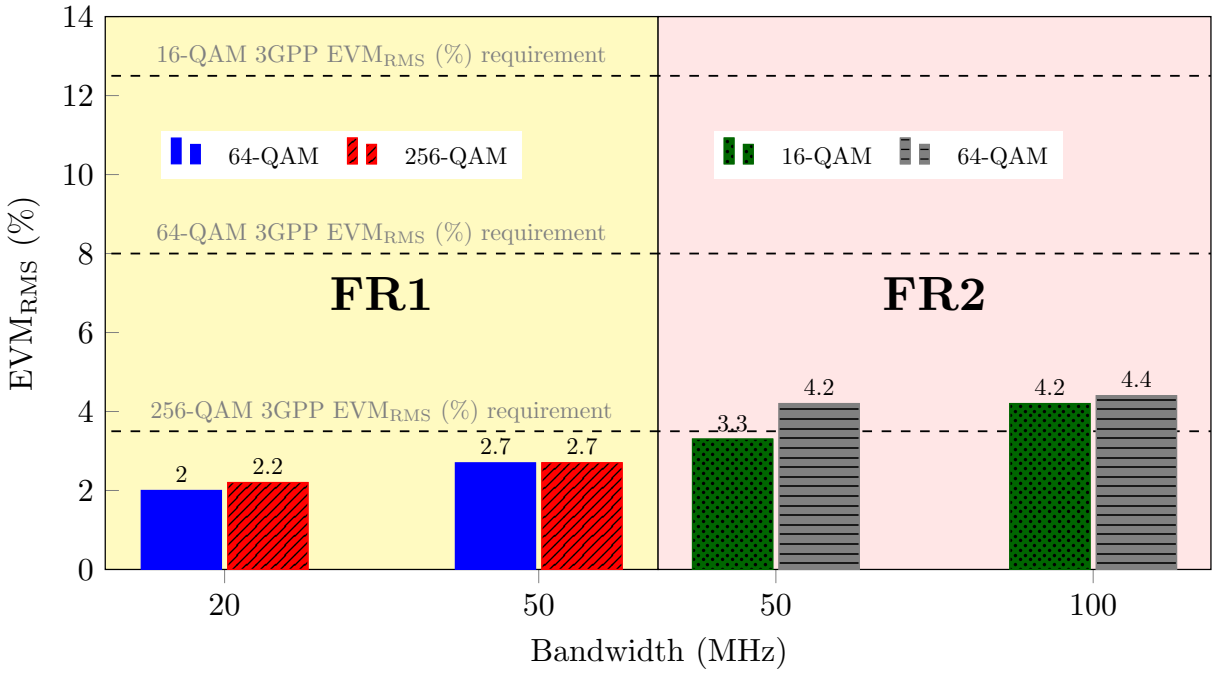

Fig. 9. 5G NR FiWi system EVM_{RMS} measurement as a function of bandwidth in the FR1 and FR2 bands.

Fig 10 illustrates the spectrum and constellation of the received 3.5 and 26 GHz signals after 10 m reach wireless transmission. In both frequency ranges, we have allocated half of the OFDM subcarriers for one user and the other half for a second user, following the orthogonal frequency division multiple access (OFDMA) operating principle. Fig.10 (a) illustrates the 50 MHz bandwidth received signal at 3.5 GHz, whereas Fig.10 (b) exhibit the 100 MHz bandwidth signal at 26 GHz. The assigned modulation orders were 64- and 256-QAM for the signal at 3.5 GHz, and 16- and 64-QAM for the signal at 26 GHz. The assigned modulation order depends on the user distance from the base stations (BS), i.e., the user located at BS proximity receives the signal with higher modulation order than that one at the cell border.

ISSN 2179-1074

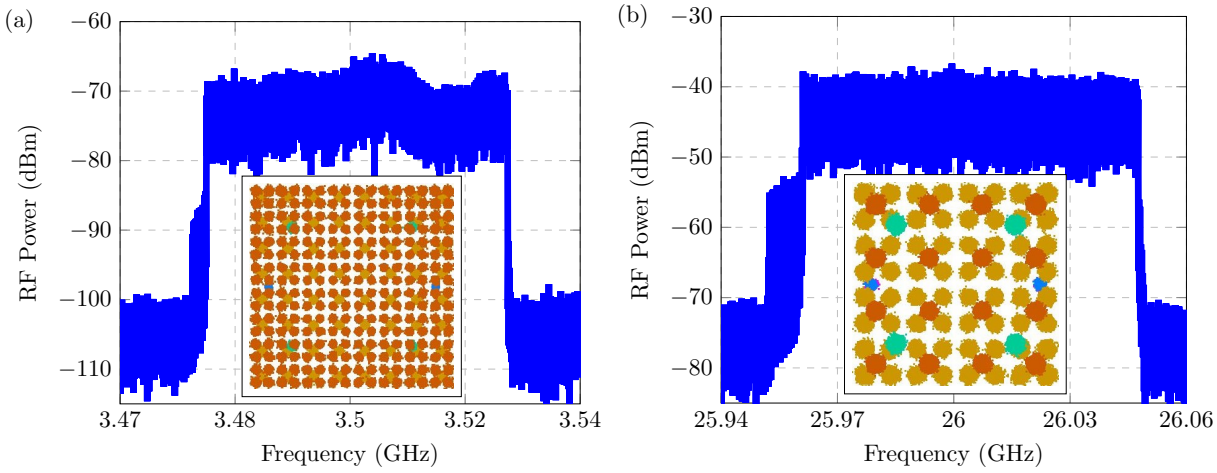

Fig. 10. Spectrum and constellation of the received signal after the wireless transmission: (a) 50-MHz bandwidth signal at 3.5 GHz; (b) 100-MHz bandwidth signal at 26 GHz.

V. Conclusions

This work reported a DPD technique based on a ML algorithm and the implementation of a multi-band FiWi system for the next-generation wireless networks. The proposed technique was applied to an OFDM signal and its performance was investigated in terms of EVM_{RMS} and ACLR. The proposed DPD scheme reduced 10.5 dB on the signal ACLR, while improving the EVM_{RMS} from 6.35 to 0.92%. This analysis demonstrated that ML algorithms can have a distinguish role in A-RoF systems employed in future FiWi communication.

We have also implemented an experimental multi-band FiWi system. In this second analysis, we were specially interested in the experimental validation of an C-RAN-based architecture for future FiWi systems. The results demonstrated our FiWi system as a potential solution for composing the transport and access network of the future communication systems. We reported an optical and electrical power characterization for the A-RoF transport network. Additionally, it was implemented a 10-m reach cell attaining 590 Mbit/s as a proof of concept. Futures works regard to join our two investigations, which means experimentally implement our proposed ML-based linearization technique in a multi-band 5G FiWi system.

Acknowledgments

This work was partially supported by FAPESP Grant No. 20/05127-2, under SAMURAI project and Rede Nacional de Ensino e Pesquisa (RNP), with resources from the Ministério da Ciência, Tecnologia e Inovações e Comunicações (MCTIC), Grant No. 01245.020548/2021-07, under the 6G Mobile Communications Systems project of the Centro de Referência em Radiocomunicações (CRR) of the Instituto Nacional de Telecomunicações (Inatel), Brazil. Authors also thank the financial support from Conselho Nacional de Desenvolvimento Científico e Tecnológico (CNPq), Coordenação de Aperfeiçoamento de Pessoal de Nível Superior (CAPES), Financiadora de Estudos e Projetos (FINEP) and Fundação de Amparo à Pesquisa do Estado de Minas Gerais (FAPEMIG).

REFERENCES

[1] M. Alsenwi, N. H. Tran, M. Bennis, A. K. Bairagi, and C. S. Hong, "eMBB-URLLC Resource Slicing: A Risk-Sensitive Approach," *IEEE Communications Letters*, vol. 23, no. 4, pp. 740–743, 2019.

[2] G. P. Fettweis, "The Tactile Internet: Applications and Challenges," *IEEE Vehicular Technology Magazine*, vol. 9, no. 1, pp. 64–70, 2014.

[3] I. Philbeck, "Connecting the Unconnected: Working Together to Achieve Connect 2020 Agenda Targets," in *Special session of the Broadband Commission and the World Economic Forum at Davos Annual Meeting*, 2017.

[4] N. Xia, H.-H. Chen, and C.-S. Yang, "Radio Resource Management in Machine-to-Machine Communications—A Survey," *IEEE Communications Surveys Tutorials*, vol. 20, no. 1, pp. 791–828, 2018.

[5] M. A. Habibi, M. Nasimi, B. Han, and H. D. Schotten, "A comprehensive Survey of RAN Architectures Toward 5G Mobile Communication System," *IEEE Access*, vol. 7, pp. 70 371–70 421, 2019.

[6] V. A. Thomas, M. El-Hajjar, and L. Hanzo, "Performance Improvement and Cost Reduction Techniques for Radio over Fiber Communications," *IEEE Communications Surveys & Tutorials*, vol. 17, no. 2, pp. 627–670, 2015.

[7] A. Udalcovs, M. Levantesi, P. Urban, D. A. Mello, R. Gaudino, O. Ozolins, and P. Monti, "Total Cost of Ownership of Digital vs. Analog Radio-Over-Fiber Architectures for 5G Fronthauling," *IEEE Access*, vol. 8, pp. 223 562–223 573, 2020.

[8] J. Wang, C. Liu, M. Zhu, A. Yi, L. Cheng, and G.-K. Chang, "Investigation of Data-Dependent Channel Cross-Modulation in Multiband Radio-Over-Fiber Systems," *Journal of Lightwave Technology*, vol. 32, no. 10, pp. 1861–1871, 2014.

[9] X. Zhang, "Broadband Linearization for 5G Fronthaul Transmission," *Frontiers of Optoelectronics*, vol. 11, no. 2, pp. 107–115, 2018.

[10] T. Ismail, C.-P. Liu, J. E. Mitchell, and A. J. Seeds, "High-Dynamic-Range Wireless-Over-Fiber Link Using Feedforward Linearization," *Journal of Lightwave Technology*, vol. 25, no. 11, pp. 3274–3282, 2007.

[11] S. Korotky and R. de Ridder, "Dual Parallel Modulation Schemes for Low-Distortion Analog Optical Transmission," *IEEE Journal on Selected Areas in Communications*, vol. 8, no. 7, pp. 1377–1381, 1990.

[12] B. Masella, B. Hraimel, and X. Zhang, "Enhanced Spurious-Free Dynamic Range Using Mixed Polarization in Optical Single Sideband Mach–Zehnder Modulator," *Journal of Lightwave Technology*, vol. 27, no. 15, pp. 3034–3041, 2009.

[13] G.-W. Lee and S.-K. Han, "Linear Dual Electroabsorption Modulator for Analog Optical Transmission," *Microwave and Optical Technology Letters*, vol. 22, no. 6, pp. 369–373, 1999.

[14] M. Noweir, Q. Zhou, A. Kwan, R. Valivarthi, M. Helaoui, W. Tittel, and F. M. Ghannouchi, "Digitally Linearized Radio-Over Fiber Transmitter Architecture for Cloud Radio Access Network's Downlink," *IEEE Transactions on Microwave Theory and Techniques*, vol. 66, no. 7, pp. 3564–3574, 2018.

[15] H. D. Rodrigues, T. C. Pimenta, R. A. A. de Souza, and L. L. Mendes, "Orthogonal Scalar Feedback Digital Pre-Distortion Linearization," *IEEE Transactions on Broadcasting*, vol. 64, no. 2, pp. 319–330, 2018.

[16] A. Hekkala, M. Hiivala, M. Lasanen, J. Perttu, L. C. Vieira, N. J. Gomes, and A. Nkansah, "Predistortion of Radio Over Fiber Links: Algorithms, Implementation, and Measurements," *IEEE Transactions on Circuits and Systems I: Regular Papers*, vol. 59, no. 3, pp. 664–672, 2012.

[17] L. A. M. Pereira, L. L. Mendes, C. J. A. Bastos-Filho, and Arismar Cerqueira, S. Jr., "Linearization Schemes for Radio Over Fiber Systems Based on Machine Learning Algorithms," *IEEE Photonics Technology Letters*, vol. 34, no. 5, pp. 279–282, 2022.

[18] M. U. Hadi, "Mitigation of Nonlinearities in Analog Radio over Fiber Links Using Machine Learning Approach," *ICT Express*, vol. 7, no. 2, pp. 253–258, 2021.

[19] S. Liu, Y. M. Alfadhli, S. Shen, M. Xu, H. Tian, and G.-K. Chang, "A Novel ANN Equalizer to Mitigate Nonlinear Interference in Analog-RoF Mobile Fronthaul," *IEEE Photonics Technology Letters*, vol. 30, no. 19, pp. 1675–1678, 2018.

[20] A. O. Mufutau, F. P. Guiomar, M. A. Fernandes, A. Lorences-Riesgo, A. Oliveira, and P. P. Monteiro, "Demonstration of a Hybrid Optical Fiber–Wireless 5G Fronthaul Coexisting With end-to-end 4G Networks," *IEEE/OSA Journal of Optical Communications and Networking*, vol. 12, no. 3, pp. 72–78, 2020.

[21] H. Zeng, X. Liu, S. Megeed, A. Shen, and F. Effenberger, "Digital Signal Processing for High-Speed Fiber-Wireless Convergence [invited]," *IEEE/OSA Journal of Optical Communications and Networking*, vol. 11, no. 1, pp. A11–A19, 2019.

[22] K. Kanta, A. Pagano, E. Ruggeri, M. Agus, I. Stratakos, R. Mercinelli, C. Vagionas, P. Toumasis, G. Kalfas, G. Giannoulis, *et al.*, "Analog Fiber-Wireless Downlink Transmission of IFoF/mmWave over In-Field Deployed Legacy PON Infrastructure for 5G Fronthauling," *IEEE/OSA Journal of Optical Communications and Networking*, vol. 12, no. 10, pp. D57–D65, 2020.

Brazilian Microwave and Optoelectronics Society-SBMO *received 0 Month 2020; for review 0 Month 2020; accepted 0 Month 2020*
Brazilian Society of Electromagnetism-SBMag *ISSN 2179-1074*

[23] C. H. de Souza Lopes, E. S. Lima, L. A. M. Pereira, R. M. Borges, A. C. Ferreira, M. Abreu, W. D. Dias, D. H. Spadoti, L. L. Mendes, and A. Junior, "Non-Standalone 5G NR Fiber-Wireless System Using FSO and Fiber-Optics Fronthauls," *Journal of Lightwave Technology*, vol. 39, no. 2, pp. 406–417, 2021.

[24] R. M. Borges, L. A. M. Pereira, H. R. D. Filgueiras, A. C. Ferreira, M. S. B. Cunha, E. R. Neto, D. H. Spadoti, L. L. Mendes, and Arismar Cerqueira S. Jr., "DSP-based flexible-waveform and multi-application 5G fiber-wireless system," *Journal of Lightwave Technology*, vol. 38, no. 3, pp. 642–653, 2020.

[25] L. Pereira, E. Lima, and A. Cerqueira, "A Multi-band 5G-NR Fiber-wireless System for Next-generation Networks," in *2021 SBMO/IEEE MTT-S International Microwave and Optoelectronics Conference (IMOC)*, pp. 1–3, 2021.

[26] 3GPP, "5G; NR; Overall description; Stage-2," *TS 38.300 version 15.3.1 Release 15*, 2018.

  ISSN 2179-1074

Paper 4: Amplified Radio-over-Fiber System Linearization Using Recurrent Neural Networks

Luiz Augusto Melo Pereira, Luciano Leonel Mendes, Carmelo José Albanez Bastos-Filho and Arismar Cerqueira Sodré Junior. "Amplified Radio-over-Fiber System Linearization Using Recurrent Neural Networks", *IEEE/Optica Journal of Optical Communications and Networking*, 2022, vol. 15, no. 3, pp. 144-154, March, 2023.

Publisher: IEEE/Optica

Amplified Radio-over-Fiber System Linearization Using Recurrent Neural Networks

LUIZ AUGUSTO MELO PEREIRA[1], LUCIANO LEONEL MENDES[1], CARMELO JOSÉ ALBANEZ BASTOS FILHO[2], AND ARISMAR CERQUEIRA SODRÉ JUNIOR[1,*]

[1] National Institute of Telecommunications (Inatel), Santa Rita do Sapucaí, MG 37400-000 Brazil
[2] University of Pernambuco- Polytechnic School of Pernambuco department, Recife, PE 50100-010 Brazil
[*] Corresponding author: arismar@inatel.br

Received 29 August 2022; revised 26 December 2022; accepted 25 January 2023; published 15 February 2023

Ubiquitous communication is an emergent feature of the future sixth generation of mobile communication (6G) networks. One of the main challenges of this upcoming mobile network is providing broadband communication wherever connectivity is necessary, including rural areas. Up to now, all previous generations of mobile networks have not satisfactorily accomplished this task, and the high cost of deploying and maintaining complex communication infrastructure in remote areas is one of the main reasons. The centralized radio access network (C-RAN) might play an important role in overcoming it, since it enables all baseband centralization in a central office (CO), simplifying the network deployment and reducing the operating/maintenance costs. Additionally, in this scenario, the analog radio over fiber (A-RoF) system might be used for transporting analog signals from CO to a simplified remote base station, only composed of an optical detector and radiofrequency (RF) front-end. However, the Mach-Zehnder modulator (MZM) and power amplifier (PA), commonly employed in A-RoF systems, introduce undesired nonlinear effects, which can severely degrade the overall system performance and prohibitively increase the out-of-band emission (OOBE). We investigate the use of machine learning (ML) algorithms applied to the linearization of an electrical-amplified A-RoF system. Particularly, a memory recurrent neural network (RNN) linearization is proposed and compared with a memoryless multi-layer perceptron (MLP) linearization. The root mean square error vector magnitude (EVM_{RMS}), normalized mean square error (NMSE) and adjacent channel leakage ratio (ACLR) metrics have been calculated to evaluate the performance of our ML-based approach. Numerical results demonstrate promising linearization performance when the RNN memory depth is equal to or higher than the amplified-A-RoF system memory depth.

http://dx.doi.org/10.1364/JOCN.474290

1. INTRODUCTION

The sixth-generation of mobile network (6G) is being currently designed and several proposals for supporting new use case scenarios and futuristic and audacious new services are being presented by researchers all over the world [1]. An unprecedented flexible physical layer (PHY) is required for supporting emergent new services and applications [2]. Moreover, the remote and rural areas communication scenario has attracted considerable attention, especially in continental-size countries [3]. Although many initiatives have been conducted to cover remote areas, the quality of experience (QoE) in this operating scenario must be enhanced [4–6]. As an example, reliable communications with latency below 10 ms and data rates up to 1 Gbit/s are necessary for enabling remote and autonomous control of the machinery on farms. In this case, enabling solutions must be employed for encompassing all these requirements, including satellite networks, multiple-input multiple-output (MIMO), TV white space (TVWS), and analog RoF (A-RoF). MIMO systems enable the exploitation of diversity for increasing the system reliability, whereas TVWS is a cost-effective solution since enables to exploit of unlicensed vacant ultra-high frequency (UHF) channels [7]. Finally, A-RoF can be used to reduce the deployment

and maintenance costs and increase the network capillarity in the remote areas scenario. However, the convergence of radiofrequency (RF) and optical systems brings undesired nonlinear effects. Linearization techniques can be employed for overcoming the non-linearities of the A-RoF systems [8–10].

Linearization techniques for A-RoF have been heavily researched in the past few years. These techniques are considered key enablers for fifth-generation of mobile network (5G) and 6G since A-RoF has an important role in future mobile networks. High-speed A-RoF systems usually employ a Mach-Zehnder modulator (MZM) for modulating the optical carrier with the RF signal. This modulation method gives rise to the A-RoF systems. A major degradation source of A-RoF is the MZM nonlinear response, which leads to in-band and out-band signal distortions [11]. The nonlinear distortions produced by the MZM become more severe as signal RF power increases, meaning that the distortion introduced by the optical modulation is a function of the signal's input power at the MZM. One solution to reduce the nonlinear distortion is to increase the back-off, i.e., reducing the input power. This approach, however, leads to low optical power at the MZM output and, consequently, to a short maximum optical link between the central office (CO) and the remote radio head (RRH). Alternatively, a linearization technique can be applied to reduce the nonlinear distortions of the signal, enabling operating with high-power RF signals [12]. In some particular cases, a dynamic RF power allocation is desirable, which is the case of the enhanced remote area communications (eRAC) scenario.

In the eRAC scenario, the users are located in remote unserved regions [7]. Low population density, infrastructure scarcity and high deployment and maintenance costs are the main challenges for the operator to provide digital services in these areas. To overcome these challenges, future mobile networks must take advantage of cost-effective solutions, where A-RoF deserves special attention [13]. The centralized radio access network (C-RAN) architecture enables sharing of processing resources among distinct services as well as simplifying the network maintenance, reducing the radio access network (RAN) implementation costs [14, 15]. In this case, the fronthaul link needs to be extended, which suggests the use of microwave and optical technologies [16]. In [17], authors have shown that an A-RoF system can be used to provide multiple services to a simple RRH without introducing performance loss among these services. The digital RoF (D-RoF) solution could also be employed in the C-RAN transport network. The aforementioned solution commonly employs Common Public Radio Interface (CPRI) or evolved Common Public Radio Interface (eCPRI) to transport baseband I/Q signals from CO to RRH [18]. Although D-RoF is currently widely employed, it might not be the best option for the eRAC scenario. For instance, the use of CPRI protocol leads to considerably large bandwidth when compared with A-RoF systems. In addition, the required analog-to-digital converter (ADC) and digital-to-analog converter (DAC) can also increase the capital expenditures (CAPEX). Therefore, the D-RoF solution presents scalability issues and the operational expenditure (OPEX) grows as the fronthaul link is extended to cover remote regions, which might hinder its application for eRAC communications [19]

This paper will extend the analysis presented in [17] by increasing the optical link length, which will require higher RF and optical power. In this case, a linearization technique must be employed, otherwise, the A-RoF dynamic range will be reduced due to RF nonlinearities. Another initiative to provide connectivity in remote areas is related to the use of TVWS opportunities [4]. However, TVWS demands low out-of-band emission (OOBE), since the spectrum will be shared with another communication service, meaning that the adjacent channel leakage ratio (ACLR) must be kept as low as possible. Since spectral mobility is essential for TVWS exploitation, the low OOBE must be achieved without the use of RF filters. All the challenges mentioned above show that a linearization technique is key for successfully covering remote areas.

Linearization of A-RoF systems might be performed both in optical and electrical domains [20–26]. Typically, electrical domain linearization is preferable compared with optical domain techniques. The optical domain linearization is hindered by the need for extremely precise and fast operations at distinct system points, using considerable additional optical components. The electrical domain linearization reduces the complexity of the linearization process. Digital pre-distortion is the most prominent electrical domain linearization technique [12, 27]. More recently, machine learning (ML) linearization techniques applied to A-RoF systems have been proposed [28–31]. Particularly, our research group has proposed two linearization schemes designed for the A-RoF system [32]. The main goal was to mitigate the nonlinearities introduced by the MZM, which might be represented by a memoryless polynomial model [33]. We have designed a multi layer perceptron (MLP) [34] artificial neural network (ANN) for estimating the A-RoF system post-inversion response, which is used for linearizing the A-RoF system [32]. However, we have not considered the nonlinearities of the base station (BS) power amplifier (PA), which amplifies the RF signal before wireless transmission.

This paper reports the proposal and implementation of two ML-based linearization schemes, specially designed for amplified-A-RoF systems. The linearization schemes are based on pre-and post-distortion concepts. The pre-distortion applies an intentional distortion to the input signal, preventing the spectral regrowth after the MZM or the PA. On the other hand, the post-distortion scheme act as an equalizer at the system output, which does not prevent spectral regrowth. We have assumed that the nonlinear response of the system comes only from the MZM and PA components. The last one presents the memory effect, which means that its output at a specific time instant depends not only on the current input but also on previous inputs [35]. The memory polynomial model has been widely used for modeling devices with memory effects, which is the case of PA [36]. Many approaches based on computational intelligence are commonly employed to deal with memory-temporal signals, including recurrent neural networks (RNNs), which present a memory structure that aids to learn complex nonlinear behavior [37–39]. Thereby, since we intend to compensate for the cascade nonlinear responses of the MZM and PA, an ANN capable of dealing with the memory effect is required. So, we have designed our pre- and post-distortion schemes based on a RNN and compared it with a memoryless MLP ANN. The goal is to investigate the impact of the memory effect on the performance of the proposed linearization schemes.

The main contribution of this paper is the proposal of two innovative ML linearization schemes, based on RNN, and their performance evaluation. The proposal was specially designed for amplified A-RoF systems, applied to the transport network of C-RAN architecture. Our goal was to demonstrate that recurrent layers of an ANN can be employed to mitigate non-linear distortions with memory effect, which can not be compensated using simple MLP ANNs. Therefore, we have not performed

an exhaustive investigation of all possible ANN architecture that enables to compensate memory effect. The RNN and long short-term memory (LSTM) were considered during the linearization scheme design. The last one has a more sophisticated architecture, capable of learning long-term temporal dependencies, which was not the case of memory from the A-RoF system. Hence we have opted for a simple RNN. This solution is particularly interesting in the context of eRAC applications since it enables the A-RoF to operate at high RF power without producing prohibitive distortions. This paper is organized as follows. Section 2 describes the nonlinear models used for modeling both MZM and PA. Section 3 presents the proposed RNN-based linearization schemes concepts, whereas Section 4 reports its results and performance evaluation. Finally, the conclusions and future works are discussed in Section 5.

2. BASE-BAND EQUIVALENT SYSTEM MODEL

Fig. 1 depicts the scenario considered in this paper, in which a C-RAN architecture can be employed to support eRAC applications. We have considered that the core network is connected to the CO using an optical-fiber backhaul link. The PHY and medium access control (MAC) functions of the BS are performed at CO, by taking advantage of software-defined radio (SDR) implementation. It will be assumed that TVWS will be used to provide eRAC services, which means that low OOBE is necessary [7]. We have also assumed that the RRH will be located in the region where the services will be provided and the optical link can be several miles long. The base-band signal generated by the SDR transmitter at the CO is upconverted to a RF channel. This RF signal modulates an optical carrier using an MZM, resulting in an A-RoF system. In this paper, we have employed the orthogonal frequency division multiplexing (OFDM) waveform as a base-band signal, which is given by

$$x_n = \sum_{m=0}^{M-1} d_m e^{-j2\pi \frac{m}{M}(n+1)}, \tag{1}$$

where d_m is the quadrature amplitude modulation (QAM) symbols, carried by the mth subcarrier, $m \in \{0, 1, 2, \ldots, M-1\}$ and $n \in \{0, 1, \ldots, N-1\}$ is the time index. The RF signal is linearized by one of the proposed linearization schemes, aiming to reduce the nonlinear distortions caused either by the MZM and/or PA components. The A-RoF TX block is composed of laser diode (LD), MZM and polarization voltage (V_{BIAS}), as illustrated in Fig. 1. Once we intend to provide communication for remote and rural areas by exploiting TVWS, the RF signal will be converted to the very high frequency (VHF) and UHF frequency bands before being transported to the RRH. At RRH, the signals are converted to the electrical domain, upconverted, amplified and radiated by remote antenna unit (RAU) to cover remote areas. The photodetector (PD) might also introduce non-linear distortions. However, for the investigated scenario, the PD will be located several miles from CO at RRH. In this case, the nonlinear distortions of the PD might be neglected due to the low optical power of the incident beam [40]. In the uplink transmission, the RAU is also responsible for receiving the signals from the users, which will be converted to the optical domain. The next subsections introduce the mathematical models used in the A-RoF transmitter (TX) block and the PA.

A. Radio over Fiber Transmitter Model

In A-RoF systems, an MZM is used in the CO to modulate the optical carrier with the RF signal. The MZM transfer function has a nonlinear behavior, which is commonly approximated by a cosine shape function [41]. In this paper, we are particularly interested in operating with high optical and RF power to overcome the optical fronthaul link extension. In this case, if no countermeasures are employed, high distortion levels will be imposed on the RF signal, leading to a prohibitive OOBE for TVWS exploitation.

The MZM nonlinearities are modeled by a memoryless polynomial. For A-RoF systems, the theoretical polynomial model is used to relate the RF power at MZM input with the RF power at A-RoF system output. In practical systems, any distortion caused by the laser optical power will be intrinsically considered by the model. The memoryless polynomial model is given by [32, 33]

$$y_n = \sum_{j=0}^{J-1} h_j |v_n|^j v_n, \tag{2}$$

where v_n is the OFDM signal at the MZM input, $n \in \{0, 1, .2., \ldots, N-1\}$ is the time index, h_j are coefficients of the memoryless nonlinear model, with $j = 0, 1, \ldots, J-1$, in which J stands for the nonlinearity model order. Similarly to [10, 32, 33], we have employed $J = 5$ in our investigation. Since the model above is linear-in-the-parameters, we can write (2) in the matrix form as

$$\mathbf{y} = \mathbf{V}\mathbf{h}, \tag{3}$$

where $\mathbf{h} = [h_0, h_1, ..., h_{J-1}]^{\mathrm{T}}, \mathbf{h} \in \mathbb{C}^{J\times 1}$ is the column vector containing the coefficients of the model, with $(.)^{\mathrm{T}}$ denoting the matrix transposition operation, $\mathbf{y} = [y_0, y_1, ..., y_{N-1}]^{\mathrm{T}}, \mathbf{y} \in \mathbb{C}^{N\times 1}$ represents the discrete output signal, whereas $\mathbf{V} \in \mathbb{C}^{N\times J}$ is the regression matrix described as follows

$$\mathbf{V} = [\mathbf{v}^0, \mathbf{v}^1, \ldots, \mathbf{v}^{J-1}], \tag{4}$$

where

$$\mathbf{v}^j = \begin{bmatrix} |v_0|^j v_0 \\ |v_1|^j v_1 \\ \vdots \\ |v_{N-1}|^j v_{N-1} \end{bmatrix}. \tag{5}$$

B. Power Amplifier Model

The PA considered in this paper is located at the RRH. This device is used to amplify the RF signal at PD output. Many memoryless models based on amplitude-to-amplitude (AM/AM) and amplitude-to-phase (AM/PM) functions can be used to represent the non-linear behavior of the PA. In most practical systems, the PA has a dynamic behavior that can not be represented by a memoryless polynomial model since a memory effect will be observed. The memory effect is a variation of the AM/AM and AM/PM functions due to the past input levels, which means that the instantaneous PA output does not depends only on the corresponding instantaneous input. The memory depth (Q) parameter defines how many previous samples have an influence on the instantaneous signal at the PA output. In this case, the memory polynomial model, which is a pruned version of the Volterra series, is widely adopted for modeling the PA behavior. The base-band signal output of the memory polynomial model as a function of an input signal z_n is expressed as

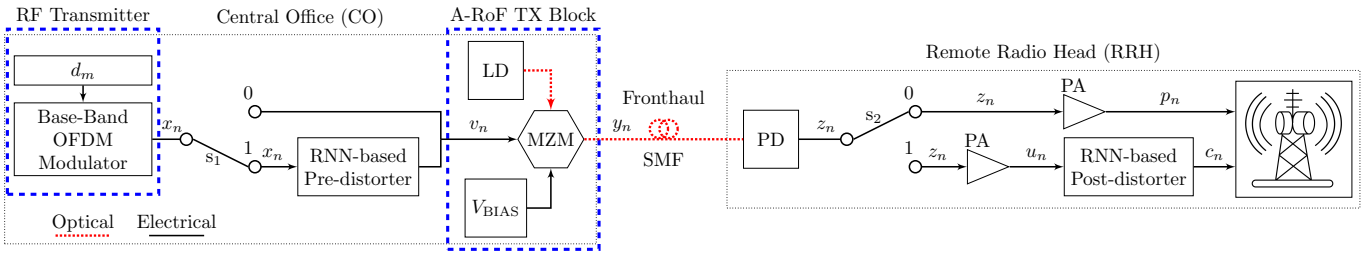

Fig. 1. Block diagram of the amplified radio-over-fiber system assisted by the proposed RNN-based linearization schemes.

$$p_n = \sum_{q=0}^{Q-1} \sum_{k=0}^{K-1} \xi_{q,k} \left| z_{n-q} \right|^k z_{n-q}, \tag{6}$$

where $\xi_{q,k}$ are coefficients of the PA model, with $q \in \{0, 1, \cdots, Q-1\}$ and $k \in \{0, 1, \cdots, K-1\}$, in which Q is the memory depth and K the model nonlinearity order.

For the sake of simplicity, (6) can be written in matrix form. Firstly, let us define $\boldsymbol{\xi}$ as the matrix of coefficient of the memory polynomial model, $\boldsymbol{\xi} \in \mathbb{C}^{Q \times K}$, which is given by

$$\boldsymbol{\xi} = \begin{bmatrix} \xi_{0,0} & \xi_{0,1} & \cdots & \xi_{0,K-1} \\ \xi_{1,0} & \xi_{1,1} & \cdots & \xi_{1,K-1} \\ \vdots & \vdots & \ddots & \vdots \\ \xi_{Q-1,0} & \xi_{Q-1,1} & \cdots & \xi_{Q-1,K-1} \end{bmatrix}, \tag{7}$$

Now, consider $\mathbf{Z} \in \mathbb{C}^{Q \times K}$, as a matrix containing samples of the input signal, which are organized as follows

$$\mathbf{Z} = \begin{bmatrix} z_n & z_n|z_n| & \cdots & z_n|z_n|^{K-1} \\ z_{n-1} & z_{n-1}|z_{n-1}| & \cdots & z_{n-1}|z_{n-1}|^{K-1} \\ \vdots & \vdots & \ddots & \vdots \\ z_{n-Q+1} & z_{n-Q+1}|z_{n-Q+1}| & \cdots & z_{n-Q+1}|z_{n-Q+1}|^{K-1} \end{bmatrix}, \tag{8}$$

where nth output sample of the memory polynomial model is given by the sum of all elements of the Hadamard product between $\boldsymbol{\xi}$ and $\mathbf{Z}$ as follows

$$p_n = \sum_{q,k} [\boldsymbol{\xi} \odot \mathbf{Z}]_{q,k}, \tag{9}$$

in which $\odot$ represents the Hadamard product, $q \in \{0, 1, \cdots, Q-1\}$ and $k \in \{0, 1, \cdots, K-1\}$. Finally, we can rewrite (6) as a column vector given by $\mathbf{p} = [p_0, p_1, \cdots, p_{N-1}]^{\mathrm{T}}, \mathbf{p} \in \mathbb{C}^{N \times 1}$. Due to the causal response of PA, the samples with a negative index in (9) are considered to be zeroed.

3. RNN-BASED LINEARIZATION SCHEMES FOR ANALOG RADIO-OVER-FIBER SYSTEMS

Linearization schemes based on ML algorithms has recently been considered as an interesting solution for practical implementation. An ANN can be used for implementing pre- and post-distortion linearization techniques based on a linear regression operation. In this case, a supervised ANN can learn a behavioral model given its input and output samples. In this work, we have used a RNN to estimate the post-inversion response of the cascade A-RoF and PA power responses, which are used later for implementing pre- and post-distortion schemes. A second RNN is used to model the cascade response of an A-RoF model and an PA component Since the PA nonlinearities have memory, an ANN capable of dealing with a system with memory effect is necessary. For this reason, we have opted for an RNN, since it has an internal memory structure. Additionally, memoryless devices, such as MZM, can be considered a special case of the memory system and, therefore, also can be modeled using this ANN architecture [42].

Volterra-series based models are often used to design a linearization scheme [12]. On the other hand, ML algorithms can be employed as a less complex solution with linearization performance similar to the classic Volterra models. In specific cases, ML-based solutions can even outperform the classic models since it has a remarkable non-linear representation and generalization capacity [43]. The next subsections present the training process of the RNN and the concepts of the proposed pre- and post-distortion schemes.

A. Recurrent Neural Network training

In the RNN training, supervised learning is employed for performing a linear regression. Many linear regression techniques can be found in the specialized literature, including autoregressive moving average (ARMA), autoregressive integrated moving average (ARIMA), RNN, LSTM and Hopfield ANNs [37, 44–47]. We have chosen the RNN since it is the most similar architecture to our previous simulations [32], enabling us to evaluate the memory effect. The RNN is composed of an input layer, L hidden layers and one output layer. Each layer has O_ℓ neurons, with $\ell \in \{0, \cdots, L+1\}$, ℓ denoting the ℓth layer. The neurons are densely connected in sequential layers, and they also have connections pointing backward, as demonstrated in Fig. 2. The RNN output is a function of the instantaneous and previous samples of the input signal in a given time step (Ts). The Ts parameter stands for the RNN memory depth. The memory depth of an RNN governs how many previous training samples are used for estimating the ANN output for a given Ts.

The ℓth hidden layer, $\ell \in \{1, \cdots, L\}$, has two sets of weights matrices $\mathbf{W}_p \in \mathbb{R}^{O_{\ell-1} \times O_\ell}$ and $\mathbf{W}_v \in \mathbb{R}^{O_\ell \times O_\ell}$, in which are stored the weights of the input vector of the current Ts and for the output of the previous Ts, respectively. The output of each hidden layer at time step t with $t \in \{1, \cdots, Ts\}$, is given by [48]

$$\hat{\mathbf{V}}_{(t)} = \phi\left(\mathbf{P}_{(t)}\mathbf{W}_p + \hat{\mathbf{V}}_{(t-1)}\mathbf{W}_v + \mathbf{b}\right), \tag{10}$$

where $\phi(.)$ is the nonlinear activation function, $\mathbf{P}_{(t)} \in \mathbb{R}^{N \times nf}$, represents the input matrix at $Ts = t$, with nf denoting the number of features of the input training instances, $\hat{\mathbf{V}}_{(t-1)} \in \mathbb{R}^{N \times O_\ell}$,

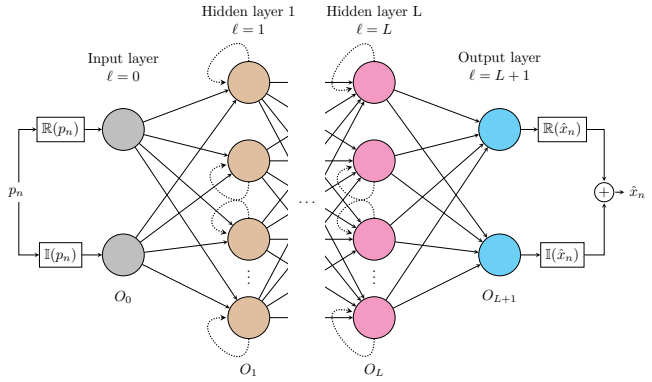

Fig. 2. Recurrent neural network architecture composed of the following layers: input layer ($\ell = 0$); hidden layers ($\ell = 1, ..., L$); output layer ($\ell = L + 1$). Each layer has O_ℓ neurons.

is the output matrix of the previous Ts and $\mathbf{b}$ is the bias vector. It is important to highlight that the output of the ℓth layer will be the input of the $(\ell + 1)$th layer. Additionally, as illustrated in Fig. 2, the input ($\ell = 0$) and output layer ($\ell = L + 1$) are composed of non-recurrent neurons, which means that $\hat{\mathbf{V}}_{(t-1)}$ and $\mathbf{W}_v$ are zeroed in these layers.

We have used the ANN for estimating the inverse cascade response of the A-RoF system and PA. Fig. 3 depicts the block diagram for the system post-inversion estimation. In this case, we have considered the switches s_1 and s_2 from Fig. 1 to be in position 0, leading to $v_n = x_n$, which corresponds to an OFDM signal generated using (1). The signal y_n at A-RoF TX block output is generated by (2) with v_n as input. Since we are only interested in nonlinear distortions caused by the MZM and PA, we have assumed that the single-mode fiber (SMF) and PD combined response is $g_n = \delta_n$, leading to

$$z_n = y_n * g_n = y_n, \tag{11}$$

where $*$ denotes the convolution operation. Sequentially, z_n is applied to the PA, which was modeled using the memory polynomial expression described by (6). In this way, p_n is generated by applying (6), with z_n as input, assuming $Q = 3$ and $K = 5$ [49]. Finally, we can use x_n as the training desired label and p_n as the RNN input.

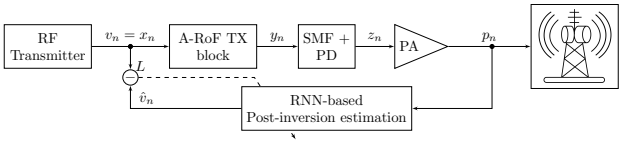

Fig. 3. Block diagram of the RNN training for post-inversion estimation.

The RNN input matrix contains the complex samples of the distorted signal at PA output. We have used the Tensorflow application programming interface (API) for implementing the RNN. Such implementation does not enable directly operating with complex signals. Hence, we have to extract the real and imaginary parts of the OFDM signal and group them into a matrix $\mathbf{P} \in \mathbb{R}^{N \times nf}$. The first column of $\mathbf{P}$, contains the real part of the signal, whereas the second column stores the imaginary part, leading to the input matrix with two features ($nf = 2$).

During the training, the backpropagation algorithm is employed for calculating each component of $\mathbf{W}_p$, $\mathbf{W}_v$ and $\mathbf{b}$ that minimize a cost function, given by

$$Loss(\mathbf{W}_p, \mathbf{W}_v, \mathbf{b}) = \frac{1}{N_{\text{TR}}} \sum_{n=0}^{N_{\text{TR}}-1} \mathcal{L}\left(x_n, \hat{x}_n(\mathbf{W}_p, \mathbf{W}_v, \mathbf{b})\right), \tag{12}$$

where N_{TR} is the number of training instances and $\mathcal{L}$ is a loss function. In our investigation, we have used a database containing 614,400 samples, in which 70% were used for training and 30% for validating the model, resulting in $N_{\text{TR}} = 430,080$. Additionally, 2,048 samples were used for testing the model. Although k-fold is commonly used to check for bias in the training dataset, this analysis was left out of scope in this work. Regarding the number of hidden layers, two are enough for modeling a system with a nonlinear response, as long as the activation function is nonlinear. We have employed two hidden layers with 64 and 32 neurons, i.e., $O_1 = 64$ and $O_2 = 32$. The number of hidden layers and neurons per hidden layer were obtained using a heuristic methodology, aiming to select the smallest configuration that produces a trade-off between performance and complexity. It is important to highlight that the number of hidden layers was selected considering the particularities of this application, which means that for less-complex systems less resources might be required.

Regarding the activation function, many of them are being proposed for performing high-nonlinear transformations by applying simple modifications to the data [50]. The data transformation is governed by the activation function type, which can be the rectified linear unit (ReLU), exponential linear unit (Elu), scaled exponential linear unit (SELU) and hyperbolic tangent (tanh), Sigmoid, Softmax, Softsign, and others. The choice of the activation function depends on the type of data to be predicted. In our investigation, the predicted value is the OFDM signal, which can assume negative or positive values. Hence, in the output layer, we can not employ ReLU, since this activation function transforms negative data to zero. Softmax and Sigmoid are commonly employed in classification problems, which is not the case for our proposed schemes [48]. So, we have tested the Elu, Leaky ReLU, Softsign, SELU, and tanh activation functions. The last one has presented the best results, therefore, it was employed in all layers of our ANN. The tanh activation function is given by [50]

$$\phi(\psi) = \frac{e^{2\psi} - 1}{e^{2\psi} + 1}, \tag{13}$$

where a represents an arbitrary set of training instances. Hence, we have used the tanh, for evaluating the linearization schemes performance. Table 1 summarizes the main hyperparameters used for training the RNN.

The training was done throughout 10,000 epochs unless the stop condition of an early stop technique is reached. The number of epochs and patient hyperparameters were heuristically selected throughout observations during the training process. Hence, the training process stops when a mean-squared error (MSE) variation higher than 10^{-9} ($\Delta_{min} = 10^{-9}$) is not observed throughout 100 epochs. During the training first epochs, MSE was about 10^{-3}. In addition, MSE rapidly decreases for the next epochs achieving $\approx 10^{-7}$. Beyond the 280 epoch, MSE remained approximately unchanged, meeting the early stop criterion with less than 350 epochs. It is important to mention that

Table 1. Recurrent Neural Network hyperparameters.

	Input Layer	Hidden Layer 1	Hidden Layer 2	Output Layer
Number of Neurons	2	64	32	2
Type of Layer	Dense	Simple RNN	Simple RNN	Dense
Activation Function	Hyperbolic Tangent (tanh)			
Kernel Initializer	Glorot Normal			
Learning Rate	10^{-3}			
Solver	Adam			
Stop Criterion	$\Delta_{\min} = 10^{-9}$			
Loss Function	Mean-squared Error			
Patience	100			
Time Step (Ts)	1, 2, 3, 4,5			
Epochs	10,000			
Batch Size	430,080 instances			

a lower batch size might also be employed with similar results. The MSE loss function is given by

$$\mathcal{L}(a_n, b_n) = (a_n - b_n)^2, \tag{14}$$

We have trained a second RNN using the same hyperparameters used in the previous RNN. The block diagram presented in Fig 4, depicts the RNN training process. This approach enables modeling an amplified A-RoF system, without knowing the coefficients of the nonlinear models that represent either the MZM and PA nonlinearities. With this purpose, we have trained the RNN using v_n as input and p_n as the desired labels.

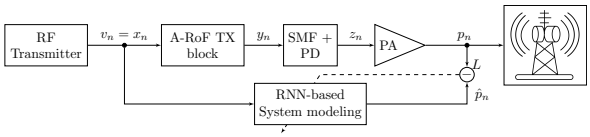

Fig. 4. Block diagram of the RNN training for modeling the amplified A-RoF system.

B. RNN-based Linearization Schemes

In Fig. 1, the switches s_1 and s_2 select which linearization scheme is employed. For s_1 in position 1 and s_2 in position 0 pre-distortion is selected, whereas changing s_1 to 0 and s_2 to 1, post-distortion is used, and, in this case, an RNN-based pre-distorter block placed between the RF transmitter and the A-RoF TX block is activated, as illustrated in Fig. 5. The pre-distortion process is carried out in two steps. The first one is the post-inversion estimation, in which the RNN is trained. In the second step, the RNN predict method is employed. This method applies the trained weights and bias and performs the non-linear transformation in the input signal, leading to the pre-distorted signal. In other words, a matrix $\mathbf{X}$, with its first column containing the real part of x_n and the second column containing the imaginary part of x_n, is used as input of pre-distortion block, which applies (10) for each RNN layer to generate a matrix of the pre-distorted signal $\hat{\mathbf{V}}$. The aforementioned matrix feeds the second RNN, which was trained for encompassing the responses of the entire A-RoF system followed by an PA. Therefore, the linearized signal $\hat{p}_n$ is obtained by applying (10) with $\hat{\mathbf{V}}$ as input. This double ANN proposal was first introduced in our previous work [43], in which an ANN-based pre-distorter scheme was exploited. We have also investigated the pre-distorter scheme capacity of compensating variations in the A-RoF system response due to temperature, aging, and fluctuations on the MZM polarization voltage. The second ANN enables to generalize the system non-linear response variation, dispensing the need for an expensive re-calibration process. Finally, the linearized signal can be transmitted exploiting TVWS without causing interference in incumbents operating in other frequency bands.

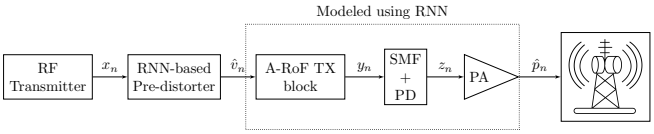

Fig. 5. Block diagram of the pre-distortion scheme.

Alternatively, the signal might be linearized by the post-distortion scheme by switching s_1 to position 0 and s_2 to position 1. The post-distortion block diagram is depicted in Fig. 6. In this case, $v_n = x_n$ and the linearization is performed at the PA's output. Again, the real and imaginary parts of v_n are extracted to create the RNN input matrix $\mathbf{V}$. The amplified A-RoF system output ($\hat{\mathbf{U}}$) is generated by applying (10) for each RNN layer considering that weights matrices and vector bias were already defined during the training process. Sequentially, the matrix $\hat{\mathbf{U}}$ containing the samples of the distorted signal feeds the RNN-based post-distorter block, which also applies (10) for obtaining the linearized signal $\hat{c}_n$.

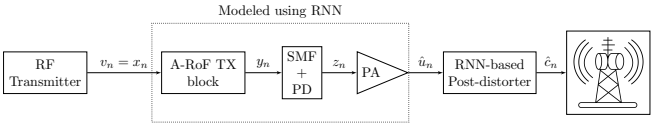

Fig. 6. Block diagram of the post-distortion scheme.

4. PERFORMANCE EVALUATION

The performance evaluation of the proposed schemes was conducted considering the exploitation of TVWS opportunities using eRAC, which means that low OOBE is required. It is important to note that the pre- and post-distortion schemes are deployed separately. In addition, both linearization schemes are also individually employed, by managing s_1 and s_2 switches position. We have employed time-domain and frequency-domain metrics to evaluate the performance of our proposed linearization schemes. The root mean square error vector magnitude (EVM_{RMS}) is used to evaluate the deviation in the coordinates of the QAM symbols introduced by the system nonlinear behavior. This metric is given by

$$\text{EVM}_{\text{RMS}}(\%) = 100\sqrt{\frac{\sum_{m=0}^{M-1} \left| d_m - \hat{d}_m \right|_2^2}{\sum_{m=0}^{M-1} |d_m|_2^2}}, \tag{15}$$

where $\hat{d}_m$ is the symbol received on the mth subcarrier, d_m is the symbol allocated in the mth subcarrier in the transmitter side and $|(.)|_p$ is the p-norm operator. We have also employed the normalized mean square error (NMSE) metric given by

$$\text{NMSE (dB)} = 10\log\left(\frac{\sum_{n=0}^{N-1}|x_n - p_n|_2^2}{\sum_{n=0}^{N-1}|x_n|_2^2}\right). \quad (16)$$

This metric enables to measure the discrepancy between the transmitted and received QAM symbols. Another important metric is the ACLR, used for evaluating the signal OOBE and is defined as

$$\text{ACLR (dB)} = 10\log\left(\frac{\int_{f\in B_O} P_{\hat{p}}(f)df}{\int_{f\in B_I} P_{\hat{p}}(f)df}\right), \quad (17)$$

where $P_{\hat{p}}(f)$ stands for the power spectrum density (PSD) of $\hat{p}_n$ at frequency f , B_I and B_O represents the in-band and out-of-bands frequencies, respectively.

The performance evaluation was conducted by varying the RF power at the MZM input from 0 to 25 dBm and Ts from 1 to 5. We have also implemented an MLP-based solution for comparing with our RNN-based proposed schemes. The MLP-based solution allows for verifying the linearization performance when the memory effect is not taken into consideration by the linearization process. We have used the same data set for RNN and MLP solutions. The last one was trained considering the hyperparameters and configurations summarized in Table 2

Fig 7 presents the linearization schemes performance in terms of EVM_{RMS}. The EVM_{RMS} limit for a 5G network operating with a given modulation order is established in the 3rd Generation Partnership Project (3GPP) Release 15 [51]. In this work, 16-QAM is assumed, which requires EVM_{RMS} below 12.5%. We can notice that either the pre- and post-distortion schemes can extend the system dynamic range for all tested Ts of the RNN. The worst performance was observed when the effect memory is not considered, which is the case of employing the MLP-based linearization. When RNN is employed, the EVM_{RMS} considerably decreases when compared with MLP since RNN has a memory structure that can be used for compensating memory effects. We can notice that EVM_{RMS} performance becomes similar for $Ts \geq 3$. However, the optimal performance is observed

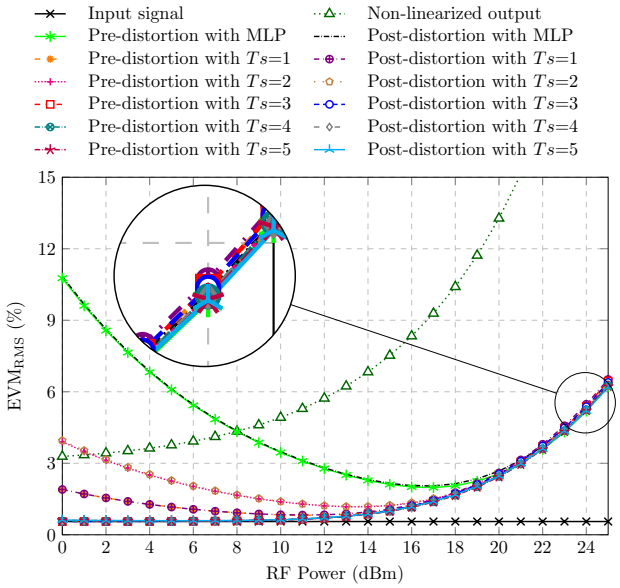

Fig. 7. EVM_{RMS} as a function of electrical power and Ts.

Table 2. Multi-layer Perceptron neural network hyperparameters.

	Input Layer	Hidden Layer 1	Hidden Layer 2	Output Layer
Number of Neurons	2	64	32	2
Type of layer	Dense			
Activation Function	Hyperbolic Tangent (tanh)			
Kernel Initializer	Glorot Normal			
Learning Rate	10^{-3}			
Solver	Adam			
Stop Criterion	$\Delta_{\min} = 10^{-9}$			
Loss Function	Mean-squared Error			
Patience	100			
Epochs	10,000			
Batch Size	430,080 instances			

when the RNN memory depth is equal to the PA memory depth, i.e., $Ts = Q = 3$.

Fig. 8 illustrates the received 16-QAM-OFDM constellations with and without linearization. It is important to mention that the non-linearized signal phase was manually compensated at the reception side. On the other hand, when the RNN-based linearization scheme is employed, both phase and magnitude of the received signal are simultaneously compensated.

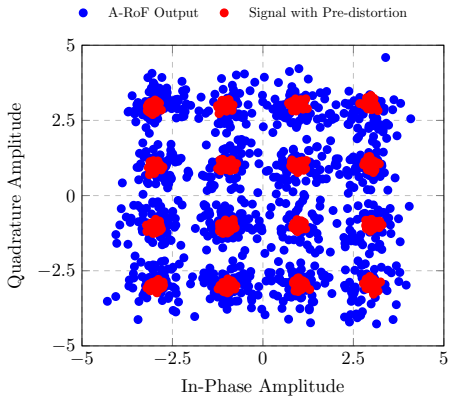

Fig. 8. Constellation diagram of the received OFDM signal.

Fig. 9 presents the NMSE between the transmitted signal (x_n) and the received signals. If a linearization technique is not applied, the estimated NMSE varied from -2.55 to 0.8 dB as the RF power is increased. The NMSE drastically decreases when a linearization technique is employed. For the RNN, despite the Ts configuration, either pre- and post-distortion schemes have presented a remarkable performance in terms of NMSE. In this result, it becomes clear that making $Ts = Q = 3$ leads to the optimal RNN performance, with the NMSE linearly increasing with the RF power. Once again, the MLP-based scheme has presented the worst performance, which is in accordance with the EVM_{RMS} results. Therefore, we can assume that Ts positively impacts on in-band distortion reduction.

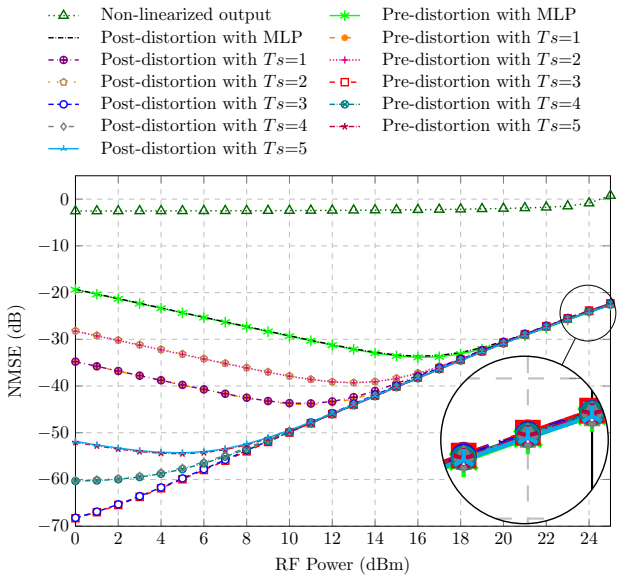

Fig. 9. NMSE as a function of electrical power and *Ts*.

We have also investigated the linearization schemes using a frequency-domain metric. The ACLR enables us to measure the ratio between the power within and outside the desired bandwidth. Considering that we intend to exploit TVWS vacant channels, the ACLR is an important metric for evaluating the signal distortions due to intermodulation products. Fig. 10 presents the ACLR as a function of RF power at MZM input. We can notice that either the pre- and post-distortion schemes have considerably reduced the ACLR. When applying the proposed linearization techniques, the system dynamic range is increased by approximately 10 dB, in comparison with the non-linearized output signal. It is important to highlight that the MLP and RNN have produced similar results in terms of ACLR. This can

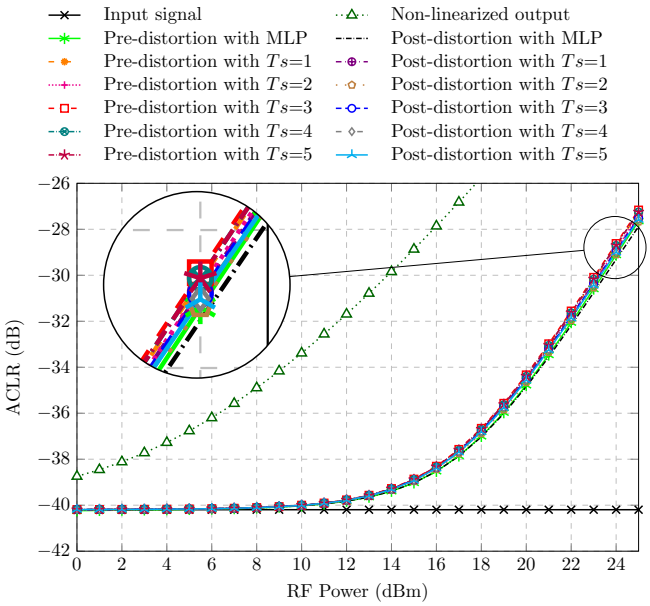

Fig. 10. ACLR as a function of electrical power and *Ts*.

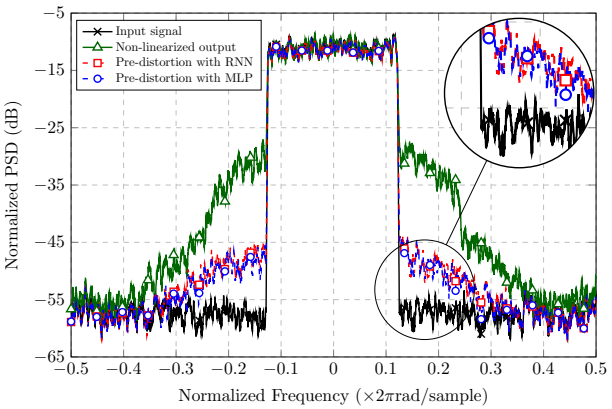

Fig. 11. Frequency spectrum for an OFDM signal for distinct pre-distortion schemes.

be explained by the ANN training process. The out-of-band distortions of the non-linearized OFDM signal are produced by correlated intermodulation products. On the other hand, the correspondent non-distorted OFDM signal, used as desired labels has a low correlation among its time samples, therefore, the memory effect does not influence on the out-of-band distortion compensation. Hence, a simple MLP ANN can be considered the best choice in the case we are only interested in the OOBE reduction, without concern about the in-band performance degradation. This statement is validated by the memoryless MLP-based linearization, which has produced similar results in terms of ACLR and the worst performance considering EVM_{RMS} and NMSE metrics. Meanwhile, the RNN presents a powerful solution for simultaneously reducing in-band and out-of-band distortions.

The normalized PSD was also investigated for the proposed schemes and compared with the non-linearized signal, as can be seen in Fig.11. For this analysis, we only consider pre-distortion with *Ts*= 3 and MLP-based linearization. The normalized PSD was plotted for OFDM signal with 20 dBm at MZM input for either the non-linearized or linearized signals. We can notice that the RNN and MLP linearization schemes have produced a similar reduction on the OOBE, which is in accordance with the ACLR analysis. Therefore, the proposed RNN linearization schemes proved to be an interesting solution for eRAC scenario, since it allows for high-level RF power without producing significant distortions. Furthermore, the significant reduction in the OOBE favors the exploitation of TVWS in remote areas.

5. CONCLUSIONS

In this paper, we have presented two approaches based on machine-learning algorithms for linearizing amplified radio over systems. The main motivation scenario for the proposed schemes is the TVWS exploitation in remote and rural areas. In this case, a simple RRH is placed in the region to be covered, while all signal processing is performed in the CO and a long optical link is used to carry the RF signal over an optical carrier among these two elements of the network. For overcoming the additional attenuation due to link extension, high-RF/optical power is required. However, as RF power increases, the nonlinear distortions become prohibitive since the intermodulation products will increase the in-band and out-of-band distortions. Our proposed schemes employ two RNN ANN for obtaining the system post-inversion response and for modeling the A-RoF

system integrated with an PA. The system post-inversion response was used for implementing the pre- and post-distortion schemes. The main advantage of our approaches relies on the capability of simultaneously reducing in-band and out-band non-linear distortions.

The performance of the proposed schemes was compared with a machine-learning linearization solution based on a multilayer perceptron implementation, which cannot deal with the nonlinear memory effect. The performance evaluation was carried out considering three metrics: ACLR, NMSE and EVM_{RMS}. The RNN outperformed MLP linearization in terms of NMSE, and EVM_{RMS}, where the memory effect of the nonlinear devices play an important role. It is important to emphasize that besides employing RNN, it is also possible to feed the neural network with past samples to compensate for the memory effect. This approach will be exploited in future works. It was demonstrated that a memoryless ANN, e.g., MLP, is capable of reducing the out-band distortions but can not satisfactorily reduce the in-band distortion. Therefore, MLP can be used when only OOBE reduction is relevant, without concern about the in-band degradation. On the other hand, our proposed RNNs simultaneously reduces in-band and out-of-band distortions. The performance of the proposed schemes in terms of NMSE and EVM_{RMS} depends on the memory depth. It was demonstrated that when the RNN memory depth is equal to or higher than the PA memory depth, i.e., $Ts \geq Q$, the performance of the linearization schemes in terms of EVM_{RMS} and NMSE is improved. The results presented in this paper show that the proposed RNN-based linearization schemes can be an important tool to assure the proper exploitation of TVWS in remote and rural areas.

For future research, we intend to add to the analysis the non-linear and linear effects of the optical fiber and other elements present in the communication chain. In addition, we also intend to investigate other ANN architecture that employs recurrent layers for compensating memory effect. Furthermore, we envisage experimentally validating our approaches in a demonstration platform, where all signals can be generated transmitted, and received in a real-world implementation.

FUNDING

SAMURAI project (20/05127-2); 6G Mobile Communications Systems project (01245.020548/2021-07); Ministério da Ciência, Tecnologia e Inovações e Comunicações (MCTIC); Instituto Nacional de Telecomunicações (Inatel); Fundação de Amparo à Pesquisa do Estado de São Paulo (FAPESP); Rede Nacional de Ensino e Pesquisa (RNP); Conselho Nacional de Desenvolvimento Científico e Tecnológico (CNPq); Coordenação de Aperfeiçoamento de Pessoal de Nível Superior (CAPES); Financiadora de Estudos e Projetos (FINEP);Fundação de Amparo à Pesquisa do Estado de Minas Gerais (FAPEMIG).

REFERENCES

1. H. Tataria, M. Shafi, A. F. Molisch, M. Dohler, H. Sjöland, and F. Tufvesson, "6G Wireless Systems: Vision, Requirements, Challenges, Insights, and Opportunities," Proc. IEEE **109**, 1166–1199 (2021).
2. Z. Zhang, Y. Xiao, Z. Ma, M. Xiao, Z. Ding, X. Lei, G. K. Karagiannidis, and P. Fan, "6G Wireless Networks: Vision, Requirements, Architecture, and Key Technologies," IEEE Veh. Technol. Mag. **14**, 28–41 (2019).
3. A. Chaoub, M. Giordani, B. Lall, V. Bhatia, A. Kliks, L. Mendes, K. Rabie, H. Saarnisaari, A. Singhal, N. Zhang, S. Dixit, and M. Zorzi, "6G for Bridging the Digital Divide: Wireless Connectivity to Remote Areas," IEEE Wirel. Commun. **29**, 160–168 (2022).
4. W. Dias, D. Gaspar, L. Mendes, M. Chafii, M. Matthé, P. Neuhaus, and G. Fettweis, "Performance Analysis of a 5G Transceiver Implementation for Remote Areas Scenarios," in *2018 European Conference on Networks and Communications (EuCNC),* (IEEE, 2018), pp. 363–367.
5. 5G RuralFirst consortium, "5G RuralFirst: New Thinking Applied to Rural Connectivity," Technical report, Departure for Digital, Culture, Media and Sports (2019). Available at: https://www.5gruralfirst.org/wp-content/uploads/2019/10/5G-RuralFirst-New-Thinking-Applied-to-Rural-Connectivity-1.pdf.
6. F. Schaich, M.-H. Hamon, M. Hunukumbure, J. Lorca, K. Pedersen, M. Schubert, E. Kosmatos, G. Wunder, and K. Reaz, "The ONE5G Approach Towards the Challenges of Multi-Service Operation in 5G Systems," in *2018 IEEE 87th Vehicular Technology Conference (VTC Spring),* (2018), pp. 1–6.
7. L. L. Mendes, C. S. Moreno, M. V. Marquezini, A. M. Cavalcante, P. Neuhaus, J. Seki, N. F. T. Aniceto, H. Karvonen, I. Vidal, F. Valera, P. A. S. M. Barreto, M. F. Caetano, W. D. Dias, and G. Fettweis, "Enhanced Remote Areas Communications: The Missing Scenario for 5G and Beyond 5G Networks," IEEE Access **8**, 219859–219880 (2020).
8. J. Wang, C. Liu, M. Zhu, A. Yi, L. Cheng, and G.-K. Chang, "Investigation of Data-Dependent Channel Cross-Modulation in Multiband Radio-Over-Fiber Systems," J. Light. Technol. **32**, 1861–1871 (2014).
9. C. Mateo, P. L. Carro, P. García-Dúcar, J. De Mingo, and Í. Salinas, "Radio-over-fiber Linearization With Optimized Genetic Algorithm CPWL Model," Opt. Express **25**, 3694–3708 (2017).
10. A. Hekkala, M. Hiivala, M. Lasanen, J. Perttu, L. C. Vieira, N. J. Gomes, and A. Nkansah, "Predistortion of Radio over Fiber Links: Algorithms, Implementation, and Measurements," IEEE Transactions on Circuits Syst. I: Regul. Pap. **59**, 664–672 (2011).
11. J. James, P. Shen, A. Nkansah, X. Liang, and N. J. Gomes, "Nonlinearity and Noise Effects in Multi-Level Signal Millimeter-Wave Over Fiber Transmission Using Single and Dual Wavelength Modulation," IEEE Transactions on Microw. Theory Tech. **58**, 3189–3198 (2010).
12. M. Noweir, Q. Zhou, A. Kwan, R. Valivarthi, M. Helaoui, W. Tittel, and F. M. Ghannouchi, "Digitally Linearized Radio-Over Fiber Transmitter Architecture for Cloud Radio Access Network's Downlink," IEEE Transactions on Microw. Theory Tech. **66**, 3564–3574 (2018).
13. A. M. Cavalcante, M. V. Marquezini, L. Mendes, and C. S. Moreno, "5G for Remote Areas: Challenges, Opportunities and Business Modeling for Brazil," IEEE Access **9**, 10829–10843 (2021).
14. M. A. Habibi, M. Nasimi, B. Han, and H. D. Schotten, "A Comprehensive Survey of RAN Architectures Toward 5G Mobile Communication System," IEEE Access **7**, 70371–70421 (2019).
15. F. Tonini, C. Raffaelli, L. Wosinska, and P. Monti, "Cost-Optimal Deployment of a C-RAN With Hybrid Fiber/FSO Fronthaul," J. Opt. Commun. Netw. **11**, 397–408 (2019).
16. V. A. Thomas, M. El-Hajjar, and L. Hanzo, "Performance Improvement and Cost Reduction Techniques for Radio Over Fiber Communications," IEEE Commun. Surv. Tutorials **17**, 627–670 (2015).
17. L. A. M. Pereira, C. H. S. Lopes, R. M. Borges, E. S. Lima, A. C. Ferreira, M. Abreu, L. L. Mendes, and Arismar Cerqueira S. Jr., "Implementation of a Multiband 5G NR Fiber-wireless System Using Analog Radio over Fiber Technology," Opt. Commun. **474**, 126112 (2020).
18. D. Wake, A. Nkansah, and N. J. Gomes, "Radio over Fiber Link Design for Next Generation Wireless Systems," J. lightwave Technol. **28**, 2456–2464 (2010).
19. A. Udalcovs, M. Levantesi, P. Urban, D. A. Mello, R. Gaudino, O. Ozolins, and P. Monti, "Total Cost of Ownership of Digital vs. Analog Radio-over-Fiber Architectures for 5G Fronthauling," IEEE Access **8**, 223562–223573 (2020).
20. T. Ismail, C.-P. Liu, J. E. Mitchell, and A. J. Seeds, "High-Dynamic-Range Wireless-Over-Fiber Link Using Feedforward Linearization," J. Light. Technol. **25**, 3274–3282 (2007).
21. S. Korotky and R. de Ridder, "Dual parallel modulation schemes for low-distortion analog optical transmission," IEEE J. on Sel. Areas Commun. **8**, 1377–1381 (1990).
22. B. Masella, B. Hraimel, and X. Zhang, "Enhanced Spurious-Free Dynamic Range Using Mixed Polarization in Optical Single Sideband

Mach–Zehnder Modulator," J. Light. Technol. **27**, 3034–3041 (2009).
23. G.-W. Lee and S.-K. Han, "Linearization of a narrowband analog optical link using integrated dual electroabsorption modulator," in *International Topical Meeting on Microwave Photonics. MWP'99. Technical Digest (Cat. No.99EX301),* (1999), pp. 21–24 vol.1.
24. X. Zhang, "Broadband Linearization for 5G Fronthaul Transmission," Front. Optoelectronics **11**, 107–115 (2018).
25. X. Zhang, S. Saha, R. Zhu, T. Liu, and D. Shen, "Analog Pre-Distortion Circuit for Radio Over Fiber Transmission," IEEE Photonics Technol. Lett. **28**, 2541–2544 (2016).
26. Y. Shen, B. Hraimel, X. Zhang, G. E. R. Cowan, K. Wu, and T. Liu, "A Novel Analog Broadband RF Predistortion Circuit to Linearize Electro-Absorption Modulators in Multiband OFDM Radio-Over-Fiber Systems," IEEE Transactions on Microw. Theory Tech. **58**, 3327–3335 (2010).
27. R. Zhu, X. Zhang, B. Hraimel, D. Shen, and T. Liu, "Broadband Predistortion Circuit Using Zero Bias Diodes for Radio Over Fiber Systems," IEEE Photonics Technol. Lett. **25**, 2101–2104 (2013).
28. S. Liu, X. Wang, W. Zhang, G. Shen, and H. Tian, "An Adaptive Activated ANN Equalizer Applied in Millimeter-wave RoF Transmission System," IEEE Photonics Technol. Lett. **29**, 1935–1938 (2017).
29. S. Liu *et al.*, "A Multilevel Artificial Neural Network Nonlinear Equalizer for Millimeter-Wave Mobile Fronthaul Systems," J. Light. Technol. **35**, 4406–4417 (2017).
30. E. Liu, Z. Yu, C. Yin, and K. Xu, "Nonlinear Distortions Compensation Based on Artificial Neural Networks in Wideband and Multi-Carrier Systems," IEEE J. Quantum Electron. **55**, 1–5 (2019).
31. M. U. Hadi, "Mitigation of nonlinearities in analog radio over fiber links using machine learning approach," ICT Express **7**, 253–258 (2021).
32. L. A. M. Pereira, L. L. Mendes, C. J. A. Bastos-Filho, and Arismar Cerqueira S. Jr, "Linearization Schemes for Radio Over Fiber Systems Based on Machine Learning Algorithms," IEEE Photonics Technol. Lett. **34**, 279–282 (2022).
33. H. Chen, J. Li, K. Xu, Y. Pei, Y. Dai, F. Yin, and J. Lin, "Experimental Investigation on Multi-dimensional Digital Predistortion for Multi-band Radio-over-fiber Systems," Opt. express **22**, 4649–4661 (2014).
34. T. Kim and T. Adali, "Fully Complex Multi-Layer Perceptron Network for Nonlinear Signal Processing," J. VLSI signal processing systems for signal, image video technology **32**, 29–43 (2002).
35. H. Ku and J. S. Kenney, "Behavioral Modeling of Nonlinear RF Power Amplifiers Considering Memory Effects," IEEE transactions on microwave theory techniques **51**, 2495–2504 (2003).
36. J. H. Vuolevi, T. Rahkonen, and J. P. Manninen, "Measurement technique for characterizing memory effects in RF power amplifiers," IEEE Transactions on microwave theory techniques **49**, 1383–1389 (2001).
37. L. Gupta, M. McAvoy, and J. Phegley, "Classification of Temporal Sequences Via Prediction Using the Simple Recurrent Neural Network," Pattern Recognit. **33**, 1759–1770 (2000).
38. B. Nakisa, M. N. Rastgoo, A. Rakotonirainy, F. Maire, and V. Chandran, "Automatic Emotion Recognition Using Temporal Multimodal Deep Learning," IEEE Access **8**, 225463–225474 (2020).
39. T. Zhang, W. Zheng, Z. Cui, Y. Zong, and Y. Li, "Spatial–Temporal Recurrent Neural Network for Emotion Recognition," IEEE Transactions on Cybern. **49**, 839–847 (2019).
40. K. Williams, R. Esman, and M. Dagenais, "Nonlinearities in p-i-n Microwave Photodetectors," J. Light. Technol. **14**, 84–96 (1996).
41. V. J. Urick, J. F. Diehl, J. D. McKinney, J. M. Singley, and C. E. Sunderman, "Nonlinear Optical Angle Modulation for Suppression of RF Interference," IEEE Transactions on Microw. Theory Tech. **64**, 2198–2204 (2016).
42. F. M. Ghannouchi, O. Hammi, and M. Helaoui, *Behavioral Modeling and Predistortion of Wideband Wireless Transmitters* (John Wiley & Sons, 2015).
43. L. A. M. Pereira, L. L. Mendes, C. J. A. Bastos-Filho, and Arismar Cerqueira S. Jr, "Machine Learning-Based Linearization Schemes for Radio Over Fiber Systems," IEEE Photonics J. **14**, 1–10 (2022).
44. A. Loukas *et al.*, "Distributed Autoregressive Moving Average Graph Filters," IEEE Signal Process. Lett. **22**, 1931–1935 (2015).
45. Y.-S. Lee and L.-I. Tong, "Forecasting Time Series Using a Methodology Based on Autoregressive Integrated Moving Average and Genetic Programming," Knowledge-Based Syst. **24**, 66–72 (2011).
46. A. Graves, "Long Short-Term Memory," Supervised sequence labelling with recurrent neural networks pp. 37–45 (2012).
47. K. Y. Lee, A. Sode-Yome, and J. H. Park, "Adaptive Hopfield Neural Networks for Economic Load Dispatch," IEEE transactions on power systems **13**, 519–526 (1998).
48. A. Géron, *Hands-on Machine Learning with Scikit-Learn, Keras, and TensorFlow: Concepts, Tools, and Techniques to Build Intelligent Systems* (" O'Reilly Media, Inc.", 2019).
49. Y. Wu, U. Gustavsson, A. G. i Amat, and H. Wymeersch, "Residual Neural Networks for Digital Predistortion," in *GLOBECOM 2020-2020 IEEE Global Communications Conference,* (IEEE, 2020), pp. 01–06.
50. I. Goodfellow, Y. Bengio, and A. Courville, *Deep learning* (MIT press, 2016).
51. 3GPP, "Group RAN; NR; base station (BS) conformance testing part 1: Conducted conformance testing," 3GPP TS **38.141-1 version 1.0.0**, Release15 (2018).

AUTHOR BIOGRAPHIES

Luiz Augusto Melo Pereira received the B.Sc. and the M.Sc. degree in telecommunications engineering from the National Institute of Telecommunications (Inatel), Brazil, in 2017 and 2020, respectively and is a PhD student in telecommunications in the same institution. Currently acts as a researcher at Inatel.

Luciano Leonel Mendes received the B.Sc. and M.Sc. degrees from Inatel, Brazil, in 2001 and 2003, respectively, and the Doctor degree from Unicamp, Brazil, in 2007, all in electrical engineering. From 2013 to 2015, he was a Visiting Researcher with the Technical University of Dresden in the Vodafone Chair Mobile Communications Systems, where he has developed his postdoctoral. Since 2001 he is a professor at Inatel, where currently he acts as the Research Coordinator of the Brasil 6G project.

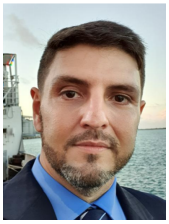

Carmelo José Albanez Bastos Filho (Senior Member, IEEE) received the B.Sc. degree in electronics engineering and the M.Sc. and Ph.D. degrees in electrical engineering from the Federal University of Pernambuco (UFPE) in 2000, 2003, and 2005, respectively. He is currently an Associate Professor with the Polytechnic School, University of Pernambuco. He authored or coauthored roughly 300 full papers in journals and conferences and advised more than 50 Ph.D. and M.Sc. candidates.

Arismar Cerqueira Sodré Junior received his Ph.D. degree from Scuola Superiore Sant'Anna-Italy in 2006. He was Invited Researcher and Professor from many world-recognized universities, such as Scuola Superiore Sant'Anna-Italy, University of Oulu, Danish Technical University-Denmark, Max-Planck Institute-Germany and University of Bath-UK. He is a holder of 12 patents, has transferred 25 products to the industry and has published over 300 scientific papers.

Paper 5: Machine Learning Applied to 6G Radio over Fiber Systems Linearization

Luiz Augusto Melo Pereira, Luciano Leonel Mendes, Carmelo José Albanez Bastos-Filho and Arismar Cerqueira Sodré Junior. "Machine Learning Applied to 6G Radio over Fiber Systems Linearization", *IEEE International Conference on Electrical, Computer, Communications and Mechatronics Engineering*, pp. 1-6, November, 2022.

Publisher: IEEE Conference

Proc. of the International Conference on Electrical, Computer, Communications and Mechatronics Engineering (ICECCME)
16-18 November 2022, Maldives

Machine Learning Applied to 6G Radio over Fiber Systems Linearization

1st Luiz A. M. Pereira
Wireless and Optical Convergent Access (WOCA) Laboratory
Instituto Nacional de Telecomunicações (Inatel)
Santa Rita do Sapucaí, Brazil
luiz.augusto@dtel.inatel.br

2nd Luciano L. Mendes
Centro de Referência em Radiocomunicações (CRR)
Instituto Nacional de Telecomunicações (Inatel)
Santa Rita do Sapucaí, Brazil
lucianol@inatel.br

3rd Carmelo J. A. Bastos-Filho
Polytechnic School of Pernambuco
Universidade Federal de Pernambuco (UFPE)
Santa Rita do Sapucaí, Brazil
carmelo.filho@upe.br

4th Arismar Cerqueira S. Jr.
Wireless and Optical Convergent Access (WOCA) Laboratory
Instituto Nacional de Telecomunicações (Inatel)
Santa Rita do Sapucaí, Brazil
arismar@inatel.br

***Abstract*—This work proposes the development and demonstrates the applicability of a machine learning (ML)-based digital pre-distortion (DPD) tool applied to the sixth-generation of mobile network (6G) analog radio over fiber (A-RoF) systems linearization. Particularly, our tool was idealized for linearizing electrically amplified A-RoF, which transport downlink signals from the central office, where the baseband unit might be implemented using a software-defined radio approach, to simplified remote radio units (RRUs). A memory recurrent neural network (RNN) DPD and its performance in terms of root mean square error vector magnitude (EVM_{RMS}) and adjacent channel leakage ratio (ACLR) are investigated for different activation functions.**

***Index Terms*—Analog radio-over-fiber, digital pre-distortion, machine learning and recurrent neural network.**

I. Introduction

Nowadays, several research institutes around the globe are proposing use cases and defining the requirements for the future sixth-generation of mobile network (6G) [1]. Although the definition of this new mobile communication network is incipient, one important application scenario named enhanced remote area communications (eRAC) [2] is gathering attention. This scenario aims to provide broadband communication in remote and rural areas, a service that the 5G New Radio (5G NR) does not support it. However, besides the technological barrier, deployment, and maintenance costs are also challenges for the eRAC success. Therefore, cost-effective solutions are required to provide the necessary infrastructure in remote areas. The centralized radio access network (C-RAN), satellite network, television (TV) white space (TVWS) and analog radio over fiber (A-RoF) technologies can play important roles in this challenging operating scenario. C-RAN allows for implementing the entire BBU using software-defined radio (SDR) approach, which can run in the central office (CO), reducing the deployment costs [3]. TVWS enables the unlicensed exploitation of vacant ultra-high frequency (UHF) channels for mobile communication [4]. Finally, A-RoF can be employed to transport analog downlink signals from the baseband unit (BBU) running in the CO to a simplified remote radio head (RRH) composed by an optical-to-electrical converter (OEC), the power amplifier (PA) and radiofrequency (RF) filters, reducing the network deployment cost and increasing its capillarity [5].

Since A-RoF is considered an essential technology for transporting analog RF signals, it is interesting to provide solutions for the main distortions introduced by this system. One challenge is to deal with the non-linearities mainly imposed by the Mach-Zehnder modulator (MZM). The MZM has a nonlinear power response that leads to the in-band and out-band interferences. Depending on the distortion level, the exploitation of TVWS will be hindered mainly by out-band distortion that can leave to severe interference in adjacent digital television (DTV) signals. In contrast, in-band distortions will degrade the mobile communication system's performance. The PA used to provide electrical power for the signal transmitted by the RRH is yet another source of non-linearities. However, while the MZM can be modeled as a memoryless nonlinear system, the PA is a nonlinear system with memory. Therefore, as mentioned earlier, considering the memory effect, a linearization technique is necessary to minimize the impacts of the distortions.

The most prominent linearization technique is based on pre-distorting the signal at the BBU, by means of applying the estimated system inverse response. This technique is known as digital pre-distortion (DPD) and is usually employed in

This work was supported by RNP-MCTIC Grant No. 01245.020548/2021-07, under the 6G project, FAPESP Grant No. 20/05127-2, under SAMURAI project, CNPq, CAPES, FINEP and FAPEMIG.

978-1-6654-7095-7/22/$31.00 © 2022 IEEE

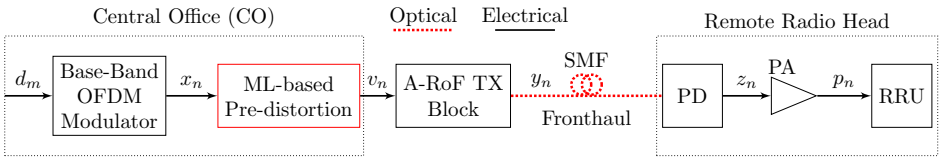

Fig. 1. Block diagram of the electrically amplified radio over fiber system assisted by the machine learning-based pre-distortion.

A-RoF systems [6–8]. Another approach to deal with the non-linearities in A-RoF is to use an equalizer placed in the RRH [9]. More recently, machine learning (ML) has also been employed for linearizing the A-RoF system by employing the DPD and equalization techniques. In [10], an artificial neural network (ANN)-based equalizer was proposed for reducing the nonlinear distortions and interference among multiple users in uplink transmissions. In-band nonlinear distortion mitigation by applying an ANN-based equalizer is proposed in [11]. In [12], authors demonstrate a DPD solution for linearizing an A-RoF system. Particularly, we have employed a multi-layer perceptron (MLP) DPD and equalization linearization schemes aimed for A-RoF [13]. However, the PA present in the RRH was not considered at that time. In [14] we have introduced a recurrent neural network (RNN)-based DPD which considers the non-linearities coming from the MZM and from the PA, meaning that the DPD must deal with the memory effect. However, the RNN hyperparameters can consider several activation functions that lead to a different performance in terms of root mean square error vector magnitude (EVM_{RMS}) and adjacent channel leakage ratio (ACLR).

This paper aims to analyze the performance of the RNN-based DPD, considering different activation functions. The main contribution of this paper is the performance evaluation of an innovative ML DPD scheme that employs a RNN to compensate for the non-linear distortions present in electrically amplified A-RoF systems that compose the transport network of a C-RAN. This paper is organized as follows. Section II describes the nonlinear models used for modeling both MZM and PA. Section III presents the proposed RNN-based DPD scheme concepts, whereas Section IV reports its results and performance evaluation. Finally, the conclusions and future works are discussed in Section V.

II. Base-Band Equivalent System Model

Fig. 1 depicts the block diagram of the electrically amplified A-RoF system. We have assumed the mobile network was in accordance with the C-RAN architecture, in which the core network is connected to the CO by an optical backhaul link. The baseband signal unit generates the orthogonal frequency division multiplexing (OFDM) signal, given by

$$x_n = \sum_{m=0}^{M-1} d_m e^{-j2\pi \frac{m}{M}(n+1)}, \tag{1}$$

where d_m is the modulated data, which are mapped in the mth subcarrier, $m \in \{0,\ 1,\ 2,\ \ldots,\ M-1\}$ and $n \in \{0, 1, \ldots, N-1\}$ is the time index. The baseband signal is pre-distorted by the proposed ML-based DPD. It is important to notice that the DPD coefficients must be previously calculated during the ANN training. Sequentially, the pre-distorted signal is applied to the A-RoF transmitter (TX) block, which is composed of an MZM and laser diode (LD). At the RRH, a photodetector (PD) converts the signal to the electrical domain for being upconverted, amplified and radiated by the remote radio unit (RRU) over the covered area. The base station (BS) medium access control (MAC) and physical layer (PHY) functions run at CO using SDR implementation. It will be assumed that TVWS will be employed aiming to enable eRAC applications. In the next subsections, the mathematical models used for modeling the nonlinearities of the A-RoF TX block and PA are presented.

A. Analog Radio over Fiber Transmitter Model

A memoryless polynomial with non-linearity order $J = 5$ has been recently used for modeling the non-linearities of the A-RoF system. Such a model has its non-linear behavior ruled by a set of coefficients, denoted by h_j, with $j \in \{0, 1, \ldots, J-1\}$. The relation between the samples at the system input (v_n) and output (y_n) is given by [15]

$$y_n = \sum_{j=0}^{J-1} h_j |v_n|^j v_n, \tag{2}$$

where v_n is the baseband signal at the MZM input, $n \in \{0, 1, 2, \ldots, N-1\}$ is the time index.

B. Power Amplifier Model

The architecture considered in this paper employs a PA at RRH to amplify the signal before wireless transmission. A memory polynomial model, a pruned version of the Volterra series, is widely employed for modeling the PA nonlinear response. This model encompasses the memory effect presented by practical PA devices. The memory effect is the dependence of the instantaneous output PA on the previous input. In other words, the PA output also depends on the samples of the previously applied signal to the PA input. The memory depth (Q) defines how many samples impact the PA output. The memory polynomial model is expressed as

$$p_n = \sum_{q=0}^{Q-1} \sum_{k=0}^{K-1} \xi_{q,k} \left| z_{n-q} \right|^k z_{n-q}, \tag{3}$$

where $\xi_{q,k}$ are coefficients of the PA model, with $q \in \{0, 1, \cdots, Q-1\}$ and $k \in \{0, 1, \cdots, K-1\}$, in which

Q is the memory depth and K is the nonlinearity order of the model.

Fig. 2 illustrates the memory and memoryless polynomial models transfer function. The same input signal z_n was employed in both polynomial models. For each normalized magnitude of the input signal, i.e, $|z_n|$, a normalized output signal $|p_n|$ is generated. It can be observed that the memory effect produces a scattered behavior in the output of the signal. Additionally, the output points' dispersion increases as the memory effect increases, which is caused by the dependency on the past samples.

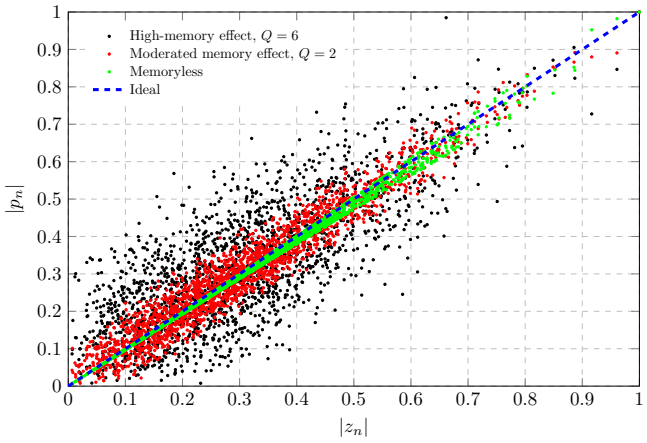

Fig. 2. Nonlinear models instantaneous transfer functions.

III. Machine Learning-based Digital Pre-Distortion

We have used an ANN to implement the DPD processing block. Once the cascade response of A-RoF TX block and PA has a memory effect, an RNN was chosen since it has a memory structure that can be used for compensating the memory effect. The proposed solution employs two ANN for modeling the amplified A-RoF system and the PA device. We refer to this solution as dual-ANN DPD. The first step for linearizing the amplified A-RoF system consists of training both ANN. Once trained, we can apply the ANN predict function to obtain the pre-distorted signal that will be applied to the MZM. The following subsections detail the ANNs training process, as well as the concepts of the proposed dual-ANN DPD scheme.

A. Artificial Neural Network Training

We have chosen the RNN since it enables us to evaluate the memory effect. The RNN is composed of an input layer, L hidden layers and one output layer. Each layer has O_ℓ neurons, with $\ell \in \{0, \cdots, L+1\}$, ℓ denoting the ℓth layer. The neurons are densely connected in sequential layers, and they also have connections pointing backward, as demonstrated in Fig. 3. The RNN output is a function of the instantaneous and previous samples of the input signal in a given time step (Ts).

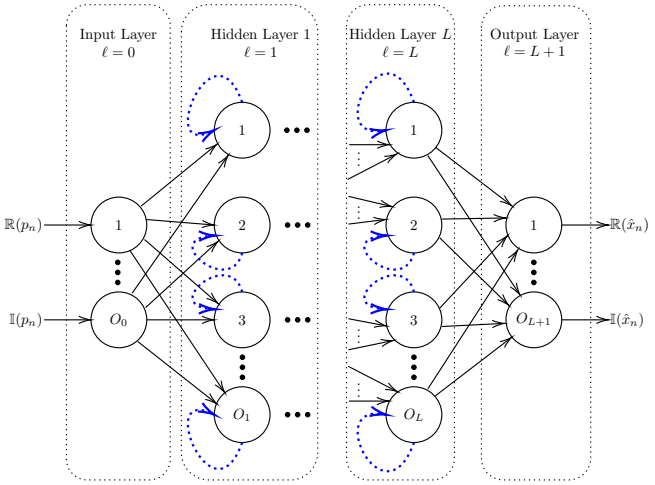

Fig. 3. Recurrent neural network architecture composed of the following layers: input layer ($\ell = 0$); hidden layers ($\ell = 1, ..., L$); output layer ($\ell = L + 1$). Each layer has O_ℓ neurons..

Our proposed dual-ANN DPD employs two neurons in the input and output layers. Accordingly to our studies, two hidden layers with 64 and 32 neurons produce a trade-off between complexity and performance. A high number of hidden layers may hinder the neural network training process since the number of hyperparameters will grow and the known vanishing gradient problem may occur. To overcome this problem, activation functions with more linear and non-saturating behavior can be used at the cost of reducing the capacity of the neural network for representing nonlinear behaviors. In this paper, only two hidden layers were enough to capture the non-linearities produced by the MZM component, which means that not exploding or vanishing gradient problems were observed. In any case, we initialize the neural network weights using the Glorot normal initializer, which mitigates the aforementioned problems. The backpropagation algorithm is used to estimate both matrix of weights ($\mathbf{W}_p$) and ($\mathbf{W}_v$). The training was performed throughout 10,000 epochs in case the early stop criterion was no reached. The employed early stop technique is based on the patience hyperparameter, which was heuristically set to 100. This means that the training process stops when a mean-squared error (MSE) variation higher than 10^{-9} ($\Delta_{min} = 10^{-9}$) is not observed throughout 100 epochs. The MSE loss function ($\mathcal{L}$) is given by

$$\mathcal{L} = \frac{1}{N_{\text{TR}}} \sum_{n=0}^{N_{\text{TR}}-1} (x_n - \hat{x}_n)^2, \tag{4}$$

where N_{TR} is the number of training instances. We have employed a data set composed of 614,400 samples, in which 30% were used for validating and 70% for training the model, which means that $N_{\text{TR}} = 430,080$. Regarding the activation function, many of them were tested, including exponential linear unit (Elu), Leaky rectified linear unit (Leaky ReLU),

Softsign, scaled exponential linear unit (SELU), and hyperbolic tangent (tanh) activation functions.

Fig. 4 depicts the block diagram of the components used to create the training data set, which was generated by applying the base-band OFDM signal to the models that represent the A-RoF TX block and PA. Mathematically, the baseband OFDM signal (x_n) is generated using (1) and then applied to (2), leading to y_n. Once in this work we are only interested in the MZM and PA nonlinearities, we have assumed that the single-mode fiber (SMF) and PD combined response is $g_n = \delta_n$, which is the unit impulse response. Therefore, the signal at PD output is given by

$$z_n = y_n * g_n + w_n, \tag{5}$$

where w_n is the additive white Gaussian noise (AWGN) and $*$ denotes the convolution operation. The signal at PD output is amplified by applying (3) with z_n as the input signal, resulting in the distorted-amplified p_n signal. After that, we can use the original non-distorted signal (x_n) as the desired label and p_n as the input of the RNN. This strategy allows for the RNN to learn the system post-inversion response, which is used for pre-distorting the baseband signal. We used a second RNN to model the amplified A-RoF system. In this case, the desired label will be denoted by p_n with x_n as the second RNN input.

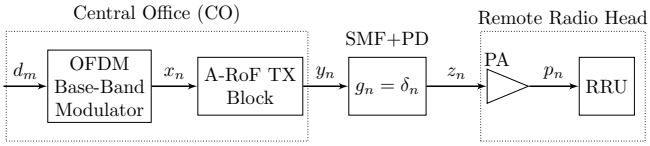

Fig. 4. Block Diagram of the architecture used for training the RNN.

The ML-based algorithm complexity is an important parameter to be taken into account. The complexity analysis was performed applying the float-point operations (flops) counter method, where one flop is defined as one multiplication followed by and addition of two float-point numbers. Considering that the employed architecture only the hidden layers are recursive, we can express the ML-based DPD complexity by

$$\mathcal{O}\left(\dim(\mathbf{P})\left[\sum_{\ell=0}^{L} O_\ell O_{\ell+1} + \sum_{\ell=1}^{L} O_\ell^2\right]\right) \tag{6}$$

where $\dim(\cdot)$ returns the size of the input training matrix. One can note that the complexity of the proposed DPD grows linearly with the dimension of the input matrix and quadratically with the number of hidden layers and number of neurons from the hidden layers.

B. Machine Learning Based Digital Pre-distortion

Considering that the RNNs have already been trained, the DPD scheme can be employed for linearizing the electrically amplified A-RoF system. Since the system cascade response presents memory effect that comes from the PA, the RNN internal memory structure needs to be used for compensating the memory effect. The Ts hyperparameter defines the RNN memory depth. Properly adjusting the Ts is a key configuration to enhance the linearization performance. Assuming that the matrix of weights was already calculated in the training process, the baseband OFDM signal (x_n) will be pre-distorted by using the prediction method of the first trained RNN. The pre-distorted signal is given by

$$\mathbf{V}_{(t)} = \phi\left(\mathbf{P}_{(t)}\mathbf{W}_p + \mathbf{V}_{(t-1)}\mathbf{W}_v + \mathbf{b}\right), \tag{7}$$

where $\phi(.)$ is the nonlinear activation function, $\mathbf{P}_{(t)}$ represents the input matrix at $Ts{=}\ t$, $\mathbf{V}_{(t-1)}$ is the output matrix of the previous Ts and $\mathbf{b}$ is the bias vector. Sequentially, the matrix of pre-distorted signal ($\mathbf{V}$) is applied to the second RNN, which was trained to mimic the amplified A-RoF response. Therefore, the linearized signal p_n is obtained by applying (7) with $\mathbf{V}$ as input. Finally, the linearized signal can be transmitted by exploiting TVWS without causing interference in the adjacent frequency bands.

We have tested several activation functions during the RNN training process. Fig. 5 presents the RNN modeling for distinct activation functions. We have compared the real part of the output of the amplified A-RoF system when (2) and (3) are applied with the RNN predict method. It can be observed that tanh has led to the best linearization performance, attaining MSE = $6.18{\times}10^{-3}$. Table I summarizes the MSE for all the tested activation functions.

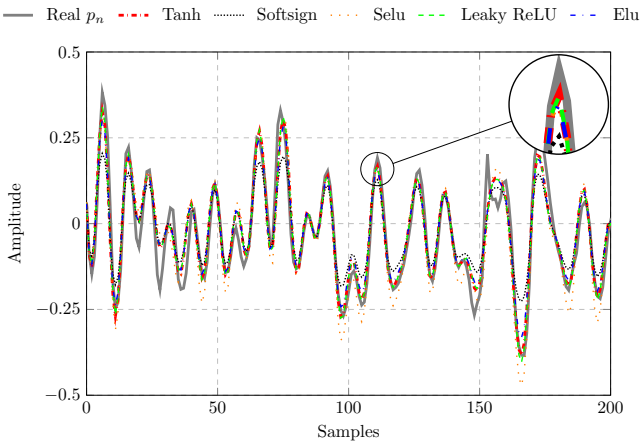

Fig. 5. Estimation of system output for distinct activation functions.

TABLE I
MEAN SQUARED ERROR

	tanh	Softsign	Selu	Leaky ReLU	Elu
MSE	$6.18{\times}10^{-3}$	$1.1{\times}10^{-2}$	$9.18{\times}10^{-3}$	$6.38{\times}10^{-3}$	$6.64{\times}10^{-3}$

IV. Performance Evaluation

This section reports the results of the proposed dual-ANN DPD performance evaluation. The proposed scheme was specially designed to enable eRAC applications by exploiting

TVWS opportunities. One important motivation for designing a DPD scheme for this scenario is the need for dynamically allocating power to cover distinct regions. This strategy inhibits the out-of-band emission (OOBE) that can interfere in the RF channels used for broadcasting TV services. The novel dual-ANN DPD was designed upon application programming interface (API) Keras. Its performance investigation was carried out considering two figures of merit, namely: EVM_{RMS} and ACLR. The EVM_{RMS} enables us to evaluate the dispersion produced in the quadrature amplitude modulation (QAM) symbols coordinates due to the nonlinear behavior of the system. The EVM_{RMS} metric is expressed as

$$\text{EVM}_{\text{RMS}}(\%) = 100\sqrt{\frac{\sum_{m=0}^{M-1}\left|d_m - \hat{d}_m\right|_2^2}{\sum_{m=0}^{M-1}|d_m|_2^2}}, \tag{8}$$

where $\hat{d}_m$ is the symbol received on the mth subcarrier, d_m is the symbol allocated in the mth subcarrier at the transmitter side and $|(.)|_p$ is the p-norm operator. We have also employed the ACLR metric for evaluating the signal OOBE, given by

$$\text{ACLR (dB)} = 10\log\left(\frac{\int_{f\in B_{\text{O}}} P_p(f)df}{\int_{f\in B_{\text{I}}} P_p(f)df}\right), \tag{9}$$

where $P_p(f)$ stands for the power spectrum density (PSD) of p_n at frequency f , B_{I} and B_{O} represent the in-band and out-of-bands frequencies, respectively.

The performance evaluation was conducted by testing several activation functions, including tanh, Softsign, SELU, Leaky ReLU with $\alpha = 0.8$ and Elu. We have used the same nonlinearity order ($J = K = 5$) of polynomial models for modeling the MZM and PA power response. It is important to highlight that the memory effect was only considered for the PA model. We have employed memory depth $Q = 3$ to model the PA power response. These parameters were chosen as a proof of concept. In practical systems, the parameters that enable properly modeling the system nonlinear devices must be firstly characterized. Nonetheless, we have typically employed values demonstrated in the specialized literature [6,15]. Regarding the RNN memory depth, our previous investigations and observation demonstrated that using Ts equal to the PA memory depth, i.e., Ts = Q =3, enhances the linearization performance. Additionally, the data set was generated considering OFDM signals at 0 dBm. Therefore, although the RNN training was performed only for 0 dBm, the linearization performance was conducted considering signals from 0 to 25 dBm. This strategy verifies the scheme generalization capability when the mobile network RF power allocation dynamically changes.

Fig 6 presents the dual-ANN linearization performance in terms of EVM_{RMS} for distinct activation functions. Once 64-QAM was used to modulate the data, the EVM_{RMS} limit, specified in the 3rd Generation Partnership Project (3GPP) Release 15 [16], will be 8%. We can notice that for the set of tested RF power, only when tanh and Leaky ReLU activation

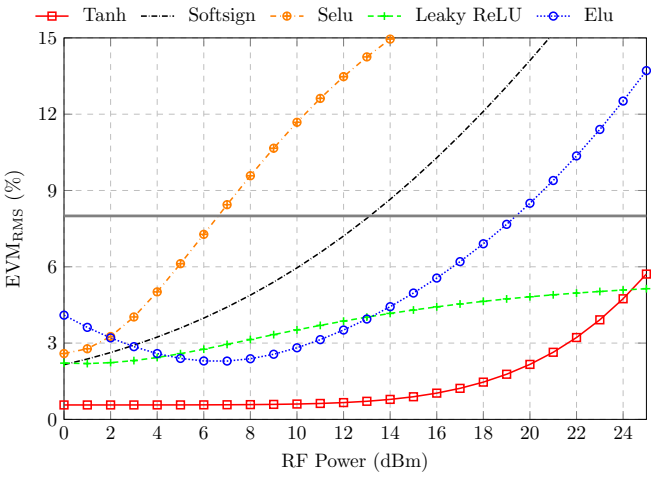

Fig. 6. Root mean squared error vector magnitude as a function of RF input power at MZM input for distinct activation functions.

functions are employed, the EVM_{RMS} was kept below the limit. Although tanh and Leaky ReLU present EVM_{RMS} below the 3GPP limit for the entire analyzed RF power range, employing tanh leads to a significant improvement compared with Leaky ReLU. Furthermore, the proposed scheme has presented an outstanding generalization capability, once no retraining was required along with the range of tested RF power.

We have also investigated the dual-ANN performance in terms of ACLR, which is a frequency-domain metric used to evaluate the signal OOBE. It is an important metric since we are interested in exploiting TVWS vacant channels for providing communication. In this case, OOBE must be kept as low as possible, aiming to avoid interference in the adjacent channels. Fig. 7 presents the ACLR for distinct activation functions. Similarly to the EVM_{RMS} analysis, we can notice that employing tanh has led to the best ACLR performance,

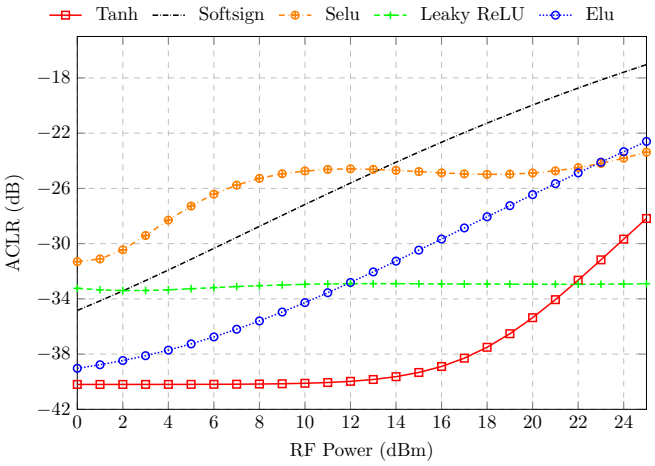

Fig. 7. Adjacent channel leakage ratio as a function of RF input power at MZM input for distinct activation functions.

which was kept below -27 dB for the entire RF power range. It is important to notice that ACLR considerably increases for RF power higher than 15 dBm.

Finally, we have investigated the normalized PSD for the proposed dual-ANN DPD, as displayed in Fig.8. In this analysis, we have considered an OFDM signal at 15 dBm applied to the MZM input. The tanh, Leaky ReLU and Elu activation functions were considered in this investigation. We can notice that only tanh has led to a low-level OOBE, which is in accordance with the previous ACLR analysis. Therefore, the proposed dual-ANN DPD presents a powerful solution for simultaneously reducing out-band and in-band distortions when the tanh activation function is employed. This result endorses the applicability of the proposed scheme to reduce the OOBE, favoring TVWS exploitation in remote areas.

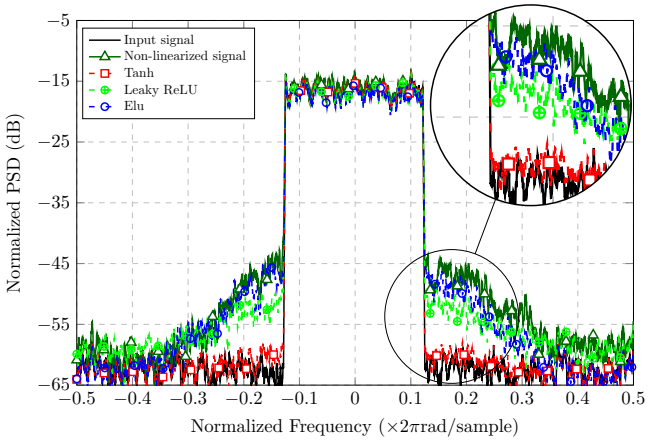

Fig. 8. Normalized power spectrum density at remote radio head for distinct activation functions.

V. Conclusions

We have tested distinct activation functions of a RNN-based DPD scheme, designed to exploit TVWS using eRAC. The activation function is one of the most important hyperparameters of an ANN since it impacts the capacity of the DPD in mitigating in-band and out-band distortions. The performance evaluation was carried out considering two metrics: EVM_{RMS} and ACLR. We investigated the impact of the activation function used in all layers of the RNN. Leaky ReLU, Elu, Softsign, SELU and tanh were considered in the investigation. The last one produced the best linearization performance. One could expect it since tanh can better represent nonlinear behaviors. The results presented in this paper demonstrate the potential of an ML solution for enhancing or even providing broadband communication in remote and rural areas. For future research, we intend to analyze the non-linear and linear effects of optical fiber and other elements present in the communication chain. Furthermore, we intend to compare our proposed solution with state-of-art DPD methods. We also envisage experimentally validating our approaches in a real-world implementation.

References

[1] M. Giordani, M. Polese, M. Mezzavilla, S. Rangan, and M. Zorzi, "Toward 6G Networks: Use Cases and Technologies," *IEEE Communications Magazine*, vol. 58, no. 3, pp. 55–61, 2020.

[2] A. Chaoub, M. Giordani, B. Lall, V. Bhatia, A. Kliks, L. L. Mendes, K. Rabie, H. Saarnisaari, A. Singhal, N. Zhang, S. Dixit, and M. Zorzi, "6G for Bridging the Digital Divide: Wireless Connectivity to Remote Areas," *IEEE Wireless Communications*, vol. 29, no. 1, pp. 160–168, 2022.

[3] M. A. Habibi, M. Nasimi, B. Han, and H. D. Schotten, "A Comprehensive Survey of RAN Architectures Toward 5G Mobile Communication System," *IEEE Access*, vol. 7, pp. 70 371–70 421, 2019.

[4] W. Dias, D. Gaspar, L. Mendes, M. Chafii, M. Matthé, P. Neuhaus, and G. Fettweis, "Performance Analysis of a 5G Transceiver Implementation for Remote Areas Scenarios," in *2018 European Conference on Networks and Communications (EuCNC)*, 2018, pp. 363–367.

[5] D. Apostolopoulos, G. Giannoulis, N. Argyris, N. Iliadis, K. Kanta, and H. Avramopoulos, "Analog Radio-over-Fiber Solutions in Support of 5G," in *2018 International Conference on Optical Network Design and Modeling (ONDM)*. IEEE, 2018, pp. 266–271.

[6] M. Noweir, Q. Zhou, A. Kwan, R. Valivarthi, M. Helaoui, W. Tittel, and F. M. Ghannouchi, "Digitally Linearized Radio-over Fiber Transmitter Architecture for Cloud Radio Access Network's Downlink," *IEEE Transactions on Microwave Theory and Techniques*, vol. 66, no. 7, pp. 3564–3574, 2018.

[7] A. Hekkala, M. Hiivala, M. Lasanen, J. Perttu, L. C. Vieira, N. J. Gomes, and A. Nkansah, "Predistortion of Radio Over Fiber Links: Algorithms, Implementation, and Measurements," *IEEE Transactions on Circuits and Systems I: Regular Papers*, vol. 59, no. 3, pp. 664–672, 2012.

[8] X. Xie, M. Hui, T. Liu, and X. Zhang, "Hybrid Linearization of Broadband Radio-over-Fiber Transmission," *IEEE Photonics Technology Letters*, vol. 30, no. 8, pp. 692–695, 2018.

[9] X. Wang, S. Yegnanarayanan, T. Hancock, and P. Juodawlkis, "Nonlinear equalization of microwave photonic links," in *2016 IEEE International Topical Meeting on Microwave Photonics (MWP)*, 2016, pp. 269–272.

[10] S. Liu, Y. M. Alfadhli, S. Shen, M. Xu, H. Tian, and G.-K. Chang, "A Novel ANN Equalizer to Mitigate Nonlinear Interference in Analog-RoF Mobile Fronthaul," *IEEE Photonics Technology Letters*, vol. 30, no. 19, pp. 1675–1678, 2018.

[11] S. Liu, M. Xu, J. Wang, F. Lu, W. Zhang, H. Tian, and G.-K. Chang, "A Multilevel Artificial Neural Network Nonlinear Equalizer for Millimeter-Wave Mobile Fronthaul Systems," *Journal of Lightwave Technology*, vol. 35, no. 20, pp. 4406–4417, 2017.

[12] A. C. Najarro and S.-M. Kim, "Nonlinear Compensation Using Artificial Neural Network in Radio-over-Fiber System," *Journal of information and communication convergence engineering*, vol. 16, pp. 1–5, 2018.

[13] L. A. M. Pereira, L. L. Mendes, C. J. A. Bastos-Filho, and Arismar Cerqueira, S. Jr., "Linearization Schemes for Radio Over Fiber Systems Based on Machine Learning Algorithms," *IEEE Photonics Technology Letters*, vol. 34, no. 5, pp. 279–282, 2022.

[14] L. A. M. Pereira, L. L. Mendes, C. J. A. B. Filho, and Arismar Cerqueira, S. Jr., "Amplified Radio-over-Fiber System Linearization Using Recurrent Neural Networks," 2022, under review.

[15] H. Chen, J. Li, K. Xu, Y. Pei, Y. Dai, F. Yin, and J. Lin, "Experimental Investigation on Multi-Dimensional Digital Predistortion for Multi-Band Radio-over-Fiber Systems," *Optics express*, vol. 22, no. 4, pp. 4649–4661, 2014.

[16] 3GPP, "Group RAN; NR; base station (BS) conformance testing part 1: Conducted conformance testing," *3GPP TS*, vol. 38.141-1 version 1.0.0, p. Release15, 2018.

Paper 6: Novel Machine Learning Linearization Scheme for 6G A-RoF Systems

Luiz Augusto Melo Pereira, Luciano Leonel Mendes, Carmelo José Albanez Bastos-Filho and Arismar Cerqueira Sodré Junior. 'Novel Machine Learning Linearization Scheme for 6G A-RoF Systems", *IEEE/Optica Journal of Lightwave Technology*, (accepted for publication in August 8, 2023, DOI:10.1109/JLT.2023.3304281).

Publisher: IEEE/Optica

Novel Machine Learning Linearization Scheme for 6G A-RoF Systems

Luiz A. M. Pereira, Luciano L. Mendes, Carmelo J. A. Bastos-Filho and Arismar Cerqueira S. Jr.

***Abstract*—This paper presents the design and implementation of a digital pre-distortion (DPD) scheme based on machine learning (ML) algorithms, which has been envisioned for the sixth generation of mobile communications (6G) analog radio over fiber (A-RoF) system. The DPD scheme employs an augmented real-valued time delay neural network (ARVTDNN) to compensate for the memory and memory-less non-linear effects introduced by the A-RoF communication chain. The ARVTDNN receives the base-band samples of the transmit waveform and stores them in a time-delay line (TDL), which means that the information necessary to compensate time correlated effects is available for the ML algorithm. Therefore, the ARVTDNN can compensate both memory and memory-less effects, including the chromatic dispersion introduced by the optical fiber. The novel DPD can bring a significant positive impact in enhanced remote areas (eRAC) applications since the proposed DPD allows A-RoF to be used to connect the base-band unit with a low cost radio frequency (RF) radio head installed in remote areas. In this case, the severe non-linearities introduced by the Mach-Zehnder optical modulator (MZM) and power amplifier (PA) and the time dispersive distortions introduced by the fiber can be mitigated, improving the quality of the signal. Furthermore, the novel ML-based linearization scheme can be flexibly tailored to cover variations in the operating scenario by adjusting its hyperparameters and training data. The root mean square error vector magnitude (EVM_{RMS}), normalized mean square error (NMSE) and adjacent channel leakage ratio (ACLR) metrics have been used to evaluate the performance of the proposed DPD. Numerical results demonstrate promising linearization performance, reducing the signal in- and out-band distortions when the fronthaul link is extended to cover remote and rural areas.**

***Index Terms*—6G, analog radio-over-fiber, digital pre-distortion, machine learning.**

I. Introduction

THE fifth-generation of mobile network (5G) is currently being deployed worldwide and although it is becoming commercially available in many countries, technical limitations have hindered it from fulfilling all the International Mobile Telecommunications-2020 (IMT-2020) visions [1]. One of the reasons is the very challenging and conflicting requirements from different use case scenarios that are imposed to the radio access network (RAN), physical layer (PHY) and medium access control (MAC) layer. The requirements for the sixth-generation of mobile network (6G) PHY will be even more challenging since new audacious and futuristic applications are being foreseen for the next generation of mobile communication networks [2]. High data rates, low latency, high robustness and large coverage must be provided to support holographic and haptic communications, remote surgeries, digital twins, global coverage and other challenging scenarios [3]. Large coverage is especially important for providing broadband communications in remote and rural areas, which is a relevant application scenario that currently cannot be properly supported by 5G networks. Therefore, 6G networks are being envisioned to fully support enhanced remote area communications (eRAC) applications.

One approach to overcome this limitation is to reduce the cost of deploying the network sites. Fully equipped base stations (BSs) with all base-band processing are expensive, complex to be installed, and costly to be maintained. One approach to tackle this problem is to implement the baseband unit (BBU) using software-defined radio (SDR) approach and running the PHY and MAC layers of the RAN in a server (or cloud), leading to the so-called centralized radio access network (C-RAN). In this case, the waveforms are entirely processed in the server, which is typically connected to the radiofrequency (RF) remote radio head (RRH) installed in the site using a fiber optic link. This approach is already used in 5G networks, but the samples are digitally transmitted to/from the RRH using Common Public Radio Interface (CPRI) or evolved Common Public Radio Interface (eCPRI) protocols, which requires high bandwidth in the optical link and expensive analog-to-digital converters (ADCs) and digital-to-analog converters (DACs) in the RRH. Analog RoF (A-RoF) is an alternative where the analog waveforms modulate the laser beam applied in the optical fiber. This approach simplifies the RRH, since only a photodetector (PD) and a Mach-Zehnder modulator (MZM) are needed to connect it to the optical network. The challenge, in this case, is that the optical link will introduce distortion to the waveform transported by the optical carrier.

The MZM and the power amplifier (PA) used in the RRH are non-linear devices, which will produce non-linear distortions that increase the out-of-band (OOB) emission and the root mean square error vector magnitude (EVM_{RMS}). For the long optical links used in remote and rural areas applications, chromatic dispersion (CD) kicks in and introduces linear distortions as well. All these interference must be compensated in a A-RoF system. Therefore, a linearization scheme must be employed [10]. In other words, the main factors that degrade the signal quality in A-RoF applied to remote communication

This work was supported by RNP-MCTIC Grant No. 01245.020548/2021-07, under the 6G project, FAPESP Grant No. 20/05127-2, under SAMURAI project, CNPq, CAPES, FINEP and FAPEMIG.

Luiz A. M. Pereira, Luciano L. Mendes and Arismar Cerqueira S. Jr are with the Inatel, Santa Rita do Sapucaí, MG 37400-000 Brazil (e-mails: luiz.melo@inatel.br, lucianol@inatel.br, arismar@inatel.br).

C. J. A. Bastos-Filho is with the University of Pernambuco, Recife, PE 50100-010 Brazil (e-mail: carmelo.filho@upe.br).

Manuscript received Month xx, 2023; revised Month xx, 2023.

TABLE I
STATE-OF-THE-ART ON ML-BASED LINEARIZATION SCHEMES.

Reference	Non-linear Device	ANN Type	Linear Distortion	Linearization Scheme	Contributions
[4]	PA	ARVTDNN	No	Pre-distortion	ARVTDNN-based digital predistorter designed to mitigate non-linear distortions introduced by PA.
[5]	MZM	MLP	No	Pre- and Post-distortions	Proposal of MLP-based digital pre- and post-distortion schemes to mitigate non-linear distortions of MZM from A-RoF systems
[6]	MZM PA	RNN	No	Pre- and Post-distortions	Introduction of a RNN-based digital pre- and post-distortion schemes to mitigate non-linear distortions of MZM and PA from A-RoF systems
[7]	MZM PA	Delay-tap MLP	No	Post-distortion	ANN-based equalizer designed to minimize multi-user interferences caused by non-linear impairments in A-RoF uplink transmissions.
[8]	PA	RVTDCNN	No	Pre-distortion	Investigation of a RVTDCNN-based pre-distorter scheme for mitigating the non-linear distortions and memory effects of PAs
[9]	PA	BiLSTM	No	Pre-distortion	Proposal of a BiLSTM-based pre-distorter scheme for reducing the non-linear distortion and memory effects of PAs
This Work	MZM PA	ARVTDNN	Yes	Pre-distortion	Proposal of an ARVTDNN-based pre-distorter to address linear chromatic dispersion and achive linearization of MZM and PA from A-RoF systems

scenario are the nonlinear effect of the MZM and PA and the linear distortion caused by CD, which occurs due to the fiber length and signal bandwidth. All these effects are modeled in the simulation, which we have designed in the Python environment. The goal was to propose a pre-distortion scheme capable of simultaneously dealing with all these issues.

The main aim of this paper is to propose a digital signal processing (DSP) scheme based on machine learning (ML) algorithm that is able to compensate the memory-less non-linear distortion from the MZM, the memory non-linear distortion from the PA and the linear chromatic dispersion from the fiber. Residual artificial neural networks (ANNs) have been used for compensating the non-linear distortions of PA [4], [11]–[15], since the residual information allows for compensating the non-linear behavior of this device. The memory effect might also be compensated by employing recurrent neural network (RNN), long short-term memory (LSTM) and gated recurrent units (GRU), which uses an internal memory structure to deal with temporal dependencies of the model [16]. Once trained, ANNs have demonstrated superior robustness and less complexity in comparison with conventional Volterra-based linearization schemes [17]. Additionally, the neural network high capability of learning complex systems might also be employed for compensated distortions produced by the interaction among several cascade non-linear devices, which is the case of A-RoF systems.

One extra benefit of using ML algorithms is that, when properly designed and trained, this class of algorithms can also deal with the linear distortion introduced by CD, reducing even further the complexity, since dispersion compensation fibers (DCFs) and DSP approaches are not required [18]–[23]. The proposed digital pre-distorion (DPD) will be evaluated in terms of OOB emissions, EVM_{RMS}, and normalized mean square error (NMSE) using simulation and the results show that the proposed DPD can effectively reduce the influence of both linear and non-linear distortions in A-RoF systems.

The remaining of this manuscript is structured as follows. Section II reports a literature review on related works, whereas Section III describes the system model whereas Section IV reports the proposed augmented real-valued time delay neural network (ARVTDNN) linearization scheme including its training process. The evaluation of the proposed DPD is presented in Section V and, finally, Section VI concludes this paper.

II. RELATED WORKS

This section is regarding a literature review on related works of linearization schemes based on ML, mainly focusing on the use of ANNs for linearizing A-RoF systems. Table I presents a comparison among our proposed approaches and other state-of-the-art linearization schemes. For instance, in our previous work, we have developed a linearization scheme for A-RoF based on multi layer perceptron (MLP) [5]. The non-linear effects only come from MZM and the PA is considered ideal. On the other hand, the current work considers the memory effects of PA and CD from the optical fiber. In this case, a simple MLP ANN is unable to compensate for the memory effect, since it lacks a memory structure to handle the memory effect. Therefore, we have developed a new technique that effectively addresses the memory effect and even considers the chromatic dispersion of the optical fiber.

ANNs have been widely explored to linearize A-RoF systems, including RNNs, which are able of capturing non-linear distortion with memory effect from PA and memoryless non-linear distortion from MZM, as demonstrated in our previous published paper [6]. However, when considering the presence of CD, the internal memory structure of RNN can not properly compensate for this linear effect, limiting the performance of the system. In this current work, we propose the use of an ANN that incorporates a time-delay line instead of an internal memory structure. This modification proves advantageous in compensating both non-linear and linear distortions from A-RoF systems.

In [7], the authors demonstrated a complex-valued multilevel ANN non-linear equalizer designed for uplink transmissions of single carrier frequency division multiple access (SC-FDMA) signals. The goal was to mitigate inter-user interference caused by non-linear distortions of A-RoF systems. Nevertheless, in this study, the authors did not consider the effect of CD due to the limited link length of 15 km, which aligns with typical fronthaul distances in mobile communications. In our current work, it was employed a transmitter-side pre-distortion scheme to reduce the operational expenditure

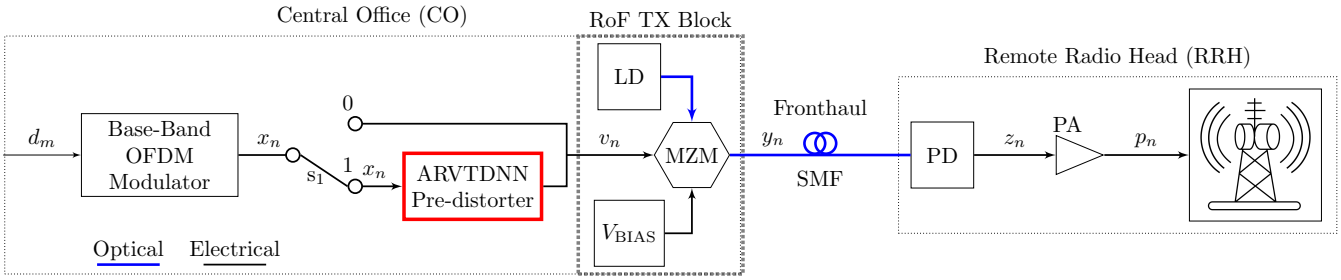

Fig. 1. Block diagram of the equivalent base-band system model of analog radio-over-fiber system.

(OPEX) and extend the link coverage to remote areas. In this context, CD and non-linear effects of A-RoF components need to be taken into account, and an ANN capable of compensating for these effects is employed.

Several types of input data sets have been investigated for ANNs, and an ARVTDNN was proposed as an alternative to traditional polynomial models [4]. Furthermore, a real-valued time-delayed convolutional neural network (RVTDCNN)-based DPD scheme was proposed by Hu *et al.* [8]. They treated the envelope-dependent terms and in-phase and quadrature (I/Q) components and as image-like representations. In addition Sun *et al.* presented in [9] a bidirectional long short-term memory (BiLSTM) ANN to linearize the PA of 5G wireless systems. However, in [8] and [9], the authors primarily concentrated on linearizing the PA, addressing the time series features and memory effects associated with this non-linear device.

III. Base-Band Equivalent System Model

Fig. 1 shows the block diagram of the equivalent base-band system model of the A-RoF system considered in this paper for the eRAC scenario. The digitally pre-distorted waveform is generated by the base-band generator, whereas an A-RoF system is employed to transport the RF signal from the central office (CO) to the RRH. The A-RoF system is composed of a laser (LD), a MZM, and a direct current (DC) polarization voltage (V_{BIAS}). A standard single-mode fiber (SMF) will be used to connect the CO to RRH. It is assumed that the RRH is deployed in a rural or remote area site, typically located $50 \sim 70$ kilometers from CO. The signal at RRH is photodetected and amplified before transmission. It is worth mentioning that we are using ANN in this specific scenario for providing broadband communication to remote and rural areas, which is a relevant application scenario for 6G networks. Nevertheless, linearization schemes based on ANNs can also cover distinct operating scenarios by appropriately adjusting their architecture, hyperparameters and training data set.

In this work, we employed orthogonal frequency division multiplexing (OFDM), which has a high peak to average power ratio (PAPR). This means that this waveform offers a more aggressive stress test for component non-linearities compared to single-carrier waveforms. Moreover, OFDM has gained widespread adoption in modern communication systems. Notwithstanding, the proposed scheme is not limited to OFDM waveform and can be adapted for other type of waveforms. The OFDM signal is given by

$$x_n = \sum_{m=0}^{M-1} d_m e^{-j2\pi \frac{m}{M}(n+1)}, \tag{1}$$

where d_m is quadrature amplitude modulation (QAM) symbol carried by the mth subcarrier, $m \in \{0,\, 1,\, 2,\, \ldots,\, M-1\}$ and $n \in \{0, 1, \ldots, N-1\}$ is the time index.

OFDM uses cyclic prefix (CP) to protect the transmitted signal from the multipath mobile channel, avoiding inter block interference (IBI) by copying the N_{CP} last samples from the OFDM block to its beginning.

If DPD is employed, the OFDM signal is applied to the ARVTDNN block (switch s_1 in Fig. 1 at position 1), otherwise it is directly applied to the MZM (switch s_1 in Fig. 1 at position 0, leading to $v_n = x_n$). Details about the ARVTDNN algorithm is presented in Section IV.

The MZM modulates the optical carrier from LD and the power of the LD beam affects the non-linear behavior of the optical device, as well as the DC voltage coming from the V_{BIAS} component. The MZM, polarized by a DC voltage provided by the V_{BIAS} block, presents a memory-less non-linear behavior that can be modeled by a transfer function given by [20]

$$y_n = \sum_{j=0}^{J-1} h_j |v_n|^j v_n, \tag{2}$$

where h_j are the polynomial model coefficients and $v_n = x_n$ (it is assumed that switch s_1 is at position 0). Here, J stands for the non-linear order of the model.

At the MZM output, the signal is launched in an SMF that can have tens of km to deliver the signal at the RRH. The SMF introduces CD that leads to a variation in the fiber frequency response, which is given by [23], [24]

$$G\left(e^{j\omega T}\right) = e^{-jA(\omega T)^2}, \;\; A = \frac{D\lambda^2 L}{4\pi c T^2}, \tag{3}$$

where D is the SMF dispersion parameter, λ is the optical carrier wavelength, L is the SMF length and c is the speed of light. The digital frequency is represented by $\omega T = 2\pi f T$, in which T stands for the sample period. The CD impulse response is given by the inverse Fourier transform of (3), which leads to non-causal and infinite impulse response (IIR). The authors in [23] have shown that the CD can be properly

represented using a finite impulse response (FIR) filter by truncating the IIR with an odd number of taps N_{t}, leading to

$$g_n = \sqrt{\frac{1}{j4A\pi}} e^{j\frac{n^2}{4A}}, -\left\lfloor \frac{N_{\mathrm{t}}}{2} \right\rfloor \leq n \leq \left\lfloor \frac{N_{\mathrm{t}}}{2} \right\rfloor, N_{\mathrm{t}} = 2\lfloor 2A\pi \rfloor + 1, \tag{4}$$

in which $\lfloor x \rfloor$ returns the largest integer smaller than the x. It is important to note that the optical fiber exhibits an impulse response at the sample signaling rate of the OFDM symbol. However, the system response is obtained through the convolution between the fiber response and the wireless channel response. This leads to spreading in the resultant impulse response. Consequently, the CP needs to be sized to cover the wireless channel convolved with the response of the fiber. Hence, the analysis will be performed at the sample signaling rate, considering the system as a whole.

Using this model and assuming that the PD does not introduce distortions, the signal delivered for PA is given by

$$z_n = y_n * g_n + w_n, \tag{5}$$

where w_n is the additive white Gaussian noise (AWGN).

The PA usually operates close to its 1-dB saturation point, introducing memory non-linear distortions that can be modeled as [25]

$$p_n = \sum_{q=0}^{Q-1} \sum_{k=0}^{K-1} \xi_{q,k} \left| z_{n-q} \right|^k z_{n-q}, \tag{6}$$

where $\xi_{q,k}$ are coefficients of the PA model, with $q \in \{0, 1, \cdots, Q-1\}$ and $k \in \{0, 1, \cdots, K-1\}$, in which Q is the memory depth and K the model non-linear order. It is important to highlight that K and Q depend on the specific components and architecture used to build the PA [25].

IV. ARVTDNN-Based Linearization Scheme for Analog Radio-over-Fiber Systems

The DPD for A-RoF must be able to compensate the memory-less and memory non-linear distortions introduced by the MZM and PA and the linear distortion introduced by the SMF. The ARVTDNN has been selected because its architecture employs a time delay line (TDL) to feed the ANN, allowing the DPD to compensate for all these distortions. Fig. 2 presents the architecture of the ARVTDNN used as DPD.

The ARVTDNN ANN is composed of $L+1$ layers. The ℓth layer has O_ℓ neurons, with $\ell \in \{0, ..., L+1\}$. The input layer depends on the PA memory depth Q and non-linear order K, since the ANN is fed with $K+1$ blocks of Q samples to compensate for the memory effect. This approach enables to capture of time-varying patterns and dependencies in the data, which is the case of the memory effect of PAs. The first 2 blocks receive the real and imaginary values of the waveform. The remaining $K-1$ blocks receive the absolute value of the Q samples raised to the k power.Therefore, the input layer has a total of $Q(K+1)$ neurons, meaning that the neural network has all the necessary information to compensate the memory effect.

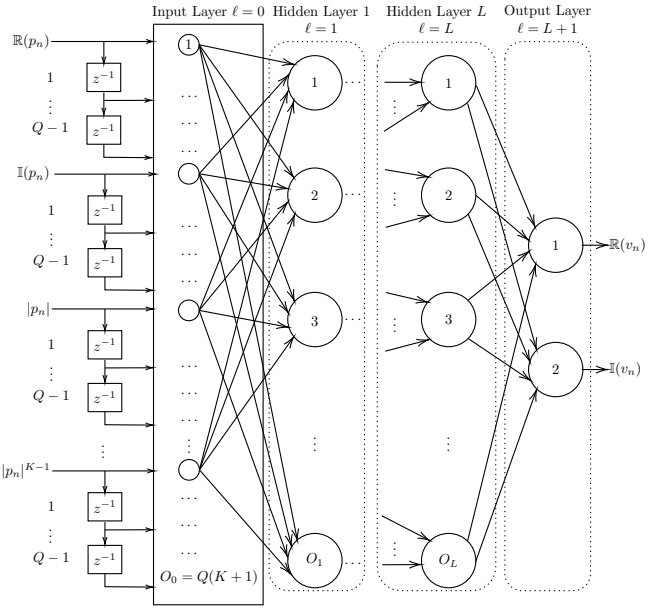

Fig. 2. ARVTDNN architecture composed of the following layers: input layer ($\ell = 0$); hidden layers ($\ell = 1, ..., L$); output layer ($\ell = L+1$). Each layer has O_ℓ neurons.

The ARVTDNN is trained using a data set containing the original input signal (v_n) and the distorted signal at PA output (p_n), as can be seen in Fig. 2. During the training phase, the target labels will be $\mathbb{R}(\mathbf{v})$ and $\mathbb{I}(\mathbf{v})$, where $\mathbf{v}$ is the vectored version of v_n with Q samples. The indirect learning is used to estimate the amplified A-RoF system post-inversion response. During the ARVTDNN training, a loss function is minimized, in other words, the ANN is trained to compensate the A-RoF by learning the inverse response of the A-RoF system. This estimated response is afterward used in the pre-distortion block, producing the desired linearization. The loss function used to train the ANN is given by

$$Loss(\mathbf{W}, \mathbf{b}) = \frac{1}{N_{\mathrm{TR}}} \sum_{n=0}^{N_{\mathrm{TR}}-1} \mathcal{L}(v_n, \hat{v}_n(\mathbf{W},\mathbf{b})), \tag{7}$$

where N_{TR} is the size of the training set and

$$\mathcal{L}(a_n, b_n) = (a_n - b_n)^2, \tag{8}$$

is the mean-squared error (MSE) function. In summary, the MSE loss function is commonly employed in regression tasks as it is easily differentiable, which makes it suitable for use with the optimization algorithms. In this work, we have used the Adaptive Momentum (Adam) optimization algorithm.

The minimization of the loss function generates the optimized weight matrix $\mathbf{W}$ and bias vector $\mathbf{b}$, which are used by the ANN to pre-distort the signal. Therefore, the signal at ARVTDNN output is given by

$$\hat{v}_n = \sum_{\ell=0}^{L+1} \phi(\mathbf{W}_\ell \mathbf{p}_\ell + \mathbf{b}_\ell), \tag{9}$$

where $\mathbf{p}$ is the input vector and $\phi(.)$ is the nonlinear activation function.

V. Performance Evaluation

The proposed DPD has been evaluated using computer simulation in terms of adjacent channel leakage ratio (ACLR), NMSE, and EVM_{RMS}. The EVM_{RMS} measures the effect of the system degradation on the signal by evaluating the received QAM symbols deviation in comparison with the transmitted symbols. This metric is given by

$$\text{EVM}_{\text{RMS}}(\%) = 100\sqrt{\frac{\sum_{m=0}^{M-1}\left|\hat{d}_m - d_m\right|_2^2}{\sum_{m=0}^{M-1}|d_m|_2^2}}, \tag{10}$$

where $\hat{d}_m$ is the received symbol on the mth subcarrier, d_m is the symbol at mth subcarrier at the transmitter side and $|(.)|_p$ is the p-norm operator.

NMSE is used to verify the discrepancy between the transmitted and received signals and it is computed as

$$\text{NMSE (dB)} = 10\log\left(\frac{\sum_{n=0}^{N-1}|p_n - x_n|_2^2}{\sum_{n=0}^{N-1}|x_n|_2^2}\right). \tag{11}$$

The last metric is related to the OOB emission since it enables measuring the signal leakage due to non-linearities. This metric is defined as

$$\text{ACLR (dB)} = 10\log\left(\frac{\int_{f\in B_\text{O}} P_{\hat{p}}(f)df}{\int_{f\in B_\text{I}} P_{\hat{p}}(f)df}\right), \tag{12}$$

where $P_{\hat{p}}(f)$ stands for the power spectrum density (PSD) of $\hat{p}_n$ at frequency f , B_I and B_O represents the in-band and out-of-bands frequencies, respectively. It is worth mentioning that the evaluation of these three performance metrics was conducted through numerical calculations.

Once the metrics used to evaluate the system performance are defined, it is necessary to specify each system model. The parameters for the MZM transfer function and PA model are presented in Table II.

TABLE II
Parameters for the MZM and PA non-linear models.

Parameter	Value
Non-linear order of the MZM	J=5
MZM non-linear coefficients	$h_j = \begin{bmatrix} 1.1+j0.4 \\ 0.2+j0.6 \\ 0.7+j0.2 \\ 0.5+j0.7 \\ 0.3+j0.5 \end{bmatrix}$
Non-linear order of the PA	K = 5
PA memory depth	Q = 3

with the coefficients for the PA non-linear model being given by

$$\boldsymbol{\xi} = \begin{bmatrix} 1.1+j0.1 & j0.1 & 0.1+j0.1 & 0.1 & 0 \\ 0.1+j0.1 & 0.1 & 0.1+j0.1 & j0.1 & 0 \\ 0 & 0.1 & 0.1 & 0.1 & j0.1 \end{bmatrix} \tag{13}$$

where the rows bring the coefficients for a given memory depth and the columns bring coefficients for a given non-linear order of the PA. The parameters and coefficients presented in Table II and (13) are typical values found in literature [13], [25]–[27]. It is worth mentioning that the coefficients of the MZM and PA components may vary across distinct MZM and PA device models. In this case, a component characterization will need to be performed.

For defining the impact of the linear distortion introduced by the SMF, two fiber lengths will be considered: 50 km and 70 km. Table III shows the parameters for the chromatic dispersion model assuming these two scenarios.

TABLE III
Simulation parameters of chromatic dispersion FIR.

L [km]	D [ps/nm/km]	λ [nm]	T [ps]	N_t	A
50	17	1553	50	3	0.2175
70	17	1553	50	3	0.3045

As mentioned in Section II, OFDM has been assumed as the waveform to be transmitted over the A-RoF system. A total of 2048 subcarriers have been used to transmit 16-QAM symbols. Moreover, the CP with 2 samples is added to the OFDM symbol to protect the signal from IBI. Therefore, each OFDM block is composed of 2050 samples.

Once the system model has been parameterized, it is possible to design the ANN to compensate for the linear and non-linear effects of the A-RoF system. The ANN hyperparameters specification and its training are the main tasks in designing the ARVTDNN. The input layer has $O_0 = Q(K+1) = 18$ neurons. Following, three hidden layers with 1024 neurons each were employed. The output layer has only two neurons, corresponding to the real and imaginary parts of the OFDM block. In this paper, the hyperbolic tangent (tanh) activation function was used in the first hidden layer and the Leaky rectified linear unit (ReLU) activation function with $\alpha = 0.01$ has been used in the other two hidden layers. Using tanh in the first hidden layer mitigates the gradient exploding problem since $|\tanh(x)| \leq 1$, preventing the gradients from getting too large. It is important to notice that other activation functions such as, scaled exponential linear unit (SELU), ReLU and exponential linear unit (Elu) can also be employed, however the DPD performance must be properly evaluated for each case. No activation function was used in the output layer, which is a common approach for regression problems. These hyperparameters were heuristically chosen to optimize the linearization performance without concerning about the algorithm complexity, which is out-of-scope of this work.

The training data set was composed of 100 OFDM blocks, leading to a data set with 205000 instances. It is important to emphasize that two separate data sets were used during the training process for distinct values of L. Specifically, one data set comprised samples of the signal transmitted over a distance of 50 km of optical fiber, while the other data set, with the same number of samples, consisted of samples from the signal transmitted over a distance of 70 km. This approach enabled the neural network to learn the inverse response of the CD for both the 50 and 70 km links. Additionally, it is noteworthy that the data set utilized to train the model is synthetic. The choice to employ a simulation-generated data set is justified by the proven ability of the utilized models to accurately represent the distortions present in the system, as confirmed by previously published empirical and practical studies. The Adam optimizer

and early stop technique were used. The training batch was composed of the entire data set, i.e. 205000 samples, which means that only one interaction is performed in each training epoch. During the training phase, 143500 samples of the data set were used for the ANN training and the remaining (61500 samples) are used for validation. On the other hand, an additional independent data set comprising 205000 samples was generated specifically to test the ANN and evaluate the performance of the proposed linearization scheme. Although a fixed number of 5000 epochs was configured, typically only around 1000 epochs were actually required for the ANN training. This means that the early stop criterion was frequently reached. In this work, the MSE value of $\Delta_{\text{min}} = 10^{-9}$ has been used as a stop criterion, with patience hyperparameter set to 100. These hyperparameters were chosen accordingly to our preliminary studies, aiming a trade-off between convergence time and linearization performance. It is important to highlight that a NVIDIA Quadro-RTX 4000 graphics processing unit (GPU) was used for the ANN training, significantly reducing the time necessary for this procedure.

Once trained, the ARVTDNN performance is evaluated by switching s_1 to position 1, which means that the pre-distortion introduced by the ARVTDNN is applied to the signal. Fig. 3 (a) and (b) compares the magnitude and phase of the signal p_n at the PA output as a function of x_n with and without the linearization scheme. We can observe that the linearization scheme corrects the magnitude of the signal, leading to a response equal to the original non-distorted signal. Likewise, the phase is also compensated, since the phase deviation between the output and the input signals is kept around zero.

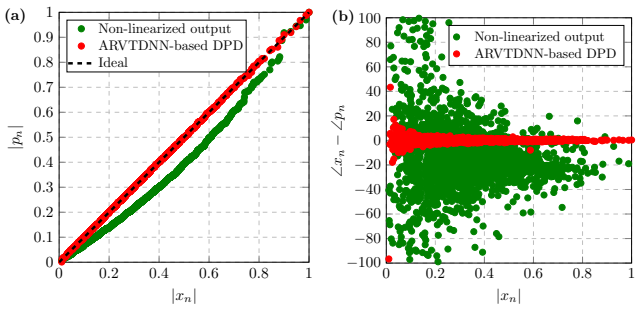

Fig. 3. Distortions compensation: (a) magnitude; (b) phase deviation.

Fig. 4 reports the EVM_{RMS} as a function of the electrical input power at MZM input. The zoom-in-view shows the transmitted and received QAM symbols for the different scenarios (with and without DPD and for $L = 50$ km and $L = 70$ km). We have compared our proposed DPD with the RNN-based DPD, which is also an ANN capable of dealing with memory effect. From Fig. 4 it is possible to notice that the EVM_{RMS} is remarkably reduced for the two evaluated link distances. This means that non-linear effects and linear CD degradation can effectively be mitigated by the proposed ARVTDNN-based scheme. Although the RNN-based solution has reduced the EVM_{RMS}, it exhibits lower linearization performance when compared with ARVTDNN DPD. This can be attributed to the recurrent neurons, which replicate the CD impulse response in the signal. The low EVM_{RMS} means that the in-band distortion are mitigated at the PA output, which means that the proposed ML based DPD is a promising solution to compensate the impairments introduced by A-RoF systems.

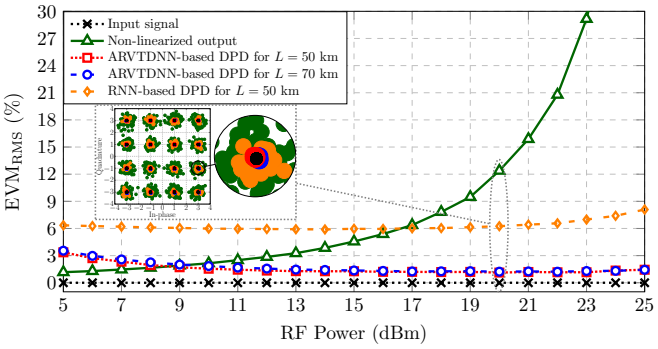

Fig. 4. EVM_{RMS} as a function of RF Power at MZM input.

Fig. 5 presents the NMSE between x_n and p_n, where it is possible to observe that it decreases considerably for the entire analyzed RF power range when the DPD is enabled. Once again, the RNN has presented lower linearization performance when compared with the ARVTDNN DPD. For the ARVTDNN DPD, the NMSE was kept below -25 dB. This result endorses the excellent generalization capability of ANN since it does not need to be re-trained for each input RF power. Nonetheless, the data set used during the training phase must contain signals with distinct RF power to increase the ANN generalization capability. Moreover, the NMSE is practically equal for the 50 and 70 km link distances. This means that the ARVTDNN was able to compensate the linear distortions introduced by distinct CD spread delay profiles.

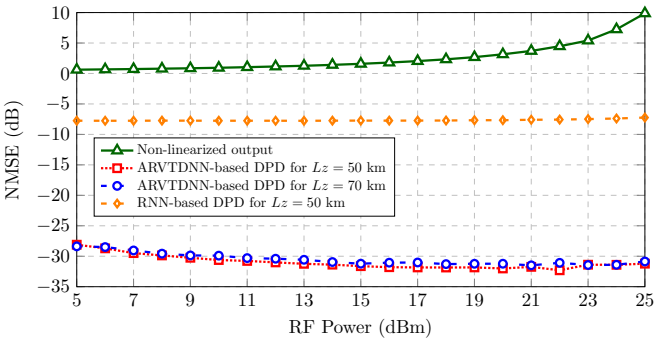

Fig. 5. NMSE as a function of RF Power at MZM input.

The ACLR was evaluated at the PA output to measure the effectiveness of the proposed DPD scheme in reducing the out-of-band emission (OOBE). Fig. 6 presents the ACLR as a function of RF power at MZM input. The ACLR was analyzed for $L = 50$ km and $L = 70$ km and the performance was practically the same for both cases, with values close to -35 dB for the entire analyzed RF power range. The RNN-based solution has also considerably reduced the ACLR when compared with the non-linearized output. It is important to mention that for RF power below 14 dBm, the ACLR of the linearized signal is higher than for the non-linearized

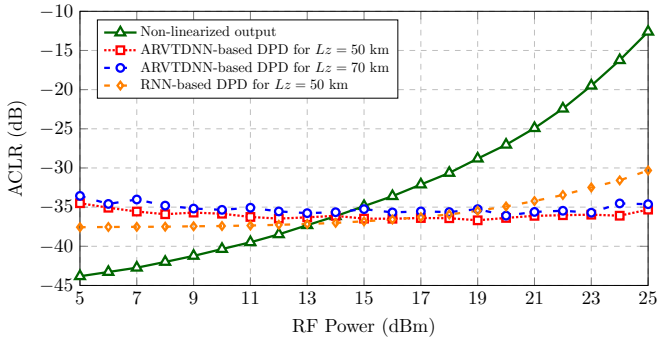

Fig. 6. ACLR as a function of RF Power at MZM input.

signal. This behavior is due the fact that, at these very low RF power, the MZM and PA do not present significant non-linearities and the pre-distortion introduced by the proposed linearization scheme slightly affects the OOBE. Nevertheless, the ACLR for RF power below 14 dBm is not prohibitive. But, if necessary, the DPD can be disabled whenever the input level is below 14 dBm, since the non-linearized signal presents acceptable EVM_{RMS} at this power range. As demonstrated by Fig. 6, in terms of ACLR, the linearization technique is indispensable when the RF power is larger than 14 dBm. It is noteworthy that the optimization of the EVM_{RMS} results in a decrease in ACLR, and vice versa. Nevertheless, despite the correlation between these metrics, the optimal point for EVM_{RMS} optimization may not necessarily coincide with the optimal point for ACLR optimization [28].

The out-band distortion was also evaluated in terms of the signal normalized PSD. The out-band distortion is the non-linear intermodulation products between the signal component frequencies, which is visualized as OOBE. Fig. 7 shows the normalized PSD for the signal at the PA output with and without DPD. We can notice that when the linearization scheme is not applied, the OOB emission might hinder the exploitation of TV white space (TVWS) since the high OOBE interfere with the adjacent channel. The RNN-based DPD has achieved a reduction of approximately 8 dB in out-band emission, while the proposed ARVTDNN has significantly lowered the out-of-band emission by approximately 20 dB.

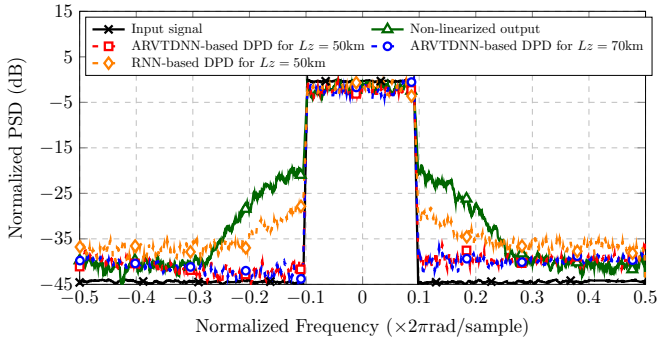

Fig. 7. Frequency spectrum for an OFDM signal at 20 dBm.

VI. Conclusions

This paper have presented and evaluated an ML-based linearization scheme designed for A-RoF systems. It employs an ARVTDNN to estimate the A-RoF post-inverse response, which is then applied to the DPD processing block. The main advantage of the ML-based approach is the simultaneously compensation of linear and non-linear impairments introduced by the A-RoF system. The proposed scheme dispenses the use of DCFs and/or DSP for mitigating CD, whereas complex Volterra-based DPD can also be eliminated. In other words, the innovative DPD simplifies the communication system, without introducing any performance disadvantages. The proposed scheme compensated in- and out-band distortions produced by the MZM and RF PA and it also allows extending the front-haul link up to 70 km by compensating the linear degradation introduced by CD. The EVM_{RMS} was kept below 3% for the entire RF power range, whereas the NMSE decreased ≈ 25 dB. The ACLR was also reduced, especially for RF power above 15 dBm. In contrast to existing approaches, the proposed novel technique demonstrated the capability to simultaneously compensate for both linear and non-linear distortions in the A-RoF system. This unique feature enables to extend the A-RoF link distance and overcomes the limitations of conventional terrestrial infrastructure. A-RoF technology aided by ML-based linearization facilitates the distribution of radio signals over long distances using fiber optic cables, providing numerous advantages for remote areas. These benefits include reliable radio coverage in challenging terrains, enhanced emergency communication systems, expanded radio services to underserved regions, improved signal quality and resilience, and reduced infrastructure costs compared to traditional radio transmission methods. In conclusion, the proposed ML-based DPD is a interesting tool for future communication systems that demands integration of long length optical front-haul and simple RRH, as it is the case of eRAC applications.

As future work, other significant effects for this scenario are being studied and will be incorporated into the simulation system. Another future action is the implementation of the proposed linearization scheme in a practical experiment.

References

[1] A. Osseiran, F. Boccardi, V. Braun, K. Kusume, P. Marsch, M. Maternia, O. Queseth, M. Schellmann, H. Schotten, H. Taoka *et al.*, "Scenarios for 5G Mobile and Wireless Communications: The Vision of the METIS Project," *IEEE communications magazine*, vol. 52, no. 5, pp. 26–35, 2014.

[2] H. Tataria, M. Shafi, A. F. Molisch, M. Dohler, H. Sjöland, and F. Tufvesson, "6G Wireless Systems: Vision, Requirements, Challenges, Insights, and Opportunities," *Proceedings of the IEEE*, vol. 109, no. 7, pp. 1166–1199, 2021.

[3] C. Han, Y. Wu, Z. Chen *et al.*, "Network 2030 A Blueprint of Technology, Applications and Market Drivers Towards the Year 2030 and Beyond," *International Telecommunication Union*, 2018. [Online]. Available: https://www.itu.int/en/ITU-T/focusgroups/net2030/Documents/White_Paper.pdf

[4] D. Wang, M. Aziz, M. Helaoui, and F. M. Ghannouchi, "Augmented Real-Valued Time-Delay Neural Network for Compensation of Distortions and Impairments in Wireless Transmitters," *IEEE Transactions on Neural Networks and Learning Systems*, vol. 30, no. 1, pp. 242–254, 2019.

[5] L. A. M. Pereira, L. L. Mendes, C. J. A. Bastos-Filho, and Arismar Cerqueira S. Jr., "Linearization Schemes for Radio over Fiber Systems Based on Machine Learning Algorithms," *IEEE Photonics Technology Letters*, vol. 34, no. 5, pp. 279–282, 2022.

[6] L. A. M. Pereira, L. L. Mendes, C. J. A. Bastos Filho, and Arismar Cerqueira S. Jr., "Amplified Radio-over-Fiber System Linearization Using Recurrent Neural Networks," *Journal of Optical Communications and Networking*, vol. 15, no. 3, pp. 144–154, 2023.
[7] S. Liu, Y. M. Alfadhli, S. Shen, M. Xu, H. Tian, and G.-K. Chang, "A Novel ANN Equalizer to Mitigate Nonlinear Interference in Analog-RoF Mobile Fronthaul," *IEEE Photonics Technology Letters*, vol. 30, no. 19, pp. 1675–1678, 2018.
[8] X. Hu, Z. Liu, X. Yu, Y. Zhao, W. Chen, B. Hu, X. Du, X. Li, M. Helaoui, W. Wang *et al.*, "Convolutional Neural Network for Behavioral Modeling and Predistortion of Wideband Power Amplifiers," *IEEE Transactions on Neural Networks and Learning Systems*, vol. 33, no. 8, pp. 3923–3937, 2021.
[9] J. Sun, W. Shi, Z. Yang, J. Yang, and G. Gui, "Behavioral Modeling and Linearization of Wideband RF Power Amplifiers Using BiLSTM Networks for 5G Wireless Systems," *IEEE Transactions on Vehicular Technology*, vol. 68, no. 11, pp. 10 348–10 356, 2019.
[10] J. Wang, C. Liu, M. Zhu, A. Yi, L. Cheng, and G.-K. Chang, "Investigation of Data-Dependent Channel Cross-Modulation in Multiband Radio-over-Fiber Systems," *Journal of lightwave technology*, vol. 32, no. 10, pp. 1861–1871, 2014.
[11] Y. Suo, W. Qiao, C. Jiang, B. Zhang, and F. Liu, "A Residual-Fitting Modeling Method for Digital Predistortion of Broadband Power Amplifiers," *IEEE Microwave and Wireless Components Letters*, vol. 32, no. 9, pp. 1115–1118, 2022.
[12] R. Hongyo, Y. Egashira, T. M. Hone, and K. Yamaguchi, "Deep Neural Network-Based Digital Predistorter for Doherty Power Amplifiers," *IEEE Microwave and Wireless Components Letters*, vol. 29, no. 2, pp. 146–148, 2019.
[13] Y. Wu, U. Gustavsson, A. G. i Amat, and H. Wymeersch, "Residual Neural Networks for Digital Predistortion," in *GLOBECOM 2020-2020 IEEE Global Communications Conference*. IEEE, 2020, pp. 01–06.
[14] Z. He and F. Tong, "Residual RNN Models With Pruning for Digital Predistortion of RF Power Amplifiers," *IEEE Transactions on Vehicular Technology*, vol. 71, no. 9, pp. 9735–9750, 2022.
[15] M. Rawat and F. M. Ghannouchi, "A Mutual Distortion and Impairment Compensator for Wideband Direct-Conversion Transmitters Using Neural Networks," *IEEE Transactions on Broadcasting*, vol. 58, no. 2, pp. 168–177, 2012.
[16] A. Shewalkar, D. Nyavanandi, and S. A. Ludwig, "Performance Evaluation of Deep Neural Networks Applied to Speech Recognition: RNN, LSTM and GRU," *Journal of Artificial Intelligence and Soft Computing Research*, vol. 9, no. 4, pp. 235–245, 2019.
[17] P. H. C. De Souza, L. L. Mendes, and M. Chafii, "Compressive Learning in Communication Systems: A Neural Network Receiver for Detecting Compressed Signals in OFDM Systems," *IEEE Access*, vol. 9, pp. 122 397–122 411, 2021.
[18] T. Ismail, C.-P. Liu, J. E. Mitchell, and A. J. Seeds, "High-Dynamic-Range Wireless-over-Fiber Link Using Feedforward Linearization," *Journal of Lightwave Technology*, vol. 25, no. 11, pp. 3274–3282, 2007.
[19] S. K. Korotky and R. M. De Ridder, "Dual Parallel Modulation Schemes for Low-Distortion Analog Optical Transmission," *IEEE journal on selected areas in communications*, vol. 8, no. 7, pp. 1377–1381, 1990.
[20] M. Noweir, Q. Zhou, A. Kwan, R. Valivarthi, M. Helaoui, W. Tittel, and F. M. Ghannouchi, "Digitally Linearized Radio-Over Fiber Transmitter Architecture for Cloud Radio Access Network's Downlink," *IEEE Transactions on Microwave Theory and Techniques*, vol. 66, no. 7, pp. 3564–3574, 2018.
[21] I. Morita, M. Suzuki, N. Edagawa, K. Tanaka, and S. Yamamoto, "Long-Haul Soliton WDM Transmission with Periodic Dispersion Compensation and Dispersion Slope Compensation," *Journal of lightwave technology*, vol. 17, no. 1, p. 80, 1999.
[22] T. Yamamoto, E. Yoshida, K. R. Tamura, K. Yonenaga, and M. Nakazawa, "640-Gbit/s Optical TDM Transmission Over 92 km Through a Dispersion-Managed Fiber Consisting of Single-Mode Fiber and" Reverse Dispersion Fiber"," *IEEE Photonics Technology Letters*, vol. 12, no. 3, pp. 353–355, 2000.
[23] S. J. Savory, "Digital Coherent Optical Receivers: Algorithms and Subsystems," *IEEE Journal of Selected Topics in Quantum Electronics*, vol. 16, no. 5, pp. 1164–1179, 2010.
[24] A. Eghbali, H. Johansson, O. Gustafsson, and S. J. Savory, "Optimal Least-Squares FIR Digital Filters for Compensation of Chromatic Dispersion in Digital Coherent Optical Receivers," *Journal of lightwave technology*, vol. 32, no. 8, pp. 1449–1456, 2014.
[25] D. R. Morgan, Z. Ma, J. Kim, M. G. Zierdt, and J. Pastalan, "A Generalized Memory Polynomial Model for Digital Predistortion of RF Power Amplifiers," *IEEE Transactions on signal processing*, vol. 54, no. 10, pp. 3852–3860, 2006.
[26] H. Chen, J. Li, K. Xu, Y. Pei, Y. Dai, F. Yin, and J. Lin, "Experimental Investigation on Multi-dimensional Digital Predistortion for Multi-band Radio-over-fiber Systems," *Optics express*, vol. 22, no. 4, pp. 4649–4661, 2014.
[27] A. Hekkala, M. Hiivala, M. Lasanen, J. Perttu, L. C. Vieira, N. J. Gomes, and A. Nkansah, "Predistortion of Radio over Fiber Links: Algorithms, Implementation, and Measurements," *IEEE Transactions on Circuits and Systems I: Regular Papers*, vol. 59, no. 3, pp. 664–672, 2011.
[28] H. D. Rodrigues, T. C. Pimenta, R. A. A. de Souza, and L. L. Mendes, "Orthogonal Scalar Feedback Digital Pre-Distortion Linearization," *IEEE Transactions on Broadcasting*, vol. 64, no. 2, pp. 319–330, 2017.

Luiz Augusto Melo Pereira received the B.Sc., M.Sc., and Ph.D. degrees in Telecommunications from the National Institute of Telecommunications (Inatel), Brazil, in 2017, 2020, and 2023, respectively. During his academic journey, he served as a tutor for Stochastic Process and Digital Communication II in the Teaching Internship Program from 2018 to 2022, gaining valuable teaching experience. Currently, he works as a Research Engineer and holds the position of post-graduate Lato Sensu professor at Inatel.

Luciano Leonel Mendes received the B.Sc. and M.Sc. degrees from Inatel, Brazil, in 2001 and 2003, respectively, and the Doctor degree from Unicamp, Brazil, in 2007, all in electrical engineering. From 2013 to 2015, he was a Visiting Researcher with the Technical University of Dresden in the Vodafone Chair Mobile Communications Systems, where he has developed his postdoctoral. Since 2001 he is a professor at Inatel, where currently he acts as the Research Coordinator of the Brasil 6G project.

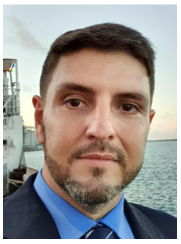

Carmelo José Albanez Bastos Filho (Senior Member, IEEE) received the B.Sc. degree in electronics engineering and the M.Sc. and Ph.D. degrees in electrical engineering from the Federal University of Pernambuco (UFPE) in 2000, 2003, and 2005, respectively. He is currently an Associate Professor with the Polytechnic School, University of Pernambuco. He authored or coauthored roughly 300 full papers in journals and conferences and advised more than 50 Ph.D. and M.Sc. candidates.

Arismar Cerqueira Sodré Junior received his Ph.D. degree from Scuola Superiore Sant'Anna-Italy in 2006. He was Invited Researcher and Professor from many world-recognized universities, such as Scuola Superiore Sant'Anna-Italy, University of Oulu, Danish Technical University-Denmark, Max-Planck Institute-Germany and University of Bath-UK. He is a holder of 12 patents, has transferred 25 products to the industry and has published over 300 scientific papers.

Paper 7: Proposal of a Fiber/Wireless System Assisted by Machine Learning Towards 6G Communications

Luiz Augusto Melo Pereira, Luciano Leonel Mendes and Arismar Cerqueira Sodré Junior. 'Proposal of a Fiber/Wireless System Assisted by Machine Learning Towards 6G Communications", *The 20th SBMO/IEEE MTT-S International Microwave and Optoelectronics Conference*, (accepted for publication in July 30, 2023).

Publisher: IEEE Conference

Proposal of a Fiber/Wireless System Assisted by Machine Learning Towards 6G Communications

1st Luiz Augusto Melo Pereira
Laboratory WOCA, Inatel
Santa Rita do Sapucaí, Brazil
luiz.melo@inatel.br

2nd Luciano Leonel Mendes
CRR, Inatel
Santa Rita do Sapucaí, Brazil
lucianol@inatel.br

3rd Arismar Cerqueira S. Jr.
Laboratory WOCA, Inatel
Santa Rita do Sapucaí, Brazil
arismar@inatel.br

***Abstract*—This paper reports the performance evaluation of a fiber/wireless (FiWi) system assisted by a machine learning (ML) algorithm envisioned for the sixth generation of mobile networks (6G). An augmented real-valued time delay neural network (ARVTDNN) is trained to learn the inverse response of the non-linear distortions introduced by the communication chain. The trained ML algorithm operates as a digital pre-distortion (DPD) scheme, which allows an analog radio-over-fiber (A-RoF) system to be used to connect the central office (CO) with a low-cost remote radio head (RRH) installed in remote areas. A Rayleigh channel was employed to model the wireless radio-frequency (RF) signal transmission. The RF signal is linearized by the DPD scheme before being radiated, aiming to provide broadband communications for remote and rural areas. Numerical results demonstrate that the ML-based DPD scheme enables the seamless integration of A-RoF into the wireless system.**

***Index Terms*—A-RoF, DPD, machine learning**

I. Introduction

While the concept of sixth-generation of mobile network (6G) is currently under discussion, the prevailing trends suggest that it will evolve into a human-centric network [1]. Therefore, enabling connectivity in remote areas stands out as an important use case of this network. The centralized radio access network (C-RAN) architecture might play a distinguished role for this communication scenario. It simplifies the communication infrastructure, centralizing the base-band processing in a central office (CO) server. In this approach, the CO might be connected to the remote radio head (RRH) by employing an analog radio-over-fiber (A-RoF) link instead of a digital RoF (D-RoF). The A-RoF simplifies the network infrastructure since the signal is transported in its analog format, dispensing expensive analog-to-digital converters (ADCs) and digital-to-analog converters (DACs). Therefore, the RRH will be composed only of an optical detector and radiofrequency (RF) front-end. The challenge, in this case, is dealing with non-linear distortions introduced especially by the Mach-Zehnder modulator (MZM) and power amplifier (PA).

The digital pre-distorion (DPD) based on machine learning (ML) algorithms have been used to compensate A-RoF system distortions [2], [3] ML solutions can learn complex interactions between linear and non-linear effects. Particularly, our research group has investigated ML-algorithms to linearize the MZM and PA components. In [4], we have used a multi layer perceptron (MLP) artificial neural network (ANN) to implement a DPD and equalizer linearization schemes to compensate the memoryless non-linear distortions of MZM. Afterward, we compared the ML-based DPD scheme with a state-of-the-art Volterra-based linearization scheme [5]. Once trained, the ML DPD scheme has demonstrated less complexity and high robustness against time variation in the system response when compared with the conventional linearization scheme. Finally, we have also considered the memory-dependent non-linear degradation of PAs [6]. In this case, a recurrent neural network (RNN) was used to compensate for the memoryless effect of MZM and the memory effect of PA.

This work presents the performance evaluation of a fiber/wireless (FiWi) system linearized by ML. An augmented real-valued time delay neural network (ARVTDNN) is used to implemented the linearization scheme [7]. The ARVTDNN receives the base-band samples of an orthogonal frequency division multiplexing (OFDM) waveform and stores them in a time delay line (TDL), which ensures that all information required to compensate memoryless and memory effects are available for the ML algorithm. After linearized, the signal can be radiated to cover remote and rural areas, giving rise to the so-called FiWi system. A Rayleigh channel is used to model the wireless transmission from the RRH to the end user.

II. Base-Band Equivalent System Model

Fig. 1 shows the block diagram of the base-band equivalent system model for an A-RoF system. The digital waveform will be generated by the OFDM base-band modulator. The pre-distorted waveform is generated by the ARVTDNN pre-distorter block, which must be previously trained. Afterwards, the pre-distorted waveform is applied to the A-RoF TX Block, which is composed of a laser diode (LD) and MZM. The optically modulated signal is transported from the CO to the RRH by employing a 50-km single-mode fiber (SMF). At RRH, the signal is amplified before being radiated to cover remote areas. A Rayleigh channel was employed to model the wireless transmission between the RRH and the user.

The utilized waveform is known as OFDM and is given by

$$x_n = \sum_{m=0}^{M-1} d_m e^{-j2\pi \frac{m}{M}(n+1)}, \tag{1}$$

in which d_m is the quadrature amplitude modulation (QAM) symbols, carried by the mth subcarrier, $m \in$

979-8-3503-2067-1/23/$31.00 © 2023 IEEE

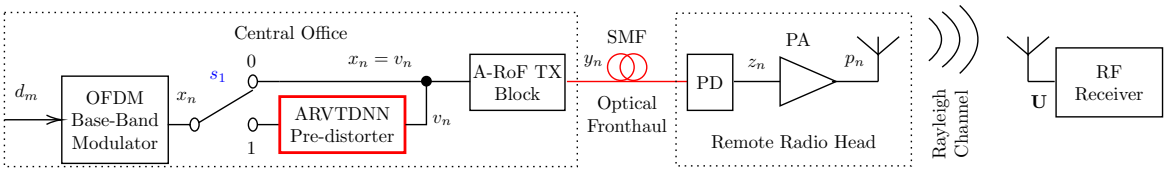

Fig. 1. Block diagram of the base-band equivalent model of analog radio-over-fiber system.

$\{0, 1, 2, \ldots, M-1\}$ and $n \in \{0, 1, \ldots, N-1\}$ is the time index. In case of DPD is employed (switch s_1 in Fig. 1 at position 1), the OFDM waveform is applied to the pre-distorter block. This signal is then applied to the MZM leading to [8]

$$y_n = \sum_{j=0}^{J-1} h_j |v_n|^j v_n, \tag{2}$$

where h_k are the polynomial model coefficients, v_n is the pre-distorted OFDM signal, $n \in \{0, 1, .2., \ldots, N-1\}$ is the time index. J stands for the nonlinearity order of the model. Once we are interested only in MZM and PA non-linear distortions, caused, we have assumed that SMF and photodetector (PD) combined response is $g_n = \delta_n$, leading to

$$z_n = y_n * g_n, \tag{3}$$

in which $*$ denotes the convolution operation

Memory non-linear distortions will be introduced PA, once it usually operates close to its 1-dB saturation point. The PA non-linearities can be modeled as [9]

$$p_n = \sum_{q=0}^{Q-1} \sum_{k=0}^{K-1} \xi_{q,k} \left|z_{n-q}\right|^k z_{n-q}, \tag{4}$$

where $\xi_{q,k}$ are coefficients of the PA model, with $q \in \{0, 1, \cdots, Q-1\}$ and $k \in \{0, 1, \cdots, K-1\}$, in which Q is the memory depth and K the model non-linear order [9].

We have assumed a Rayleigh channel to model the wireless transmission between the RRH and the RF receiver from the end user. Therefore, the signal at the end user RF receiver can be modeled as

$$\mathbf{U} = \mathbf{P} \odot \mathbf{H} + \mathbf{w}, \tag{5}$$

where $\odot$ stands for the Haddamard product, $\mathbf{P} = \mathscr{F}(\mathbf{p}), \mathbf{p} \in \mathbb{C}^{N\times 1}$ is the frequency-domain vectored version of p_n, $\mathbf{H} \in \mathbb{C}^{N\times 1}$ is the frequency response of Rayleigh channel and $\mathbf{w} \in \mathbb{C}^{N\times 1}$ is the additive white Gaussian noise (AWGN). Finally, a single-tap frequency domain equalization can be performed for compensating the effects of the wireless channel.

III. Performance Evaluation

We evaluated the performance of the FiWi system via computer simulation using the root mean square error vector magnitude (EVM_{RMS}) and symbol error rate (SER) metrics. Moreover, we have used a polynomial-based solution as a benchmark. The coefficients of the polynomial based solution was calculated by employing the know closed-form solution. Before evaluating the proposed system performance, it is necessary to specify the parameters of the base-band equivalent system model. We have assumed $J = 5$ for the MZM memoryless model and $K = 5$ and $Q = 3$ for the PA memory model, which are typical values found in literature [8], [9].

The DPD designed for A-RoF applications needs to mitigate both memory-less and memory non-linear distortions caused by the MZM and PA, as well as counteract the linear distortion originating from the SMF. To address this complex distortion scenario, the ARVTDNN has been chosen. This selection is attributed to the innovative architecture of ARVTDNN, which incorporates a TDL mechanism to intelligently supply input to the ANN. Through this strategic design, the DPD can seamlessly alleviate the diverse range of distortions mentioned earlier, thereby ensuring enhanced the signal quality.

We have performed preliminary studies by heuristically varying the ANN hyperparameters to maximize the system performance. In the ANN input layer a TDL structure was employed, leading to 18 input neurons. This approach enables feeding the ANN with all necessary information to compensate for the memory effect. Three hidden layers were employed, each one of them composed of 1024 neurons. The hyperbolic tangent (tanh) activation function was used in the first hidden layer for dealing with the gradient exploding problem, whereas Leaky rectified linear unit (ReLU) ($\alpha = 0.01$) has been used in the other two hidden layers. The ANN employs two neurons in the output layer for estimating the real and imaginary parts of the OFDM symbol. The DPD performs a regression task, which typically means that a identity activation might be used in the output layer. The training data set was composed of 15 OFDM blocks, leading to a data set with 30720 samples. It was required 300 epochs to train the model by employing the Adaptive Momentum (Adam) optimizer.

Fig. 2 reports the EVM_{RMS} as a function of RF power at MZM input. The EVM_{RMS} measures the received symbols coordinates deviation compared with the original transmitted signal. In this study, we utilize 16-QAM modulation. Additionally, we explore an OFDM signal with a 20-GHz bandwidth, representing the aggregated bandwidth of multiple users. We can notice that the ML-based DPD has considerably reduced the EVM_{RMS} even for high RF power. Moreover, the EVM_{RMS} was close to polynomial-based DPD, which was used as a benchmark. This outcome demonstrates the feasibility of allocating RF power within the range of 5 to 25 dBm, all while maintaining the transmission quality unimpaired.

The out-band distortion was also evaluated. Fig 3 shows the

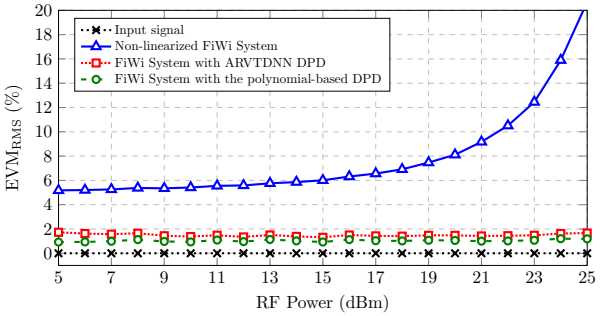

Fig. 2. EVM$_{RMS}$ as a function of RF Power at MZM input.

normalized power spectral density for the signal at the end-user receiver with and without the DPD scheme. When the DPD scheme is employed the out-of-band emission is reduced, which means that the proposed scheme solution is also a remarkable solution to compensate for out-band distortions. Furthermore, the proposed scheme demonstrates comparable outcomes when juxtaposed with the benchmark of polynomial-based DPD that was utilized.

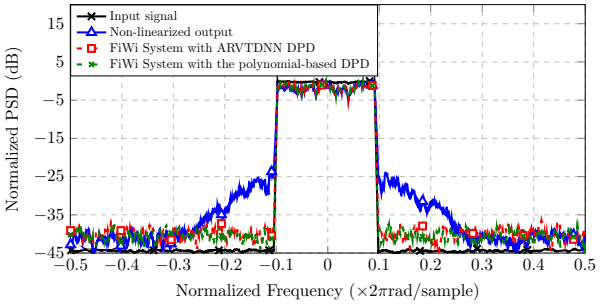

Fig. 3. Frequency spectrum for an OFDM signal at 20 dBm.

Finally, we have evaluated the SER of the FiWi system. Fig. 4 presents the results of our proposed system compared with the theoretical OFDM transmission in Rayleigh channels. We have considered 26 dBm of RF power at MZM input. It can be observed that the ML-based DPD was practically equal to the polynomial based DPD. Moreover, one can observe that the A-RoF system was practically transparent to the wireless system since the SER is almost not affected when the A-RoF is employed. On the other hand, the SER will be severely affected in the case of the proposed scheme in not employed. This achievement proves the remarkable linearization performance of the ML-based DPD scheme, in case non-linear distortions are introduced by MZM and PA. Utilizing ARVTDNN-based DPD offers a compelling approach to tackle the drawbacks of polynomial-based DPD. These drawbacks include the need for precise polynomial degree selection to avert overfitting, susceptibility to outliers, and limited handling of highly correlated signals. This can compromise accurate coefficient estimation in the regression model, causing coefficients to be overly sensitive to minor data variations and resulting in unreliable and unstable results.

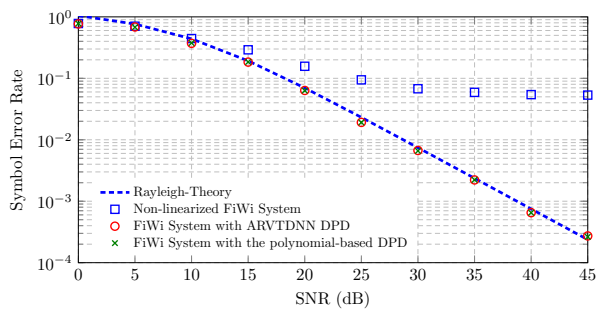

Fig. 4. Symbol error rate as a function of SNR.

IV. Conclusions

In this paper, we have presented and evaluated a ML-based DPD scheme designed for future 6G FiWi systems. The proposed DPD remarkably compensated non-linear distortions produced by the MZM and PA. The proposed scheme allowed dynamically allocating RF power to cover distinct remote areas. Moreover, the DPD scheme allowed seamless integration of an A-RoF into a wireless system since the SER of the system was practically not affected. This solution can be considered a powerful tool for future communication systems that enables dealing with A-RoF system degradation.

Acknowledgments

This work was partially supported by Brazil 6G project founded by RNP/MCTIC (01245.020548/2021-07), by the Advanced Academic Education in Telecommunications Networks and Systems founded by Huawei (PPA6001BRA23032110257684), by the SAMURAI project founded by FAPESP (20/05127-2). The authors also thank the financial support from CNPq, CAPES, FINEP and FAPEMIG.

References

[1] H. Tataria *et al.*, "6G Wireless Systems: Vision, Requirements, Challenges, Insights, and Opportunities," *Proceedings of the IEEE*, vol. 109, no. 7, pp. 1166–1199, 2021.

[2] S. Liu *et al.*, "A Multilevel Artificial Neural Network Nonlinear Equalizer for Millimeter-Wave Mobile Fronthaul Systems," *Journal of Lightwave Technology*, vol. 35, no. 20, pp. 4406–4417, 2017.

[3] Q. Zhou *et al.*, "Enhanced Multi-Level Signal Recovery in Mobile Fronthaul Network Using DNN Decoder," *IEEE Photonics Technology Letters*, vol. 30, no. 17, pp. 1511–1514, 2018.

[4] L. A. M. Pereira *et al.*, "Linearization Schemes for Radio Over Fiber Systems Based on Machine Learning Algorithms," *IEEE Photonics Technology Letters*, vol. 34, no. 5, pp. 279–282, 2022.

[5] L. A. M. Pereira *et al.*, "Machine Learning-Based Linearization Schemes for Radio Over Fiber Systems," *IEEE Photonics Journal*, vol. 14, no. 6, pp. 1–10, 2022.

[6] L. A. M. Pereira *et al.*, "Amplified Radio-over-Fiber System Linearization Using Recurrent Neural Networks," *Journal of Optical Communications and Networking*, vol. 15, no. 3, pp. 144–154, 2023.

[7] D. Wang *et al.*, "Augmented Real-Valued Time-Delay Neural Network for Compensation of Distortions and Impairments in Wireless Transmitters," *IEEE Transactions on Neural Networks and Learning Systems*, vol. 30, no. 1, pp. 242–254, 2018.

[8] H. Chen *et al.*, "Experimental Investigation on Multi-dimensional Digital Predistortion for Multi-band Radio-over-fiber Systems," *Optics express*, vol. 22, no. 4, pp. 4649–4661, 2014.

[9] D. R. Morgan *et al.*, "A Generalized Memory Polynomial Model for Digital Predistortion of RF Power Amplifiers," *IEEE Transactions on signal processing*, vol. 54, no. 10, pp. 3852–3860, 2006.

Chapter 4

Conclusions and Future Works

This work proposed and evaluated ANN-based linearization schemes designed for A-RoF systems. Such schemes are based on pre- and post-distortion concepts. The main goal was to mitigate the non-linear distortions produced by the A-RoF components. The ANN-based linearization performance was compared with the conventional DPD solution. This work presented several insights regarding the linearization of A-RoF systems:

- The implementation of digital pre- and/or post-distortion ML-based algorithms and its linearization performance evaluation: the simulation results demonstrated that pre- and/or post-distortion techniques might be employed to linearize A-RoF systems. The memoryless polynomial model was used to represent the MZM non-linearities since, in this case, a memory effect will not be significantly observed. The pre-distortion scheme slightly outperformed the post-distortion scheme, since it prevents the spectral regrowth produced by the MZM non-linearities. Moreover, the pre-distortion scheme operates with higher SNR when compared with the post-distortion, since it is implemented at the transmitter side. Therefore, the noise statistics on the receiver side are unchanged. On the other hand, the post-distortion is employed at the RRH side, which means that it can also be used for compensating linear distortion, operating as an equalizer. Nonetheless, considering that the linear distortions are not observed, it is expected that the pre-distortion scheme outperforms the post-distortion since post-distortion will not prevent the spectral regrowth.
- The implementation ML-based DPD for time-variant A-RoF systems: the simulations results showed that ANN-based DPD can accommodate variations on the coefficients of the models that represent the non-linear response of the A-RoF components. The time-variant response might come from temperature varia-

tions, aging or, fluctuation in the electro-optic modulator polarization voltage. A dual-ANN architecture was employed to model the A-RoF system and to obtain its post-inversion response in order to generalize possible variations of the A-RoF systems components. The linearization performance of the proposed dual-ANN scheme was compared with a conventional state-of-art DPD solution (OSFL) when the time-invariant and variant scenarios were considered. For the time-invariant scenario, the proposed dual-ANN solution has presented similar performance compared with the conventional OSFL DPD solution. On the other hand, when the time-variant scenario is considered, the proposed DPD outperforms the OSFL, which requires to be re-calibrated to accommodate the variations in the coefficients of the model.

- The implementation of pre- and/or post distortion schemes for amplified-A-RoF systems: in this specific operating scenario, we were interested in including the PA to our analysis. The PA considered in this case is located at RRH. In contrast to MZM, the PA introduces memory non-linear distortions. Therefore, the memory effect must be considered during the linearization. Since we intend to compensate for the cascade nonlinear responses of the MZM and PA, the employed ANN must be capable of simultaneously dealing with memory and memoryless effects. Therefore, we implemented a RNN-based linearization scheme and compared it linearization performance with a MLP scheme, which is not capable of dealing with memory effect. The simulations demonstrated that MLP, is capable of reducing the out-band distortions but can not satisfactorily reduce the in-band distortion. Therefore, MLP can be used when only OOBE reduction is relevant, without concerning about the in-band degradation. On the other hand, the RNNs simultaneously reduce in-band and out-of-band distortions. The linearization performance of the RNN-based schemes depends on the memory depth. When the RNN memory depth is equal to or higher than the PA memory depth, the performance of the linearization schemes is improved. The proposed RNN-based linearization scheme can be an important tool to assure the proper exploitation of TVWS in remote and rural areas.
- The implementation of pre- and/or post distortion schemes for amplified-A-RoF systems considering chromatic dispersion: in this analysis, the CD effect was included because it was assumed that the optical link can reach tens of kilometers. An ARVTDNN was employed for compensating the memoryless and memory non-linear distortions as well as the linear chromatic effect. A remarkable linearization performance was observed showing that the proposed scheme is potential to 5G and future 6G communication systems. One extra benefit

of this method was that, when properly designed and trained, this class of algorithms could also deal with the linear distortion introduced by CD, reducing even further the complexity, since dispersion compensation fibers (DCFs) and digital signal processing (DSP) approaches were not required. The proposed scheme was eventually employed in a FiWi system.

The suggestions for further works rely on applying the ML-based linearization algorithms in real FiWi systems using an experimental data set. For instance, one can transmit OFDM symbols and storage the system output to create the data set. For this, it is necessary synchronizing the transmitter and receiver to ensure that an input sample is matched with its corresponding output sample. In other words, Becomes required to precisely identify the beginning and end of OFDM symbol. One approach to overcome this issue is to incorporate a preamble with a known sequence at the beginning of the OFDM symbol. Synchronization between transmitter and receiver is achieved by performing a correlation operation between the known sequence from the preamble with the received symbol. However, this is a very challenging and not-trivial operation.

One another possible approach is to employ reinforcement learning, which is a non-supervised learning method. In this scenario, the data set is not required since the algorithm will be adapted through its interaction with the A-RoF system, where it receives positive or negative feedbacks. Finally, deploying practical linearization schemes might also include challenges regarded to algorithm complexity and energy consumption. New studies might be performed aiming to reduce the algorithm complexity by modifying the ANN architecture and hyperparameters, leading to a trade-off between complexity and performance. Moreover, the energy consumption might also be carefully managed, especially for large-scale deployments. This can involve the utilization of intelligent power management strategies to minimize energy consumption, while simultaneously maintaining system performance.

References

[1] Z. Zhang, Y. Xiao, Z. Ma, M. Xiao, Z. Ding, X. Lei, G. K. Karagiannidis, and P. Fan, "6G Wireless Networks: Vision, Requirements, Architecture, and Key Technologies," *IEEE Vehicular Technology Magazine*, vol. 14, no. 3, pp. 28–41, 2019.

[2] 3GPP, "Release 15 Description; Summary of Rel-15 Work Items," 2018, TR 21.915, version 0.5.0, Release 15.

[3] 3GPP-ETSI, "Study on New Radio Access Technology," Oct. 2017, TR 38.912 version 14.1.0 Release 14. [Online]. Available: https://www.etsi.org/deliver/etsi_tr/138900_138999/138912/14.01.00_60/tr_138912v140100p.pdf

[4] M. ITU-R, "Framework and Overall Objectives of the Future Development of IMT for 2020 and Beyond," 2014.

[5] L. Nielsen, A. Gavras, M. Dieudonne, I. Mesogiti, P. Roosipuu, D. Houatra, and E. Kosmatos, "Beyond 5G/6G KPIs and Target Values," Jun. 2022. [Online]. Available: https://doi.org/10.5281/zenodo.6577506

[6] 3GPP, "5G; Service Requirements for Next generation New services and Markets," 2019, TS 22.261 version 15.8.0 Release 15.

[7] ITU-R, "M. 2083, IMT Vision Framework and Overall Objectives of the Future Development of IMT for 2020 and Beyond," *ITU-R, Sep*, 2015.

[8] A. Osseiran, F. Boccardi, V. Braun, K. Kusume, P. Marsch, M. Maternia, O. Queseth, M. Schellmann, H. Schotten, H. Taoka, H. Tullberg, M. A. Uusitalo, B. Timus, and M. Fallgren, "Scenarios for 5G Mobile and Wireless Communications: The Vision of the METIS Project," *IEEE Communications Magazine*, vol. 52, no. 5, pp. 26–35, 2014.

[9] H. Tullberg, P. Popovski, Z. Li, M. A. Uusitalo, A. Hoglund, O. Bulakci, M. Fallgren, and J. F. Monserrat, "The METIS 5G System Concept: Meeting the 5G Requirements," *IEEE Communications Magazine*, vol. 54, no. 12, pp. 132–139, 2016.

[10] J. R. Bhat and S. A. Alqahtani, "6G Ecosystem: Current Status and Future Perspective," *IEEE Access*, vol. 9, pp. 43 134–43 167, 2021.

[11] G. Kalfas, C. Vagionas, A. Antonopoulos, E. Kartsakli, A. Mesodiakaki, S. Papaioannou, P. Maniotis, J. S. Vardakas, C. Verikoukis, and N. Pleros, "Next Generation Fiber-Wireless Fronthaul for 5G mmWave Networks," *IEEE Communications Magazine*, vol. 57, no. 3, pp. 138–144, 2019.

[12] M. Kamel, W. Hamouda, and A. Youssef, "Uplink Coverage and Capacity Analysis of mMTC in Ultra-Dense Networks," *IEEE Transactions on Vehicular Technology*, vol. 69, no. 1, pp. 746–759, 2020.

[13] C. Bockelmann, N. Pratas, H. Nikopour, K. Au, T. Svensson, C. Stefanovic, P. Popovski, and A. Dekorsy, "Massive Machine-Type Communications in 5G: Physical and MAC-layer Solutions," *IEEE Communications Magazine*, vol. 54, no. 9, pp. 59–65, 2016.

[14] P. Yang, Y. Xiao, M. Xiao, and S. Li, "6G Wireless Communications: Vision and Potential Techniques," *IEEE Network*, vol. 33, no. 4, pp. 70–75, 2019.

[15] N. Chen and M. Okada, "Toward 6G Internet of Things and the Convergence With RoF System," *IEEE Internet of Things Journal*, vol. 8, no. 11, pp. 8719–8733, 2020.

[16] L. L. Mendes, C. S. Moreno, M. V. Marquezini, A. M. Cavalcante, P. Neuhaus, J. Seki, N. F. T. Aniceto, H. Karvonen, I. Vidal, F. Valera *et al.*, "Enhanced Remote Areas Communications: The Missing Scenario for 5G and Beyond 5G Networks," *IEEE Access*, vol. 8, pp. 219 859–219 880, 2020.

[17] A. M. Cavalcante, M. V. Marquezini, L. Mendes, and C. S. Moreno, "5G for Remote Areas: Challenges, Opportunities and Business Modeling for Brazil," *IEEE Access*, vol. 9, pp. 10 829–10 843, 2021.

[18] W. Dias, D. Gaspar, L. L. Mendes, M. Chafii, M. Matthé, P. Neuhaus, and G. Fettweis, "Performance Analysis of a 5G Transceiver Implementation for Remote Areas Scenarios," in *2018 European Conference on Networks and Communications (EuCNC)*, 2018, pp. 363–367.

[19] F. Schaich, M.-H. Hamon, M. Hunukumbure, J. Lorca, K. Pedersen, M. Schubert, E. Kosmatos, G. Wunder, and K. Reaz, "The ONE5G Approach Towards the Challenges of Multi-Service Operation in 5G Systems," in *2018 IEEE 87th Vehicular Technology Conference (VTC Spring)*, 2018, pp. 1–6.

[20] 5G RuralFirst consortium, "5G RuralFirst: New Thinking Applied to Rural Connectivity," Departure for Digital, Culture, Media and Sports, Techni-

cal Report, October 2019, available at: https://www.5gruralfirst.org/wp-content/uploads/2019/10/5G-RuralFirst-New-Thinking-Applied-to-Rural-Connectivity-1.pdf.

[21] M. A. Habibi, M. Nasimi, B. Han, and H. D. Schotten, "A Comprehensive Survey of RAN Architectures Toward 5G Mobile Communication System," *IEEE Access*, vol. 7, pp. 70 371–70 421, 2019.

[22] F. Tonini, C. Raffaelli, L. Wosinska, and P. Monti, "Cost-Optimal Deployment of a C-RAN With Hybrid Fiber/FSO Fronthaul," *Journal of Optical Communications and Networking*, vol. 11, no. 7, pp. 397–408, 2019.

[23] V. A. Thomas, M. El-Hajjar, and L. Hanzo, "Performance Improvement and Cost Reduction Techniques for Radio Over Fiber Communications," *IEEE Communications Surveys Tutorials*, vol. 17, no. 2, pp. 627–670, 2015.

[24] L. A. M. Pereira, C. H. S. Lopes, R. M. Borges, E. S. Lima, A. C. Ferreira, M. Abreu, L. L. Mendes, and Arismar Cerqueira S. Jr., "Implementation of a Multiband 5G NR Fiber-wireless System Using Analog Radio over Fiber Technology," *Optics Communications*, vol. 474, p. 126112, 2020.

[25] J. Wang, C. Liu, M. Zhu, A. Yi, L. Cheng, and G.-K. Chang, "Investigation of Data-Dependent Channel Cross-Modulation in Multiband Radio-Over-Fiber Systems," *Journal of Lightwave Technology*, vol. 32, no. 10, pp. 1861–1871, 2014.

[26] T. Ismail, C.-P. Liu, J. E. Mitchell, and A. J. Seeds, "High-Dynamic-Range Wireless-Over-Fiber Link Using Feedforward Linearization," *Journal of Lightwave Technology*, vol. 25, no. 11, pp. 3274–3282, 2007.

[27] M. Noweir, Q. Zhou, A. Kwan, R. Valivarthi, M. Helaoui, W. Tittel, and F. M. Ghannouchi, "Digitally Linearized Radio-over Fiber Transmitter Architecture for Cloud Radio Access Network's Downlink," *IEEE Transactions on Microwave Theory and Techniques*, vol. 66, no. 7, pp. 3564–3574, 2018.

[28] J. He, J. Lee, S. Kandeepan, and K. Wang, "Machine Learning Techniques in Radio-over-Fiber Systems and Networks," in *Photonics*, vol. 7, no. 4. Multidisciplinary Digital Publishing Institute, 2020, p. 105.

[29] F. N. Khan, Q. Fan, C. Lu, and A. P. T. Lau, "An Optical Communication's Perspective on Machine Learning and Its Applications," *Journal of Lightwave Technology*, vol. 37, no. 2, pp. 493–516, 2019.

[30] S. Liu, M. Xu, J. Wang, F. Lu, W. Zhang, H. Tian, and G.-K. Chang, "A Multilevel Artificial Neural Network Nonlinear Equalizer for Millimeter-Wave Mobile Fronthaul Systems," *Journal of Lightwave Technology*, vol. 35, no. 20, pp. 4406–

4417, 2017.

[31] K. J. Williams, R. D. Esman, and M. Dagenais, "Nonlinearities in pin Microwave Photodetectors," *Journal of lightwave technology*, vol. 14, no. 1, pp. 84–96, 1996.

[32] H. Ku and J. S. Kenney, "Behavioral Modeling of Nonlinear RF Power Amplifiers Considering Memory Effects," *IEEE transactions on microwave theory and techniques*, vol. 51, no. 12, pp. 2495–2504, 2003.

[33] J. H. Vuolevi, T. Rahkonen, and J. P. Manninen, "Measurement technique for characterizing memory effects in RF power amplifiers," *IEEE Transactions on microwave theory and techniques*, vol. 49, no. 8, pp. 1383–1389, 2001.

[34] L. Gupta, M. McAvoy, and J. Phegley, "Classification of Temporal Sequences Via Prediction Using the Simple Recurrent Neural Network," *Pattern Recognition*, vol. 33, no. 10, pp. 1759–1770, 2000.

[35] B. Nakisa, M. N. Rastgoo, A. Rakotonirainy, F. Maire, and V. Chandran, "Automatic Emotion Recognition Using Temporal Multimodal Deep Learning," *IEEE Access*, vol. 8, pp. 225 463–225 474, 2020.

[36] T. Zhang, W. Zheng, Z. Cui, Y. Zong, and Y. Li, "Spatial–Temporal Recurrent Neural Network for Emotion Recognition," *IEEE Transactions on Cybernetics*, vol. 49, no. 3, pp. 839–847, 2019.

[37] W. B. Bridges and J. H. Schaffner, "Distortion in Linearized Electrooptic Modulators," *IEEE Transactions on Microwave Theory and Techniques*, vol. 43, no. 9, pp. 2184–2197, 1995.

[38] Y. Shen, B. Hraimel, X. Zhang, G. E. R. Cowan, K. Wu, and T. Liu, "A Novel Analog Broadband RF Predistortion Circuit to Linearize Electro-Absorption Modulators in Multiband OFDM Radio-Over-Fiber Systems," *IEEE Transactions on Microwave Theory and Techniques*, vol. 58, no. 11, pp. 3327–3335, 2010.

[39] L. Roselli, V. Borgioni, F. Zepparelli, F. Ambrosi, M. Comez, P. Faccin, and A. Casini, "Analog Laser Predistortion for Multiservice Radio-over-Fiber Systems," *Journal of Lightwave Technology*, vol. 21, no. 5, p. 1211, 2003.

[40] J. Ning, Y. Dai, F. Yin, J. Li, Q. Lv, and K. Xu, "Digital Linearization for Broadband Multicarrier Analog Photonic Link Incorporating Downconversion," *Optical Engineering*, vol. 55, no. 3, pp. 031 102–031 102, 2016.

[41] W. Jiang, Q. Tan, W. Qin, D. Liang, X. Li, H. Ma, and Z. Zhu, "A Linearization Analog Photonic Link With High Third-Order Intermodulation Distortion Suppression Based on Dual-Parallel Mach–Zehnder Modulator," *IEEE Photonics Journal*, vol. 7, no. 3, pp. 1–8, 2015.

[42] B. Masella, B. Hraimel, and X. Zhang, "Enhanced Spurious-Free Dynamic Range Using Mixed Polarization in Optical Single Sideband Mach–Zehnder Modulator," *Journal of Lightwave Technology*, vol. 27, no. 15, pp. 3034–3041, 2009.

[43] S. Korotky and R. de Ridder, "Dual Parallel Modulation Schemes for Low-Distortion Analog Optical Transmission," *IEEE Journal on Selected Areas in Communications*, vol. 8, no. 7, pp. 1377–1381, 1990.

[44] L. Torrijos-Morán, C. Catalá-Lahoz, D. Pérez-López, L. Xu, W. Tianxiang, and D. Pérez-Galacho, "Linearization of a Dual-Parallel Mach-Zehnder Modulator Using Optical Carrier Band Processing," *Journal of Lightwave Technology*, 2023.

[45] S. Li, X. Zheng, H. Zhang, and B. Zhou, "Highly Linear Radio-over-Fiber System Incorporating a Single-Drive Dual-Parallel Mach–Zehnder Modulator," *IEEE Photonics Technology Letters*, vol. 22, no. 24, pp. 1775–1777, 2010.

[46] X. Zhang, S. Saha, R. Zhu, T. Liu, and D. Shen, "Analog Pre-Distortion Circuit for Radio Over Fiber Transmission," *IEEE Photonics Technology Letters*, vol. 28, no. 22, pp. 2541–2544, 2016.

[47] C. Yin, J. Li, H. Chen, Q. Lv, Y. Fan, F. Yin, Y. Dai, and K. Xu, "Behavioral Modeling and Digital Compensation of Nonlinearity in Multi-Band Externally-Modulated Radio-over-Fiber Links," in *2016 25th Wireless and Optical Communication Conference (WOCC)*. IEEE, 2016, pp. 1–4.

[48] J. Li, C. Yin, H. Chen, F. Yin, Y. Dai, and K. Xu, "Behavioral Modeling and Digital Compensation of Nonlinearity in DFB Lasers for Multi-Band Directly Modulated Radio-over-Fiber Systems," in *Semiconductor Lasers and Applications VI*, vol. 9267. International Society for Optics and Photonics, 2014, p. 92670K.

[49] H. D. Rodrigues, T. C. Pimenta, R. A. A. de Souza, and L. L. Mendes, "Orthogonal Scalar Feedback Digital Pre-Distortion Linearization," *IEEE Transactions on Broadcasting*, vol. 64, no. 2, pp. 319–330, 2017.

[50] R. M. Borges, L. A. M. Pereira, H. R. D. Filgueiras, A. C. Ferreira, M. S. B. Cunha, E. R. Neto, D. H. Spadoti, L. L. Mendes, and Arismar Cerqueira S. Jr., "DSP-Based Flexible-Waveform and Multi-Application 5G Fiber-Wireless System," *Journal of Lightwave Technology*, vol. 38, no. 3, pp. 642–653, 2019.

[51] R. Zhu, X. Zhang, D. Shen, and Y. Zhang, "Ultra Broadband Predistortion Circuit for Radio-over-Fiber Transmission Systems," *Journal of Lightwave Technology*, vol. 34, no. 22, pp. 5137–5145, 2016.

[52] H.-H. Lu, S.-J. Tzeng, and Y.-L. Liu, "Intermodulation Distortion Suppression

in a Full-Duplex Radio-on-Fiber Ring Network," *IEEE Photonics Technology Letters*, vol. 16, no. 2, pp. 602–604, 2004.

[53] A. Hekkala, M. Hiivala, M. Lasanen, J. Perttu, L. C. Vieira, N. J. Gomes, and A. Nkansah, "Predistortion of Radio Over Fiber Links: Algorithms, Implementation, and Measurements," *IEEE Transactions on Circuits and Systems I: Regular Papers*, vol. 59, no. 3, pp. 664–672, 2011.

[54] X. Xie, M. Hui, T. Liu, and X. Zhang, "Hybrid Linearization of Broadband Radio-over-Fiber Transmission," *IEEE Photonics Technology Letters*, vol. 30, no. 8, pp. 692–695, 2018.

[55] L. A. M. Pereira, L. L. Mendes, C. J. A. Bastos-Filho, and Arismar Cerqueira S. Jr, "Linearization Schemes for Radio Over Fiber Systems Based on Machine Learning Algorithms," *IEEE Photonics Technology Letters*, vol. 34, no. 5, pp. 279–282, 2022.

[56] S-H. Lee, J.-M. Kang, I.-H. Choi, and S.-K. Han, "Linearization of DFB Laser Diode by External Light-Injected Cross-Gain Modulation for Radio-over-Fiber Link," *IEEE photonics technology letters*, vol. 18, no. 14, pp. 1545–1547, 2006.

[57] M. Noweir, M. Helaoui, D. Oblak, W. Chen, and F. M. Ghannouchi, "Linearization of Radio-Over-Fiber Cloud-RAN Transmitters Using Pre-and Post-Distortion Techniques," *IEEE Photonics Technology Letters*, vol. 33, no. 7, pp. 339–342, 2021.

[58] B. Hraimel, X. Zhang, W. Jiang, K. Wu, T. Liu, T. Xu, Q. Nie, and K. Xu, "Experimental Demonstration of Mixed-Polarization to Linearize Electro-Absorption Modulators in Radio-over-Fiber Links," *IEEE Photonics Technology Letters*, vol. 23, no. 4, pp. 230–232, 2010.

[59] Y. Cui, Y. Dai, F. Yin, Q. Lv, J. Li, K. Xu, and J. Lin, "Enhanced Spurious-Free Dynamic Range in Intensity-Modulated Analog Photonic Link Using Digital Postprocessing," *IEEE Photonics Journal*, vol. 6, no. 2, pp. 1–8, 2014.

[60] K. B. Letaief, W. Chen, Y. Shi, J. Zhang, and Y.-J. A. Zhang, "The Roadmap to 6G: AI Empowered Wireless Networks," *IEEE communications magazine*, vol. 57, no. 8, pp. 84–90, 2019.

[61] A. C. Najarro and S.-M. Kim, "Nonlinear Compensation Using Artificial Neural Network in Radio-over-Fiber System," *Journal of information and communication convergence engineering*, vol. 16, no. 1, pp. 1–5, 2018.

[62] M. U. Hadi, M. Awais, M. Raza, K. Khurshid, and H. Jung, "Neural Network DPD for Aggrandizing SM-VCSEL-SSMF-Based Radio over Fiber Link Per-

formance," in *Photonics*, vol. 8, no. 1. Multidisciplinary Digital Publishing Institute, 2021, p. 19.

[63] Q. Zhou, F. Lu, M. Xu, P.-C. Peng, S. Liu, S. Shen, R. Zhang, S. Yao, J. Finkelstein, and G.-K. Chang, "Enhanced Multi-Level Signal Recovery in Mobile Fronthaul Network Using DNN Decoder," *IEEE Photonics Technology Letters*, vol. 30, no. 17, pp. 1511–1514, 2018.

[64] S. Liu, Y. M. Alfadhli, S. Shen, M. Xu, H. Tian, and G.-K. Chang, "A novel ANN Equalizer to Mitigate Nonlinear Interference in Analog-RoF Mobile Fronthaul," *IEEE Photonics Technology Letters*, vol. 30, no. 19, pp. 1675–1678, 2018.

[65] I. A. Alimi, A. L. Teixeira, and P. P. Monteiro, "Toward an Efficient C-RAN Optical Fronthaul for the Future Networks: A tutorial on Technologies, Requirements, Challenges, and Solutions," *IEEE Communications Surveys & Tutorials*, vol. 20, no. 1, pp. 708–769, 2017.

[66] A. Checko, H. L. Christiansen, Y. Yan, L. Scolari, G. Kardaras, M. S. Berger, and L. Dittmann, "Cloud RAN for Mobile Networks—A Technology Overview," *IEEE Communications surveys & tutorials*, vol. 17, no. 1, pp. 405–426, 2014.

[67] CPRI Consortium and others, "Common Public Radio Interface (CPRI); Interface Specification," *CPRI specification*, vol. 7, p. 0, 2015.

[68] A. De la Oliva, J. A. Hernandez, D. Larrabeiti, and A. Azcorra, "An Overview of the CPRI Specification and Its Application to C-RAN-Based LTE Scenarios," *IEEE Communications Magazine*, vol. 54, no. 2, pp. 152–159, 2016.

[69] M. Xu, Z. Jia, J. Wang, L. A. Campos, and G.-K. Chang, "Statistical Data Compression and Differential Coding for Digital Radio-over-Fiber-Based Mobile Fronthaul," *Journal of Optical Communications and Networking*, vol. 11, no. 1, pp. A60–A71, 2019.

[70] M. Xu, F. Lu, J. Wang, L. Cheng, D. Guidotti, and G.-K. Chang, "Key Technologies for Next-Generation Digital RoF Mobile Fronthaul with Statistical Data Compression and Multiband Modulation," *Journal of Lightwave Technology*, vol. 35, no. 17, pp. 3671–3679, 2017.

[71] I. Chih-Lin, H. Li, J. Korhonen, J. Huang, and L. Han, "RAN Revolution With NGFI (xHaul) for 5G," *Journal of Lightwave Technology*, vol. 36, no. 2, pp. 541–550, 2017.

[72] T. Pfeiffer, "Next Generation Mobile Fronthaul and Midhaul Architectures," *Journal of Optical Communications and Networking*, vol. 7, no. 11, pp. B38–B45, 2015.

[73] G.-K. Chang and L. Cheng, "The Benefits of Convergence," *Philosophical Transactions of the Royal Society A: Mathematical, Physical and Engineering Sciences*, vol. 374, no. 2062, p. 20140442, 2016.

[74] C. Lim, A. Nirmalathas, M. Bakaul, P. Gamage, K.-L. Lee, Y. Yang, D. Novak, and R. Waterhouse, "Fiber-Wireless Networks and Subsystem Technologies," *Journal of lightwave technology*, vol. 28, no. 4, pp. 390–405, 2009.

[75] G. P. Agrawal, *Fiber-Optic Communication Systems*. John Wiley & Sons, 2012.

[76] V. J. Urick, J. F. Diehl, J. D. McKinney, J. M. Singley, and C. E. Sunderman, "Nonlinear Optical Angle Modulation for Suppression of RF Interference," *IEEE Transactions on Microwave Theory and Techniques*, vol. 64, no. 7, pp. 2198–2204, 2016.

[77] F. Musumeci, C. Rottondi, A. Nag, I. Macaluso, D. Zibar, M. Ruffini, and M. Tornatore, "An Overview on Application of Machine Learning Techniques in Optical Networks," *IEEE Communications Surveys & Tutorials*, vol. 21, no. 2, pp. 1383–1408, 2018.

[78] W. S. McCulloch and W. Pitts, "A Logical Calculus of the Ideas Immanent in Nervous Activity," *The bulletin of mathematical biophysics*, vol. 5, no. 4, pp. 115–133, 1943.

[79] A. Géron, *Hands-on Machine Learning With Scikit-Learn, Keras, and TensorFlow: Concepts, Tools, and Techniques to Build Intelligent Systems*. O'Reilly Media, 2019.

[80] I. Goodfellow, Y. Bengio, and A. Courville, *Deep learning*. MIT press, 2016.

[81] W. Tang, M. Hui, T. Liu, D. Shen, and X. Zhang, "A Simple Envelope-Assisted RF/IF Digital Predistortion Model for Broadband RoF Fronthaul Transmission," *Journal of Lightwave Technology*, vol. 36, no. 19, pp. 4305–4311, 2018.

[82] H. Chen, J. Li, K. Xu, Y. Pei, Y. Dai, F. Yin, and J. Lin, "Experimental Investigation on Multi-Dimensional Digital Predistortion for Multi-Band Radio-over-Fiber Systems," *Optics express*, vol. 22, no. 4, pp. 4649–4661, 2014.

[83] B. D. Laki and C. J. Kikkert, "Adaptive Digital Predistortion for Wideband High Crest Factor Applications Based on the WACP Optimization Objective: A Conceptual Overview," *IEEE Transactions on Broadcasting*, vol. 58, no. 4, pp. 609–618, 2012.

[84] F. M. Ghannouchi, O. Hammi, and M. Helaoui, *Behavioral Modeling and Predistortion of Wideband Wireless Transmitters*. John Wiley & Sons, 2015.

[85] D. R. Morgan, Z. Ma, J. Kim, M. G. Zierdt, and J. Pastalan, "A Generalized

Memory Polynomial Model for Digital Predistortion of RF Power Amplifiers," *IEEE Transactions on signal processing*, vol. 54, no. 10, pp. 3852–3860, 2006.

[86] N. Safari, T. Roste, P. Fedorenko, and J. S. Kenney, "An Approximation of Volterra Series Using Delay Envelopes, Applied to Digital Predistortion of RF Power Amplifiers With Memory Effects," *IEEE microwave and wireless components letters*, vol. 18, no. 2, pp. 115–117, 2008.

[87] Å. Björck, *Numerical Methods for Least Squares Problems*. SIAM, 1996.

[88] S. J. Savory, "Digital Coherent Optical Receivers: Algorithms and Subsystems," *IEEE Journal of Selected Topics in Quantum Electronics*, vol. 16, no. 5, pp. 1164–1179, 2010.

[89] A. Eghbali, H. Johansson, O. Gustafsson, and S. J. Savory, "Optimal Least-Squares FIR Digital Filters for Compensation of Chromatic Dispersion in Digital Coherent Optical Receivers," *Journal of lightwave technology*, vol. 32, no. 8, pp. 1449–1456, 2014.